Lithography Using an Atomic Force Microscope and Ionic Self-assembled Mulitlayers

Moataz Khalifa

Dissertation Submitted to the faculty of Virginia Polytechnic Institute and State University in partial fulfillment of the requirements for the degree of

Doctor of Philosophy
In
Physics

James R. Heflin
(Committee Chair)
Eric Sharpe
Hans D. Robinson
Chenggang Tao

February 20, 2015

Blacksburg, VA

Keywords: Atomic Force Microscope (AFM), Nanolithography, Selective Deposition, Nanografting

Lithography Using an Atomic Force Microscope and Ionic Self-assembled Mulitlayers

Moataz Khalifa

Abstract

This thesis presents work done investigating methods for constructing patterns on the nanometer scale. Various methods of nanolithography using atomic force microscopes (AFMs) are investigated. The use of AFMs beyond their imaging capabilities is demonstrated in various experiments involving nanografting and surface electrochemical modification. The use of an AFM to manipulate a monolayer of thiols deposited on a gold substrate via nanografting is shown in our work to enable chemical modification of the surface of the substrate by varying the composition of the monolayer deposited on it. This leads to the selective deposition of various polymers on the patterned areas. Conditions for enhancing the selective deposition of the self-assembled polymers are studied. Such conditions include the types of polymers used and the pH of the polyelectrolyte solutions used for polymer deposition. Another method of nanolithography is investigated which involves the electrochemical modification of a monolayer of silanes deposited on a silicon substrate. By applying a potential difference and maintaining the humidity of the ambient environment at a certain level we manage to change the chemical properties of select areas of the silane monolayer and thus manage to establish selective deposition of polymers and gold nanoparticles on the patterned areas. Parameters involved in the patterning process using surface electrochemical modification, such as humidity levels, are investigated. The techniques established are then used to construct circuit elements such as wires.

This thesis is dedicated to my parents Mohamed and Salwa Hammad, my wife Shannon, my son Ibrahim, Paul and Beth Besaw.

Table of Contents

Preface

List of Figures

Chapter 1

Chapter 2

Chapter 3

Chapter 4

Chapter 5

Chapter 6

List of Tables

Chapter 4

Chapter 6

CHAPTER 1

INTRODUCTION

In 1959 Richard Feynman delivered a speech to the American Physical Society titled "Plenty of Room at The Bottom". He spoke, in what many consider to be the birth of nanotechology, about "the problem of manipulating and controlling things on a small scale". [(1)] In this speech Feynman cleverly touched on some of the issues that would face such an effort within a few decades. Among the issues mentioned in the speech is the fact that classical physical laws do not still apply when we scale down the dimensions of the systems.[(1)] Physical laws and phenomena are quite different at the molecular and atomic level. Indeed these have been the two challenging aspects facing efforts to miniaturize circuits.

The interest in miniaturizing circuits and individual circuit elements has been an important topic of investigation in physics and electronics for decades. The drive to develop experimental methods for making circuit elements smaller and then finding ways of making such methods commercially available can be understood to be due to various reasons. These include the primary goal to increase the number of circuit elements that can fit on a chip, which can in turn improve the performance of the chips in terms of processing speed, power consumption, power dissipation, and the cost of manufacturing such high performance devices. Attempts to achieve this goal using various methods have had to deal with fundamentally different phenomena and limitations. The methods explored have spanned several techniques such as photolithography, X-ray lithography, and various scanning probe lithography techniques. Another trend being explored for the miniaturization of circuits is to try to build them from molecular components. This last approach is known as molecular electronics. Successful endeavors in molecular electronics have managed

to construct molecular diode rectifiers from molecular layers. [2], [3], [4], [5] Other attempts have been successful in constructing molecular wires in attempts to provide connections between molecular devices. [6] Studies of the conductive properties of carbon nanotubes have been done employing them as molecular wires between co-planar electrodes.[6], [7] Among the promising trends in molecular electronics is the use of carbon nanotubes as field effect transistors. Such a trend depends on the robustness of the carbon nanotubes and their chemical inertness among a host of other desirable characteristics making them an excellent candidate in the miniaturization efforts.[8], [9],[10]

In this dissertation we discuss efforts at developing a method for fabricating circuit elements on the nanometer scale. The method we have developed depends essentially on using an atomic force microscope (AFM) as a patterning tool. The AFM is used to pattern monolayers of self-assembled materials on various substrates. The patterning takes place via two different techniques. The first method is known as nanografting.[11],[12],[13] The second mode of patterning is electrochemical surface modification using an AFM.[14],[15] With these techniques, one can lay out patterns on a surface as charged templates and then self-assemble a variety of nanomaterials of arbitrary thickness onto these templates using layer-by-layer deposition. We establish in this dissertation a comparison between this new method of circuit element fabrication and other available methods used in constructing circuits and circuit elements. The comparisons established here examine aspects of the fabrication processes such as the smallest sizes achievable using each method, the ease of use for each of the methods, and the appropriate uses of each of the methods in varied applications and demands in the fields of electronics.

1.1 Lithography

Lithography in its most general form stands for techniques used in transferring patterns from one substrate to the other.[21] The origin of the word means stone writing. Some of the oldest forms date back to 3000 B. C.[22] The forms of lithography we are concerned with in the field of electronics and nanoelectronics are primarily photolithography and scanning probe lithography.

1.1.1 Photolithography

Photolithography is a process of transferring a pattern using optical means from a mask to a substrate for etching. Photolithography was invented in 1855 by the French chemist, engineer and photographer Alphonse Louis Poitevin. Poitevin discovered that exposing a ferro-gallat gum mixture to light changes its chemical properties. Exposing such a mixture to light hardens the mixture in proportion to the exposure time. The exposed parts of the mixture become water insoluble. Using such a technique provided the basis for better quality photographs and blueprints.[23],[24] The modern process of photolithography depends on the same principles of photosensitivity of certain chemicals and their becoming soluble or insoluble after being exposed to light.[25],[26] Coating a silicon substrate with certain types of materials, for example, poly(methyl methacrylate) (PMMA), as a photoresist and exposing the material to ultraviolet light of certain wavelengths breaks down bonds within the polymer and renders it soluble in certain types of solvents. This case is known as a positive photoresist. Developing the exposed substrates in the appropriate developer solutions etches away the layer of photoresist that was exposed to the UV light. This procedure allows for further processing of the silicon substrates in a multitude of ways. A similar result is achieved by using a negative resist where the exposed parts of the photoresist become insoluble in the developer solutions due to crosslinking. The versatility of this technique

and its enormous throughput due to the parallel processing nature of the technique make it a cornerstone of the semiconductor industry. However, several limitations on this process exist making it difficult to extend for much further miniaturization of circuits. The major limiting factor is the fact that once the smallest dimensions of the circuit near the tens of nanometers limit we run into interference effects from the light sources used in the photolithography.

1.1.2 Scanning Probe Lithography

Using scanning probes such scanning tunneling microscopes (STM) and atomic force microscopes (AFM) for patterning and manipulating surfaces is a strong, promising and versatile tool in the world of nanoelectronics. The main focus of this dissertation is a novel form of atomic force microscope based lithography.

1.1.2.1 Atomic Force Microscopes

The AFM is an imaging device that relies on the atomic force interactions between a very small, sharp tip, which has an average diameter of a few nanometers, and the surface of the scanned sample. Monitoring the reflection of a laser beam from the back of the AFM tip allows a feedback system to monitor changes in how the tip is deflected due to interactions with the surface. The observed changes in the reflected beam are then utilized by a feedback system to control the motion of the AFM tip to maintain either a constant distance or force to the scanned surface or constant oscillation amplitude of the tip depending on which mode of operation of the AFM is employed. A detailed discussion of the principles of operation of the AFM and the different modes of its operation will follow in Chapter 3 of this dissertation. The uses of AFMs and scanning tools have by far exceeded their straightforward use in imaging decades ago.[27] The two main techniques in which we use the AFM in AFM-based nanolithography are nanografting and surface electro-

chemical modification. Nanografting depends on applying a large force to the AFM tip such that this force shaves off some of the molecules that existed as a monolayer deposited on the substrate. Shaving the monolayer molecules takes place in the presence of an ambient solution in the liquid cell of the AFM so that the shaved molecules are replaced by another species of molecules from the ambient solution. The new molecules which have been grafted into the background monolayer are chosen based on their terminal functional group to change the chemistry of the surface in the horizontal direction parallel to the surface. In the second mode, the AFM is used to chemically modify the chemistry of the surface in certain chosen patterns. This is done by applying potential differences between the AFM tip and the monolayer deposited on the surface. The potential differences are used to either reduce or oxidize the monolayer. The oxidized or reduced parts of the surface establish patterns of different chemical properties than the backgrounds they are imbedded in. After the patterning is done, the designed patterns get covered with different materials to construct the desired circuit elements. Among the materials used for this deposition process are polymers, gold nanoparticles, and charged carbon nanotubes. All of these materials are deposited on the patterned areas in the form of self-assembled layers.

1.2 Self-Assembled Monolayers

Self-assembled monolayers (SAMs) are very thin layers that are a single molecule thick, deposited on surfaces from vapor or liquid phases. In the work reported in this dissertation, we utilize this method of deposition for various types of molecules. In the case of depositing monolayers as backgrounds on the substrates we deposit thiol monolayers on gold substrates, silane monolayers on silicon substrates and polymer multilayers on the patterned surfaces. SAMs are characterized mainly by the autonomous manner in which the molecules arrange themselves on the designated surfaces in organized forms with precisely controlled thickness. The mechanism by which each

of these deposits on the surface differs between the different cases. In the case of depositing thiols on gold, the attachment of the molecules depends on the interaction between the head group of the molecule with the gold substrate. In the case of thiols, these head groups contain sulfur atoms. Due to the strong affinity of sulfur to attach to gold these head groups attach themselves very well to the gold surface forming a monolayer of thiols on the gold substrate. In the case of silanes, the attachment to the surface is achieved using a Si-O-Si bond between the head group of the silanes containing silicon atoms and the substrate, which is consists of silicon. In the case of polymer layers, deposition on the patterned areas is achieved primarily via electrostatic interactions between the patterned areas of the substrates and the electrically charged polymer chains. Figure (1.1) below shows a schematic diagram for a monolayer attached to a substrate.

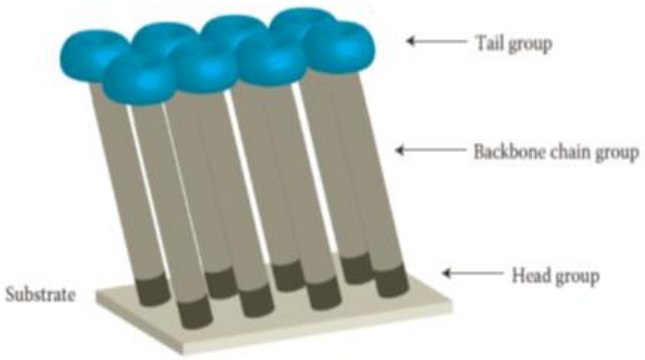

Figure (1.1): A schematic diagram of a monolayer of molecules attached to the surface of a substrate. The head group contains an atom or a molecule with affinity for binding with the surface of the substrate.[28] Reprinted with permission from: [Rogers, Pennathur, and Adams, Nanotechnology: Understanding Small Systems, 2nd Edition CRC Press, 2011]

One of the goals of this work is to demonstrate the various steps taken towards being able to build nanowires and transistors using self-assembly. The first step demonstrated is to design and execute a process to accomplish selective deposition of polymer layers and other nanomaterials on designated patterned areas. This first step is then followed by several steps aimed at selecting different materials suited for building circuit elements to be deposited using selective deposition.

1.3 Document Organization

This chapter is followed by the literature review of Chapter 2, in which we discuss some of the major trends in the world of nanoelectronics and the various methods used to fabricate nanoscale circuit elements. The methods discussed include photolithography, X-ray lithography, and scanning probe lithography, and we primarily focus on AFM based lithography techniques. In Chapter 3, we discuss in depth the experimental details of the methods and equipment used in our work. The discussion covers polymers, AFM systems and techniques, thiols, silanes and nanoparticles used in our work.

In Chapter 4, we describe the first stage of the work where we use gold-plated glass slides that we cover with a monolayer of uncharged thiols. Nanografting is then performed on the thiol monolayer in a liquid environment containing a solution of a different thiol to replace the background thiol deposited on the surface with another one thus establishing a pattern consisting of molecules terminated with charged groups within an uncharged background. The next step is to use Layer-by-Layer deposition of polyelectrolytes to selectively deposit polymer multilayers on the patterned areas. This allowed us to study the nature of this guided deposition process and to examine the factors affecting it such as pH levels and deposition times. The efforts from the first stage culminated in establishing a repeatable technique for nanografting and selective deposition

of multilayers of polymers. The technique developed also allows us a high degree of control on the thickness of the layers deposited and the sizes of the patterns they form.

In chapter 5, we describe the second stage of the work where we extend the procedure to silicon substrates covered by a monolayer of silanes.[7],[8] The silanes are then patterned using two different methods. The first method is the same AFM based nanografting method we used in the first stage. The second method is the chemical surface modification method. In this latter method, the applied potential difference between the AFM and the surface of the monolayer of silanes causes the functional groups at the end of the silane chains to change to a different desired functional group. The change in the chemical properties of the patterned areas of the silane monolayer establishes a pattern. The designed patterns are then used to guide the deposition of polymers, gold nanoparticles and charged carbon nanotubes. The extension to silicon substrates is an essential step since our goal is to build circuit elements. Circuit elements constructed by Layer-by-Layer deposition on a conductive background such as gold present an unworkable option due to the interference of the conductive substrate with device performance. Using silicon as a substrate on which the devices can be built provides a solution for this due to its semiconducting property. The second stage led to the development of a technique to construct nanowires whose widths ranged between 20 – 500 nm. The second stage of the project, also allowed us to develop a an approach that could be used to construct transistors on the nanometer scale and to integrate the nanometer scale circuit elements with standard cleanroom technology.

In Chapter 6 we discuss mechanical means of swelling and deswelling polymer multilayers by the AFM tip. The efforts in this dissertation led to the discovery of a new method to mechanically swell and de-swell polymer multilayers and to find a direct method to study the already known effect of changing pH levels on the thickness of polymer multilayers[9].

In Chapter 7 we present a discussion of the results achieved in this dissertation and an overview of future work currently under way and possible directions in which the project could be expanded using different conjugated polymers and nanomaterials.

References:

1. http://www.phy.pku.edu.cn/~qhcao/resources/class/QM/Feynman's-Talk.pdf
2. Iniewski, Krzysztof, “Nanoelectronics: nanowires, molecular electronics, and nanodevices”, McGraw-Hill, 2011.
3. D. Vuillaume, B. Chen and R.M. Metzger, Langmuir 15, 4011 (1999).
4. B. Chen and R.M., Metzger, J. Phys. Chem. B 103, 4447 (1999).
5. R.M. Metzger, J. Mater. Chem. 9, 2027 (1999); ibid 10, 55 (2000).
6. S. J. Tans, M. H. Devoret, H. Dal, A. Thess, R. E. Smalley, L. J. Geerligs and C. Dekker, Nature 386, 475 (1997).
7. C. Dekker, Physics Today, 22 (May 1999)
8. Dekker, Cees; Tans, Sander J.; Verschueren, Alwin R. M. (1998). "Room-temperature transistor based on a single carbon nanotube". Nature 393 (6680): 49.
9. Martel, R.; Schmidt, T.; Shea, H. R.; Hertel, T.; Avouris, Ph. (1998). "Single- and multi-wall carbon nanotube field-effect transistors". Applied Physics Letters 73 (17): 2447
10. H. Dai, A. Javey, E. Pop, D. Mann, Y. Lu, "Electrical Properties and Field-Effect Transistors of Carbon Nanotubes," Nano: Brief Reports and Reviews 1, 1 (2006).
11. Song Xu and Gang-Yu Liu, “Nanometer-Scale Fabrication by Simultaneous Nanoshaving and Molecular Self-Assembly”, Langmuir 13, 127-129, (1997).

12. Luis G Rosa and Jian Liang, “Atomic force microscope nanolithography: dip-pen, nanoshaving, nanografting, tapping mode, electrochemical and thermal nanolithography”, J. Phys.: Condens. Matter 21 483001, (2009).
13. Paulo Samori, “Scanning probe microscopies beyond imaging “, J. Mater. Chem. **14**, 1353-1366, (2004).
14. Hiroyuki Sugimura, Nagahiro Saito, Kazuyuki Hayashi, Noriya Maeda and Osamu Takai, “Scanning Probe Surface Modification: Chemical Conversion of Terminal Functional Groups on Organosilane Self-Assembled Monolayers”, Scanning Tunneling Microscopy/Spectroscopy and Related Techniques: 12th International Conference STM'03. AIP Conference Proceedings , Volume 696, pp. 150-157, (2003).
15. N. Saito, N. Maeda, H. Sugimura, and O. Takai, “Generation of Amino -Terminated Surfaces by Chemical Lithography Using Atomic Force Microscopy”, Langmuir **20**, 5182-5184, (2004).
16. A. Tulpar, Z. Wang, C.-H. Jang, V. Jain, J.R. Heflin, W.A. Ducker, "Nanoscale Patterning of Ionic Self-Assembled Multilayers," Nanotechnology **20**, 155301:1-5 (2009).
17. N. Saito, N. Maeda, H. Sugimura, and O. Takai, “Generation of Amino -Terminated Surfaces by Chemical Lithography Using Atomic Force Microscopy”, Langmuir **20**, 5182-5184, (2004).
18. Michael V. Lee, Kyle A. Nelson, Laurie Hutchins, Hector A. Becerril, Samuel T. Cosby, Jonathan C. Blood, Dean R. Wheeler, Robert C. Davis, Adam T. Woolley, John N. Harb, Mathew R. Linford, "Nanografting of Silanes on Silicon Dioxide with Applications to

DNA Localization and Copper Electroless Deposition", Chem. Mater. 2007,19, 5052-5054.

19. Lee. D., Nolte. A. J., Kunz. A.L., Rubner. M. F., Cohen. R. E. pH-Induced Hysteretic Gating of Track-Etched Polycarbonate Membranes: Swelling/Deswelling Behavior of Polyelectrolyte Multilayers in Confined Geometry. J. AM. CHEM. SOC. **128**, 8521-8529, (2006).

20. C. Binning, C. F. Quate, Ch. Gerber. "Atomic Force Microscope", Physical Review Letters, Volume 56, Number 9, (1986).

21. Weaver, Peter. The Technique of Lithography. London: B.T. Batsford, (1964)

22. Andrew George, ed.: Cuneiform Royal Inscriptions and Related Texts in the Schøyen Collection, Cornell University Studies in Assyriology and Sumerology, vol. 17, Manuscripts in the Schøyen Collection, Cuneiform texts VI. CDL Press, Bethesda, MD, 2011, text 24, p. 50, pl. XX

23. Robert Hirsch. *Seizing the Light: A Social History of Photography*. (McGraw-Hill, 2009).

24. https://indico.cern.ch/event/34040/material/slides/1?contribId=13

25. Jaeger, Richard C. *Introduction to Microelectronic Fabrication* 2nd ed. (Upper Saddle River: Prentice Hall, 2002).

26. https://www.ee.washington.edu/research/microtech/cam/PROCESSES/PDF%20FILES/Photolithography.pdf

27. Rachel K. Smith, Penelope A. Lewis, Paul S. Weiss, “Patterning self-assembled monolayers”, Progress in Surface Science **75**, 1-68, (2004).

28. Rogers, Pennathur, and Adams, *Nanotechnology: Understanding Small Systems*, 2nd Edition CRC Press, 2011.

Chapter 2

Literature Review

2.1 Introduction and historical background

Printing as a method of transferring patterns from one substrate to the other has been known since 3000 B. C.[1] The surviving evidence shows that in Mesopotamia and ancient Egypt molds of carved stones were used to transfer patterns into soft materials like wet clay. The form of printing that shares a common principle and also resembles, in essence, the methods utilized in this work is known as lithography and was invented in 1796 A. D.[2] Lithography, which comes from a Greek origin where lithos means stone and graphein means to write, is a form of printing that depends on transferring a pattern from an etched stone to paper. It was invented by German actor and writer Alois Senefelder.[2] The method depended on painting a pattern with wax or fat on the surface of a piece of limestone. After that, the surface of the stone was exposed to a corrosive acid that etched away the parts of the stone that were not covered with wax. This developed a topographic pattern on the surface of the stone which was used later to print the original picture on paper.[3] Figure (2.1) below shows an example of an image produced by using lithographic methods.

Figure (2.1): William L. Breton, Residence of Washington in High Street, Philada, John Fanning Watson, Annals of Philadelphia (1830), opp. p. 361.[52] (Public Domain). Wikipedia: http://en.wikipedia.org/wiki/Lithography#mediaviewer/File:PhiladelphiaPresidentsHouse.

In modern day technology, lithography has played a key role in the development and later flourishing of the semiconductor industry as we know it today. The various types of lithography used in semiconductor fabrication will be discussed shortly. One of the main trends in the electronics industry and research is the interest in increased miniaturization of all possible elements of a circuit for reasons that include improved computational capabilities and power consumption. Such a trend has led to great advances in the methods used to manufacture circuit elements. Developments are constantly being achieved in both lithographic methods and materials used in making circuit elements. One of the main frontiers for developing new lithographic techniques is the smallest size of a circuit element that can be produced. The advances towards smaller and smaller circuit elements also brings up a few issues concerning the fabrication methods needed to achieve this goal. Along with the examination of the fabrication methods comes the search for alternative approaches to nanoelectronics as some of the mainstream methods reach fundamental

limitations. In what follows in this chapter, we discuss some of the different approaches to nanoelectronics. These approaches span current methods that are used in circuit manufacturing and other new and novel techniques. For each of the cases, we examine devices that have been manufactured using these methods and examine the strengths and weaknesses of the different methods as we approach smaller and smaller sizes for the circuit elements.

2.2 Techniques of lithography

Constructing circuit components is accomplished via various methods of lithography in the semiconductor industry. The following is a short discussion of some of the most commonly used methods

2.2.1 Photolithography

Photolithography is a process of transferring a pattern using optical means from a mask to a substrate for etching. Photolithography was invented in 1855 by the French chemist, engineer and photographer Alphonse Louis Poitevin. Poitevin discovered that exposing a ferro-gallat gum mixture to light changes its chemical properties. Exposing such a mixture to light hardens the mixture in proportion to the exposure time. The exposed parts of the mixture become water insoluble. Using such a technique provided the basis for better quality photographs and blueprints.[(4),(5)] The modern process of photolithography used in the semiconductor industry depends on the same principles of photosensitivity of certain chemicals and their becoming soluble or insoluble after being exposed to light.[(6),(7)]

The first step in the modern photolithography process is cleaning a substrate of silicon. The cleaning process exposes silicon layers by etching away silicon dioxide layers and other organic and inorganic materials from the surface of the substrate.

After the cleaning step, the substrate is covered with a photoresist material. The photoresist is a substance that is sensitive to light and changes its chemical properties as it is exposed to ultraviolet radiation in this specific type of photolithography. Figure (2.2) shows a general scheme for photolithography alignment and exposure.

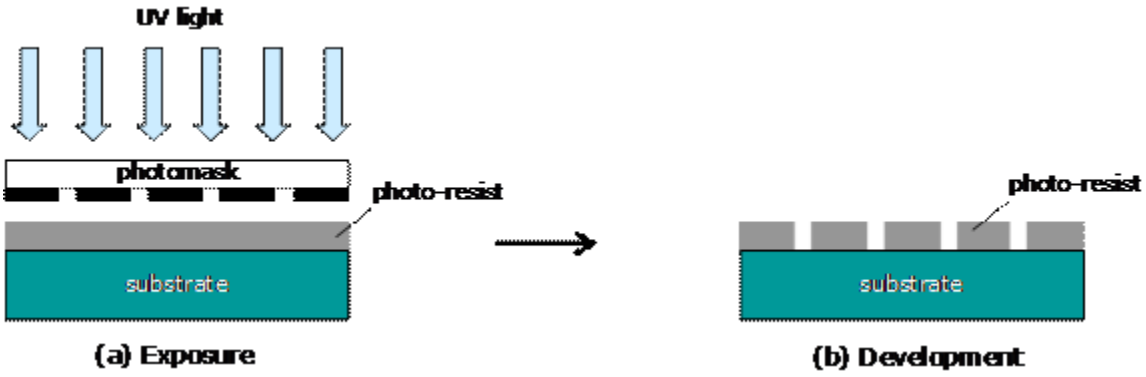

Figure (2.2): (a) The basic process of exposing a substrate covered with a photoresist to UV light and then developing it. (b) Developing an exposed substrate.[13] Reprinted with permission from [PIMPIN, A., SRITURAVANICH, W. "Review on Micro- and Nanolithography Techniques and Their Applications", Engineering Journal, Thailand, 16, nov. 2011]

The case in which the exposed regions become soluble is called positive photoresist and the counterpart in which the exposed parts become insoluble is called negative photoresist. After the substrates are covered with a layer of the photoresist material of choice using the process of spin coating, the substrates are baked for a very short period of time to drive off excess solvents and harden the photoresist.[7] The next step is to expose the substrates to ultraviolet (UV) light through a photomask. Masks for photolithographic processes are made out of material that is transparent

to UV light. The most commonly used material is a sodalime substrate. Then on this substrate electron or ion beam lithography is used to implement a pattern that ultimately we need to transfer to the silicon substrate. The part of the mask that is designed to absorb the UV light is made of copper. Different photoresists are designed to be sensitive to different wavelengths in the UV light range. Once the substrates are exposed to the UV light, the photoresist can be developed using solvents that dissolve either the exposed or the non-exposed parts of the photoresist. Depending on the type of photoresist used, the exposed parts can either be soluble in the photoresist solvent or can become insoluble. Materials used as photoresists include poly(methyl methacrylate) (PMMA), poly(methyl glutarimide) (PMGI), and phenol formaldehyde resin (DNQ/Novolac). The chemical process by which the positive resist DNQ becomes soluble in the developers is shown in Figure (2.3) below.

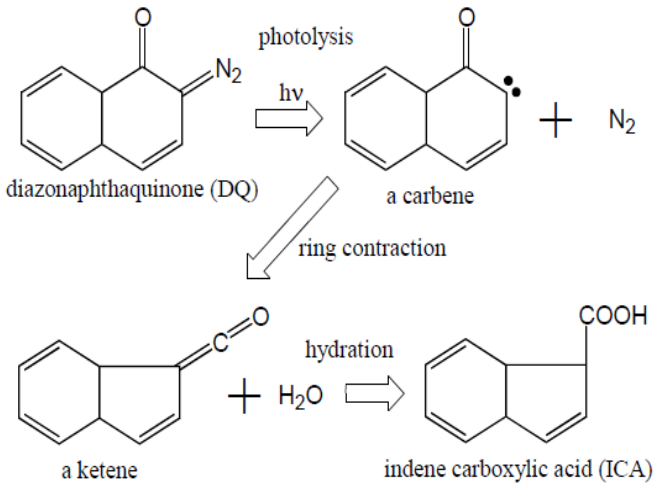

Figure (2.3): The main reaction of a DNQ positive photoresist when exposed to light. The formation of an acid leads to an increased solubility in a water/base mixture of a developer.[52] [Fair use]: http://www.microchem.com/Tech-LithoTerms.htm

Once this step is done, the substrates are ready to be processed in a variety of ways. Such a process leaves the substrate ready for building conductive wire connections, semiconductor channels, insulating regions and other device components. Among the factors making photolithography a very powerful tool in the commercial scale production of semiconductor devices is the massive capability for parallel processing. Billions of transistor components can be produced simultaneously in a few seconds using available cleanroom equipment at any production facility. This reduces the cost per bit for the produced devices. On the other hand, as we proceed in investigating the possibilities of 3-D circuitry and nanoscale electronics, we will run into some of the limitations of photolithography. Among the prominent limitations is the smallest size that can be produced using photolithography. The smallest sizes for the features that can be produced is limited by the wavelengths, the optical systems used for the exposure, and the smallest size that can be put on the mask. The effects of these factors can be understood in the context of the method of alignment and exposure used in photolithography. There are three main ways of exposure used in this type of lithography. The first type is what is known as contact lithography. In this mode, the mask comes into physical contact with the photoresist covered substrate. This ensures that any limitations due to diffraction effects are eliminated. In this mode, theoretically speaking, the limit on the smallest feature producible is the smallest feature achievable on the mask. However, this approach has an intrinsic problem that repeated contact between the photoresist coating and the mask leaves residue on the mask and cleaning is required every single time the mask is used and this causes the quality of the mask to deteriorate over time. Among the other factors affecting the success of this method is how flat and clean the substrate is. Any dust particles or discrepancies with how flat the surface is leads to gaps between the mask and the substrate opening the door to other limiting effects such as diffraction effects. Contact photolithography is thus not used in

semiconductor mass production. The second type of alignment and exposure in photolithography is what is known as proximity printing. In this type of exposure, a very small gap is maintained between the mask and the substrate. The following equation provides a measure on the smallest feature producible using proximity printing:[14]

$$W_{min} \approx \sqrt{(g*\lambda)} \qquad (1)$$

where g is the gap between the mask and the substrate during the exposure and λ is the wavelength used for UV exposure of the photoresist. The problem of maintaining a constant gap between the mask and the substrate presents a challenge in this type of lithography. This is usually caused by the dependence on a mechanical design to maintain such precision over a very short distance for the gap and the flatness of the substrate. The third mode of printing which is the foundation of the semiconductor industry is known as projection printing. In this mode, the separation of the mask and substrate is a considerable one, normally around 0.5 m. At such a separation, a system of lenses is usually used to produce a reduced projection of the mask on the substrate. Figure (2.4) below shows a schematic of the three different types of printing in photolithography

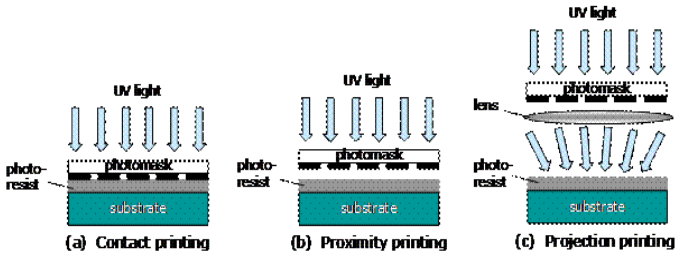

Figure (2.4): Different types of photolithography. (a): Contact printing where the mask comes into physical contact with the substrate. (b): Proximity printing where there is a very small gap maintained between the mask and the substrate. (c) Projection printing where the distance between the mask and the substrate is increased to the order of 0.5 m and optical components are used to provide shrinking of the mask pattern on the substrate.[13] Reproduced with permission from: [PIMPIN, A., SRITURAVANICH, W. "Review on Micro- and Nanolithography Techniques and Their Applications", Engineering Journal, Thailand, 16, nov. 2011]

Using a simple Fresnel diffraction analysis, we find that the smallest size for a feature of a circuit on the surface of the substrate is given by[14]

$$R \approx (k_1 * \lambda)/NA \qquad (2)$$

where R is smallest feature feasible, k_1 is a constant pertaining to the printing process and the photoresist used and NA is the numerical aperture of the system. The k_1 value is approximated to be at around unity for many of the processes in the semiconductor industry. Using this projection system presents its own set of problems related to the depth of focus affecting the sizes achieved at the smallest scale possible. The smallest sizes achieved using a combination of resolution enhancement techniques and specially designed photoresists are now on the order of 20 nm lines.[14]

Another way around the diffraction problem while still providing access to smaller feature dimensions and resolution is what is known as extreme ultraviolet lithography. Using higher energy ultraviolet sources means using shorter wavelengths in the range 10-14 nm. In this technique, the exposure is done via projection patterning. The main problem that faces this technique is the need for improved reflective mirrors and optical components since, at such short wavelength, absorption is a major problem. The smallest sizes currently achieved using this technique are in the range of 40 nm, although much smaller sizes are possible. [24]

2.2.2 X-Ray lithography

X-Ray lithography is a very strong candidate for the future of lithography. In this type of lithography, the exposing energy source is collimated X-rays.[8] The short wavelength

characteristic of the X-rays used, less than 1 nm, allows a much smaller resolution limit imposed by diffraction effects. The principle of operation for X-ray lithography is very similar to that of photolithography.[8] Masks used for X-ray lithography are made of materials that are characterized by low atomic number. Typical materials used for this process are diamond, beryllium, or polyimide. The parts that shield the photoresists from the X-rays are made of X-ray absorbing materials characterized by high atomic numbers such as gold. The photoresist used in this case is often PMMA. In spite of using similar photoresists to the ones used in UV photolithography, the thicknesses of the layers are adjusted to accommodate the fact that X-rays penetrate deeper into exposed materials than UV does. One of the main advantages to using X-ray lithography is that due to its penetrating power it allows for construction of higher structures on the substrates. On the other hand, the main disadvantage of using X-ray lithography is the high cost of the equipment used to produce the X-rays needed for the exposure process.[9] Another limiting factor on using X-ray lithography is the lack of the ability to reduce the projected features from the masks. This leads to the smallest sizes possible to achieve being restricted by the mask production technology. The smallest sizes reported are in the range of 30 nm.[25]

2.2.3 Ion Beam lithography

Ion beam lithography is one of the most versatile tools that exist in the various endeavors of patterning surfaces.[25] The technique depends on exposing the surface to be patterned to a highly energetic beam of ions. The exposure takes place via two main methods. The first method is a projection method similar to the photolithographic method where the ion beam passes through a mask first before it encounters the substrate.[26] The other method is known as direct write ion beam lithography where the ion beam is focused to form a very small probe and then is manipulated directly onto the surface that is to be patterned. In this latter method, the beam is

controlled such that it moves on the surface of the substrate tracing the pattern that is to be transferred to the surface. The mechanism by which the patterning takes place varies from resist exposure to milling and etching.[25] The heavy mass of the ions coupled with the high accelerating voltages with which the ions are accelerated leads to high momentum for the ions. This in turn leads to very low diffraction effects and excellent feature sizes. Ion beam lithography offers a range of very small feature sizes depending on the source used to produce the ions.[25],[27] For a plasma source, the feature sizes can range from 100 nm to 1 μm. For a gas field-ionization source, the feature sizes range from 5 nm to 10 nm.[25]

2.2.4 Nanoimprint lithography

Nanoimprint lithography (NIL) was introduced in 1996 by Stephen Chou[10]. The main idea behind this method is to manufacture, using micromachining techniques, a mold that carries the desired pattern and then bring it into contact at elevated temperatures with a layer of polymer material that is spun onto a substrate to transfer the pattern to the polymer layer. Once that is done, the "mold" and the substrate are separated and the pattern is established on the polymer on the substrate. Different etching techniques are used after that to further transfer the pattern imprinted on the polymer to the substrate underneath it. This nanolithography method has resulted in many variations on the same technique. The earliest of them is what is known as Thermoplastic nanoimprint lithography (T-NIL), which was introduced by Chou in his paper in 1996[10].

2.2.5 Scanning probe lithography

Scanning probe lithography refers to lithographic methods of patterning surfaces on the micro and nano scales using probes that were originally intended for scanning, imaging and characterizing surfaces[11]. Among the scanning devices used by these lithography methods are atomic force

microscopes and scanning tunneling microscopes.[11] Various techniques exist for establishing the desired patterns on select substrates. All the patterning techniques depend on energy transfer to the surface. The form of energy transferred can either be chemical, mechanical, thermal, or electrical. The choice of technique and device used for the patterning depends on the materials used and the goal to be achieved by the design. The work in this dissertation uses atomic force microscope lithography as a primary tool, and it will be discussed in much more detail below.

2.2.5.1 Dip-pen nanolithography (DPN)

DPN is a lithography method that depends on using an AFM to deliver a chemical pattern using the AFM tip as a writing device and the chemical material used to pattern the surface as ink.[12] In DPN, the AFM tip is covered with the "ink" material that will establish the pattern on the surface. The patterning process begins by bringing the AFM tip close to the surface. Due to the humidity in the air surrounding the AFM tip and the sample, a miniscule droplet of water is formed between the two. The water droplet delivers the material from the AFM tip to the surface establishing a chemical pattern on the surface where the tip scans the sample.[12] Figure (2.5) below shows a schematic diagram of how this process takes place.

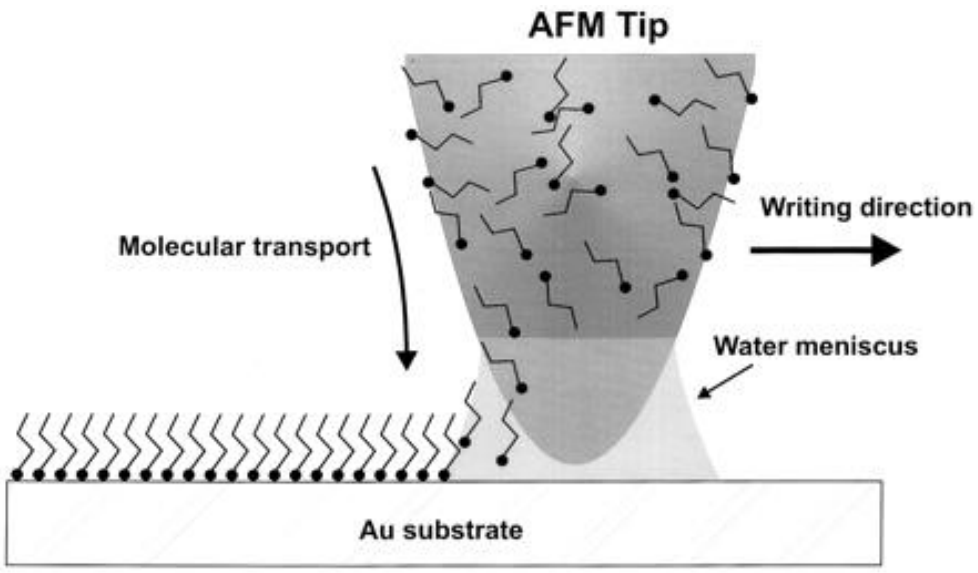

Figure (2.5): An illustration of how DPN works. The ink molecules that are covering the AFM tip diffuse through the water droplet between the tip and the surface to deposit on the surface in the areas scanned by the AFM tip.[12] [Fair use]: Piner, R. D.; Zhu, J.; Xu, F.; Hong, S.; Mirkin, C. A. ""Dip-Pen" Nanolithography," Science 283, 661-663 (1999)

The size of the patterns that can be constructed using DPN techniques are limited by two factors. The first limiting factor is the size of the AFM tip used. The second factor is the relative humidity in the environment in which the pattering takes place. Some of the smallest sizes of patterns constructed using DPN are in the range of 15 – 50 nm.[15],[16] In their first paper published describing this technique, Mirkin *et al*. successfully deposited 1-Octadecanethiols (ODT) on gold surfaces. The technique involved dipping a silicon nitride tip in a saturated solution of ODT in acetonitrile for one minute. The tip was then dried under a stream of compressed diflouroethane. The substrates used for patterning were prepared by evaporating 30 Å of gold onto a substrate of

mica. When the AFM tip was brought in contact with the gold surface the ODT molecules were transported from the tip to the surface via the water meniscus formed in the narrow gap between the tip and the surface. Lateral force measurements of the patterned surfaces revealed a detectable difference between the areas of the surface that were covered with ODT molecules and the areas that were not treated. Figure (2.6) shows images from these patterning attempts.[12]

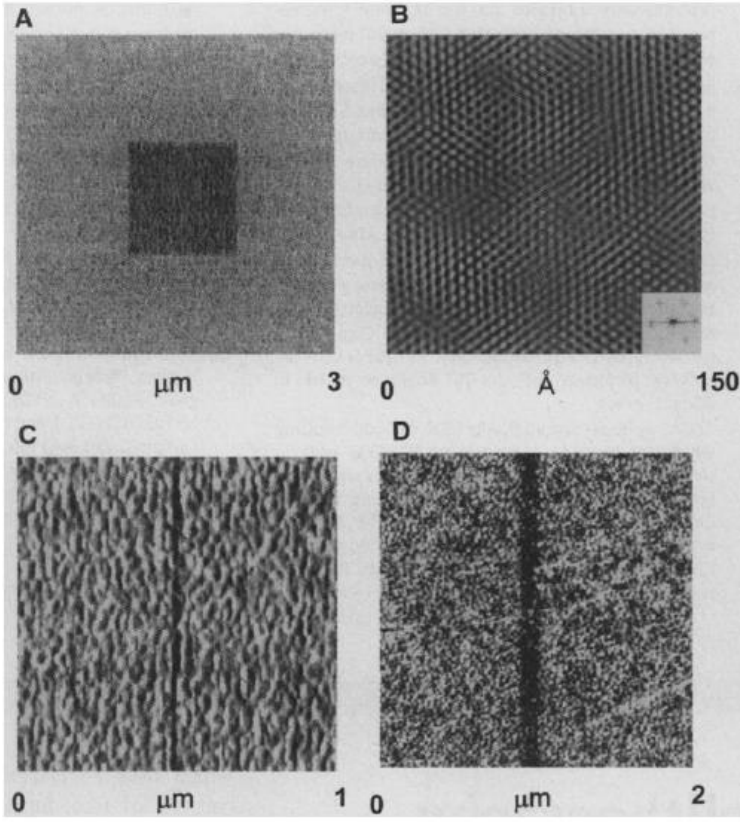

Figure 2.6: Lateral force measurements of patterns made using DPN of ODT on gold surfaces. (a) A lateral force image of a 1 µm X 1 µm square of ODT deposited on gold. The patterning was done at a relative humidity of 39% and the scan rate used during the patterning is 1 Hz. (b) A lattice resolved image of an ODT patterned area. (c) A 20 nm wide wire of ODT patterned on gold suing DPN. (d) A 100 nm wide wire of ODT on a gold substrate.[12] [Fair use]: Piner, R. D.; Zhu, J.; Xu, F.; Hong, S.; Mirkin, C. A. ""Dip-Pen" Nanolithography," Science 283, 661-663 (1999)

Various exciting applications of DPN have been developed since its debut. Among the very interesting applications for this patterning method is the construction of nanoarrays for biosensors.[35] Nanoarrays of biological molecules have the ability to hold a large number of features, around 10^5 more, compared to microarrays of similar molecules. In a study performed by Lee *et al.*, DPN was used to immobilize anti-p24 in nanoarrays to screen for the human immunodeficiency HIV-1 (HIV-1) p24 antigen in serum samples.[33] The antibody nanoarrays were fabricated using DPN to pattern the surface of a gold substrate with molecules of 16-Mercaptohexadecanoic acid (MHA). After the antibodies were immobilized on the MHA patterned areas, the substrates were dipped in serum samples. When the p24 particles were attached to the antibodies, the height of these patterned areas increased. To amplify the height difference samples were then exposed to a solution of gold nanoprobes that were functionalizes with anti-ps4 which attached themselves to the immobilized p24 particles resulting in higher features on the gold substrates. Such techniques are used to enable the studying of virus binding and detection techniques. A schematic of the procedure used in this experiment is shown in Figure (2.7)[33], [35]

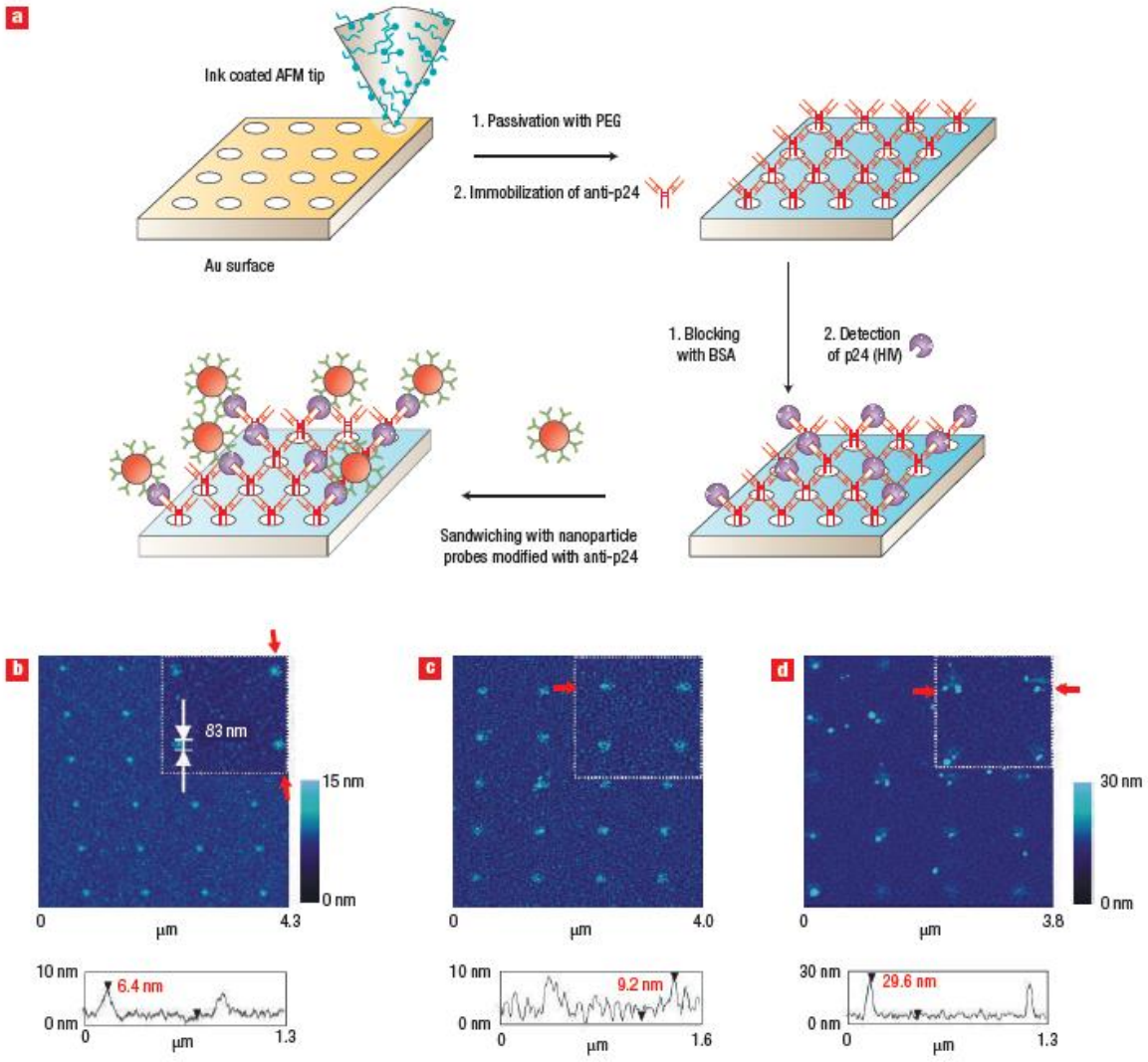

Figure 2.7: (a) Using DPN to pattern the gold surface with MHA molecules. After the patterning is complete the anti-p24 get immobilized on the patterned areas. Exposing the immobilized anti-p24 particles to serum samples allows the p24 to bind to immobilized antibodies. To amplify the height difference resulting from the binding of p24 to the immobilized anti-p24 the substrate is further exposed to a solution of gold nanoprobes functionalized with anti-p24. (b) Topographic image and map of the MHA templated areas. (c) The topographic image and height profile of immobilized anti-p24. The height difference is in the range of 2.3±0.6 nm compared to the template areas. (d) Topographic image and height profile of the substrate after sandwiching the immobilized p24 particles with a layer of anti-p24 functionalized gold propbes.[33] [Fair use]: Lee, K. B, Kim, E. Y., Mirkin, C. A. and Wolinsky, S. M., "The Use of Nanoarrays in highly sensitive and selective human immunodeficiency virus type 1 in plasma", Nano Lett. 4, 1869-1872, (2004)

Among the interesting investigations carried out using DPN is the investigation of the interaction between carbon nanotubes and areas patterned with MHA in a background of a passivating ODT. Hong and coworkers studied the binding behavior of carbon nanotubes to sites that were patterned in circular shapes of MHA. The affinity of the carbon nanotubes to binding to the –COOH terminated MHA led to very interesting results. Using specially strained carbon nanotubes that are longer than the circumference of the patterned circles caused the nanotubes to wrap around themselves in circular shapes to fit on the patterns. Figure (2.8) shows the results of the investigations carried out by Hong *et al*. Such studies allow for examining the details of directed assembly of carbon nanotubes and other nanoscale building blocks.[36]

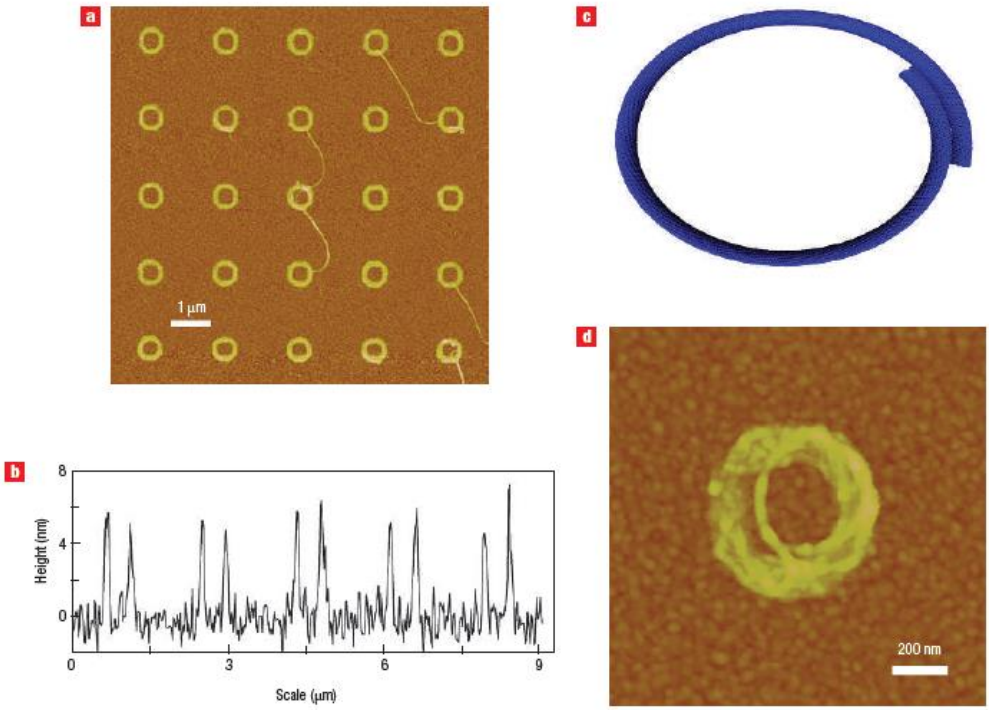

Figure (2.8): (a) A tapping mode topographic image of multiple single walled nantubes coiled and stacked on top of one another on the template areas. (b) Height profile of the stacked carbon nanotubes showing relative uniformity. (c) A model for the coiled nanotube. (d) A zoomed in image of one of the patterned sites showing the stacked nanotubes.[36] [Fair use]: Rau, S. G., Huang, L., Steyawan, W., Hong, S. H., Large-scale assembly of carbon nanotubes, Nature, 425, 36-37, (2003)

Among the positive aspects of using DPN techniques is that they are very versatile and easy to perform methods possible to carry out on virtually any AFM. However, among the drawbacks of this method is the fact that it is a serial processing method making it a slower process when compared to parallel processing methods such as photolithography or microcontact printing. In an effort to address the parallel processing limitations of the DPN method, Mirkin *et al*. developed an array of AFM tips that carried 55,000 tips in the form of a 2-D array.[37] This array was designed and fabricated using photolithographic methods. In their design, a high clearance was created between the apex of each of the tips and the supporting substrate to allow for higher tolerance and maneuverability with respect to the surface topography. Instead of using a massively complicated feedback system to control the positioning of these tips with respect to the surface, the tips were controlled by gravitational effects managing their separation from the surface in an interplay with the repulsive forces that the tips feel from the surface. Areas of 1 cm^2 size were patterned simultaneously with resolution below the 100 nm limit. Figures (2.9) and (2.10) show images of the 55,000 tip array and the patterns resulting from using ODT as an ink on a gold substrate respectively.

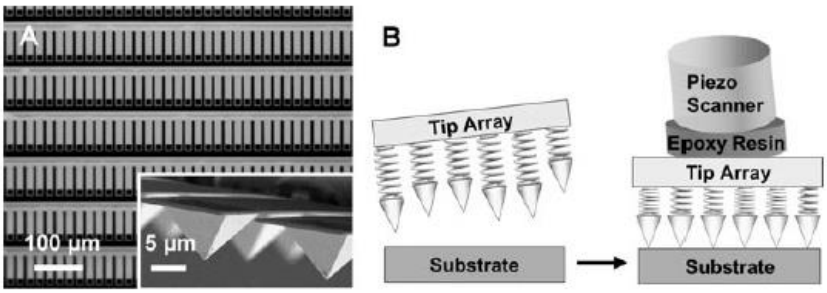

Figure 2.9: (a) An array of cantilevers used in parallel DPN. The inset image is an SEM image of some of these cantilevers. (b) Schematic view of the design of the gravity-aligned array and how it is controlled. [37] [Fair use]: Salaita, K. Wang, Y., Faragala, J., Vega, R. A., Liu. C., Mirkin, C. A., Massively Parallel Dip-Pen Nanolithography with 55,000-Pen Two Dimensional Arrays, ANgew. Chem. Int. Ed., 45, 7220-7223, (2006)

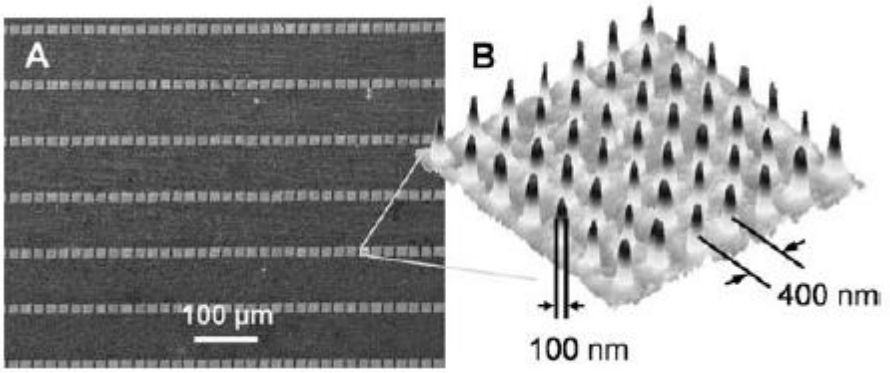

Figure (2.10): (a) SEM image of an 88,000,000 gold dot array patterned using massively parallel DPN. (b) AFM topographical image of part of the patterned array. The dot to dot distance is 400 nm and the dot width is 100 ± 20 nm. [37] [Fair use]: Salaita, K. Wang, Y., Faragala, J., Vega, R. A., Liu. C., Mirkin, C. A., Massively Parallel Dip-Pen Nanolithography with 55,000-Pen Two Dimensional Arrays, ANgew. Chem. Int. Ed., 45, 7220-7223, (2006)

In another study by Mirkin and co-workers, DPN was paired with LbL deposition methods to achieve directed deposition of polymer multilayers on patterned surfaces.[51] In this study, Mirkin and his colleagues used mercaptohexadecanoic acid (MHA) as ink to write dot and line features on a gold surface. The dot features were 80 - 500 nm in diameter and the line features were 200 nm wide. After the features were written, the gold surface was passivated using octadecanethiol (ODT), 16-mercapto-1-hexadeanol (MHD), and 11-mercaptoundecyl-tri(ethylene glycol) (PEG). After completing the passivation process, the patterned substrates were dipped in 40 mM solutions of poly(diallyldimethylammonium chloride) (PDDA) and poly(sodium-4-styrenesulfonate) (PSS) alternatively. No pH modification of the polyelectrolyte solutions was needed given that both of them are strong polyelectrolytes that are strongly charged regardless of the pH of the solution. Each dipping step lasted 10 minutes and was followed by a rinse in deionized (DI) water and a 10 second sonication in DI water. To examine the ability of such a technique to immobilize various molecules, it was used to immobilize fluorescein sodium salts. The deposited patterns of MHA

were found to be 2 nm on average for all the patterns written. The average height for each layer deposited of PDDA and PSS was found to be 2.3 nm on average. When the concentration of the solutions was lowered to 20 mM the average height increase per layer deposited of the polymer was reduced by 0.5 nm. The average height of the deposited multilayers was similar for the features regardless of the feature size. Surfaces passivated with PEG demonstrated better deposition selectivity than those passivated with ODT and MHD. Figure (2.11) shows images demonstrating these results.[51]

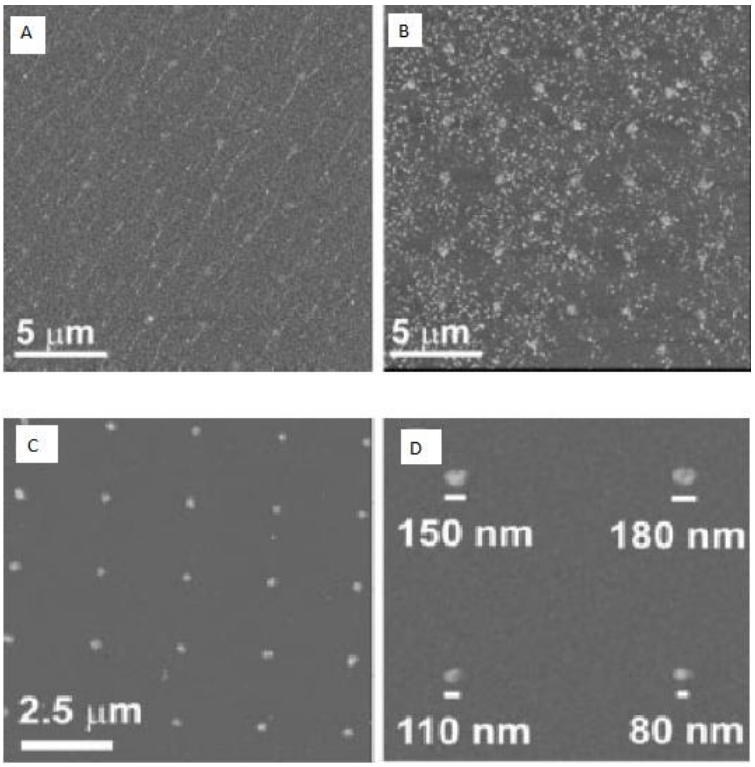

Figure (2.11): Polyelectrolyte multilayers deposited on patterned disks of MHA (a) 200 nm disks on ODT passivated background. (b) 200 nm disks MHO passivated background. (c) 200 nm disks on PEG passivated background. (d) 80 – 180 nm disks on PEG passivated background. The better selectivity of the deposition process on the PEG passivated substrate can be seen clearly in the difference of deposition of the polymer multilayers on the background in the different cases shown.[51] [Fair use]: Seung Woo Lee, Raymond G. Sanedrin, Byung-Keun Oh, and Chad A. Mirkin, "Nanostructured Polyelectrolyte Multilayer Organic Thin Films Generated via Parallel Dip-Pen Nanolithography", Adv., 17, 2749–2753, 2005

2.3 Carbon Nanotube Field Effect Transistors

Carbon nanotubes are cylindrical structures made of wrapped graphene sheets to create cylindrical shapes that have walls that are a single atom thick. Carbon nanotubes fall into two main categories known as single-walled carbon nanotubes (SWNT) and multi-walled carbon nanotubes (MWNT) based on the number of sheets that are needed to produce the tubes.[22],[23] Carbon nanotubes are characterized by very small diameter to length ratios. SWNT have been made with diameters measuring down to 1 nm while their lengths have been realized up to millions of times their diameter. Carbon nanotubes have unique strength, electric, and thermal properties. These properties are closely related to their diameters. One of the main properties of carbon nanotubes is their unique strength. This strength is explained by considering the type of chemical bonding that takes place between the carbon atoms in the unique structure that distinguishes these tubes. The chemical bonds are of the sp^2 type which are extremely strong and thus explain the strength of the carbon nanotubes.[22],[23] The way the graphene sheets are rolled into carbon nanotubes determine many of their properties.[21],[22],[23] There are several ways of rolling carbon nanotubes such as zigzag, chiral, and armchair. The rolling method determines the electric properties of the carbon nanotubes as either metallic or semiconducting. In our experiments, we deposit charged carbon nanotubes on patterned areas on silane monolayers. Our goal for doing this is to utilize the carbon nanotubes semiconducting properties as channels for nanotransistors.

Figure (2.12) shows the different chiralities of carbon nanotubes.

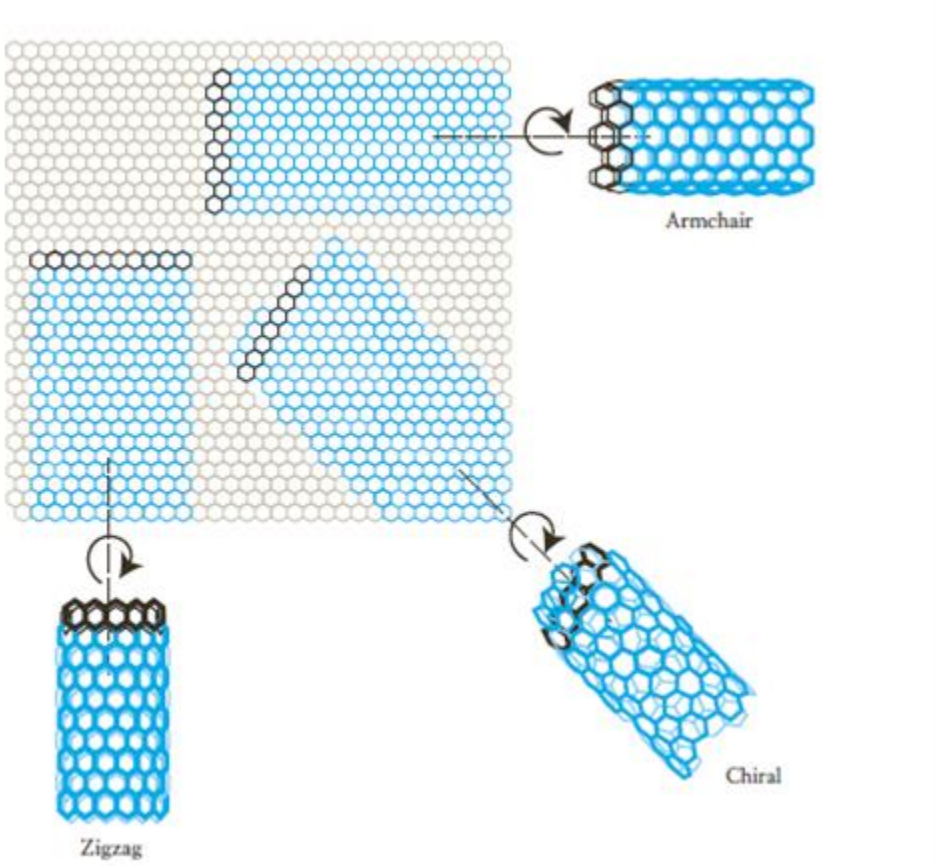

Figure (2.12): The three types of chirality carbon nanotubes can have. The chirality of the carbon nanotube depends on the way in which the grapheme sheet is rolled up. Chirality determines the physical properties of the carbon nanotubes.[21] Reproduced with permission from: Rogers, Pennathur, and Adams, Nanotechnology: Understanding Small Systems, 2nd Edition CRC Press, 2011

Carbon nanotubes enjoy a host of mechanical, chemical, thermal and electrical properties that make them a very attractive and versatile candidate for structures on the nanoscale.[14] The fact that all of these properties can be tuned by controlling the chirality of the nanotube and its dimensions is very important. In 1998 it was shown that the high electron mobility and the adjustable band gap of carbon nanotubes allows for their use in constructing single carbon nanotube transistors.[30],[31] In their work, Martel and co-workers examined the possibility of using

a single SWNT and a single MWNT to construct a field effect transistor (FET). The SWNTs they used were fabricated using laser ablation of graphite doped with nickel and cobalt. The nanotubes were then cleaned in an H_2SO_4/H_2O_2 solution. The MWNTs were produced by an arching technique and used as produced without any further cleaning or processing. The nanotubes were then deposited across gold electrodes that were fabricated using ion beam lithography. The nanotubes and the electrodes rested on a 140 nm thick background of silicon dioxide on top of a silicon substrate. For each nanotube, two gold electrodes functioned as a source and drain and the silicon substrate acted as a back gate. Figure (2.13) shows a schematic diagram for the design of the device.

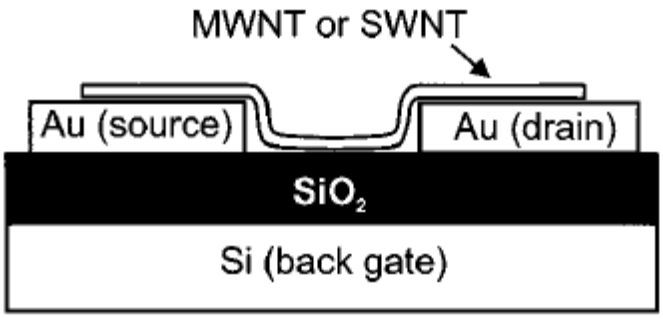

Figure (2.13): A schematic design for the experimental set up used by Martel and co-workers to examine the possibility of using a SWNT or a MWNT as an FET. The two gold electrodes function as a source and a drain and the silicon substrate functions as the gate for the FET.[31] [Fair use]: Martel, R.; Schmidt, T.; Shea, H. R.; Hertel, T.; Avouris, Ph. (1998). "Single- and multi-wall carbon nanotube field-effect transistors". Applied Physics Letters 73 (17): 2447

Connecting a SWNT between two electrodes, changing the potential difference between the source and the drain, (V_{SD}), and examining its effect on the current that flows through the nanotube, (I) at various gate potential values, (V_G) revealed a behavior characteristic of FETs. When V_G was set

to zero, a linear relationship was found between the V_{SD} and the current. For this particular V_G value the resistance of the SWNT was concluded to be around 2.9 MΩ. [31]

When V_G is varied such that V_G is negative, the relationship remains linear. When the V_G assumes large positive values nonlinearity appears in the I-V_{SD} relationship until the current diminishes completely for large values of V_G. Figure (2.14) shows the relationship between V_{SD} and the current in the nanotube for different values of V_G.

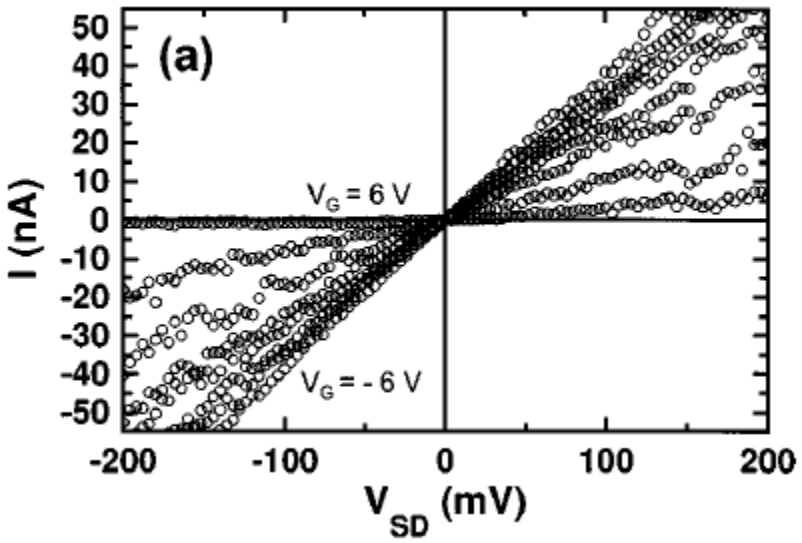

Figure (2.14): The I-V_{SD} relationship in a SWNT connected between two electrodes while the back gate V_G is varied. For $V_G \leq 0$ the relationship is fairly linear. When V_G is at a high positive value the I-V_{SD} starts becoming nonlinear.[31] [Fair use]: Martel, R.; Schmidt, T.; Shea, H. R.; Hertel, T.; Avouris, Ph. (1998). "Single- and multi-wall carbon nanotube field-effect transistors". Applied Physics Letters 73 (17): 2447

The SWNT behaves as a p-doped FET and the explanation for this behavior rests on one of two assumptions. The first is that positive charge carrier concentration is inherent in SWNTs. The second is that the positive carriers are injected into the SWNT at the electrodes due to electrons leaking out from the SWNT to the gold electrode due to the higher work function of gold. Figure (2.15) shows the relationship between I and V_G for a SWNT.

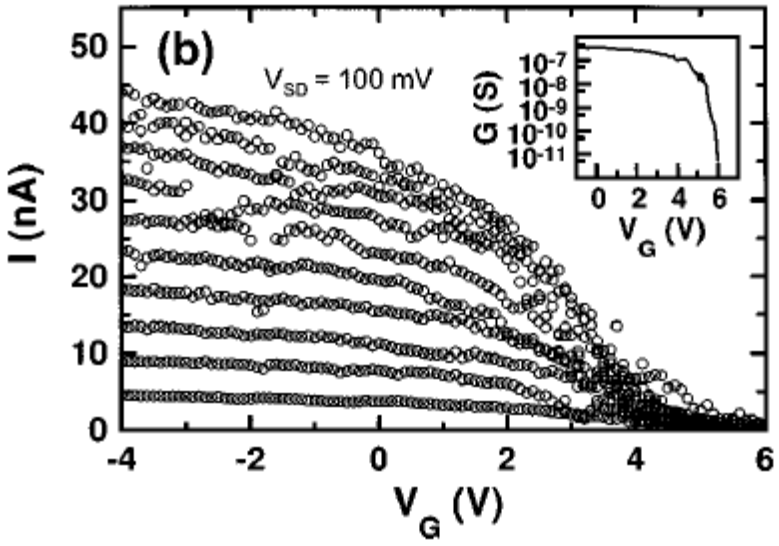

Figure (2.15): The relationship between I and V_G in a SWNT FET. As the V_G assumes larger values the current diminishes.[31] [Fair use]: Martel, R.; Schmidt, T.; Shea, H. R.; Hertel, T.; Avouris, Ph. (1998). "Single- and multi-wall carbon nanotube field-effect transistors". Applied Physics Letters 73 (17): 2447

When similar examinations were carried out using a MWNT, it was discovered that MWNTs that are intact do not exhibit any V_G dependence in their I-V_{SD} curves. However, structurally damaged MWNT exhibit FET behavior due to the change in their electric properties.[31] Figure (2.16) shows the relationship between V_G and I for a MWNT.

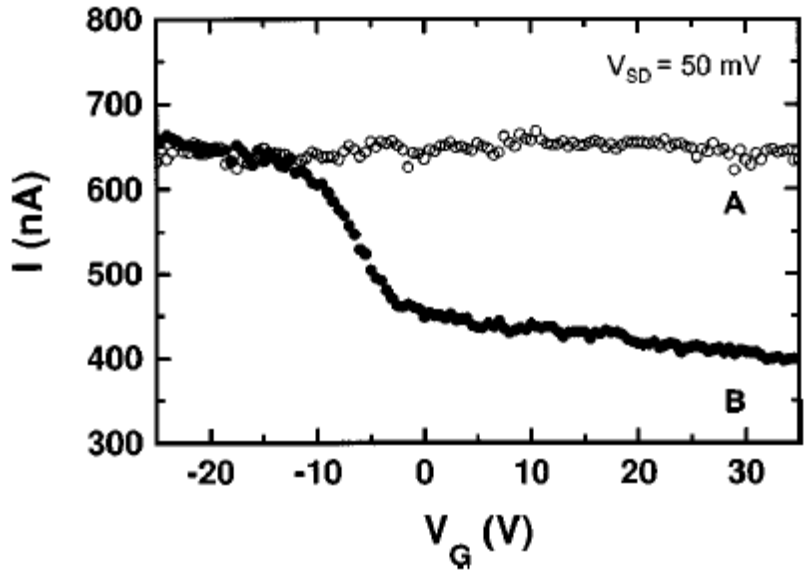

Figure (2.16): The relationship between I and V_G for a MWNT connected between two gold electrodes. The case for an intact MWNT, the light colored curve, shows that there is no dependence of I on the V_G. Once structural damage is introduced to the MWNT, it starts exhibiting FET behavior as seen represented by the solid black curve.[31] [Fair use]: Martel, R.; Schmidt, T.; Shea, H. R.; Hertel, T.; Avouris, Ph. (1998). "Single- and multi-wall carbon nanotube field-effect transistors". Applied Physics Letters 73 (17): 2447

In a similar fashion, Dekker *et al*. showed that it is possible to construct a field effect transistor using a single semiconducting carbon nanotube that is operational at room temperature.[30] This was accomplished using a semiconducting single walled carbon nanotube. The construction was that of a backgated transistor. The nanotube was laid across three terminals made out of Pt. A silicon dioxide layer on top of silicon substrate on which the entire construction rested served as a gate.[30] In spite of the success of the experiment, there were a few problems surrounding this construction. Among the biggest problems was the poor conduction between the nanotube and the electrodes. To remedy this problem several other geometries exist for constructing nanotube field effect transistors. Some of the examples are top gated transistors and Gate-All-Around single carbon nanotube FET. [28],[29]

2.4 Self-Assembly

Photolithography, deep ultra violet lithography, X-ray lithography, and ion beam lithography, which constitute the forerunners in the present and future of the semiconductor industry, are considered examples of the top-down approach of design. The top-down approach starts with a large scale object and reduces it to the desired size. As we have seen in the discussion above, this approach is beginning to run into a host of technical problems challenging its ability to continue leading the way in miniaturizing electronics. Since the limits of circuit miniaturization circuits is expected to eventually deal with dimensions on the order of individual molecules, an alternative approach, bottom-up assembly, to miniaturization seems to be a promising option. In the bottom-up approach, the building blocks are individual molecules or nanostructures that are used either individually or in aggregates for their electronic properties. The process of assembling the molecular building blocks offers control on the dimensions of the system down to fractions of nanometers.

Self-assembly is one of main techniques used in the bottom up approach. In self-assembly, we use molecules that assemble themselves into the desired forms and structures. Such an approach offers control on the molecular level.[14] The success of such a process depends on what type of interaction will allow these molecules to adhere together in one structure and how to establish a form of recognition between the molecules to form a discriminative assembly system.[14, 32] The interactions binding the molecules can be electrostatic interactions, hydrogen bonding, π-π interactions, dispersion forces, hydrophobic effects, or dative bonding.[14]

Among the forms of self-assembly are self-assembled monolayers (SAMs). In this type of assembly, molecules chemisorb spontaneously on the surfaces of substrates in a one molecule thick layer.

One of the important examples of SAM is the deposition of alkanethiolates on a gold substrate. The alkanethiolates are alkane chains that have a head group containing sulfur and hydrogen atoms (SH) at the end of the chain. Alkanethiolates can be deposited on gold substrates using spin coating, vapor deposition or dipping in a solution. The method we use in our work is the last one. Alkanethiolate molecules attach themselves to the gold surface by establishing a dative bond between the SH head group and the gold atoms in the substrate. Once the bond is established between the sulfur atom in the head group and the gold substrate, the alkanethiolate chains are tilted at an angle of 30° to maximize the van der Waals forces between the neighboring chains.[14] This forms a long range ordering of closely packed molecules on the gold surface. The deposited layer of alkanethiolate is one molecule thick, and its thickness is determined by the length of the molecular chain of the compound. Figure (2.17) shows a schematic diagram for alkanethiols arrangements on a god surface.

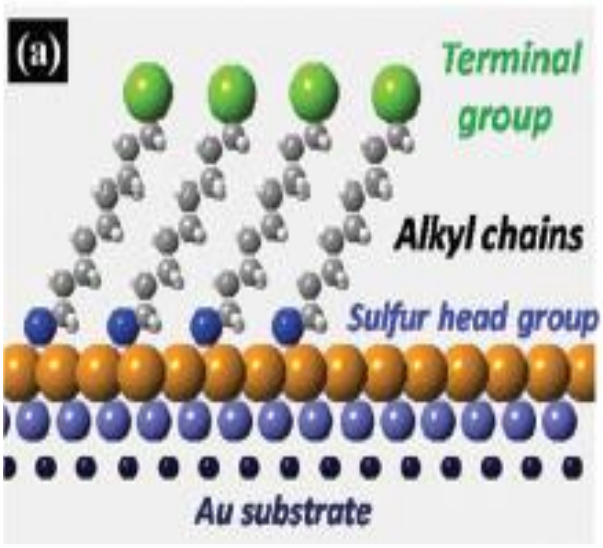

Figure (Figure 2.17): A monolayer of alkanethiols deposited on a gold surface. The thiol molecules have an SH head group that binds to the gold through sulfur gold bonding and a terminal group that determines that changes the chemistry of the surface on which the monolayer is deposited. The alkane chains between the head and terminal groups are erected at 30° to maximize the van der Waals forces between them.[49] [Fair use]: Quanmin Guo and Fangsen Li, "Selff-assembled alkanethiol monolayers on gold surfaces, resolving the complex structure at the interface by STM", Phys. Chem. Chem Phys., 16, 19074 – 19090, (2014)

SAMs in general have a mechanism for eliminating errors in the formations of smooth compact layers except for errors arising from the deposition process or the defects in the surfaces on which they are deposited.[14] The following is an equation for the chemical reaction that takes place when the (SH) group attaches itself to the gold substrate[14]

$$X(CH_2)_nSH + Au^0 \rightarrow X(CH_2)_nS^- + Au^1 + (1/2)\, H_2$$

2.4.1 Polymer Multilayers and Layer-by-Layer Deposition

Another important example of self-assembly is ionic self-assembled multilayers (ISAM). In this type of self-assembly, the main force at play is electrostatic interactions between the molecules to be deposited and the surface they deposit on. The surface and molecules are oppositely charged and that drives the molecules to adsorption on the surface. The thickness of the layer deposited is normally a few nanometers, offering a great control of the construction dimensions. One of the important applications of ISAM deposition in our research is deposition of polyelectrolyte layers from solution. Polyelectrolytes are polymer chains, which are large molecules that are made of smaller repeated molecular units, with electrolyte groups on their repeating units. The electrolyte groups are either on the backbone of the polymer or exist as a side group. The electrolyte groups dissociate in water and become charged. Figure (2.18) shows two examples of common polyelectrolytes.

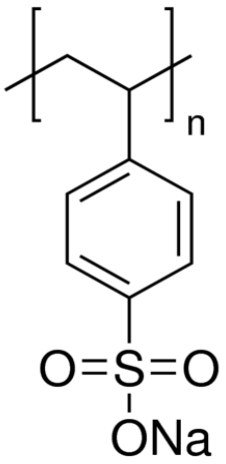

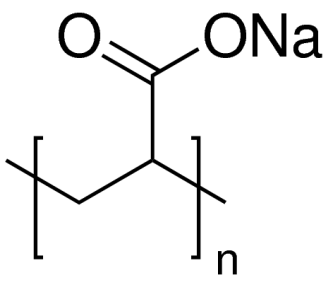

Figure (2.18): (a): Poly(sodium 4-styrenesulfonate) (PSS) is a strong polyelectrolyte that becomes negatively charged due to the SO_3Na molecule dissociating into $(SO_3)^-$ and Na^+. (b): Poly(acrylic acid, sodium salt) is a weak polyelectrolyte.[53] Reproduced with permission from: http://www.sigmaaldrich.com/catalog/product/aldrich/243051?lang=en&region=US

Other examples of polymers we use are poly(allylamine hydrochloride) (PAH) and poly[1-[4-(3-carboxy-4-hydroxyphenylazo)-benzensulfonamido]-1,2-ethanediyl sodium salt] (PCBS). Figures (2.19) and (2.20) below show the structure of the PAH and the PCBS polymers respectively.

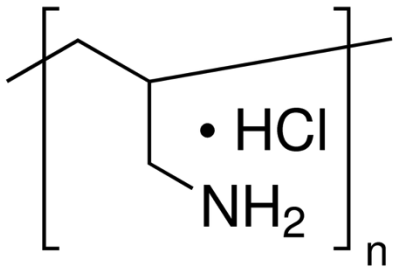

Figure (2.19): Poly(allylamine hydrochloride) (PAH).[53] Reproduced with permission from: http://www.sigmaaldrich.com/catalog/product/aldrich/283215?lang=en&region=US

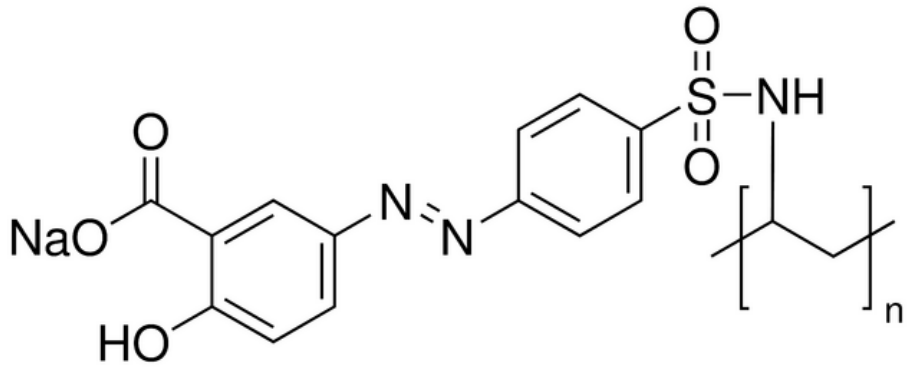

Figure (2.20): poly[1-[4-(3-carboxy-4-hydroxyphenylazo)-benzensulfonamido]-1,2-ethanediyl sodium salt] (PCBS).[53] Reproduced with permission from: http://www.sigmaaldrich.com/catalog/product/aldrich/346411?lang=en&region=US

The fact that the polymers we use are charged in aqueous solution gives rise to the possibility of depositing alternating layers of polymers that are oppositely charged on selected surfaces. This is the basis of the layer-by-layer (LbL) deposition method of polymer multilayers. LbL is credited to R. K. Iler who used it to deposit microparticles back in 1966 while working for DuPont[12]. The substrates on which the polymers are deposited vary from glass to plastics to silicon and other materials. The fabrication of such polymer multilayers is achieved by alternately dipping the substrates of choice, after cleaning them, in oppositely charged polyelectrolyte solutions.[17] The electrostatic interaction between the oppositely charged layers and the substrate causes the alternating layers to adhere to each other and to the substrate. Figure (2.21) shows a schematic diagram of how LbL deposition of multilayers of polymers works.

The dipping times and pH of the polyelectrolyte solutions affect the smoothness and the thickness of the layers deposited. The effects of changing the pH of the polyelectrolyte solution on the resultant film thickness and physical properties is examined in various papers by Rubner *et al*[38] .

The degree of ionization of weak polyelectrolytes depends on the pH level of the solution. Weak positively-charged polyelectrolytes such as PAH are highly ionized at low pH. However, they lose protons as the pH of the solution goes above a characteristic pH value known as the pK_a (at which 50% of the groups are charged). Negatively-charged polyelectrolytes exhibit the opposite behavior where they are highly ionized at high pH. One of the observations made by Rubner *et al*. is that deposition of a positively-charged polymer and a negatively-charged polymer at pH values where both are fully ionized, for example PAH at pH 2 and PAA at pH 8, results in very thin polyelectrolyte multilayers. On the other hand, the deposition of a positively-charged weak polyelectrolyte layer in a high pH solution where it is not fully ionized on top of a negatively-charged weak polyelectrolyte layer that was deposited from a solution where it was fully ionized at high enough pH results in a thick layer of the positively-charged polymer and thicker multilayers in general. This can be explained in terms of the degree of ionization of both polymers. If both polymers are fully ionized, the outermost layer deposits in a flat configuration covering the largest possible area to neutralize the charge from the previously deposited layer. When a polymer layer is deposited at a pH where it is not fully ionized as the outermost layer on a previously deposited layer that was fully ionized when deposited, there will be an entropic penalty for spreading flat to cover the surface charge beneath it and the enthalpic gain to the free energy of adsorption is not going to be enough to compensate for the penalty. In this situation a segment of the partially ionized chains gets more ionized and adheres to the previously deposited layer while the rest of the chain tries to avoid the surface increasing the loop structure in the layer and thus increasing the thickness of the layer. The degree of ionization of different polymers vary depending on the polymer and its structure leading to different pK_a for each polymer. When Rubner and co-workers sequentially deposited layers of PAH and PAA at various pH values that ranged from 2.5 to 4.5

they were able to study surface wettability, organization and layer thickness of the deposited polymer layers.[38] Water contact angle for the deposited multilayers was found to be determined by the first 5-10 Å of the outermost deposited polymer layer.[38] A possible explanation for this phenomenon can be given in terms of the interpenetration of the sequentially deposited polymer layers. The thickness of the outermost layer determines the degree of interpenetration of the layer beneath it. When the outermost layer is thick, it limits the interpenetration from the layer under it and thus becomes the main determining factor to affect the contact angle of the polymer multilayer system. Making the outermost layer thinner by changing the pH of the deposition solution allows for more interpenetration from the layers below and thus allows for the lower layers to affect the water contact angle of the system. Changing the pH of deposition solutions, the water contact angles of bilayers of PAH/PAA, PAH/poly(methacrylic acid) and other combinations of polymer bilayers was changed systematically from < 5° to 72 ± 3°.[38] The surfaces exhibiting the lowest contact angles < 5° were associated with the outermost layer being an aliphatic polyacid such as PAA. On the other hand, hydrophobic surfaces exhibiting contact angles 50-60° are associated with aromatic polyacids such as poly(styrene sulfonate) (SPS).[38] Such a method of fine tuning the water contact angles for surfaces can be used to fabricate antifogging coatings for mirrors and lenses. Figure (2.22) shows some of the results of the experiments performed by Rubner and his group to study the dependence of the polymer layers on the pH levels of the deposition solutions. Figure (2.23) shows the effect of changing the deposition pH on the water contact angle for the polymer multilayers.

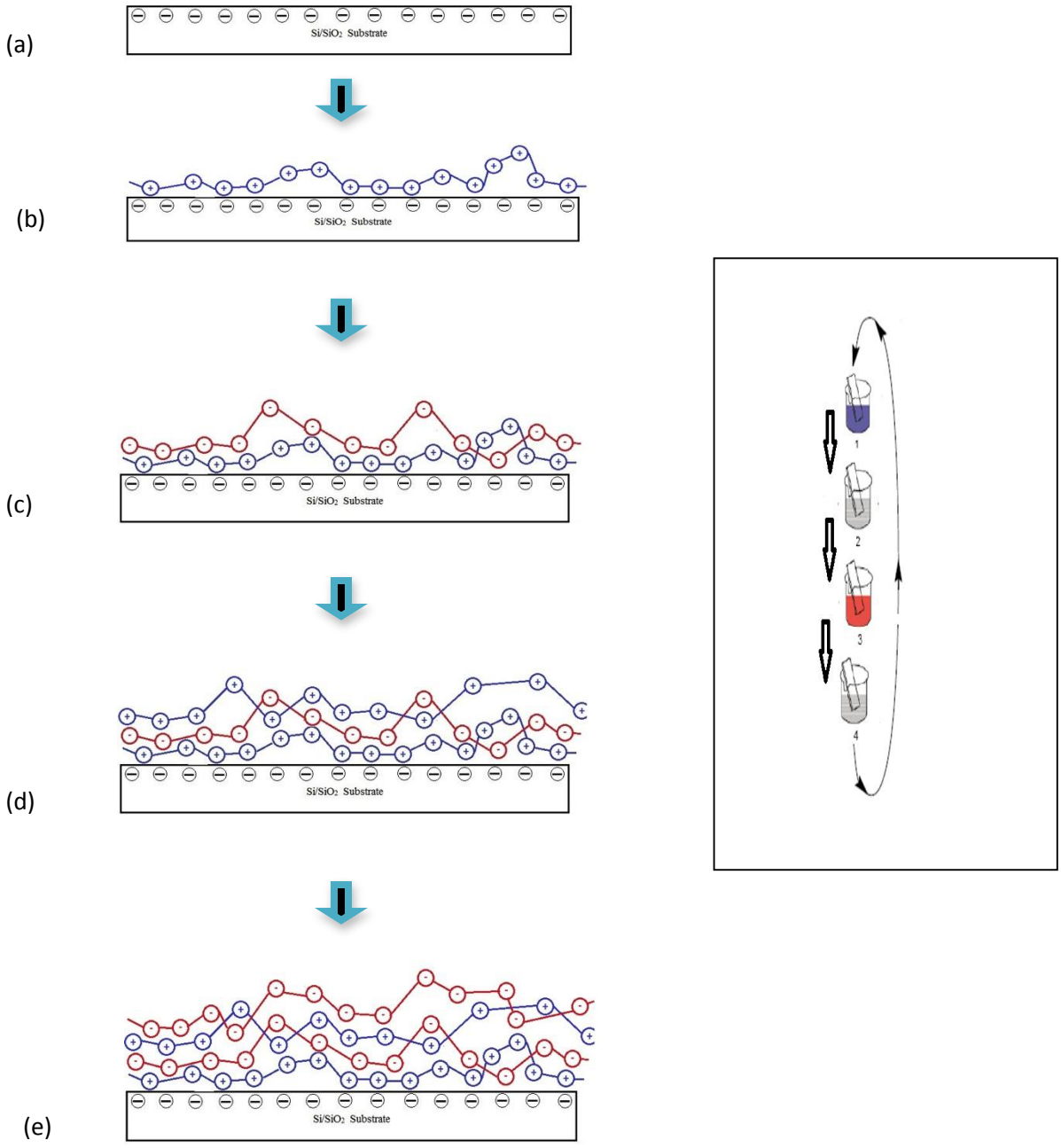

Figure (2.21): Layer by Layer deposition of polymers. Starting with a suitable substrate (in this case the substrate is made of glass), the substrate can have a charge on it. Dipping the substrate in positive and negative polymer solutions causes the deposition of multilayers of alternating polymer films.

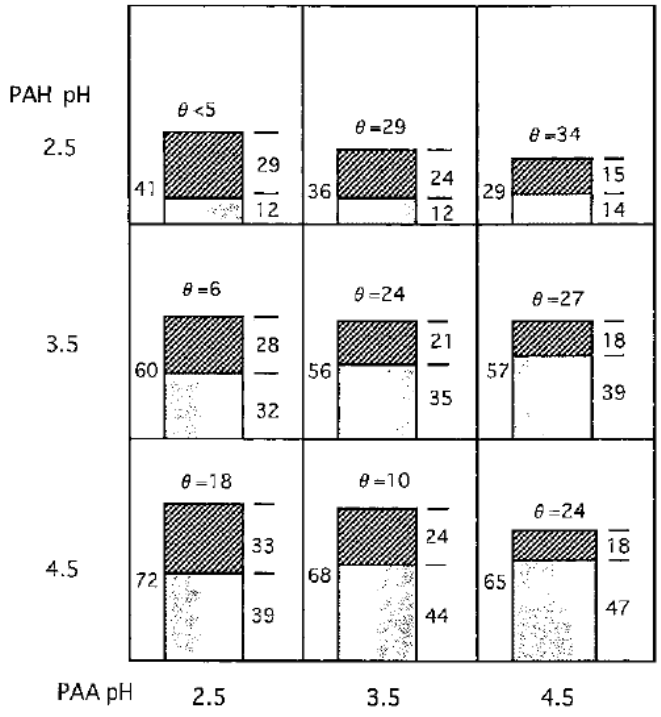

Figure (2.22): The changes in the thickness of a layer of PAH and a layer of PAA depending on the pH level of the deposition solutions. The dark color is use to represent the PAA layer and the light color is used for the PAH layer. The measurements represented here are in Å. The θ measurement provided is the water contact angle of 8 layers of polymers with PAA being the outermost layer.[38] [Fair use]: Yoo, D., Shiratori, S. S., and Rubner, M. F., "Controlling Bilayer Composition and Surface Wettability of Sequentially Adsorbed Weak Polyelectrolytes", Macromolecules, 31, 4309-4318, (1998).

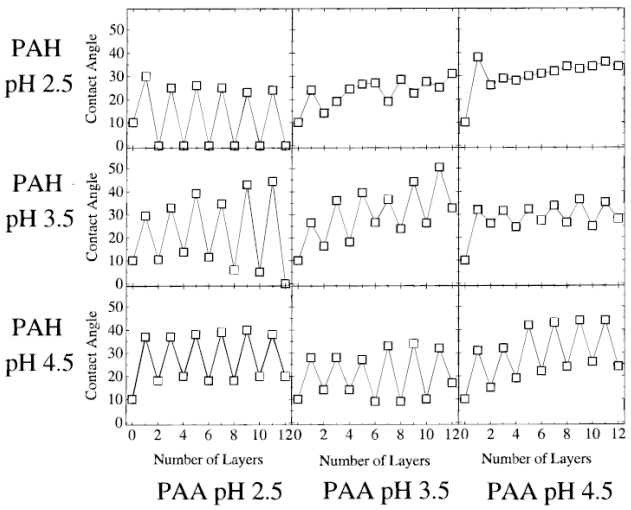

Figure (2.23): Contact angle measurements for different numbers of layers of PAH/PAA as a function of layer numbers and pH level of the deposition solutions. Cases of odd numbers of layers are cases with PAH as an outermost layer while cases with even number of layers are cases with PAA as an outermost layer.[38] [Fair use]: Yoo, D., Shiratori, S. S., and Rubner, M. F., "Controlling Bilayer Composition and Surface Wettability of Sequentially Adsorbed Weak Polyelectrolytes", Macromolecules, 31, 4309-4318, (1998).

In another study, Rubner and his group studied the correlation between the deposition solution pH and the thickness of the deposited multilayers of PAH/PAA. Depositing a multilayer of PAH/ PAA at the same pH level yielded the results represented in Figure (2.24)[39]

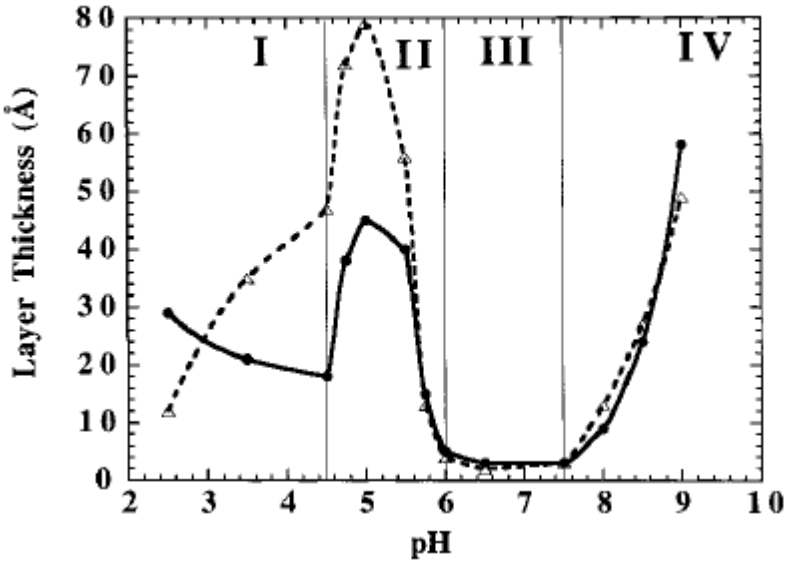

Figure (2.24): Average incremental thickness contribution of PAH and PAA to multilayers deposited from solutions where PAH and PAA are maintained at the same pH as a function of pH values.[39] [Fair use]: Shiratori, S. S., and Rubner, M. F., "pH Dependent Thickness Behavior of Sequentially Adsorbed Layers of Weak Polyelectrolytes", Macromolecules, 33, 4213-4219, (2000).

The thicknesses of the deposited layers were characterized by three main transitions in the layer thickness depending on the deposition pH. The thickness of the deposited layers depended on the level of ionization of each of the polyelectrolytes at the various pH levels. The PAA degree of ionization changes between 20% at pH 2.5 and increases to 100% at pH 6.5. The PAH chains are fully ionized up to pH 7 where they start losing protonation. Part I in Figure (2.24) shows that as the pH level increases, The PAH layers get thicker and the PAA layers get thinner. This can be explained by the fact that the PAH chains are fully ionized throughout this increase but the PAA chains are becoming more ionized and thus the PAA layers are getting thinner while the PAH

layers are getting thicker to neutralize the increasing surface charge of PAA on which they deposit. The trends of thickness changes in segment II of the graph in Figure (2.24) are explained by considering the fact that as the pH is lowered the PAH chains are strongly ionized while the PAA chains are partially ionized and that explains the tremendous increase in the thickness of each of the layers. The deposition thicknesses in part III of the graph are explained by the fact that both polyelectrolytes are fully ionized in this range of pH values leading to very thin deposited layers. Part IV of the graph is explained by considering the fact that at this range of pH levels the degree of ionization of the PAH is decreasing where its chains are almost fully ionized but they are starting to lose protonation. Meanwhile at these ranges of pH the PAA chains are fully ionized. The deposition of a nearly fully charged polyelectrolyte onto a fully ionized one gives us the well documented increases in layer thickness. Figure (2.25) shows the data collected by Rubner and his group in depositing PAH/PAA bilayers at a matrix of pH levels for each of the polyelectrolytes.[39]

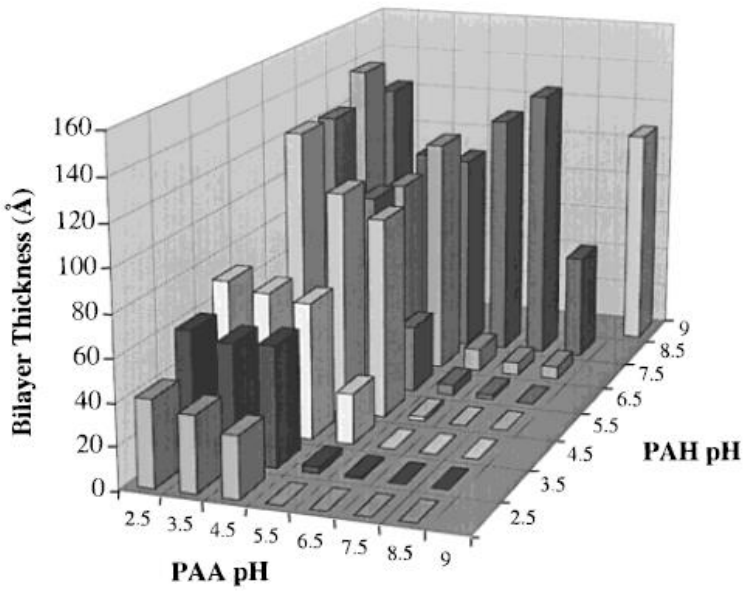

Figure (2.25): Values of the bilayer thickness of PAH/PAA systems as a function of pH values for both solutions.[39] [Fair use]: Shiratori, S. S., and Rubner, M. F., "pH Dependent Thickness Behavior of Sequentially Adsorbed Layers of Weak Polyelectrolytes", Macromolecules, 33, 4213-4219, (2000).

Another interesting property of polymer multilayers is the ability to change their thickness post deposition by dipping them in solution with varying pH levels. Rubner *et al*. studied this phenomenon in detail and found a correlation between the assembly pH and the degree to which the multilayers can change their thickness in response to changing the immersion soultion pH post-assembly.[40), (41), (42), (43)] The systematic deposition of PAH and SPS at different pH levels and soaking them post deposition in DI water with pH levels ranging from 2 to 10.5 revealed that PAH/SPS bilayers that were deposited at pH < 8.5 exhibit pH independent swelling behavior for no more than 15% of their thickness when measured after drying them. However, bilayers deposited at pH >8.5 exhibited a strong dependence on the pH of the dipping solutions post assembly. The increase in the thickness levels of the bilayers in the latter case reached 380%. Thickness measurements in these experimental trials were performed using ellipsometry. Figure (2.26) showed the data collected in the experiment described above

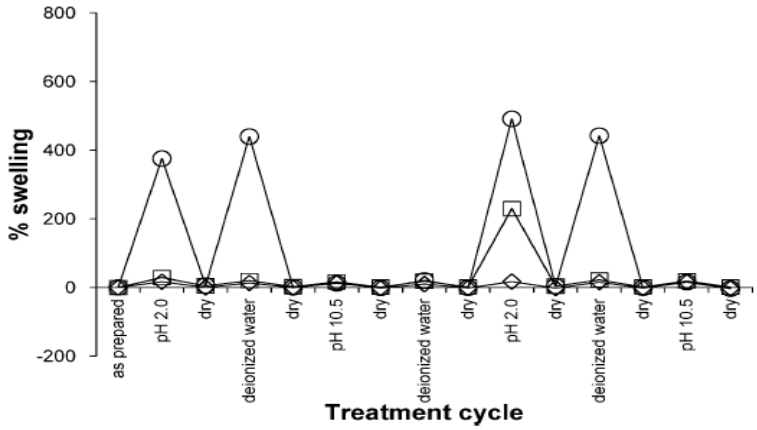

Figure (2.26): Depositing PAH/SPS bilayers at different levels of pH and immersing them in DI water with different pH levels shows a discontinuous response in the thickness changes of the layers depending on their deposition pH levels. The circles, squares and diamonds represent deposition conditions of pH 9.3, pH 8.5, and pH 7.5 respectively. The immersion in DI water lasted three minutes before thickness measurements were done.[41] [Fair use]: Itano. K., Choi. J., Rubner. M. F. Mechanism of the pH-Induced Discontinuous Swelling/Deswelling Transitions of Poly(allylamine hydrochloride)-Containing Polyelectrolyte Multilayer Films. Macromolecules 38, 3450-3460, (2005).

This behavior can be attributed to the use of a weak polyelectrolyte and a strong polyelectrolyte to fabricate the bilayers. Due to the dependence of the ionization level of the weak polyelectrolyte on the pH of the solution it is immersed in, it can be perceived that the change in ionization degree causes the electrostatic interactions between the differently charged layers to fluctuate and this allows for other effects such as hydrogen bonding and hydrophobicity to play a larger role in the layers binding. This can be seen to be the case when one considers reported data of using two strong polyelectrolytes, PDAC and SPS, to fabricate the multilayers where the reported change in thickness does not exceed 30% of the dry film thickness.[41], [42]

Layer by layer deposition of polymers has a wide range of applications attracting attention from different disciplines. Among the interesting applications are an antireflection coating that depends on the pH swelling and deswelling behavior of polymer multilayers. Rubner *et al*. reported successfully fabricating pH responsive antireflection coatings. By depositing layers of PAH/PAA at pH 8.5 and 3.5 respectively and then immersing the layers in an acidic solution of pH 1.8 a phase separation occurs rendering the top most layer porous. Such structure allows for pores of air to exist inside the polymer layers changing its effective refractive index. Subsequently immersing the layers in DI water of different pH levels causes the polymer layers to either shrink to the point where the pores close completely or swell where the pores become larger. Such pH induced change in the size of the pores causes the refractive index of the layers to change. Rubner *et al*. showed that a particular refractive index can be secured against further pH changes by thermally treating the layers. Such a mechanism of controlling the refractive index of the various layers, stabilizing the refractive index of the individual layers and the ability to deposit various layers sequentially allows for the creation of antireflection coatings that change their refractive indices gradually.

Such coatings can be effective for wide ranges of the spectrum. Such techniques can also be used for creating pH gated delivery systems for molecular exchanges or medication delivery systems.[40]

Another approach to fabricating antireflection coating using polymer multilayers and LbL deposition is the one taken by Heflin and co-workers.[48] In their work reported in 2006, they found that depositing silica nanoparticles of average diameters 15, 45, and 85 nm in bilayers with PAH allowed them to achieve reflectivity levels $\geq 2\%$, $\leq 2\%$, and $\leq 2\%$ for the wavelength range λ = 350 – 700 nm for the diameters of silica particles listed above, respectively. The idea behind designing an effective antireflective coating starts with having a coating of thickness $\lambda/4$. This requirement was met by utilizing LbL deposition of PAH and the silica nanoparticles. This deposition technique offers fine-tuning and control down to the nanometer scale. The second requirement is that the refractive index of the coating needs to meet the requirement of $n_c = (\sqrt{n_1 n_2})$ where n_1 and n_2 are the refractive indices of the materials on both sides of the coating. For an antireflective coating between air and glass, the n_c = 1.22. Such a small value for the refractive index was possible to achieve by utilizing the void spaces between the deposited silica nanoparticles due to their shapes.[48]

Another application of LbL deposition of polymers is in the fabrication of electrochromic devices. Heflin *et al*. showed for the first time in 2009 the possibility of producing electrochromic devices, devices that change their color due to oxidation or reduction reaction when voltage is applied to them, using LbL deposition methods. Until that point all of the electrochromic devices produced were fabricated using spin coating, thermal evaporation, or surface polymerization. In one example of their electrochromic work, Heflin and co-workers used bridged polysilsesquioxane nanoparticles to be deposited with poly[2-(acrylamido)-2-methyl-1-propanesulfonic

acid] (PAMPS) using LbL deposition methods. The choice of the nanoparticles was made given the fact that the surface area they have enhances the color contrast of the device. Also the porosity of the surfaces produced given the spherical shapes of the nanoparticles allows for faster switching times.[45]

A multitude of other uses for multilayer deposition using the LbL method exist including biosensors[44], microstructure fabrication[46] and a host of other applications.

Selective deposition of ISAM layers on charged regions written via an atomic force microscope is a crucial aspect of this dissertation. We therefore will discuss in great detail the excellent work of Paula Hammond's research group in understanding the variables that control the selective deposition of these films on templated surfaces.[18],[19],[20] In their papers, Clark and Hammond, reason that the possibility of directing the deposition of polymer layers to specific regions is due to the following effects[18],[19]

a) Electrostatic

b) Secondary interactions

c) Steric repulsion effects

In their work they use three different polyamines which are PAH, branched poly(ethyleneimine) solution (BPEI), and linear polyethyleneimine (LPEI), which are to be deposited with different polyacids in LbL deposition. They divided the runs into two categories based on the polyacid used in the run. One set of runs used poly(acrylic acid) (PAA) as the polyacid and the other used poly(methacrylic acid) (PMAA). The deposition of the multilayers takes place on gold surfaces patterned with materials ending with the functional group –COOH (serving as an ionizable surface

for the polyion adsorption) and regions of oligoethylene oxide (EG) (serving as a resist surface to prevent the adsorption of polyions). Preventing polyions from depositing on the EG layer depends on hydration and low interfacial free energy of the EG layer with water and its ability to shield the deposition of charged polymer chains and proteins.

In what follows I summarize the key points in their papers:

a) At pH 4.8 the region of preferred adsorption of the more hydrophobic polyamines was generally the EG surface. The more hydrophilic species like LPEI preferred to deposit on the –COOH regions at this pH level.

b) It is proposed that PAH goes through a process of complexation with the EG surface based on hydrophobic and hydrogen bonding interactions at moderate pH levels.

c) LPEI has a hydrated backbone and is strongly believed to undergo a process of large steric repulsion with the EG surface, thus resulting in deposition only on the –COOH regions of the surface.

d) The region of preferred adsorption also varied with the pH level

    i. At low pH: the hydrogen bonding of the PAA played an important role in directing the deposition to the –COOH regions

    ii. At high pH: the electrostatic interactions became dominant when all systems were highly charged

The authors state that in previous work of theirs they were able to establish a set of rules for the selective adsorption of strong polyions.[19],[20] These rules are based on:

a) Electrostatic interactions

b) Shielding effects

c) Secondary effects

The authors further note the following points:

At moderate to low ionic strength (of the solutions), strong highly charged polyelectrolytes deposit almost solely on the –COOH regions with very little to no deposition on the EG. The reason for this is that for strong polyelectrolytes, electrostatic interactions play the predominant role in the selectivity.

- The use of weak electrolytes provides an opportunity to use the pH level as a tool to manipulate the selectivity of deposition on different surfaces. As the pH is varied, the degree of ionization of the weak electrolytes is altered as well as the number of sites available for hydrogen bonding (hydrogen bonding plays an important role in the case of the weak electrolytes).

- The authors found a strong correlation between the chemical structure of the polyion, specifically the hydrophobic or hydrophilic nature of the polymer backbone and the surface region of preferred deposition (this will be explained in more detail later).

Examining the details of the experiments and results Clark and Hammond have in their work yields the following observations[(18),(19),(20)]

- At neutral pH both the polyamine and polyacid are highly charged and unshielded and therefore adsorb to the surface in thin layers. Moving up or down in pH levels from this

point increases the ionization of one weak polyelectrolyte while decreasing the other, resulting in thick films for the least ionized component.

- In all the different trials performed, the deposition process began with deposition of the polyamine (PAH, BPEI and LPEI). The authors notice that the polyamine will deposit on both the –COOH and EG functionalized areas. This is not the case when the authors use strong polyelectrolytes where they deposit only on one of the areas with high selectivity that goes up to 90%. However, once the PAH, BPEI and LPEI combined with polyacids start developing multilayers on top of the patterned surface, the authors observe that the structure is higher on one of the regions than the other. Using this observation they develop a selectivity measure that is given by[18]

Selectivity = (COOH_th – EG_th)/(the greater of COOH_th ,EG_th)

where:

- COOH_th is the thickness of the film that deposited on the area of the substrate functionalized with COOH
- EG_th is the thickness of the film that deposited on the area of the substrate functionalized with EG

For this definition of selectivity

+ve values = more preference to deposit on the –COOH surface

-ve values = more preference to deposit on the EG surface.

- For weak polyelectrolytes the effect of the underlying surface becomes less important as more layers are added. The authors observe the following

  a) For polyion pairs with low to moderate absolute values of selectivity, the pattern starts to vanish after 20-40 deposition cycles.

  b) The surface on which the deposition process takes place can influence the multilayer film thickness for at least 10-15 bilayers. This can be understood given the large degree of interpenetration between layers in polyelectrolyte multilayer films. Individual polyions in the multilayer films penetrate up to 10-15 layers above and below their originally deposited layer. For these reasons, the authors observe that the influence of the underlying surface in these patterned films is maintained up through many multiple layers – at least 15-30 bilayers.

Figure (2.27) shows the selectivity of different combinations of Polyamines/PAA in the first set of experimental trials.[18]

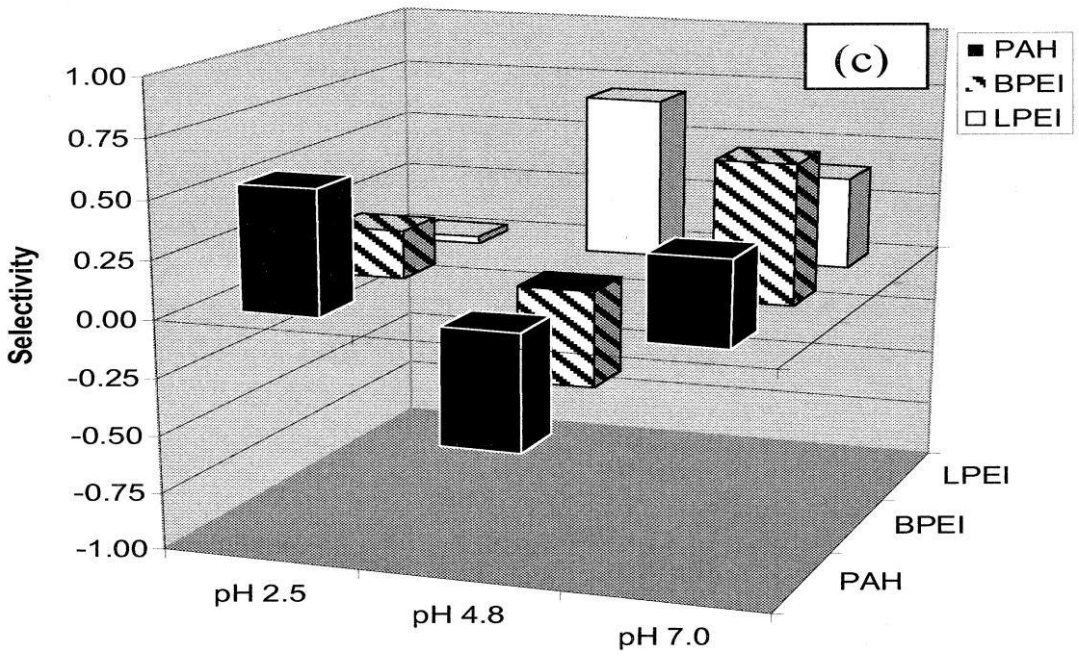

Figure (2.27): After depositing 10 bilayers of a Polyamine/PAA combination on a gold coated substrate that is functionalized with COOH and EG the thickness of the deposited films on both areas were measured. Using equation (1) above the selectivity of the deposition process was assessed. [18] [Fair use]: Sarah L. Clark and Paula T. Hammond, "The role of secondary interactions in Selective Electrostatic Multilayer deposition", Langmuir 16 (26), pp 10206-10214, (2000).

The positive selectivity in the graph indicates a preference for the films to deposit on the COOH surface and the negative selectivity indicates preference to deposit on the EG surface.

The following is a summary of the detailed information provided in the papers[18],[19],[20]

1. Low pH levels (pH 2.5):

   a) Observation:

      i. The systems of polyamine and PAA exhibit low to moderate preferential adsorption on the –COOH surface.

ii. This is different than the case of preferential adsorption on the EG surface observed for the PAH and BPEI polyamines when they were coadsorbed with a sulfonated dye molecule.

b) Explanation:

i. The first step in the adsorption process is the deposition of the polyamine on the surface. It is expected that this will lead to a very thin layer of PAH due to the very low degree of ionization of the –COOH surfaces at such a pH level.

ii. It is probable that acid sites remain accessible to the surface on the COOH regions after the first polyamine layer is adsorbed.

iii. In this case we should expect hydrogen-bond dimerization to take place between the next adsorbing layer of polyacid and the underlying COOH SAM. This should enhance adsorption of the polyacid on the COOH surface at low pH.

iv. In each subsequent adsorption cycle, interpenetrated acid groups underlying the top polyamine layer can again promote polyacid deposition compounding the effect of hydrogen bonding from one layer to the next on the COOH stamped surface regions.

v. In turn it appears that after the first polyamine/polyacid bilayer is deposited, polyamine adsorption happens on the regions with the largest relative amount of polyacid.

vi. The net result is preferential adsorption on the COOH surface.

2. Moderate pH (pH 4.8):

a) Observations:

i. The selectivity changes dramatically in this case from what it was before.

ii. Multilayers with PAH and BPEI tend to have a preference to adsorb on the EG surface rather than the COOH surface (greater negative selectivity is observed for the PAH-based films).

iii. At pH 4.8, LPEI/PAA multilayers preferred to adsorb on the COOH surface with very high positive selectivity.

b) Explanation:

i. One way of addressing this is by considering the charged state of both the surfaces and the polyions as well as the potential for intermolecular interactions.

ii. At pH 4.8, both the COOH SAM and PAA are moderately ionized and this greatly decreases the hydrogen –bonding interactions between acid groups on the surface and the polymer backbone that encouraged the deposition on the COOH surface at pH 2.5.

iii. In the weak electrolyte multilayer systems, the influence of COOH-COOH hydrogen bonding is diminished with increasing pH; without this mediation between the protonated acid groups, the polyamine structure plays a more important role in determining selectivity.

iv. On the basis of electrostatics alone it would be expected that deposition takes place only on the ionized COOH surface. They note that the ionization of the three polyamines at pH 4.8 ranges from 60% to 95% and they conclude that all three polyamines are significantly charged.

v. The large differences in selectivity must arise from differences in the polyamine structures and their interactions with the COOH and EG surfaces.

vi. A hydrogen bonding argument between the polyamines and the surface groups might be posed based on the results above. The EG monolayer presents four hydrogen bond acceptor groups per molecule in the form of ether and alcohol oxygen, whereas the COOH surface presents one such site only. For this reason only it might be expected that protonated polyamines, which are strong hydrogen bond donors, would prefer the EG regions at lower pH.

vii. However, hydrophobicity can also be important in determining the selectivity behavior observed here.

viii. When a polyamine with an alkyl backbone interacts with the EG resist, the dispersion interactions of the polyamine backbone with the ethylene group of the EG repeat may be optimized while still maintaining complementary H-bonding interactions with the ether oxygen.

ix. We observe a progression in the preferred region of deposition from the COOH to the EG surface with increasing hydrophobicity of the polyion

backbone. Deposition mediated by these nonpolar dispersion interactions apparently leads to a reversal of the deposition selectivity in PAH and BPEI polyamines in going from low to moderate pH levels.

x. LPEI polyamine multilayers were selective towards the COOH surface at all pH conditions, with a maximum selectivity observed at pH 4.8. The linear structure of LPEI is composed entirely of secondary amine groups resulting in a polyelectrolyte with a highly hydrated structure. It is likely that LPEI chains undergo repulsive interactions with the similarly hydrated EG brush layer at pH 4.8 and 7.0.

xi. Only at the lowest pH (pH 2.5) is the LPEI chain actually adsorbed in relatively high quantities to the EG surface, although the actual selectivity remains positive. In this case, hydrogen bonding with ether oxygens in the EG layer is probably the primary driving force toward adsorbing LPEI on the EG at pH 2.5.

3. High pH (pH 7):

a) Observations:

i. The AFM images of these patterned surfaces indicate that each system is again selective to the ionized COOH surface as at pH 2.5.

ii. The final multilayers are very thin due to the extended highly ionized configuration of the adsorbed chains.

iii. The average polyamine pair thicknesses were 1.1, 0.5, and 0.5 nm respectively for multilayers containing PAH, BPEI and LPEI on COOH surfaces.

b) Explanation:

i. PAA and the polyamine are both highly ionized and adsorb in a manner similar to systems of strong polyelectrolytes

ii. They observe that the adsorption behavior was consistent with what will be expected from two highly ionized polyions; the polymers adsorb as very thin flat films to maximize charge compensation and avoid self-repulsive segmental interactions.

iii. The high degree of ionization on the COOH surface achieved at pH 7 also increases electrostatic interactions such that the hydrophobic interactions of the polyamines are much less in this case. Thus, in this case all three polyamine/polyacid systems indicate preference to deposit on the COOH surface.

When the second set of trials was executed by adsorbing the polyamines PAH, BPEI, and LPEI with the polyacid PMAA, the following observations were made by the authors.[18],[19],[20]

a) Poly(ethylene oxide) (PEO), the polymer analogue of the EG surface readily complexes with PAA and PMAA at low pH, when the polyacids have a low degree of ionization.

b) PMAA chains at low degrees of ionization are much more hydrophobic than PAA chains due to the presence of the additional methyl group and tertiary carbon.

c) These additional hydrophobic interactions along with hydrogen bonding drive a strong complexation of PMAA with PEO.

The selectivity graph for this case is shown in Figure (2.28).

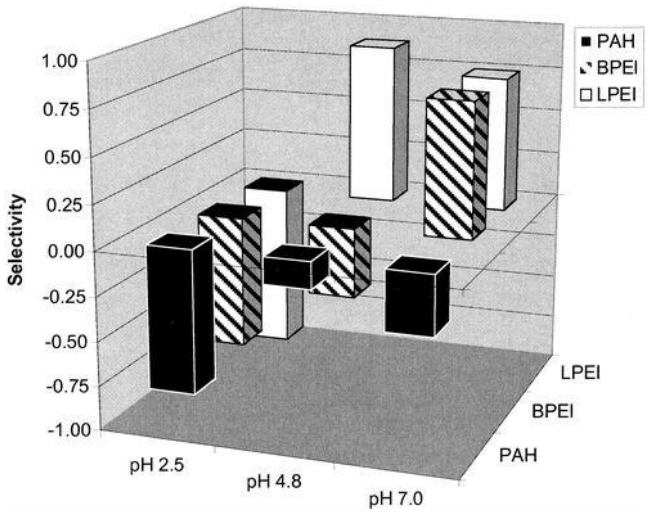

Figure (2.28): The selectivity behavior for various polyamines deposited in 10 bilayers with PMAA. The positive selectivity in the graph indicates a preference for the films to deposit on the COOH surface and the negative selectivity indicates preference to deposit on the EG surface. These results pertain to the case of polyamine/PMAA systems [18] [Fair use]: Sarah L. Clark and Paula T. Hammond, "The role of secondary interactions in Selective Electrostatic Multilayer deposition", Langmuir 16 (26), pp 10206-10214, (2000).

The following is a summary of the observed data and analysis reported by the authors. [18],[19],[20]

1. Low pH (pH 2.5):

a) Observations:

i. The selectivity of all the PMAA/polyamine combinations were all highly negative (prefer to adsorb to the EG surface)

b) Explanation:

i. Unlike the PAA systems, the potential for hydrogen bonding and hydrophobic interactions with PMAA on the EG surface overcome the

potential for hydrogen bond dimerization with the underlying COOH surface.

ii. Comparing these results with the positive selectivity exhibited in the case of PAA/polyamine combinations, it seems that ionic interactions with the surface functional groups have a lesser influence on the preferred adsorption location at low pH.

iii. Selective adsorption in these two cases of low pH levels is based solely on the difference of the single methyl group on PMAA, which rendered the polyanion more hydrophobic and more readily bound to the EG surface.

2. Moderate pH (pH 4.8):

a) Observations:

i. At pH 4.8, PMAA has a higher degree of ionization than at pH 2.5.

ii. PMAA polymer chains exist as a compact random coil at lower pH values isolating a hydrophobic core with brush like acid layer.

iii. A slight increase in ionization includes an abrupt transition to moderately ionized extended chains.

b) Explanation:

i. The adsorption behavior of the more highly ionized PMAA chain is no longer influenced by hydropobic interactions between the methyl group and

the EG ethylene groups as the polymer chains become more charged and solvated.

ii. For the above reason, the chemical structures of the poyamines again guide the selective adsorption at pH 4.8 like in the case of PAA/Polyamine layers.

3. High pH (pH 7.0):

a) Observations:

i. PMAA/polyamine films adsorption behavior at pH 7 matches that of strong highly ionized polyelectrolytes resulting in thin films with preference for equally highly ionized COOH surfaces. This is similar to what has been observed for the PAA/polyamine films at pH 7.

Finally, performing some comparisons of adsorption on hydrophobic versus charged surfaces leads us to the following.[18],[19],[20]

a) They have proposed so far that the positive and negative selectivity values of the PAA/polyamine patterned multilayers adsorbed at pH 4.8 result from a balance between ionic interactions with the COOH surface and secondary interactions with the EG surface. To confirm these observations, two different functional monolayer surfaces with simpler interactions were substituted for the COOH and EG surfaces. An $(SO_3)^-$ Na^+ terminated SAM provided a strongly ionized surface without the pH-dependent behavior and hydrogen bonding interactions of the COOH surface in the pH range of interest.

b) A CH_3-terminated SAM provided an alkyl, purely hydrophobic analogue to the EG surface.

c) Substrates patterned with $(SO_3)^- Na^+$ /EG and $COOH/CH_3$ were used for the adsorption of 10 bilayer films of each of the polyamine/PAA pairs at pH 4.8.

d) In each case there is striking resemblance to the original COOH/EG patterned films at pH 4.8.

e) It appears that qualitative aspects of selectivity can be generated using an all alkyl chain in place of the EG surface at 4.8. It is also apparent that the COOH surface is much like the highly ionized sulfonate surface at pH 4.8.

2.5 Molecular Electronics

Electronic devices built from a single molecule or a small group of molecules is a strong candidate for extending Moore's law and leading the way in miniaturizing electronics. This idea was suggested in the mid seventies.[47]. Such an approach offers the positive point of reducing the size of the electronic elements to molecular sizes. However, due to the size of these elements, techniques utilizing this idea have to deal with a few fundamental issues. One of the major technical issues is the fabrication of leads on the molecular size scale to contact molecules and allow measurements on these devices. The problem of characterizing the electronic properties of a single molecule or a small group of molecules has been tackled in various ways in the literature so far. Three of the most important and successful ways such measurements have been performed

are break-junction techniques, the use of electromigration to form nanogaps, and the use of scanning tunneling microscopes to probe the conductivity of single molecules.

(a) Break-Junction Techniques

In this technique, a very thin conducting wire is constructed on the nanometer scale. The wire is then fixed on top of a flexible substrate. The wire is tnotched using a sharp tool or a focused ion beam. The flexible substrate is mounted on top of a piezoelectric element. By virtue of the piezoelectric properties, which will be discussed in details in the following chapter, applying a potential difference to the piezoelectric element causes the element to twist or expand depending on the piezoelectric element design. Once the piezoelectric element is expanded, it bends the substrate and the nanowire fixed to it. When the nanowire is bent beyond a certain limit, it breaks. The flexible substrate and the wire mounted on top of the piezoelectric element allows one to control the width of the gap introduced by breaking the wire. Such a setup is known as a mechanically controlled break-junction. Having the gap in the wire immersed in a solution of molecules that can self-assemble will result in a self-assembled monolayer of molecules between the electrodes. The break-junction technique was the method used by Mark Reed and colleagues for measuring the conductance of benzene-1,4-dithiolate molecules. Immersing a gold nanowire in a solution of benzene-1,4-dithiolate and then breaking the wire while in solution caused the benzene-1,4-dithiolate molecules to deposit on the newly formed electrodes in a self-assembled monolayer. After the solution was evaporated, a potential difference was applied to the electrodes and the gap size between them was reduced until conduction was first observed. This allowed for the measurement of the conductance of a single molecule of benzene-1,4-dithiolate. The gap size at which conductance was first observed was estimated to be 0.8

nm. The 0.8 nm corresponds to the legth of a single benzene-1,4-dithiolate molecule. Figure (2.29) shows the setup for the mechanically controlled break-junction and a schematic diagram for its use in measuring the conductance of benzene-1,4-ditholate molecules.

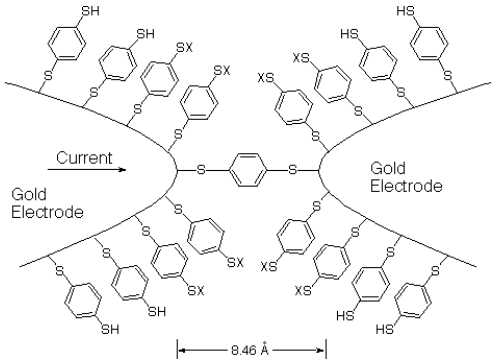

(a)

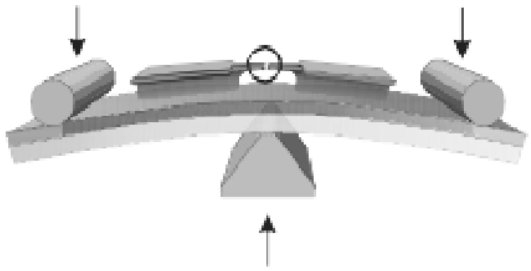

(b)

Figure (2.29): (a) A schematic diagram of benzene-1,4-dithiolate molecule connected between two electrodes of a mechanically controlled break-junction to measure its conductivity.[14] (b) Schematic diagram showing the design of a mechanically controlled break-junction.[50] [Fair use]: Massimiliano Ventra, Stephane Evoy, James R. Heflin, "Introduction to Nanoscale Science and Technology (Nanostructure Science and Technology)", Springer; 2004 edition. [Fair use]: N. Kang, A Erbe, and E. Scheer, "Electrical characterization of DNA in mechanically controlled break-junctions", New Journal of Physics, 10, 2008.

(b) Electromigration

When an electric current travels in a conductor, the interactions of the electrons making up the current with the atoms of the conductor can lead to removal of some of the atoms of the conductor from their equilibrium positions. This physical phenomenon is known as electromigration. If a current of high enough density is sent though a nanowire, some of the atoms of the wire can be moved out of their equilibrium positions and cause a gap to exist in the wire. This method can be used as an alternative method of fabricating a gap in the conductive wire. Self-assembling materials on the wire and in the gap can lead to similar uses and results to what has been accomplished using the break-junction technique.[14]

Scanning Tunneling Microscopes

Scanning tunneling microscopes depend on bringing a very small, sharp, and conductive tip near the surface of a sample and applying a potential difference between the tip and the sample. Measuring the tunneling current while the tip scans the surface allows for the production of a topographic map of the sample surface. Such a map can be produced in one of two ways. The first way is to keep the height constant between the tip and the surface and to measure the fluctuations in the current and to use that to build the topographical map of the surface. The second mode of running the scanning tunneling microscope depends on keeping the current constant by using a feedback loop to change the separation between the tip and the sample. In this second mode, the current stays constant due to its dependence on the tunneling distance between the tip and the sample surface. Such a method of measurement was proven useful in determining the conductance of single molecules. When

a single conducting molecule is introduced into a background matrix of insulating molecules where there is a height difference between the introduced molecule and the background, it becomes easy for the STM tip to find this molecule and measure its electric properties. A few problems face such measurements. Among the problems that face this technique is the very high "contact" resistance between the tip. The methods developed for increasing the electrical contact between the molecules and the STM tip have come a long way during the past decade. Various trials have been done where the molecule to be tested is functionalized with a thiol molecule to facilitate interaction with the STM tip to reduce contact resistance. Other methods developed to increase interaction between molecules and electrodes include trapping individual molecules in nanopores and sandwiching a single layer of molecules between two electrodes by physically evaporating the electrode on top of the molecular layer.[14]

References:

1. Andrew George, ed.: Cuneiform Royal Inscriptions and Related Texts in the Schøyen Collection, Cornell University Studies in Assyriology and Sumerology, vol. 17, Manuscripts in the Schøyen Collection, Cuneiform texts VI. CDL Press, Bethesda, MD, 2011, text 24, p. 50, pl. XX

2. Weaver, Peter. The Technique of Lithography. London: B.T. Batsford, (1964)

3. A. B. Hoen, Discussion of the Requisite Qualities of Lithographic Limestone, with Report on Tests of the Lithographic Stone of Mitchell County, Iowa, Iowa Geological Survey Annual Report, 1902, Des Moines, 1903.

4. Robert Hirsch. *Seizing the Light: A Social History of Photography*. (McGraw-Hill, 2009).

5. https://indico.cern.ch/event/34040/material/slides/1?contribId=13

6. Jaeger, Richard C. *Introduction to Microelectronic Fabrication* 2nd ed. (Upper Saddle River: Prentice Hall, 2002).

7. https://www.ee.washington.edu/research/microtech/cam/PROCESSES/PDF%20FILES/Photolithography.pdf

8. J.A.Samson and D.L.Ederer. *Vacuum Ultraviolet Spectroscopy II.* (Academic Press 1998).

9. Jackson, Mark. *Micro and Nanofabrication.* (Springer 2007)

10. Chou, S.Y.; Krauss, P.R.; Renstrom, P.J.. "Imprint Lithography with 25-Nanometer Resolution". Science **272** (5258): 85–7. (1996)

11. Rachel K. Smith, Penelope A. Lewis, Paul S. Weiss, “Patterning self-assembled monolayers”, Progress in Surface Science **75**, 1-68, (2004).

12. Piner, R. D.; Zhu, J.; Xu, F.; Hong, S.; Mirkin, C. A. “”Dip-Pen” Nanolithography,” Science **283**, 661-663 (1999)

13. PIMPIN, A., SRITURAVANICH, W. “Review on Micro- and Nanolithography Techniques and Their Applications”, Engineering Journal, Thailand, 16, nov. 2011

14. Massimiliano Ventra, Stephane Evoy, James R. Heflin, “Introduction to Nanoscale Science and Technology (Nanostructure Science and Technology)”, Springer; 2004 edition.

15. Donna L. Wilson, Raquel Martin, Seunghun Hong, Mark Cronin-Golomb, Chad A. Mirkin, and David L. Kaplan, “Surface organization and nanopatterning of collagen by dip-pen nanolithography”, Proceedings of the National Academy of Sciences of the United States of America, vol. **98** no. 24, (2001).

16. Seunghun Hong, Jin Zhu, Chad A. Mirkin, “Multiple Ink Nanolithography: Toward a Multiple-Pen Nano-Plotter”, *Science* **286**, 523 (1999).

17. A. Tulpar, Z. Wang, C.-H. Jang, V. Jain, J.R. Heflin, W.A. Ducker, "Nanoscale Patterning of Ionic Self-Assembled Multilayers", Nanotechnology **20**, 155301:1-5 (2009).

18. Sarah L. Clark and Paula T. Hammond, “The role of secondary interactions in Selective Electrostatic Multilayer deposition”, Langmuir **16** (26), pp 10206-10214, (2000).

19. Sarah L. Clark, Martha F. and Paula T. Hammond, "Ionic Effects of Sodium Chloride on the Templated Deposition of Polyelectrolytes Using Layer-by-Layer Ionic Assembly", Macromolecules **30**, 7237-7244, (1997).
20. Sarah L. Clark and Paula T. Hammond, "Engineering the Microfabrication of Layer-by-Layer Thin Films", Advanced Materials, Volume 10, Issue 18, Pages 1515-1519, December (1998).
21. Rogers, Pennathur, and Adams, *Nanotechnology: Understanding Small Systems*, 2nd Edition CRC Press, 2011.
22. Loiseau, A., Launois-Bernede, P., Petit, P., Roche, S., Salvetat, J.-P. (Eds.), *Understanding Carbon Nanotubes*, Lecture Notes in Physics, Vol. 677, Springer 2008.
23. Thomas Ebbesen, , "Carbon Nanotubes", Physics Today, Vol. 49 Issue 6, (1996).
24. T. Kozawa et al., "Point Spread Function for the Calculation of Acid Distribution in Chemically Amplified Resists for Extreme Ultraviolet Lithography", Appl. Phys. Exp. 1, 027001 (2008).
25. Alexandra Joshi-Imre and Sven Bauerdick, "Direct-Write Ion Beam Lithography," Journal of Nanotechnology, vol. 2014, Article ID 170415, 26 pages, 2014
26. F. Watt, A. A. Bettiol, J. A. Van Kan, E. J. Teo, and M. B. H.Breese, "Ion beam lithography and nanofabrication: a review," International Journal of Nanoscience, vol. 4, no. 3, pp. 269–286, 2005
27. H. D. Wanzenboeck and S. Waid, "Focused ion beam lithography", in Recent Advances in Nanofabrication Techniques and Applications, B. Cui, Ed., InTech, Rijeka, Croatia, 2011.

28. Wind, S. J.; Appenzeller, J.; Martel, R.; Derycke, V.; Avouris, Ph. (2002). "Vertical scaling of carbon nanotube field-effect transistors using top gate electrodes". Applied Physics Letters 80 (20): 3817

29. Chen, Zhihong; Farmer, Damon; Xu, Sheng; Gordon, Roy; Avouris, Phaedon; Appenzeller, Joerg (2008). "Externally Assembled Gate-All-Around Carbon Nanotube Field-Effect Transistor". IEEE Electron Device Letters 29 (2): 183

30. Dekker, Cees; Tans, Sander J.; Verschueren, Alwin R. M. (1998). "Room-temperature transistor based on a single carbon nanotube". Nature 393 (6680): 49

31. Martel, R.; Schmidt, T.; Shea, H. R.; Hertel, T.; Avouris, Ph. (1998). "Single- and multi-wall carbon nanotube field-effect transistors". Applied Physics Letters 73 (17): 2447

32. J. –M. Lehn, Supramolecular Chemistry (VCH, Weinhein, 1995)

33. Lee, K. B, Kim, E. Y., Mirkin, C. A. and Wolinsky, S. M., "The Use of Nanoarrays in highly sensitive and selective human immunodeficiency virus type 1 in plasma", Nano Lett. **4**, 1869-1872, (2004)

34. Wang, Y. *et al*, "Controlling the shape, orientation, and linkage of nanotube features with nano affinity templates", Proc. Natl. Accad. Scie. USA, **103**, 2026-2031, (2006)

35. Salaita, K., Wang, Y., Mirkin, C. A., "Applications of dip pen nanolithography", Nature Nanotechnology, **2**, 145-155, (2007)

36. Rau, S. G., Huang, L., Steyawan, W., Hong, S. H., Large-scale assembly of carbon nanotubes, Nature, **425**, 36-37, (2003)

37. Salaita, K. Wang, Y., Faragala, J., Vega, R. A., Liu. C., Mirkin, C. A., Massively Parallel Dip-Pen Nanolithography with 55,000-Pen Two Dimensional Arrays, ANgew. Chem. Int. Ed., **45**, 7220-7223, (2006)

38. Yoo, D., Shiratori, S. S., and Rubner, M. F., "Controlling Bilayer Composition and Surface Wettability of Sequentially Adsorbed Weak Polyelectrolytes", Macromolecules, **31**, 4309-4318, (1998).

39. Shiratori, S. S., and Rubner, M. F., "pH Dependent Thickness Behavior of Sequentially Adsorbed Layers of Weak Polyelectrolytes", Macromolecules, **33**, 4213-4219, (2000).

40. Hiller. J, Mendelsohn. J. D., Rubner. M. F. Reversibly Erasable Nanoporous Anti-reflection Coatings from Polyelectrolyte Materials. Nat. Mat. 59-63.

41. Itano. K., Choi. J., Rubner. M. F. Mechanism of the pH-Induced Discontinuous Swelling/Deswelling Transitions of Poly(allylamine hydrochloride)-Containing Polyelectrolyte Multilayer Films. Macromolecules **38**, 3450-3460, (2005).

42. Hiller. J., Rubner. M. F. Reversible Molecular Memory and pH-Switchable swelling transitions in Polyelectrolyte Multilayers. Macromolecules **36**, 4078-4083, (2007).

43. Lee. D., Nolte. A. J., Kunz. A.L., Rubner. M. F., Cohen. R. E. pH-Induced Hysteretic Gating of Track-Etched Polycarbonate Membranes: Swelling/Deswelling Behavior of Polyelectrolyte Multilayers in Confined Geometry. J. AM. CHEM. SOC. **128**, 8521-8529, (2006).

44. Wang, Z., Heflin, J.R., Van Cott,K. Stolen, R. H., Ramachandran, S., Ghalmi, S., "Biosensors Employing Ionic Self-Assembled Multilayers Adsorbed on Long-Period Fiber Gratings,", Sensors and Actuators B **139**, 618-623 (2009).

45. Jain, V., Yochum, H., Wang, H., Montazami, R., Hurtado, M. A. V., Mendoza-Galvan, A., Gibson, H. W., Heflin, J. R., "Solid-state Electrochromic Devices via Ionic Self-Assembled Multilayers of a Polyviologen," Macromol. Chem. Phys. **209**, 150-157 (2008).

46. Hammond, P. T., "Formation of Polymer Microstructures by Selective Deposition of Polyion Multilayers using Patterned Self-Assembled Monolayers", Macromolecules, 28, 7569-7571, (1995).

47. Aviram, A., and ratner, M. A., Chem. Phys. Lett., **29**, 277 (1974)

48. Yancey, S. E., Zhong, W., Heflin, J. R., and Ritter, A. L., "The influence of void spaceon antireflection coating of silica nanoparticle self-assembled monolayers", Journal of Applied Physics, **99**, 034313 (2006).

49. Quanmin Guo and Fangsen Li, "Selff-assembled alkanethiol monolayers on gold surfaces, resolving the complex structure at the interface by STM", Phys. Chem. Chem Phys., **16**, 19074 – 19090, (2014).

50. N. Kang, A Erbe, and E. Scheer, "Electrical characterization of DNA in mechanically controlled break-junctions", New Journal of Physics, **10**, 2008.

51. Seung Woo Lee, Raymond G. Sanedrin, Byung-Keun Oh, and Chad A. Mirkin, "Nanostructured Polyelectrolyte Multilayer Organic Thin Films Generated via Parallel Dip-Pen Nanolithography", Adv., **17**, 2749–2753, 2005.

52. http://www.microchem.com/Tech-LithoTerms.htm

53. http://www.sigmaaldrich.com

Chapter 3

Experimental details

All of the work in this dissertation utilizes an atomic force microscope as a lithographic and imaging tool. Thus it is appropriate to describe in detail the principle and modes of operation of such a versatile device.

3.1 Atomic Force Microscopes (AFM):

The AFM was invented by Gerd Binning a few years after the invention of the scanning tunneling microscope (STM) by Binning and Heinrich Rohrer in Zurich in 1981.[(1)] The AFM is an imaging device that relies on the atomic force interactions between a very small, sharp tip, which has an average diameter of a few nanometers, and the surface of the scanned sample. The main idea behind the operation of the AFM is to record these interactions between the AFM tip and the surface and use that information in a variety of ways depending on the imaging mode in which the AFM is being used. AFM systems either have the tip or the sample to be scanned attached to a piezoelectric scanner that moves either the tip or the sample. The piezoelectric scanner receives its data from a feedback system that collects the interaction data between the tip and the surface. The manner in which the piezoelectric scanner moves and the data extracted from that depends again on the mode in which the AFM is being run and the parameters set to optimize the measurements. Piezoelectric scanners were traditionally made of three different piezoelectric crystals to control the motion of the scanner in three spatial dimensions. Piezoelectric crystals are used for this purpose because of the precision they offer in positioning the AFM tip or surface. The piezoelectric effect is the phenomenon that certain crystal materials such as quartz, lead titanate, lead zirconate

titanate and various other materials generate electric potential difference internally if they are subjected to strain. The inverse of this phenomenon is also exhibited by the same crystals where they change their shapes if they are subjected to electric potential differences. Modern AFM scanners use what is known as piezoelectric tubes. Piezoelectric tubes were developed in 1986 for the first time to be used on STMs.[18] Among the most commonly used materials to construct the piezoelectric tubes is lead zirconate titanate. The first step in preparing the tube is to have the material in powder form. The following step is to press the material in close packed cylindrical forms. Heating the material afterwards melts it and causes it to form a solid. However, cooling the material under such conditions causes the polycrystalline material to have random orientations for it dipoles. If the dipoles remain in such a random state they lack the ability to exhibit the desired piezeoelectric induced motion. To overcome this, the material is heated to 200 °C. A strong electric field is applied to the material to organize the dipole moments of the molecules. This process is known as polling the crystal. Once this is done, the piezoelectric tube has the ability to move under electric potential differences in three dimensions. For most AFMs ,the range of motion in the X and Y directions is around 100 µm and 10 µm in the Z direction. Figure (3.1) below shows a schematic diagram of a piezoelectric tube and its axes of motion.

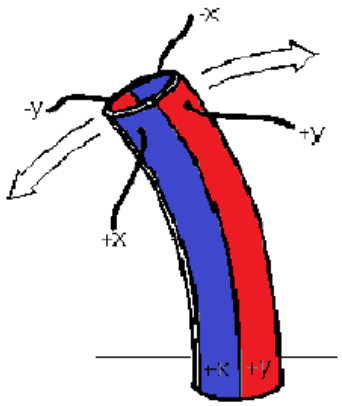

(a)

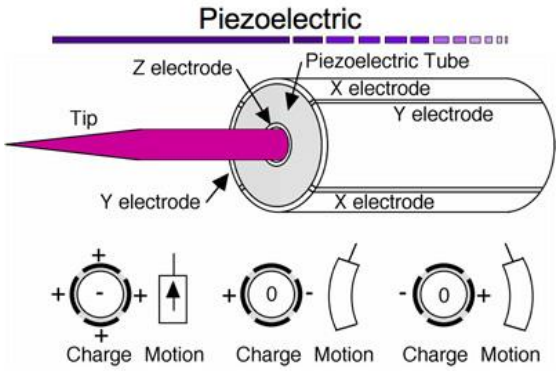

(b)

Figure (3.1): (a) A schematic diagram of the motion induced in a piezoelectric tube when potential difference is applied to its sides. The tube is divided into quarters and each diagonally opposite ones control the direction in one of the horizontal directions. (b): A diagram of a piezoelectric tube showing the electrodes in the Z-direction.[22] [Fair use]: http://chemistry.beloit.edu/edetc/SlideShow/slides/contents/scanning.html

The AFM tip can be made of a variety of materials including silicon, silicon nitride, and diamond. The tips can be used as they are or can be coated with conductive materials such as aluminum depending on the measurements to be done. Figure (3.2) shows images of different AFM tips and the substrates they are loaded on. These tips are then loaded into specially designed holders known as probe holders. These probe holders secure the tips in place and allow access to the surface to be imaged. Probe holders exist for a variety of designs to allow different types of measurements. Certain probe holders are designed to operate in air while others are designed to allow imaging in a liquid environment.

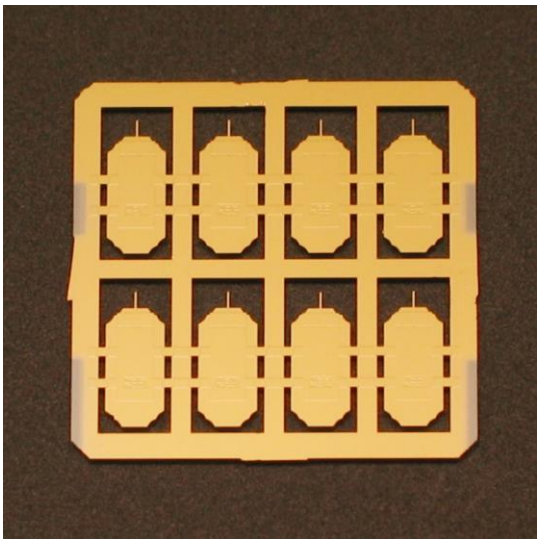

(a)

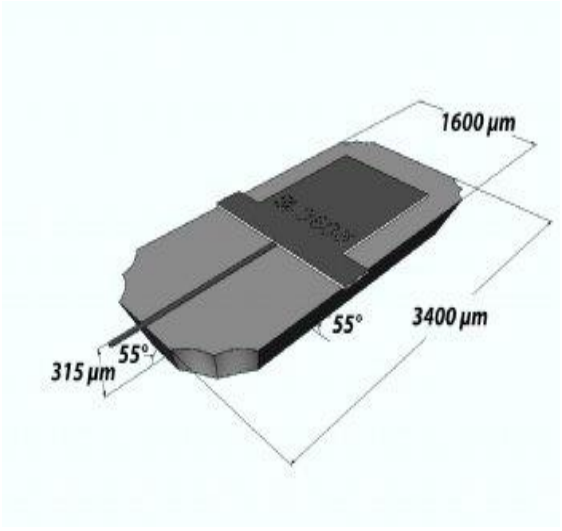

(b)

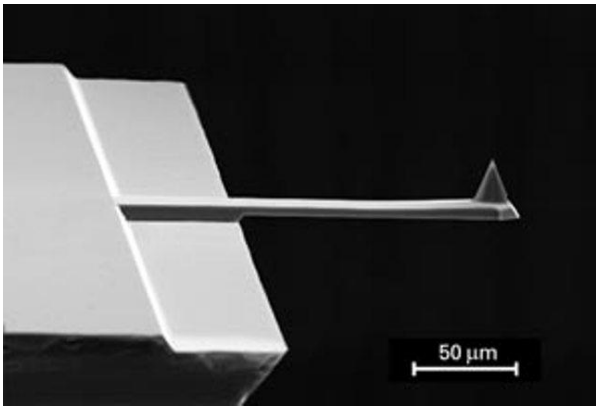

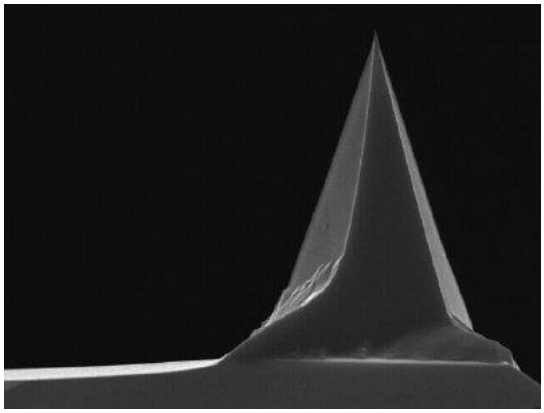

(c) (d)

Figure (3.2): Various pictures of AFM tips. (a) Gold coated AFM tips. (b) Schematic diagram illustrating the dimensions of a standard AFM tip. (c) and (d) Zoomed in pictures of AFM tips.[23] Reproduced with permission from: http://team-nanotec.de/index.cfm?fuseaction=show_product&productid=80

For the AFM to be able to image the surface of any given sample, the AFM tip has to be very close to the surface of the sample. This is done through what is known as an engaging process. When the tip has engaged the surface, the distance between them is such that a host of forces come into play and influence the interaction. Among the forces at play when the tip and surface are engaged are strong repulsive forces at very small separation distances, capillary attractive forces due to water molecules on the surface of the sample and van der Walls attractive forces at large distances. During the engaging process, the AFM tip is brought to a close proximity with the surface of the sample to be scanned. The average tip sample separation is between 0.1 nm to 10 nm.[2] Such a fine measure of

distance is achieved by shining a laser beam on the back of the tip and having it reflect to a designated detector cell. The detector cell is made of 4 photodiode cells. Figure (3.3) shows a simplified diagram of how an AFM works.

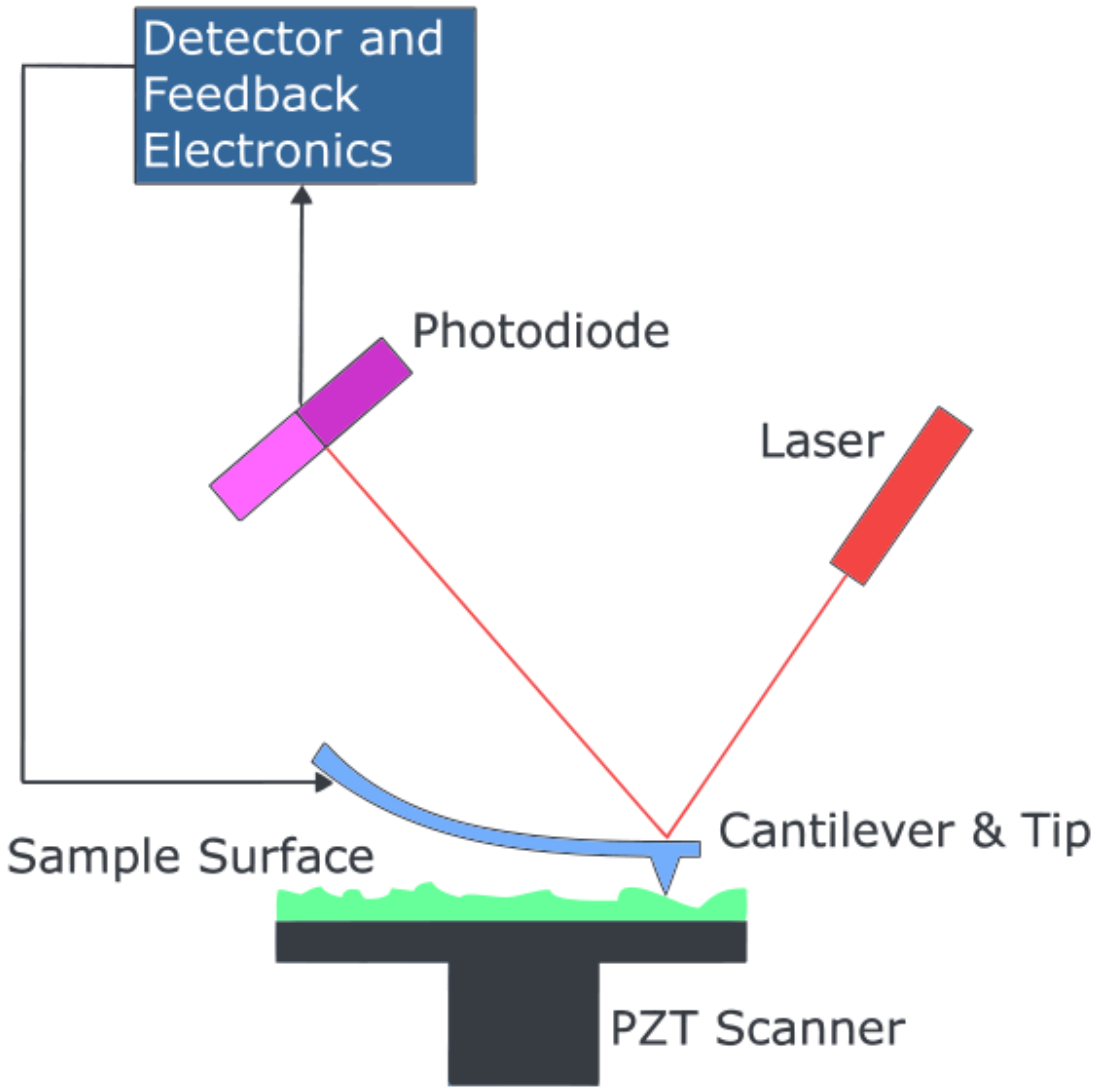

Figure (3.3): The Atomic Force Microscope has a tip made of silicon and etched by classical semiconductor cleanroom technology. The tip, which is installed on a cantilever that is on average 60 um wide reflects a laser beam that is shining on its back. The changes in the position of the reflected laser beam are used by a feedback loop to raise and lower the AFM head/stage to keep a constant distance between the tip and the sample. The data used to control the distance is then recorded and used to reproduce the topography of the surface of the sample.[24] [Public domain]:

http://en.wikipedia.org/wiki/Atomic_force_microscopy

The very small separation between the nanometer scale tip and the surface allows for atomic interactions between the material making up the surface of the sample and the AFM tip. Variations of amplitudes around 10^{-4} Å were reported measurable in the first paper detailing the invention of the AFM.[1] However, most commercially available AFMs are only capable of angstrom scale measurements. The interactions cause the reflected laser beam to change its location on the photodiode detector cell as the tip is deflected upwards or downwards. These changes in location of the reflected beam are then recorded, analyzed, and used by a feedback loop to redirect the imaging process according to a set of parameters that pertain to each imaging mode.

AFM imaging modes:

Contact mode:

In this imaging mode, the AFM tip is brought to very close proximity with the sample surface. The operational engaged distance for contact mode is on the order of angstroms. This mode is called contact mode because the atoms in the AFM tip and the atoms in the sample surface come into such close proximity that overlapping in electronic orbitals exists. The predominant force in contact mode is thus a repulsive force. AFM tips used for contact mode imaging are usually characterized by low spring constants such that the net force the tip exerts on the surface being imaged is less than the interatomic forces between the atoms in the surface. As we set the AFM to operate in this mode ,we have to set a few parameters to optimize its performance depending on the sample being imaged. One of the first parameters considered is the deflection level. This is set by deciding the position of

the reflected laser before it engages the surface. The photodiode detector is made of four different cells designed as shown in Figure (3.4)

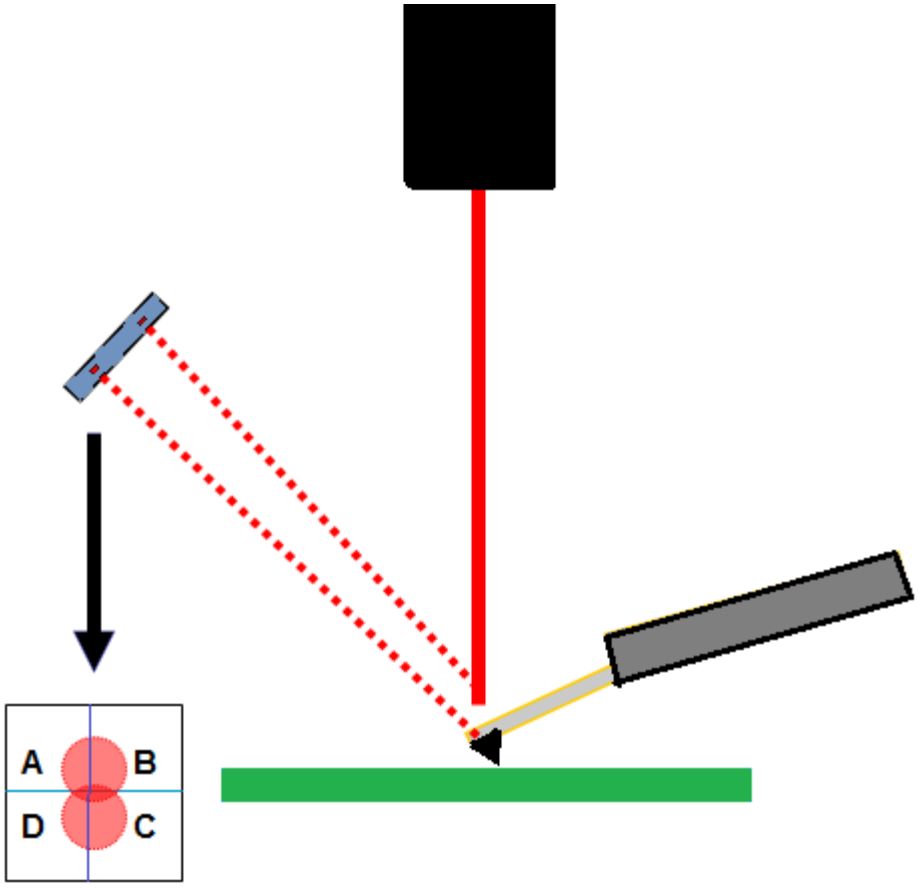

Figure (3.4): The laser beam reflected from the back of the cantilever holding the AFM tip is received on a photodiode detector made out of 4 individual cells. The relative position on the photodiode cells is used to operate the AFM and direct the piezoelectric scanner of the AFM.[25] [Fair use]: http://web.physics.ucsb.edu/~hhansma/biomolecules.htm

The original deflection point is defined by the position of the reflected laser beam with respect to the top quadrants and the lower two quadrants on the photodiode detector. If the spot is originally set more on the lower two quadrants, this will mean that we have set the

deflection to point to a negative value. The lower the position of the deflected spot becomes, the more negative the value it has. The second parameter to be determined is the set point. When the AFM tip approaches the surface of the sample it experiences a variety of forces as we discussed above. Figure (3.5) shows the progression of these forces as the tip approaches the surface. When the AFM tip is brought close enough to the surface for them to be in contact, it will start experiencing a repulsive force that will deflect the tip upwards. Once the tip is deflected upwards, the reflected spot on the photodiode will move upwards as well. The parameter "set point" determines at which level of deflection is the AFM considered engaged and the approaching action between the tip and surface is to be stopped. The difference between the set point and the deflection point determines how much force is exerted by any tip on the surface being imaged.

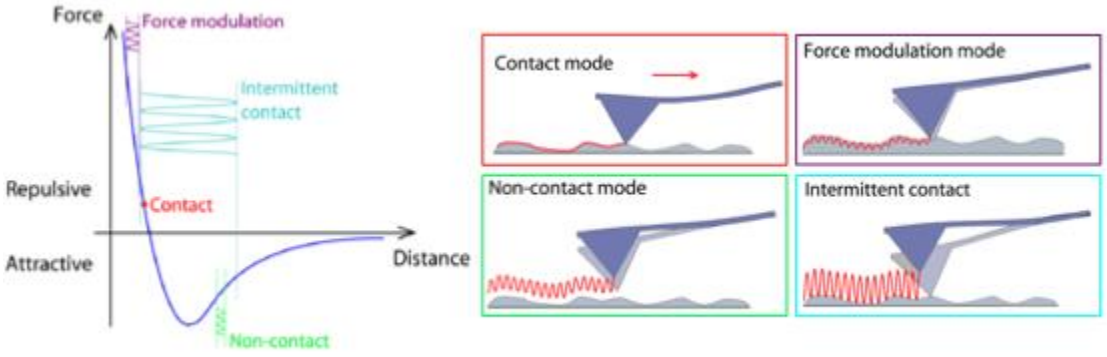

Figure (3.5): Force – Distance curve of a typical AFM tip approaching the surface to be imaged. At large distances the tip experiences weak attractive forces that keep increasing as the tip approaches the surface. When the tip comes closer to the surface the attractive forces start getting stronger due to contributions from the capillary forces from the water layer forming on the sample surface. These forces are around 10^{-8}N. As the tip keeps approaching the surface it experiences strong repulsive forces and starts deflecting away from the surface.[26] [Fair use]: http://www-liphy.ujf-grenoble.fr/Microscopie-a-force-atomique-AFM

Once the tip is deflected enough for the reflected laser spot to reach the set point on the diode, the AFM is considered engaged and it starts imaging the surface. The imaging is done by biasing the piezoelectric scanner such that it oscillates in the X and Y direction in a manner that allows the tip to raster the surface. The direction and speed with which the tip moves across the surface are subject to determination based on the application. In most cases, when using the AFM in contact mode, the tip moves in the manner depicted in Figure (3.6).

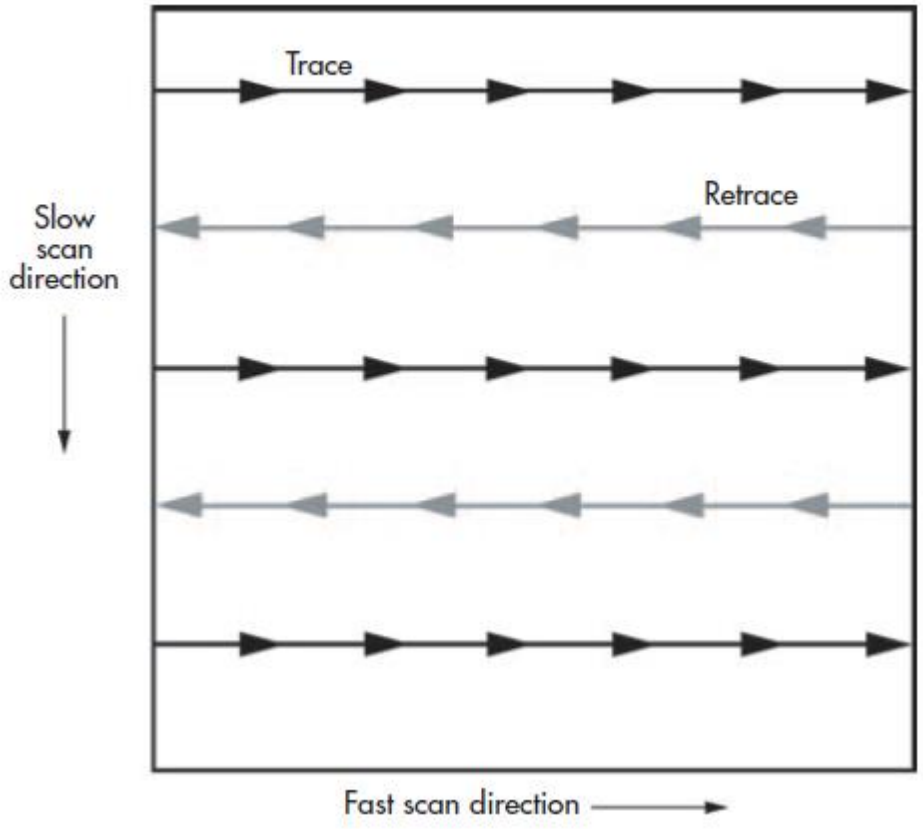

Figure (3.6): The trace and retrace motion of the AFM scanner as it scans the surface of the sample.[19] Reproduced with permission from: A Practical Guide to Scanning Probe Microscopy. A training and user manual by Bruker®

Contact mode is known for the high resolution it provides. However, it is an unsuitable technique for softer samples since it exerts a relatively large force constantly on the sample. This mode can be used in two different manners. In the first one, called constant deflection mode, we operate the AFM in contact mode with the feedback loop turned on. In this case, as the tip scans across the surface, the interactions between the tip and the sample surface will cause the tip to deflect up and down. As this is registered by the photodiode detector, it feeds this information into the feedback system to control the piezoelectric scanner such that it either extends or retracts so that the deflection of the tip stays the same throughout the scanning process. The signals used to control the piezoelectric scanner are then compiled and used to produce a topographic map of the surface of the sample. The second manner in which we can run contact mode, called constant height mode, depends on having the feedback loop being turned off. In this mode, we engage the tip until it reaches the predetermined set point of deflection. That will indicate a certain separation between the tip and the sample. Once the tip has engaged the sample, we start scanning. While the tip gets deflected up and down due to interactions with the sample surface, we record the changes in the position of the reflected laser spot on the photodiode. These changes are later used to reconstruct a topographic map of the sample surface. This mode of operating the AFM is known for the very high resolution down to the atomic level it provides. The high resolution observed in this mode is to the absence of noise signals resulting from moving the scanner up and down in the Z direction. However, this mode of operating the AFM is only possible if the sample is very flat, otherwise we run the risk of breaking the AFM tip or damaging the sample due to any possible crashes caused by large topographic changes. The topographic images that can be produced from this mode include images that

characterize heights that may not resemble the accurate shape of the objects being imaged. Another type of image is possible to extract from this mode of imaging that has better resemblance to the shape being imaged. This type of image is known as a deflection error image. It depends on calculating the difference between the deflection point and the set point and using that to produce what is known as an error image. These error images are known for outlining the shapes of the objects properly. Another way of extracting information from contact mode is to record what are known as friction images. These images depend on recording the torsional oscillations that the tip experiences while it is scanning the surface. This is done by comparing the changes in the distribution of the reflected laser point on the photodiode between the right and left halves of the detector. To maximize these torsional effects, the tip is set to raster the surface in a direction that is 90° perpendicular to what is shown in Figure (3.6). These images provide qualitative information about the friction that different regions of the scanned surface have with the tip. Such friction can be due to different chemical groups or electric charges. We use these type of images in this dissertation. The way friction and lateral force imaging forces are recorded is shown in the schematic diagram shown in Figure (3.7).

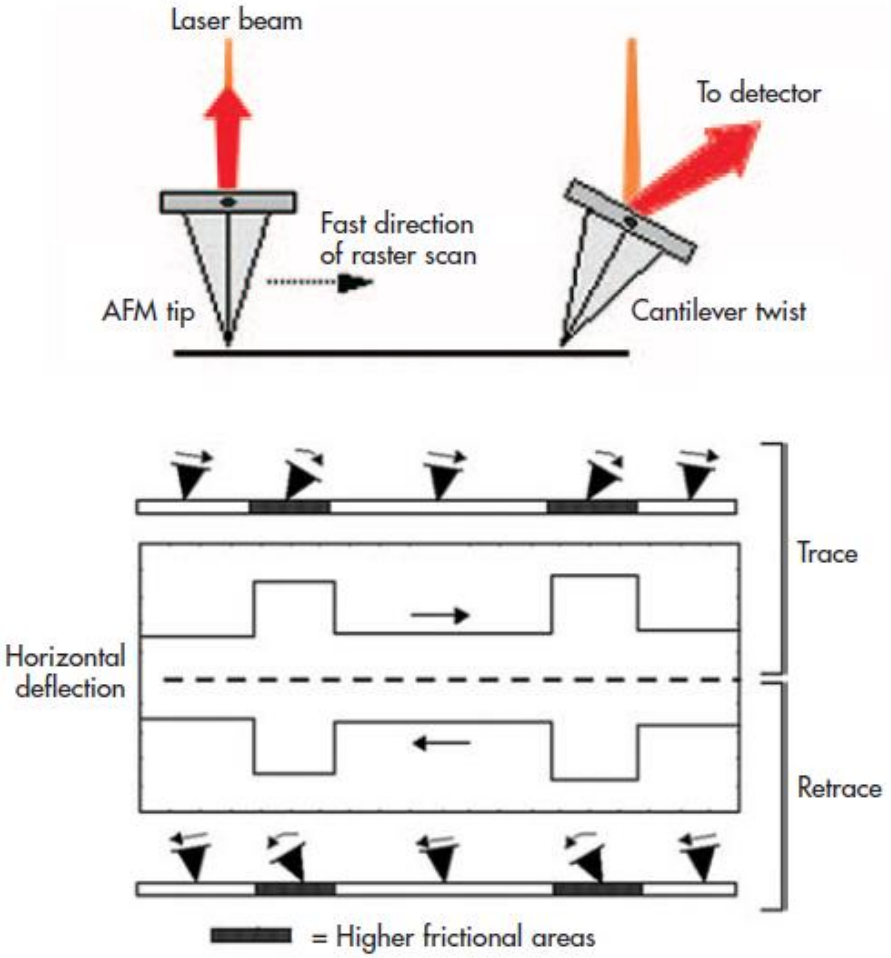

Figure (3.7): When the AFM scanner scans the surface in a direction that is 90° with respect to the normal imaging direction, the interactions between the molecules on the surface and the AFM tip causes the cantilever carrying the tip to oscillate. These oscillations are recorded and information is extracted from it about the friction properties of the surface.[19] Reproduced with permission from: A Practical Guide to Scanning Probe Microscopy. A training and user manual by Bruker®

Tapping mode:

In tapping mode, the AFM tip is brought to within a few hundred nanometers of the surface of the sample. In this mode, the AFM tip is oscillated near its resonant frequency at an optimum amplitude. The oscillations are achieved using a piezoelectric element placed in

the probe holder. The tips used for this mode of imaging are characterized with higher spring constant to prevent them from oscillating out of control with large amplitudes. The spring constants for tips used for tapping mode imaging range between 20 N/m to 120 N/m. The amplitudes of oscillations are usually on the order of tens of nanometers. As the tip scans the surface while it is oscillating, the changes in the topography of the surface will affect the amplitude of the oscillation. Monitoring these changes and using this data through the feedback loop to extend or contract the piezoelectric scanner to minimize these changes produces a topographic map of the surface of the sample. When the parameters are set properly for this imaging mode, the forces exerted by the tip on the surface can be minimized. The parameters essential for this force minimization are the amplitude of the oscillation and the set point of the reflected laser point. Making the oscillation amplitude larger than what is optimally chosen by the software running the AFM causes large forces to be exerted on the samples and can cause severe damage to the sample surface. Manipulating the set point manually can also lead to brining the tip too close to the sample and thus leading to possible damage of the sample surface. Among the advantages of this imaging mode is that it avoids lateral forces that can disrupt the imaging and reduce the resolution of the images. Another advantage of tapping mode is that it avoids the attractive force near the surface due to the very thin layer of water that gets formed on the sample surface in ambient conditions. Monitoring the rate of change of the oscillation amplitude as a function of position on the sample allows for the extraction of what are known as amplitude images. These images belong to what is known as error images and give slopes of the objects being imaged thus leading to more accurate images. Another type of information that can be extracted from tapping mode scans are known as phase images. In

producing phase images, the errors that happen in the phases of oscillation of the tip compared to what it is supposed to be, due to attractive or repulsive forces when the tip is near the surface while oscillating are observed and used to produce a map that depicts the different types of interactions the tip has with the sample surface. Phase images contain information about the softness or stiffness of the different parts of the sample.

Non-contact mode:

This is another mode of imaging that depends on oscillating the tip near its resonant frequency. In this mode, the separation distance between the tip and the sample surface is larger than it is in contact mode but much smaller than it is in tapping mode. The tip – sample separation in this mode is between tens to hundreds of angstroms. The oscillation amplitudes are also between tens to hundreds of angstroms. In this imaging mode, the smallest separation between the tip and the surface is larger than both in tapping and contact modes. Keeping the distance relatively large between the tip and the surface prevents the strong repulsive forces from interacting with the tip. In this mode of imaging, the system monitors both the amplitude and frequency of oscillation of the tip. Any changes in either the amplitude or the frequency are used through the feedback system to control the piezoelectric scanner in the Z direction as to minimize these effects and maintain the original amplitude and frequency of oscillation.

Figure (3.8) shows a schematic of both contact and tapping mode imaging for AFM systems.

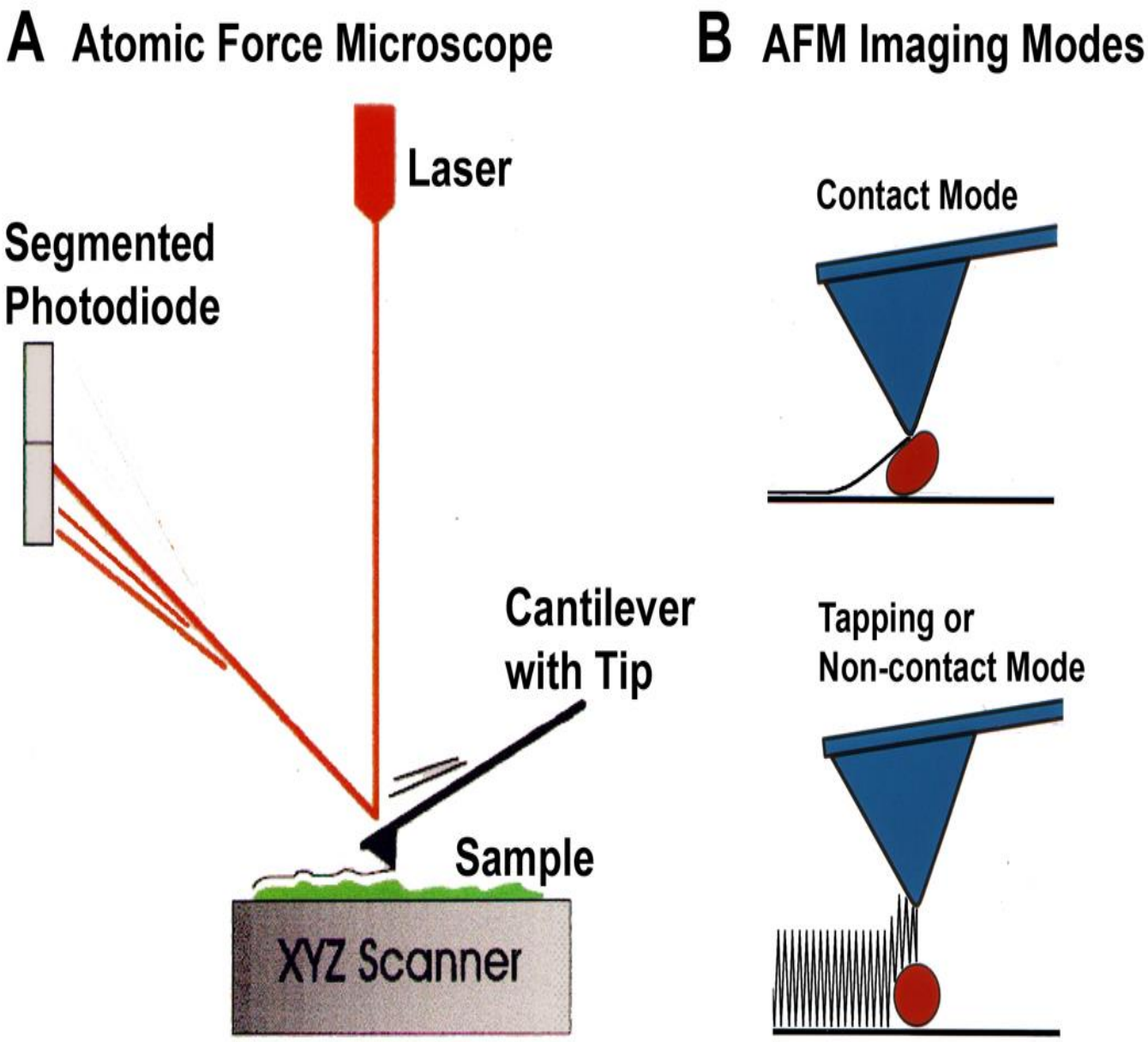

Figure (3.8): A) The general mechanism of the Atomic Force Microscope operation. B) The two modes of operation for an AFM. Contact mode where a constant distance is maintained between the AFM tip and the surface and adjustments are made to the system to maintain that distance. The second mode depicted is the tapping mode, which depends on vibrating the AFM tip at its resonance frequency and monitoring disturbances in the amplitude of the oscillations resulting from interactions between the tip and the surface and using this information to maintain the oscillation amplitude at a constant value. [Fair use]: http://web.physics.ucsb.edu/~hhansma/biomolecules.htm

The AFM systems used in our work

MultiMode® AFM system

Figure (3.9) shows the MultiMode® AFM system that was used in parts of our work. It is a very versatile system capable of performing contact, tapping, and non-contact imaging. It employs a variety of scanners that can be used one at a time. The ranges for scanning vary from 10 µm X 10 µm in the XY direction and 2.5 µm in the Z direction to 40 µm X 40 µm in the XY directions and 15 µm in the Z direction. The different scanners offered varied ranges of resolution and suitability for different imaging needs and scanned areas. Samples are inserted on top of the scanners in this particular system, and the scanner controls the position of the sample and controls the separation between it and the tip. In other words, when the system is engaging, it brings the sample up to the tip. When the system is imaging, it moves the sample with respect to the tip. The system is mounted on a pneumatic vibration isolation table. It also comes with a tripod carrier system that offers vibration insulation along with a vibration dampening cover for performing high resolution imaging. This system is known for the high resolution capabilities. This system was used in the early part of our work on selective deposition using thiols and gold substrates. Due to the absence of a closed loop feedback system on this system, it lacked accurate repositioning of the tip on the sample in repeated scanning efforts. Such accuracy is crucial for lithography work. The sample holder on this system requires the samples to be cut down to 4 mm X 4mm or smaller in order for them to fit inside the optical head.

Figure (3.9): The MultiMode AFM system. It is capable of performing contact, non-contact, and tapping mode imaging. It utilizes a Veeco IV controller. This system is known for the high resolution it offers.[20] Reproduced with permission from: www.bruker.com

Dimension Icon®:

Figure (3.10) shows the Dimension Icon® AFM system we used for the majority of our work in this dissertation. The scanner in this system controls the position of the tip while the sample remains stationary on the sample chuck underneath the AFM head that contains the scanner. This system comes with one scanner. The scanner used in this system has and XY range of 90 µm X 90 µm. The Z range for this system is 13.5 µm. This system is capable of a variety of imaging modes and probing techniques. Among the imaging modes that can be performed on this system are contact, tapping, non-contact, lateral force, electric force microscopy, electric potential microscopy, and magnetic force microscopy modes. This system is also capable of performing nanolithography, nanoindentation, and nanomanipulation procedures. These later set of procedures provide a host of nanomanipulation tools starting from mechanically modifying the surfaces of the system and ending with chemically modifying the sample surface on a few nanometer scale. The

system comes with a pneumatic vibration insulation table operated with compressed air to minimize the vibrational noise from the floor. The system also has an optional vibration insulation hood. Due to difficulty in securing extra funds for the insulation hood we designed and built our own. The system is known for its high precision in the repositioning of the tip to selected areas on the surface. The sample holding chuck on this system is designed to hold a full silicon wafer without need for cutting or reshaping the sample.

Figure (3.10): Dimension Icon® is an AFM system that offers great nanoscale manipulation tools. It is equipped with a closed-loop scanner offering great precision for repositioning the tip on the sample. It has a piezo scanner based on a piezotube.[20] Reproduced with permission from: www.bruker.com

Probe holders for AFM systems:

Several types of AFM tip holders exist to accommodate the various needs for imaging different samples. One of the main classes of probe holders that are widely used are probe holders that are functional in air or gas. Figure (3.11) shows a few of the available holders functional in air or gaseous environment. These probe holders are capable of performing both contact and tapping

mode imaging. The probe holder has a specially designed groove for the AFM tip to slide into and to be fastened in place securely with maximal exposure to both the laser beam to reflect from the back of the cantilever and for the tip to reach the surface without any obstructions. The probe loading into the probe holder is one of the most delicate tasks one has to perform manually while dealing with the AFM. The probe holders employ spring loaded mechanisms to keep the tip secure. Handling a small tip manually whose largest dimension is a fraction of a millimeter and securing it in place in a spring loaded holder can prove challenging.

(a) (b)

Figure (3.11): (a): A probe holder that can be used with a MultiMode® system. After the tip is loaded into the holder, the holder gets loaded into an optical system that holds in place directly over the piezoelectric scanner. (b): A probe holder that fits on the Dimension Icon® system. The system employs a spring loaded lever system to hold the tip in place. This holder fits directly on the piezoelectric scanner.[20] Reproduced with permission from: www.bruker.com

Liquid probe holders (liquid cells):

Another class of probe holders used with AFM systems is known as liquid cell probe holders. To overcome the problem caused by the thin layer of water on top of the imaged surfaces, AFMs have been developed to image in liquid environments. By submerging the tip and the sample in a liquid environment, such a problem as the distortion caused by capillary forces is circumvented. Liquid cells are AFM probe holders that provide containment for the liquids and the tips while protecting the AFM scanners and electronics from the damage that can be caused by the liquids used during the imaging. Given that the largest area that can be scanned at any one time by the AFM is normally less than 100 µm X 100 µm, liquid cells have small enclosures for the liquid and the small part of the surface to be imaged. Figure (3.12) shows two different liquid cells that were used in our work. Both probes shown in the figure are capable of performing contact and tapping mode measurements. The method by which the cell performs this enclosure of the liquid and tip differs between the two cells. The cell used with the MultiMode® AFM houses the tip and employs a spring loaded system to fasten it in place. It also has an O-ring that seals the liquid inside it between the transparent top where the tip is and the sample surface, which forms the bottom of the enclosure. A tubing system is then used to pump the liquid in and out of the cell. The tip is mounted inside the cell without any liquid present and then the whole liquid cell goes into the optical system, which then gets mounted on top of the piezoelectric scanner. Once it is fastened in place, we start bringing the tip and the surface closer to each other. A tubing system is then used to pump the liquid in and out of the cell when the O-ring has sealed any separation between the cell and the surface of the sample. Special considerations must be taken for the kind of liquids that can be used in the liquid cell. Any corrosive liquids, solvents, or acids are very dangerous for the system as they leak out of the cell and can easily ruin the piezoelectric scanner.

(a)

(b)

Figure (3.12): (a) liquid cell used with the MultiMode® system. This cell encloses the liquid and the AFM tip inside it and employs an O-ring to seal the liquid against the sample surface. (b): Liquid cell used with the Dimension Icon®. This cell houses the AFM tip and uses the surface tension in liquids like water to form a droplet of liquid around the tip and then image the surface through this liquid droplet when the cell and the surface are brought closer together. Using this cell with liquids that have low surface tension has proven nearly impossible.[20] Reproduced with permission from: www.Bruker.com.

The cell used with the Dimension Icon® is used in a slightly different manner than the previous one. In this case, the cell depends on using the surface tension between in the liquid used in the imaging to form a droplet that will be shared with the surface to be imaged. This droplet of liquid functions as the liquid medium. The tip is loaded while the cell is dry. The cell is mounted on the scanning head of the Dimension Icon®. Then a protective sleeve is placed on top of the liquid cell and the scanning head to protect the head from any damage. After that the tip is brought close to the surface to within a fraction of a millimeter. The next step is to use a micropipette to put a droplet of the liquid on the cell and to place the scanning head with the cell mounted on it back in its place. This makes the droplet shared between the cell and the surface as a liquid medium for the scanning. This later form of liquid cell performs very poorly when the liquid to be used has

very small surface tension. To be able to perform our experiments using a Dimension Icon® liquid cell, we had to use a small container that functioned as a liquid container for the liquid cell submersion. We had to resort to this measure since some of our work was performed in liquids like ethanol and toluene.

AFM artifacts:

Due to the geometry of the AFM tips, they can influence how the images produced resemble the actual shapes being imaged. Figure (3.13) shows some of the artifacts that can be seen in an AFM image that do not correspond to the shape of the imaged object.

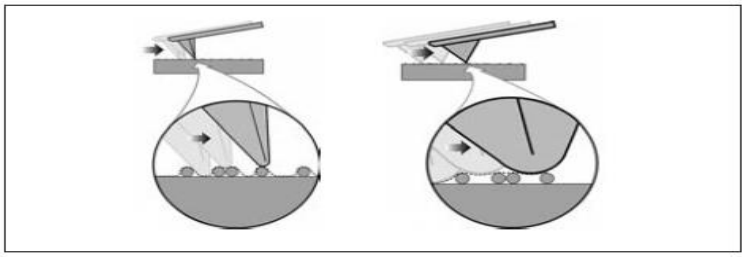

(a)

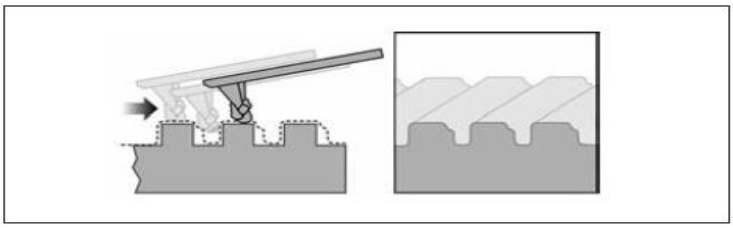

(b)

Figure (3.13): (a) The shape and size of the AFM tip affects how we see the objects it scans. (b) If the tip becomes dirty it can produce inaccurate images.[19] Reproduced with permission from: A Practical Guide to Scanning Probe Microscopy. A training and user manual by Bruker®

3.1.1 Nanoshaving and Nanografting

Nanoshaving and nangrafting were reported for the first time in 1996 by Song Xu and Gang-Yu Liu.[3] Both nanoshaving and nanografting are performed on self-assembled monolayers. Self-assembled monolayers are single layers of molecules such as thiols or silanes that arrange themselves on the surface of selected substrates due to electrostatic interactions and other secondary effects like hydrophobicity and hydrophilicity of the molecules forming the monolayer.[4],[5],[6] The nanoshaving process is performed by applying a large force on the AFM tip once it is in contact with the surface that we need to pattern. Once the applied force crosses a certain threshold, the bonds between the molecules and the surface will be broken for the molecules under the AFM tip.[3] Such dislocation or "shaving" of the molecules will expose the underlying substrate. This establishes a pattern based on the height difference between the molecules that form the monolayer on the substrate and the exposed substrate. Figure (3.14) shows an illustration of how nanoshaving works.

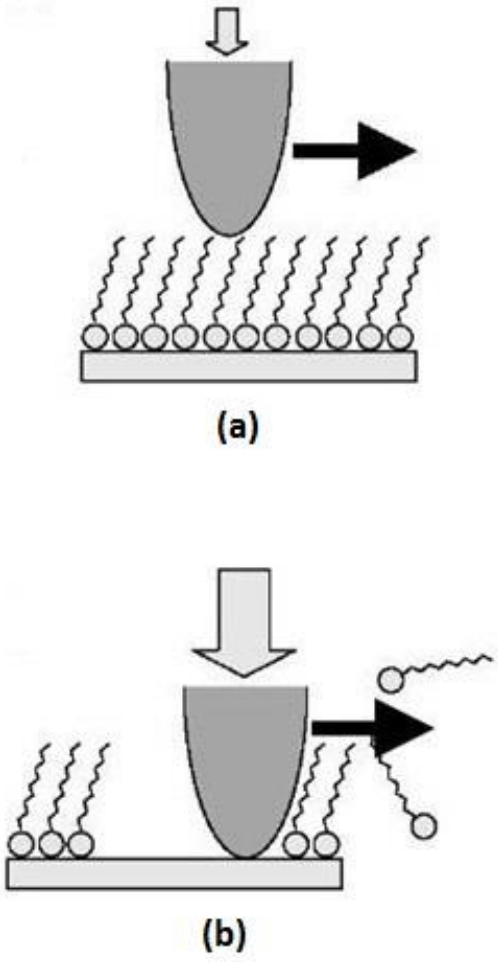

Figure (3.14): Nanoshaving is a process in which a large force is applied to the AFM tip while it is in contact with the surface being imaged. Once the force crosses a certain limit, molecules from the underlying monolayer are forced out of place exposing the substrate underneath.[7] [Fair use]: Gang-Yu Liu,* Song Xu, and Yile Qian, "Nanofabrication of Self-Assembled Monolayers Using Scanning Probe Lithography", Acc. Chem. Res. 33, 457-466, (2000)

In the nanografting process, the nanoshaving step is performed while the substrate is immersed in a medium containing molecules from another chemical species. The chemical in the solution surrounding the substrate is intended to replace the regions of the monolayer that were removed from the substrate. Once the AFM is in contact with the surface while the tip and the substrate are

submerged inside a medium containing the replacement molecules, the force applied to the AFM is increased. Once the threshold is reached, molecules from the monolayer deposited on the substrate are removed and replaced by molecules from the ambient solution. Figure (3.15) below shows a schematic diagram of nanografting.

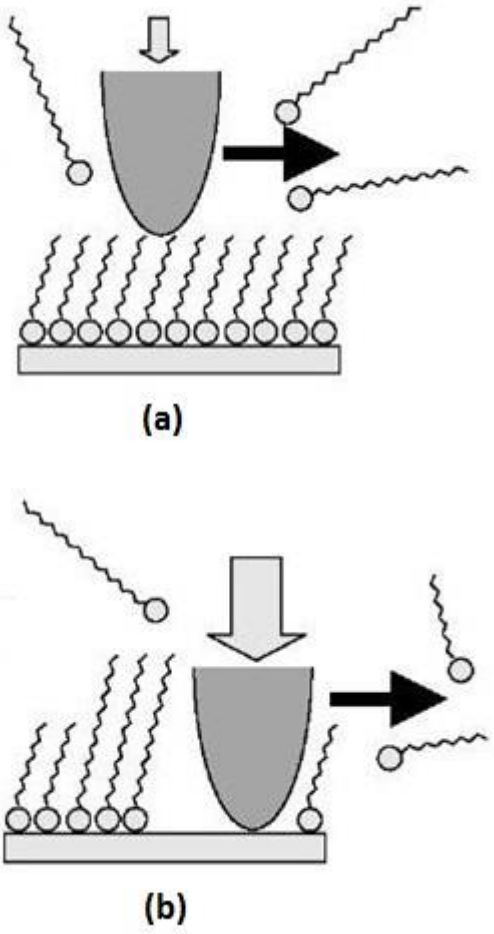

Figure (3.15): The first step in the nanografting process is to bring the AFM tip into contact with the surface and the monolayer deposited on it in a liquid medium containing a different chemical than the one deposited on substrate. For this initial contact, the AFM is being run in the imaging mode so minimal force is applied as to avoid damaging the monolayer. Once the force applied to the AFM tip is increased beyond a certain limit, the molecules under the AFM tip will be forced out of their place. The empty places in the monolayer will be occupied by different molecules from the ambient solution.[7] [Fair use]: Gang-Yu Liu,* Song Xu, and Yile Qian, "Nanofabrication of Self-Assembled Monolayers Using Scanning Probe Lithography", Acc. Chem. Res. 33, 457-466, (2000)

In the earliest work by Song Xu and Gang-Yu Liu[3] on nanoshaving and nanografting, they demonstrated both mechanisms successfully by grafting patches of octadecanethiols ($C_{18}S$) into a background matrix of decanethiols ($C_{10}S$) deposited on a gold substrate. The grafted patches were in the form of rectangular areas 3 X 5 nm in size. Figure (3.16) shows their successful results.

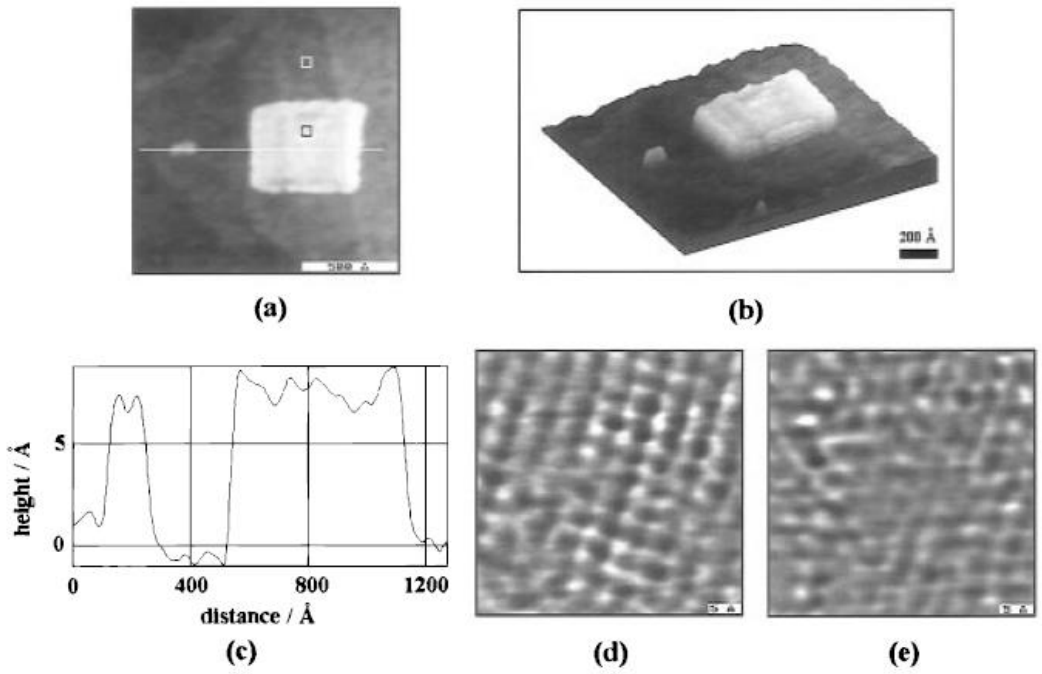

Figure (3.16): (a) A square grafted of $C_{18}S$ into a background of $C_{10}S$. The size of the square is 50 X 50 nm^2. (b) A 3-D rendition of the topographic map collected by the AFM during imaging. (c) Height profile of the grafted patterns. The height difference between the grafted areas and the background is 8.8 Å which is consistent with the theoretical value for the difference in the length between the chains for $C_{10}S$ in the background and $C_{18}S$ in the grafted patches. (d) and (e) Molecular resolution images obtained using an AFM of an area of 5 X 5 nm^2 from the matrix of $C_{10}S$ and the grafted patch $C_{18}S$ respectively.[3] [Fair use]: Song Xu and Gang-Yu Liu, "Nanometer-Scale Fabrication by Simultaneous Nanoshaving and Molecular Self-Assembly", Langmuir 13, 127-129, (1997).

A prominent application of nanografting is in the immobilization of DNA molecules and antibodies on selectively patterned areas to construct biosensors and bio-analysis experiments.

Scoles and co-workers used AFM nanografting to graft single-strand DNA into a background monolayer matrix of ethylene glycol, which was used to functionalize a gold surface. These patterned patches are then used to bind with cDNA-conjugated proteins. The procedure starts by functionalizing a clean gold surface with protein-repellent ethylene glycol terminated alkylthiol ($HS\text{-}(CH_2)_{11}\text{-}OCH_2CH_2)_3\text{-}OH$). Then the authors utilize nanografting to introduce patches of single strand DNA into the ethylene glycol background. When the patterned substrates are exposed to proteins modified with cDNA sequences, the proteins are immobilized on the patterned areas generating a ready to use biosensor for binding studies in biological systems.

Figure (3.17) shows the procedure for nanografting single strand DNA molecules into the alkylthiol background and the immobilization of cDNA-modified proteins.[21]

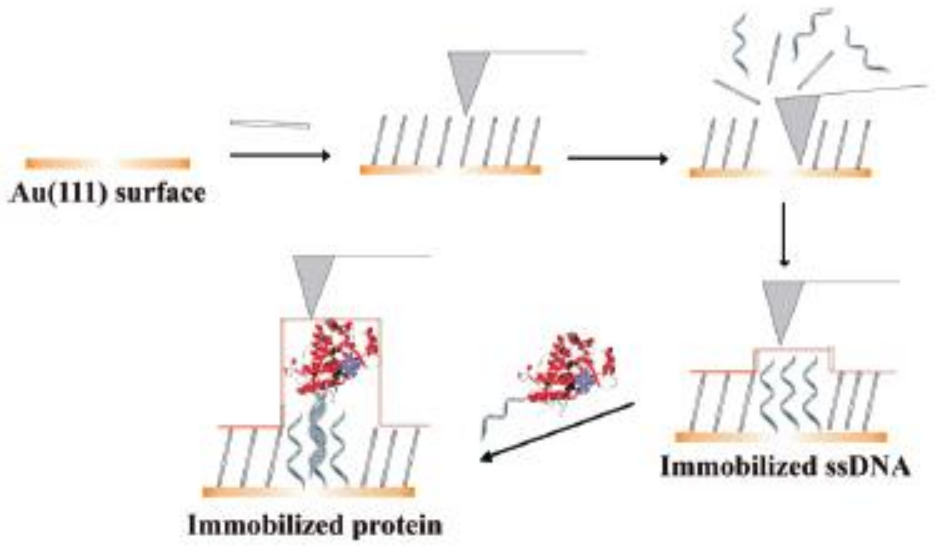

Figure (3.17): The immobilization of single strand DNA molecules is carried out by using AFM based nanografting. The next step is to allow cDNA modified proteins to attach to the immobilized single strand DNA molecules.[21] [Fair use]: Bano, F., Fruk, L., Sanavio, B., Gelletteberg, M., Casalis, L., Niemeyer, C. M., Scoles, G., "Toward Multiple Protein Nanoarrays Using Nanografting and DNA Immobilization of Proteins". Nano Letters, Vol 7, No 9, 2614-2618, (2009)

When the group used covalent DNA streptavidin conjugate (D1-STV) to immobilize and bind with anti-STV IgG, the height measurements using the AFM revealed measurable height differences corresponding to the sizes of the molecules trapped. Figure (3.18) shows the results of this experiment.[21]

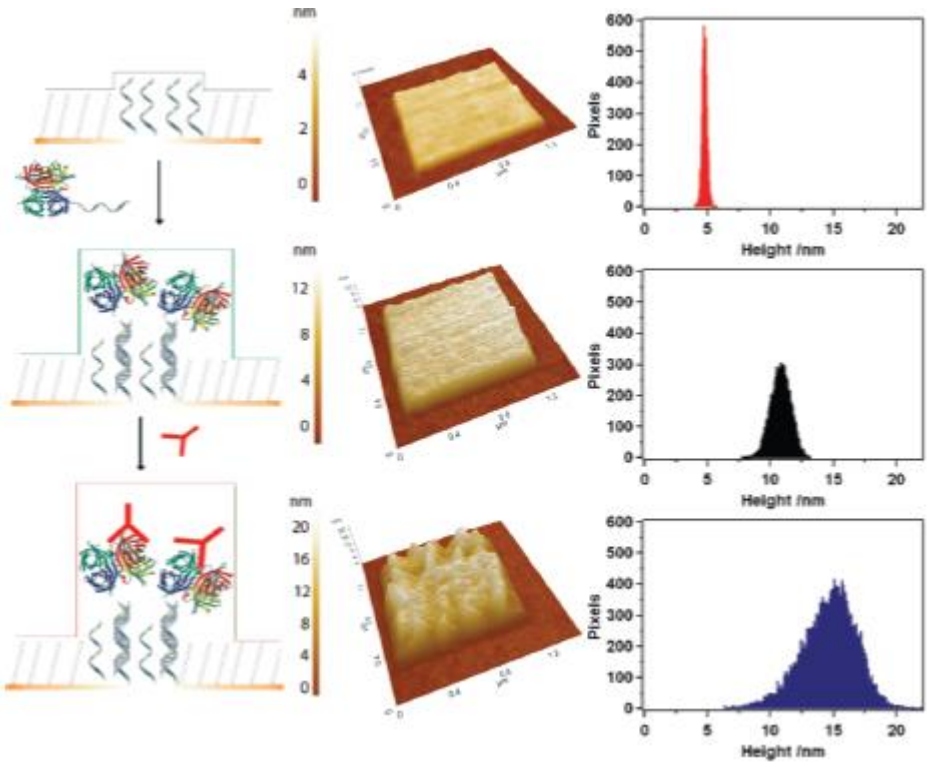

Figure (3.18): A schematic diagram showing the process of immobilizing D1-STV in patches in a background of ethylene glycol terminated alkylthiol followed by allowing anti-STV IgG combined with height measurement histograms for the different steps.[21] [Fair use]: Bano, F., Fruk, L., Sanavio, B., Gelletteberg, M., Casalis, L., Niemeyer, C. M., Scoles, G., "Toward Multiple Protein Nanoarrays Using Nanografting and DNA Immobilization of Proteins". Nano Letters, Vol 7, No 9, 2614-2618, (2009)

3.1.2 Surface electrochemical modification

Surface electrochemical modification is another method of nanopatterning that utilizes AFM systems.[8] In this method, a potential difference is applied between the AFM tip and the surface

of the sample. For this particular method, the AFM tips used are covered with conductive coatings such as aluminum or gold. When the AFM tip is brought in "contact" with the surface of the substrate and the monolayer covering it, a meniscal droplet of water forms between the tip and the surface. The possibility of forming this water droplet and its resultant size are dependent on the relative humidity in the ambient atmosphere in which the experiment is being conducted[8],[9],[10] By applying a potential difference between the AFM tip and the monolayer covering the substrate, a change in the chemistry of the monolayer, either oxidation or reduction, can be induced. This change in the chemistry of the areas scanned by the AFM while under such potential difference establishes the pattern desired by the designer. Figure (3.19) below shows a schematic diagram of how this process occurs.

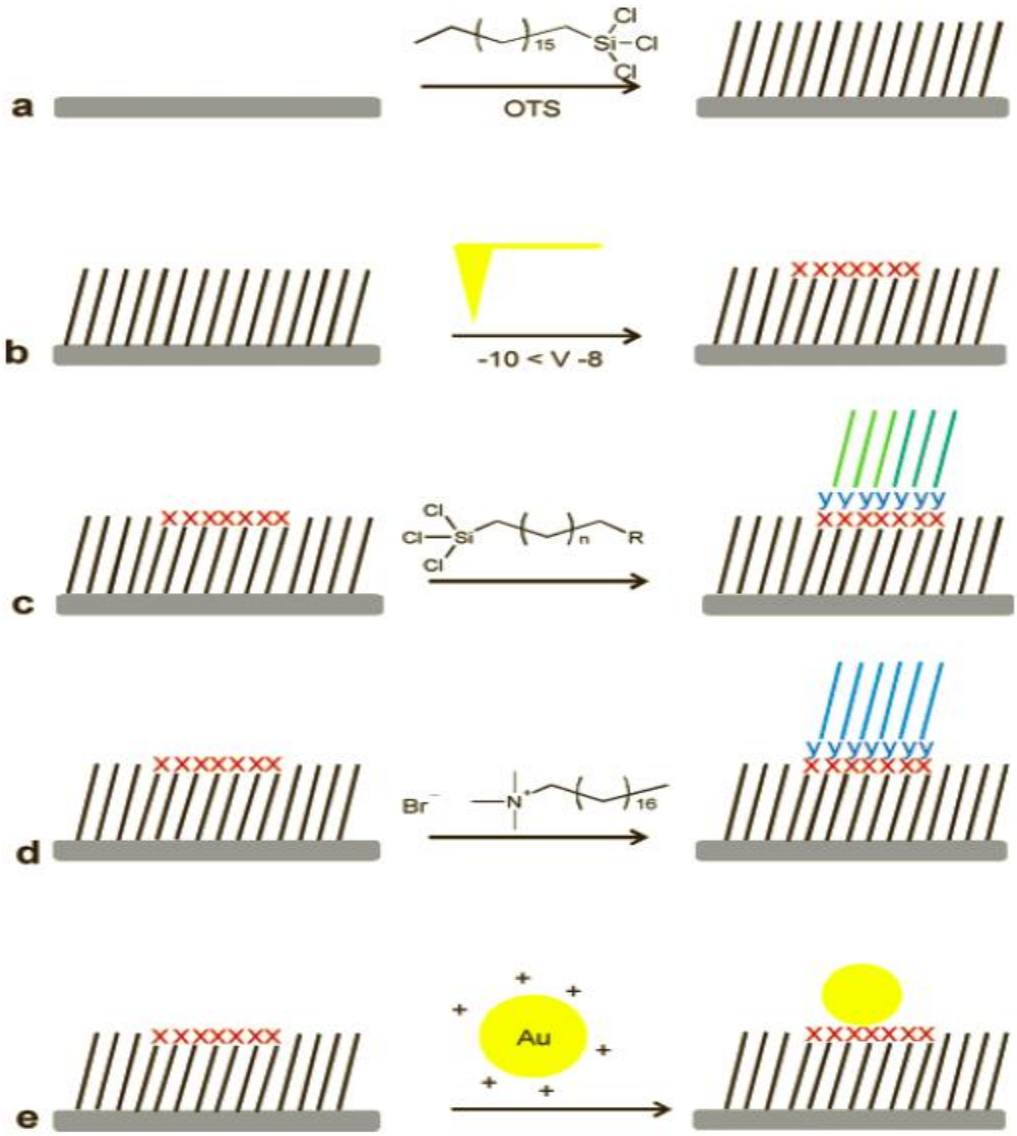

Figure (3.19): Steps of surface electrochemical modification using an atomic force microscope.[9] (a) Functionalization of a silicon substrate with octadecyl trichlorosilane (OTS). This silane is terminated with methyl functional group. (b) Using the AFM probe to oxidize the SAM (by applying negative potential to the AFM tip between -8 V and -10 V results in changing the functional group into a carboxylic group represented here by X. (c) One of the experiments carried was to allow OTS to bind with the functionalized patterns. R = CH_2 and n = 9. R becomes y as the OTS binds with the oxidized pattern. (d) Another variation of the experiment is to allow is to allow 11 – undecyl tricholorosilane (UTS) to bind with the oxidized patterns. (e) Another variation of the experiment is to have positively charged gold nanoparticles attach to the oxidized patterns.[9] [Fair use]: Daan Wouters and Ulrich S. Schubert, "Constructive Nanolithography and Nanochemistry: Local Probe Oxidation and Chemical Modification", Langmuir 19, 9033-9038, (2003).

Another way of using electrochemical modification is to oxidize silicon substrates in certain patterns such that when they are subjected to wet acid etching, the oxidized parts act as protective masks protecting the layers underneath them from being etched away by the acid. Such a technique can establish three-dimensional patterns in silicon substrates on the order of 30 nm. Kakooei and co-workers were able to show the possibility of producing a 31 nm gap using oxidation patterning of a silicon layer. In their experiment, they used a silicon-on-insulator (SOI) substrate with a 100 nm silicon device layer on top of a 150 nm of silicon dioxide layer. The substrate was first cleaned using the RCA cleaning procedure by soaking it in deionized (DI) water:NH_4OH:H_2O_2 (5:1:1) for 10 minutes at 75 °C followed by a DI water : HF (100:1) dip for 11 s followed by an DI water:HCl:H_2O_2 (6:1:1) acid solution for 10 minutes at 75 °C. The substrate was then rinsed with DI water and dried with nitrogen. The substrate was then templated by applying a potential difference of 9 V between the substrate and the tip (the tip being held at negative potential), which allowed for the oxidation of the top silicon layer of the substrate. Wet etching the silicon substrate in KOH dilute solution at 40 °C resulted in removing the top silicon layer in 2 s. The silicon dioxide mask was then removed using an HF bath of DI water : HF (100:1) for 17 s. Figure (3.20) and (3.21) show the schematic procedure for how the oxidation process and patterning process take place, respectively.

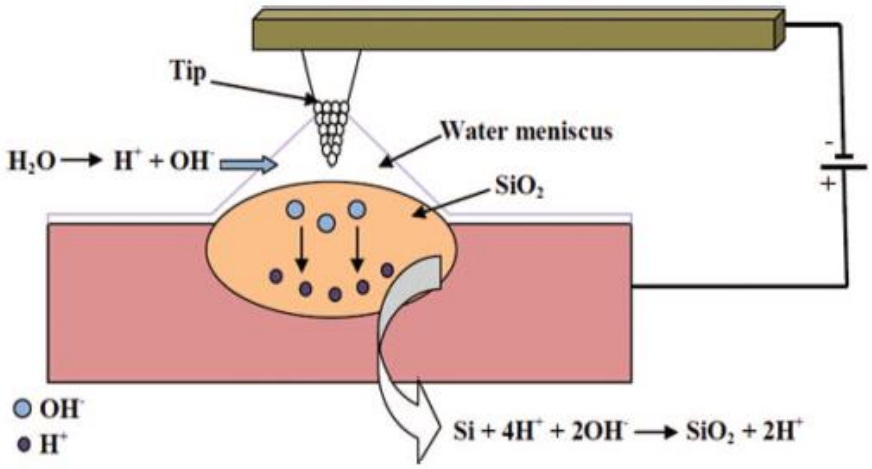

Figure (3.20): A schematic diagram of nano-oxidation process used to construct a silicon dioxide mask on the silicon substrate.[11] [Fair use]: Jalal Rouhi, Shahrom Mahmud, Sabar Derita Hutagalung and Saeid Kakooei, "Fabrication of nanogap electrodes via nano-oxidation mask by scanning probe microscopy nanolithography", J. Micro/Nanolith. MEMS MOEMS 10(4), 043002 (2011).

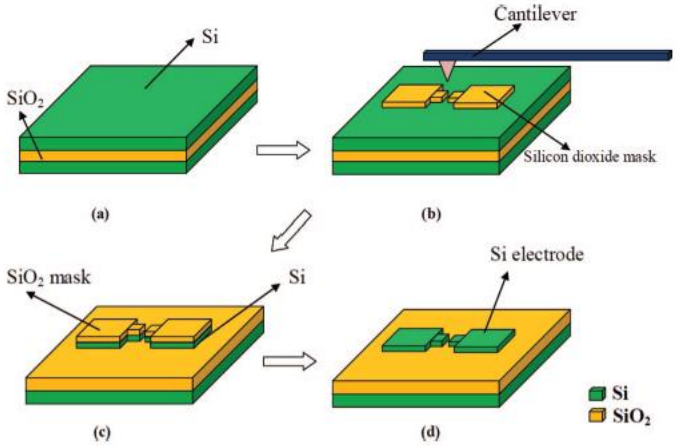

Figure (3.21): (a) The substrate used with 100 nm silicon layer on top of a 150 nm silicon dioxide layer. (b) Carrying out the nano-oxidation process produces a silicon dioxide mask on the silicon layer. (c) Removing the unmasked silicon layer using wet etching. (d) An HF bath is used to remove the silicon dioxide mask.[11]) [Fair use]: Jalal Rouhi, Shahrom Mahmud, Sabar Derita Hutagalung and Saeid Kakooei, "Fabrication of nanogap electrodes via nano-oxidation mask by scanning probe microscopy nanolithography", J. Micro/Nanolith. MEMS MOEMS 10(4), 043002 (2011).

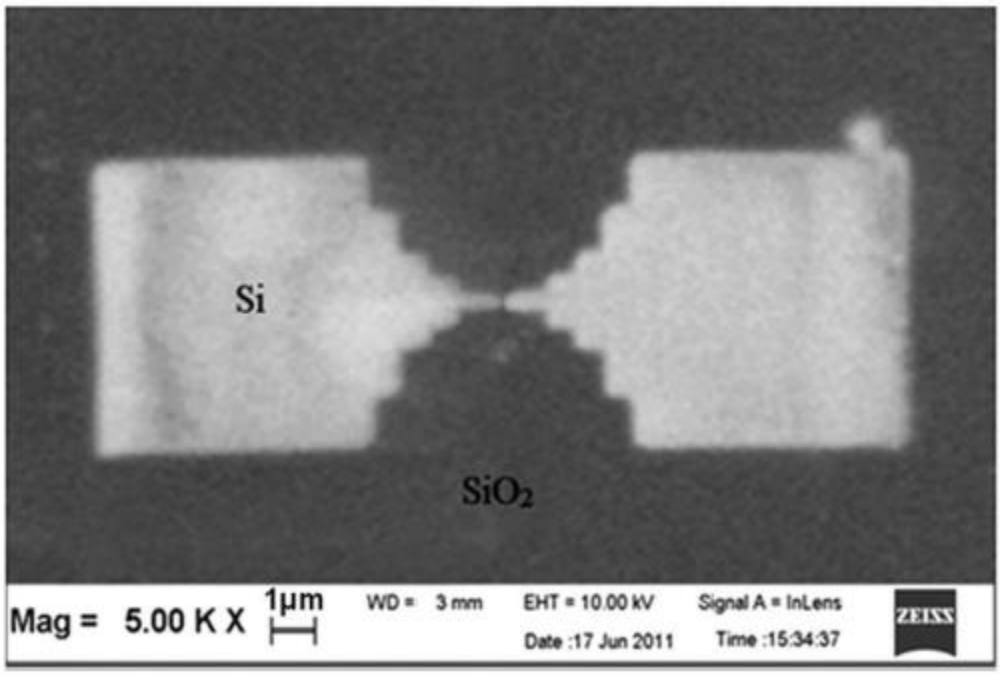

Figure (3.22): A scanning electron microscope image of the resulting construction. The gap between the electrode is 31 nm.[11]) [Fair use]: Jalal Rouhi, Shahrom Mahmud, Sabar Derita Hutagalung and Saeid Kakooei, "Fabrication of nanogap electrodes via nano-oxidation mask by scanning probe microscopy nanolithography", J. Micro/Nanolith. MEMS MOEMS 10(4), 043002 (2011).

In an attempt to utilize this technique in our work, we carried out a variation of the above detailed technique. In our trial, we cleaned a silicon substrate using a piranha solution cleaning method by soaking the substrate in a solution of H_2SO_4:H_2O_2 (3:1) at 80 °C for 15 minutes. The purpose of this step was to expose the silicon surface and remove any silicon dioxide layer on the surface. Immediately following the cleaning step, the substrate was loaded into the AFM and we patterned on it several patterns of squares of various sizes. The oxidation was carried out at a potential difference of 10 V with the tip held at -10 V while grounding the substrate. The substrate was then dipped in a DI water: HF (100:1) bath for 5 s. The HF bath etched away the oxidized parts of the

surface layer of the silicon substrate leaving behind patches of depths of 5 nm on average. One of the attempts we did yielded results exhibited in Figure (3.23).

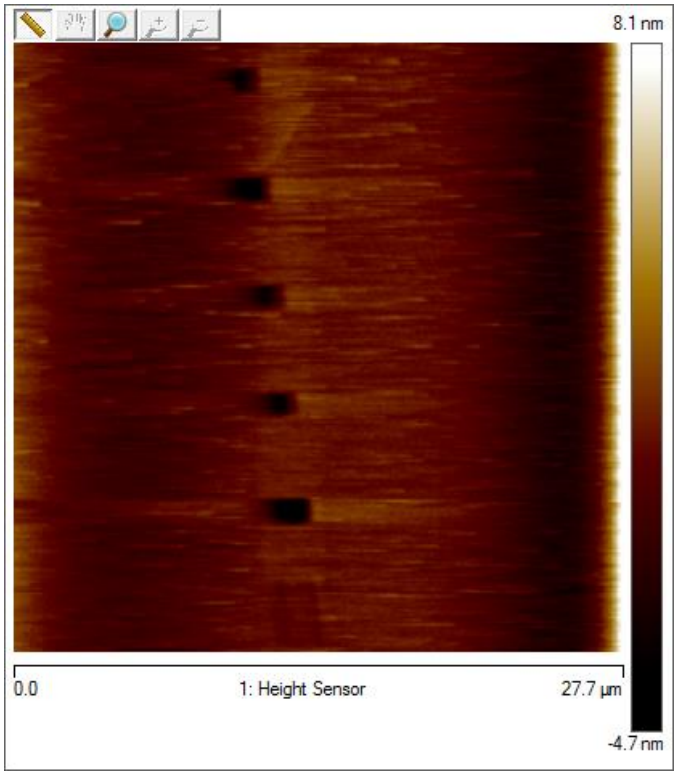

(a)

(b)

Figure (3.23): (a) Using a voltage difference of 10 V between the AFM tip and a layer of silicon on holding the tip at -10 V while the substrate is grounded oxidizes the silicon and produces a silicon dioxide layer in the patterned areas. Following this by an HF bath etches away the oxidized squares and leaves the rest of the substrate intact resulting in 3-D patterns in the silicon substrate. (b) A cross-sectional view of the depth profile of the patterned squares.

References:

1. C. Binning, C. F. Quate, Ch. Gerber. “Atomic Force Microscope”, Physical Review Letters, Volume 56, Number 9, (1986).

2. http://asdlib.org/onlineArticles/ecourseware/Bullen/SPMModule_BasicTheoryAFM.pdf

3. Song Xu and Gang-Yu Liu, “Nanometer-Scale Fabrication by Simultaneous Nanoshaving and Molecular Self-Assembly”, Langmuir 13, 127-129, (1997).

4. Gero Decher. Fuzzy Nanoassemblies : Toward Multilayerd Polymeric Multicomposites. Science **277**, 1232 (1997).

5. R. K. Iler (1966). "Multilayers of co lloidal particles". *Journal of Colloid and Interface Science* **21**: 569

6. G. Decher, J.D. Hong, J. Schmitt, “Buildup of ultrathin multilayer films by a self-assembly process: III. Consecutively alternating adsorption of anionic and cationic polyelectrolytes on charged surfaces”, Thin Solid Films Volumes **210-211**, (1992)

7. Gang-Yu Liu,* Song Xu, and Yile Qian, “Nanofabrication of Self-Assembled Monolayers Using Scanning Probe Lithography”, Acc. Chem. Res. **33**, 457-466, (2000)

8. Rachel K. Smith, Penelope A. Lewis, Paul S. Weiss, “Patterning self-assembled monolayers”, Progress in Surface Science **75**, 1-68, (2004).

9. Daan Wouters and Ulrich S. Schubert, “Constructive Nanolithography and Nanochemistry: Local Probe Oxidation and Chemical Modification”, Langmuir **19**, 9033-9038, (2003).

10. Hiroyuki Sugimura, Nagahiro Saito, Kazuyuki Hayashi, Noriya Maeda and Osamu Takai, “Scanning Probe Surface Modification: Chemical Conversion of Terminal Functional Groups on Organosilane Self-Assembled Monolayers”, Scanning Tunneling Microscopy/Spectroscopy and Related Techniques: 12th International Conference STM'03. AIP Conference Proceedings , Volume 696, pp. 150-157, (2003).

11. Jalal Rouhi, Shahrom Mahmud, Sabar Derita Hutagalung and Saeid Kakooei, “Fabrication of nanogap electrodes via nano-oxidation mask by scanning probe microscopy nanolithography”, J. Micro/Nanolith. MEMS MOEMS 10(4), 043002 (2011).

12. R. K. Iler (1966). "Multilayers of co lloidal particles". *Journal of Colloid and Interface Science* **21**: 569

13. G. Decher, J.D. Hong, J. Schmitt, “Buildup of ultrathin multilayer films by a self-assembly process: III. Consecutively alternating adsorption of anionic and cationic polyelectrolytes on charged surfaces”, Thin Solid Films Volumes **210-211**, (1992)

14. A. Tulpar, Z. Wang, C.-H. Jang, V. Jain, J.R. Heflin, W.A. Ducker, "Nanoscale Patterning of Ionic Self-Assembled Multilayers", Nanotechnology **20**, 155301:1-5 (2009).

15. D. Yoo, S. S. Shiratori, M. F. Rubner, “Controlling Bilayer Composition and Surface Wettability of Sequentially Adsorbed Multilayers of Weak Polyelectrolytes”, Macromolecules, **31**, 4309, (1998).

16. S. S. Shiratori, M. F. Rubner, “pH-Dependent Thickness Behavior of Sequentially Adsorbed Layers of Weak Polyelectrolytes”, Macromolecules, **33**, 4213, (2000).

17. Vaibhav Jain, PhD Thesis Dissertation, Virginia Polytechnic Institute and State University 2009.

18. Binnig, G.; Smith, D. P. E. (1986). "Single-tube three-dimensional scanner for scanning tunneling microscopy". *Review of Scientific Instruments* **57** (8): 1688.

19. A Practical Guide to Scanning Probe Microscopy. A training and user manual by Bruker®

20. Bruker's website

21. Bano, F., Fruk, L., Sanavio, B., Gelletteberg, M., Casalis, L., Niemeyer, C. M., Scoles, G., "Toward Multiple Protein Nanoarrays Using Nanografting and DNA Immobilization of Proteins". Nano Letters, Vol 7, No 9, 2614-2618, (2009)

22. http://chemistry.beloit.edu/edetc/SlideShow/slides/contents/scanning.html

23. http://team-nanotec.de/index.cfm?fuseaction=show_product&productid=80

24. http://en.wikipedia.org/wiki/Atomic_force_microscopy

25. http://web.physics.ucsb.edu/~hhansma/biomolecules.htm

26. http://www-liphy.ujf-grenoble.fr/Microscopie-a-force-atomique-AFM

Chapter 4

Atomic Force Microscope Patterned Surfaces and Selective Deposition of Polymers.

4.1 Introduction

In this chapter we examine selective deposition of polymers using the LbL method on areas that have been patterned using AFM-based nanografting techniques. The goal of this endeavor is to establish the optimum conditions and materials for selectively depositing polymers on selected areas of the substrates. This comes as a necessary step towards utilizing AFM-based nanografting to construct circuit elements on the nanoscale using self-assembly as the main method of material deposition. This set of experiments is an extensionsof nanografting efforts that have been reported and worked on previously by our group in successful attempts of nano-patterning of self assembled monolayers [(1)]. The work we report here involves patterning a single deposited layer of thiols on a gold surface using an atomic force microscope (AFM) and then using the LbL deposition technique to further provide selective growth on specific areas on the chosen surfaces. We further study the correlation between the size of the patterned areas, pH levels of the polymer solutions, the height of the resulting structures and the selectivity of deposition of the polymers on the designated patterned areas in an effort to extend and further utilize previously done research that tackles these points [(2),(3),(4)].

In this chapter, we examine the correlation between various parameters involved in the type of nanolithography known as nanografting and use it to pattern and construct nanoscale structures of polymers deposited selectively at various locations on chosen surfaces. The advantage such a method offers is the ability to control the chemistry and composition of surfaces in the horizontal dimension and consequently offering a chance to pattern the surfaces of substrates according to our choice. Such a technique can potentially be used to construct circuit elements on the nanoscale. The technique used in this experiment to template the surface, which is known as nanografting using an AFM, is discussed in chapter 3 [5],[6],[7],[8]. This technique depends on having a surface covered by a monolayer of a certain molecule. In this case it is a thiol terminated with an –OH terminal group, which is then replaced in parts of this monolayer with a different thiol terminated with a –COOH group. The replacement process happens as a result of using the AFM tip to remove some of the molecules of the background material and thus allowing their place to be taken by other molecules that exist in the environment in which the grafting is taking place.

4.2 Experimental Details:

4.2.1 11-Mercaptoundecanol

In this experiment, the -OH terminated thiol we chose is 11-Mercaptoundecanol (11-MUD), and its structure is shown in Figure (4.1). 11-MUD was used as a 2 mM solution dissolved in ethanol. It was purchased from Sigma-Aldrich and used as received.

$HSCH_2(CH_2)_9CH_2OH$

Figure (4.1): 11 - Mercaptoundecanol

4.2.2 16-Mercaptohexadecanoic acid

The –COOH terminated thiol is 16-Mercaptohexadecanoic acid (16-MHDA) and its chemical structure is shown in Figure (4.2). The 16-MHDA was used as a 2 mM solution dissolved in ethanol. It was purchased from Sigma-Aldrich and used as received.

$HS(CH_2)_{15}CO_2H$

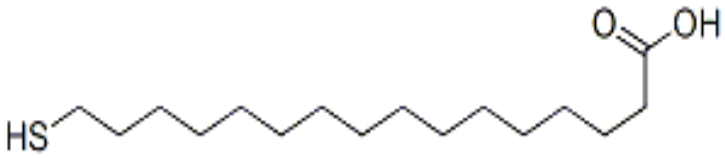

Figure (4.2): 16 – Mercaptohexadecanoic acid

4.2.3 Poly(allylamine hydrochloride) (PAH)

PAH is a positively-charged polymer when in aqueous solution. This polymer was used as a 10 mM solution in DI water at pH~7. It was purchased from Sigma-Aldrich and used as received.

4.2.4 poly[1-[4-(3-carboxy-4-hydroxyphenylazo)-benzensulfonamido]-1,2-ethanediyl sodium salt] (PCBS)

PCBS is a negatively-charged polymer when in aqueous solution. We used this polymer as a 10 mM solution in DI water at varying pH levels.

4.2.5 Slides

We used glass slides that are coated with a gold layer of thickness 1000 Å deposited on an adhesive layer of Cr of thickness 50 Å. The slides were purchased from EMF Corp. Figure (4.3) shows an image of one of the slides.

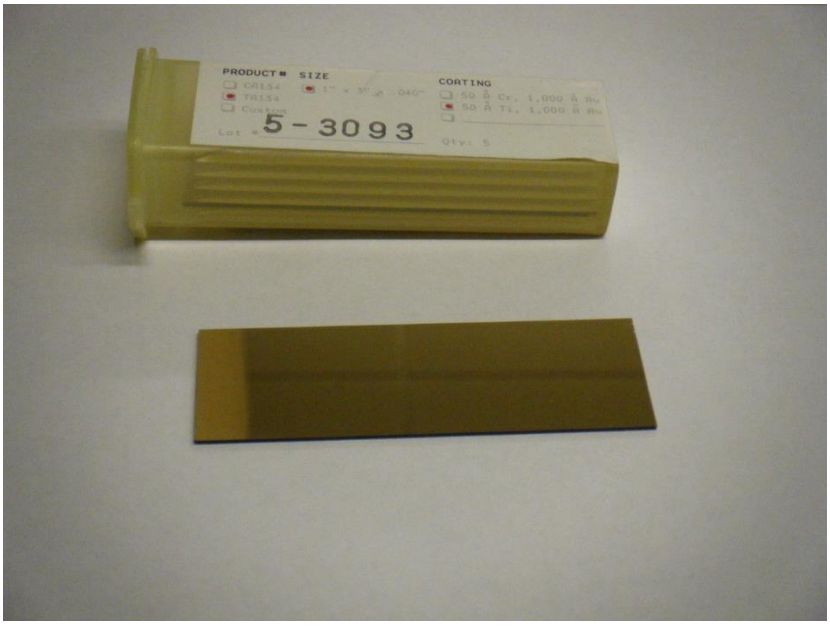

Figure (4.3): A glass slide coated with a thin film of gold. The gold layer is 1000 Å thick on top of a 50 Å layer of Cr used for adhesion between the gold and the glass surface.

4.2.6 Atomic force microscope

We used two different AFM systems for this experiment. The first system used was a Veeco Multimode with a Nanoscope V controller. The second AFM used in this experiment is a Bruker Dimension Icon with a NanoScope V controller.

4.2.7 AFM tips

We used different types of tips in the work reported here. The first set of tips used here were made by Veeco. They were made of silicon nitride cantilevers carrying silicon tips. The cantilevers had a nominal spring value of 42 N/m. The second set was also made by Veeco of silicon nitride cantilevers carrying silicon tips. The cantilevers had a nominal spring constant of 0.6 N/m, The third set of tips used in these experiments are Bruker (which purchased Veeco) SNL 10. These tips are made of silicon nitride cantilevers carrying silicon tips with a nominal spring constant of 0.7 N/m. We chose the second and third sets because of their low spring constant. It is crucial not to use a strong tip when imaging or patterning soft surfaces like gold.

4.3 Experimental Procedure

The first step in the process is cleaning the gold-coated slides purchased from EMF Corp. The cleaning process normally takes place by placing the gold substrates in a plasma cleaner for 1 minute. However, given the excellent condition of the substrates we had, no such treatment was required. The cleaning process in our case was done by boiling the gold substrates in ethanol for 45 minutes followed by rinsing them with fresh ethanol and finally drying them with pure nitrogen. After cleaning, the slides were dipped in a 2 mM solution of 11-MUD dissolved in ethanol. The

slides were left in the solution for at least 48 hours. After removing the samples from the 11-MUD solution, they were rinsed in fresh ethanol then sonicated in ethanol for 2 minutes then rinsed again in ethanol and finally dried with nitrogen. At the end of this process, a closely packed monolayer of 11-MUD is formed on the gold surface as schematically illustrated in Figure (4.4). The sulfur at one end of the 11-MUD chain binds with the gold atoms forming a network of covalent bonds between the sulfur atoms in thiols and the gold atoms on the surface of the gold film[(9)]. The thiol molecules undergo a two-phase process by which they end up in an erect position on the gold surface. The molecules, in the first step, align themselves in a horizontal manner with respect to the surface. Then in the second step they change their positions to a more erect position with respect to the surface as the density increases. The second phase is known as an all trans position and forms a typical angle of 30 degrees with respect to the surface[(10)].

The 11-MUD forms an -OH terminated monolayer that acts as a passive background on the surface of the substrate. The role of this passive layer is to prevent polymers from electrostatically depositing on the substrate on areas covered by the 11-MUD. When this passive background is replaced with the -COOH terminated 16-MHDA acid, this substitution forms an active region that allows for selectivity in deposition of subsequent layers of charged polymers. The idea behind the nanografting technique used here, as discussed earlier in this dissertation, is to apply a strong force to the tip of the AFM while it is in contact with the surface of the sample in a liquid environment where this force breaks the bonds between the background molecules already deposited on the surface and frees these molecules. The liquid environment contains a different chemical, in this case a 2mM solution of 16-MHDA, which will replace the one initially on the surface in a monolayer, in this case 11-MUD, in specific parts of that monolayer. The areas and patterns in which the 16-MHDA replaces the 11-MUD are chosen to be of different shapes and sizes to suit

our experimental design. The shapes grafted from the 16-MHDA into the 11-MUD background were squares of sizes 2 µm X 2 µm, 1 µm X 1 µm, 500 nm X 500 nm, 200 nm X 200 nm and 100 nm X 100 nm. The liquid environment of 16-MHDA is contained in a liquid cell designed specifically for the AFM for imaging in liquids. In our case, the liquid cell used was a simple in-house solution designed to suit our purposes. Given the design of the standard liquid cell of the Bruker Dimension Icon®, we were not able to immerse the sample in a solution containing 16-MHDA to perform the grafting step. To remedy this issue we used a small petri dish with low walls to serve as a reservoir in which we can immerse the sample while it is being patterned.

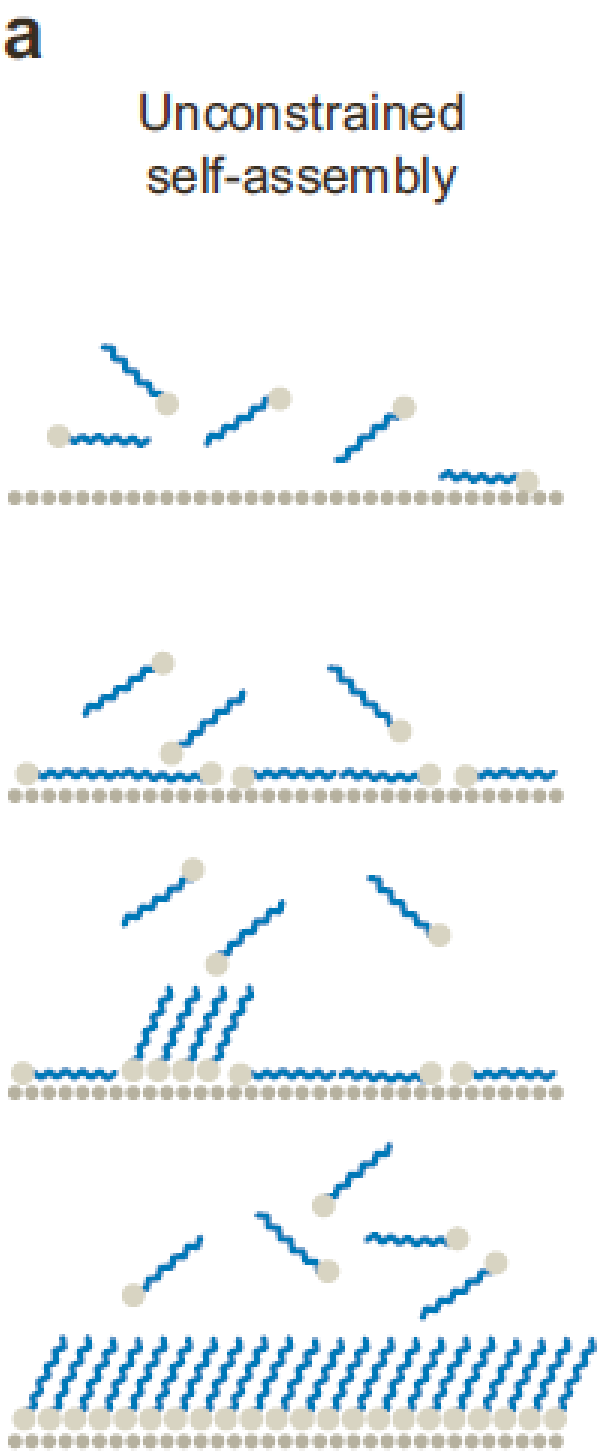

Figure (4.4): The two phases through which thiol molecules go until they align in a tightly packed upright formation on the gold surface.[10] [Fair use]: Mauzi Liu, Nabil A. Amro, and Gang-Yu Liu, "Nanografting for Surface Physical Chemistry", Ann. Rev. Phys. Chem 59: 367 – 86 (2008).

4.4 Results and discussion

To perform the nanografting step, the slides were then placed in the liquid cell of the AFM. The samples were immersed completely in a 2 mM solution of 16-MHDA in the liquid cell. Using Veeco manufactured AFM tips made of silicon and of nominal spring constant 42 N/m proved futile as the tips indented the gold layer on the substrate even at the smallest of forces possible with the AFM. Figure (4.5) shows an example of the indentations caused by too much force applied to the AFM tip.

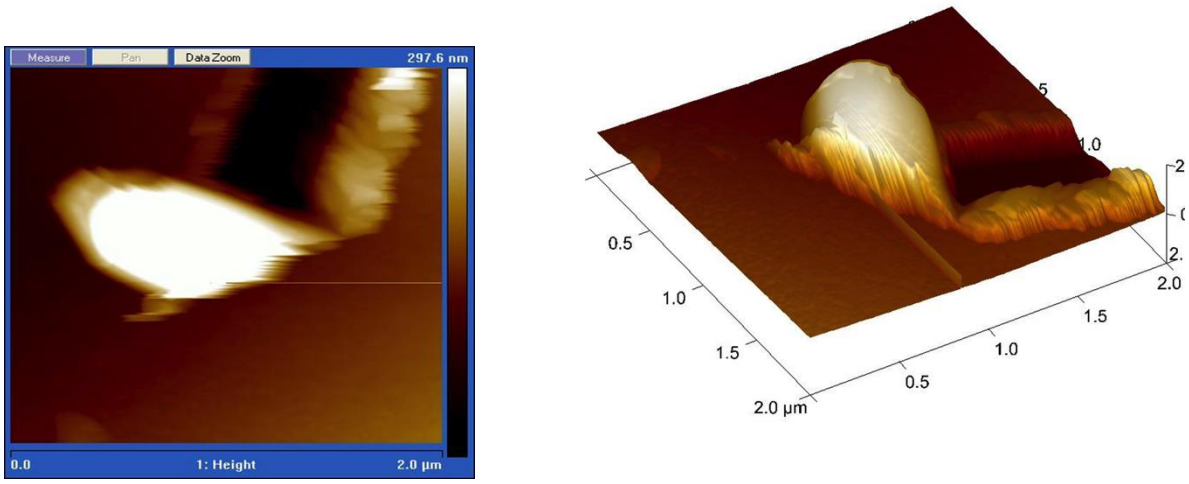

(a) (b)

Figure (4.5): Excessive forces applied to the AFM tip caused an indentation of the gold layer deposited on the substrate. (a) A Height image of gold sample after the gold removal. The tip scanning direction was from the top to the bottom. As the tip removed the gold from the surface of the sample it piled it up near the end of its scanning range. (b) 3-D rendition of the topographic image collected while the AFM is imaging.

Given the negative results of the large spring constant tips, we switched to using softer tips. We therefore switched to tips manufactured by Veeco made of silicon nitride and of nominal spring constant of 0.6 - 4 N/m. In the next step, we attempted to graft patches of the 16-MHDA in the 11-MUD monolayer deposited on the surface of the gold substrate. Unfortunately, after countless attempts, we were not able to obtain any positive results. Troubleshooting the problem led us to examining the surface of the samples using XPS. The results came back negative and indicated there were no thiol monolayers adhering to the surface. This conclusion was based on the absence of sulfur peaks from the spectrum obtained. Figure (4.6) shows the results of the XPS obtained through Virginia Tech's facilities at the Nanoscale Characterization and Fabrication Laboratory (NCFL).

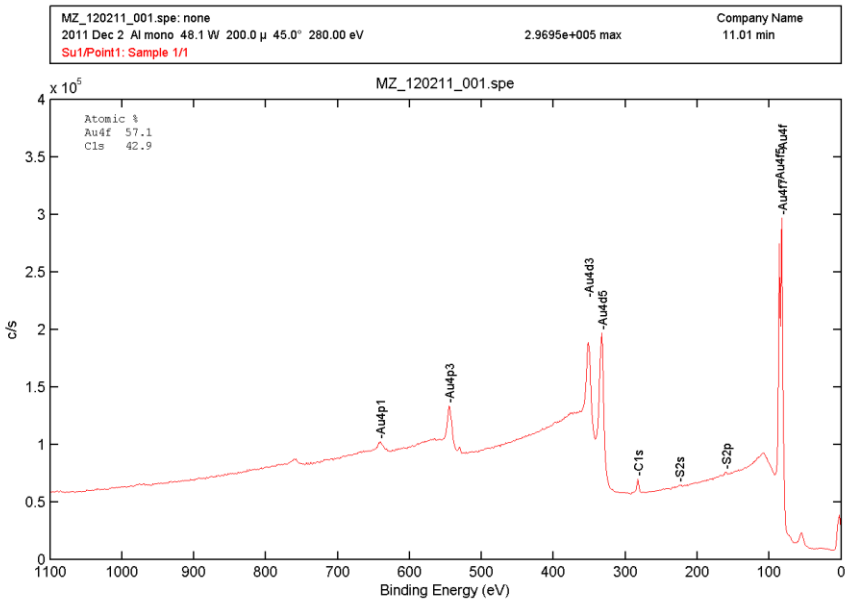

Figure (4.6): XPS results for samples with monolayers of 11-MUD supposedly deposited on it. The test showed that the thiols were not binding with the gold surface.

This was a clear indication that there was something wrong with the chemicals we were using. The next step we took was to use some other thiols from some of the group members to replace the ones we were using to eliminate the possibility that they are expired in spite of them being newly purchased.

Figure (4.7) shows attempts at shaving patches from a monolayer of 1-Octanethiol deposited on gold substrates. The image shows two parallelogram shapes with sides of size 1 µm. The shapes were supposed to be squares but due to some drifting problems in the AFM and the lack of a closed loop feedback system on the AFM used at the time the shapes were turned into parallelograms. This successful shaving was performed in a liquid cell containing fresh ethanol. The set point of the AFM, which determines the force between the tip and the sample in contact mode, was set to 8 V. The tip used in this shaving process had a nominal spring constant of 0.6 N/m. The imaging speed at which the shaving was done was 3 Hz.

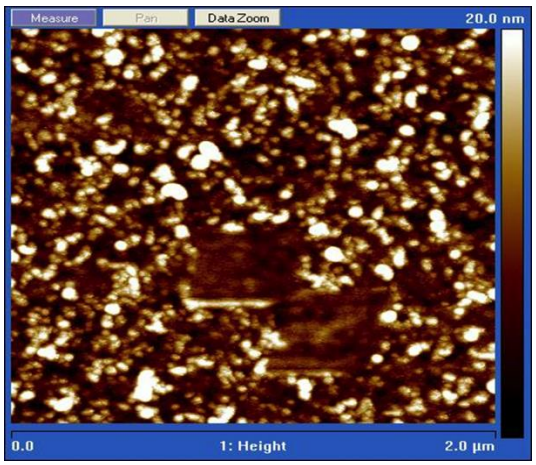

Figure (4.7): AFM nanoshaving of a monolayer of 1-Octdecanethiol deposited on a gold substrate.

Another example of successful nanoshaving is shown in Figure (4.8).

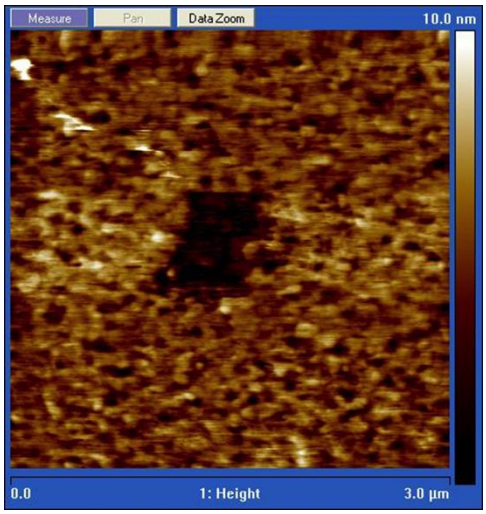

Figure (4.8): Nanoshaving of 1-Octanethiol deposited on gold.

Dr. William Ducker of the Department of Chemical Engineering supplied us with a small amount of 11-MUD. The trials yielded the first positive results of our endeavors. Figure (4.9) shows successful shaving of a monolayer of 11-MUD deposited on a gold substrate.

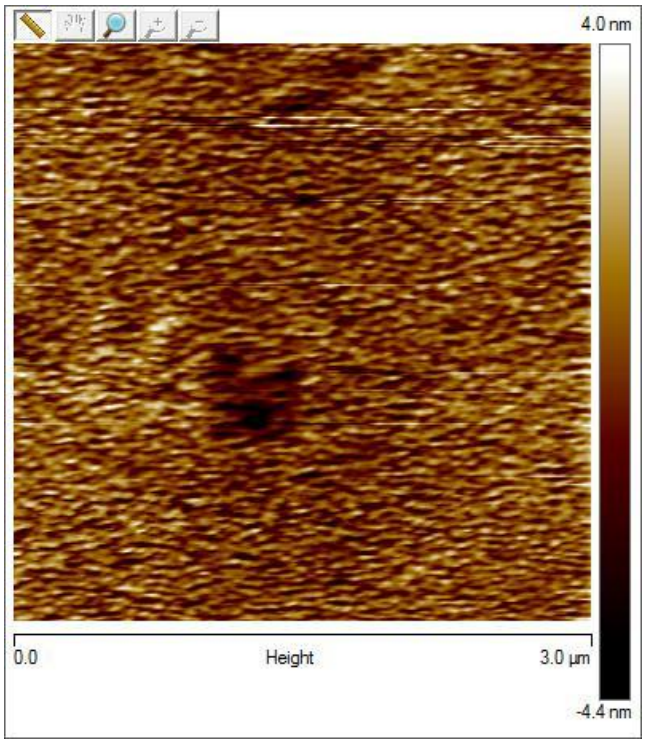

(a)

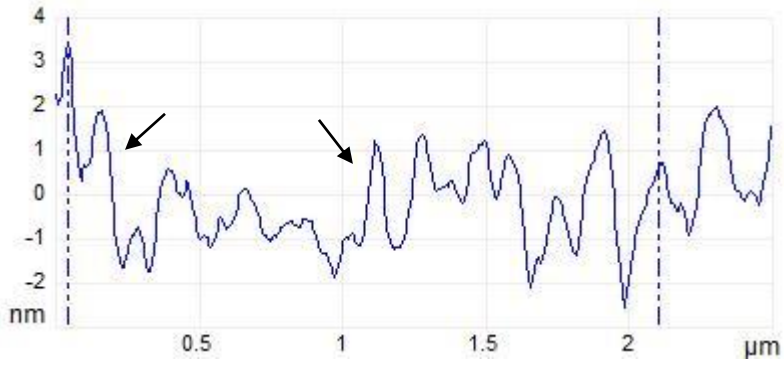

(b)

Figure (4.9): (a) Successful shaving of a square area of a monolayer of 11-MUD deposited on a gold substrate. The tilting in the square is due to drifting in the AFM scanner. (b) Height profile of the shaved area. The height difference was 1 nm which is in agreement with the theoretical value proposed for the size of the 11-MUD chain. The arrows indicate the edges of the shaved area.

The next step was to perform nangrafting on the samples covered with a monolayer of 11-MUD. Figure (4.10) illustrates the process of simultaneous nanoshaving and grafting patches of monolayers of thiols we performed. We notice here that the 16-MHDA molecules do not undergo the regular two-phase process to align on the surface and instead achieve the proper alignment on the surface in one step. This is anticipated due to the highly constrained size of the area they have to fill on the shaved gold surface.[10]

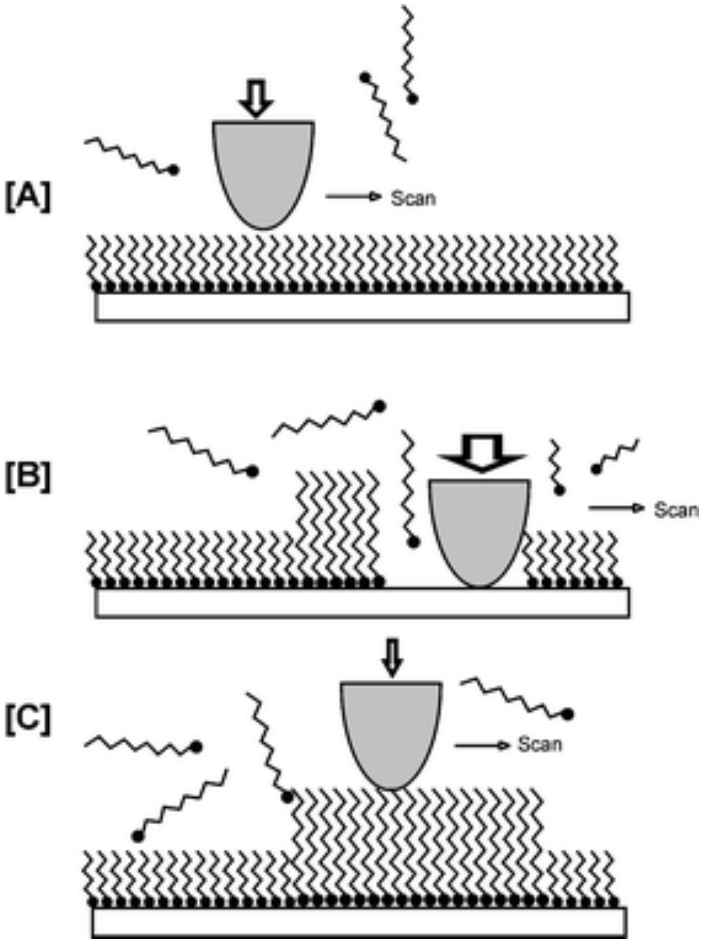

Figure (4.10): Nanografting process (a) The initial imaging is done using a very small force to minimize the effects of imaging on the deposited monolayer of 11-MUD. (b) When we increase the force applied by the AFM tip on the surface it starts removing some of the 11-MUD molecules and they are replaced by 16-MHDA molecules from solution. The replacement, also, allows the new thiol to assemble on the surface in one step instead of the usual two step process. (c) A final scan is performed with minimal force to image the modification that takes place on the surface of the slide.[10] [Fair use]: Mauzi Liu, Nabil A. Amro, and Gang-Yu Liu, "Nanografting for Surface Physical Chemistry", Ann. Rev. Phys. Chem 59: 367 – 86 (2008).

The patches of 16-MHDA were introduced in repeated patterns of squares that varied in size between 2 microns X 2microns to 100 nm X 100 nm. After the grafting process was done we rinsed the slides in fresh ethanol very well and then filled the liquid cell with ethanol and imaged the results of the grafting process. As expected, the grafted squares were clearly visible and the height difference was around 0.6-1.5 nm on average. The height difference corresponds to the extra atoms in the 16-MHDA that add to the chain length of the molecule as opposed to the 11 – MUD which is 6 Å according to theoretical calculations. Figure (4.11) shows how the grafted patch of the -COOH terminated thiol stands out against the background of the passive -OH terminated thiol background. This was our first successful trial of nanografting.

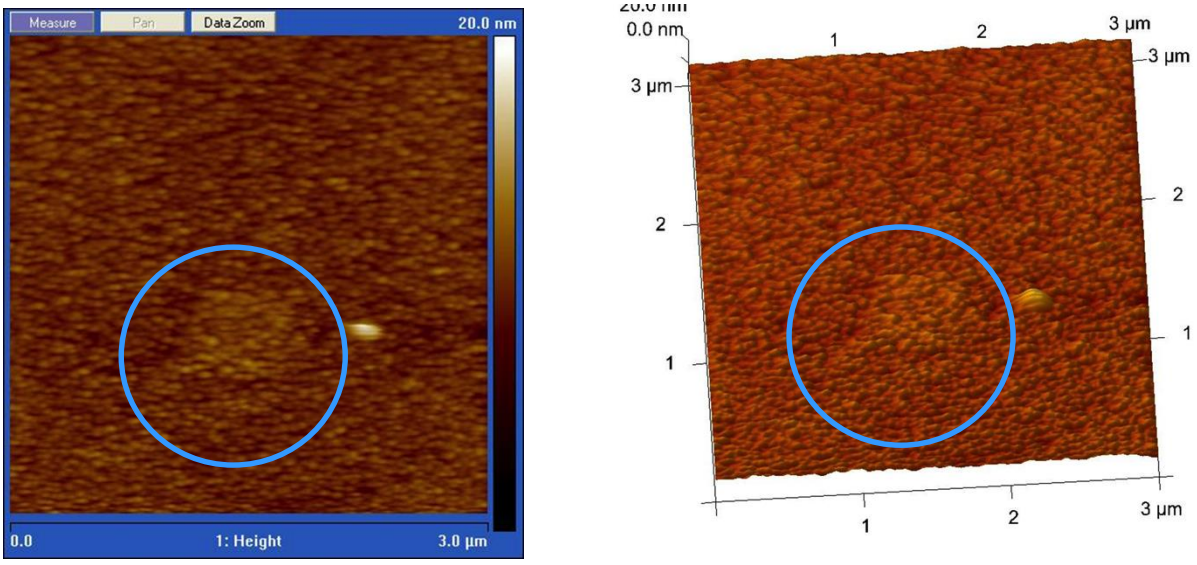

Figure (4.11): (a) A height 2-D image of a grafted square 500 nm X 500 nm of 16-MHDA onto a background of 11-MUD. (b) A 3-D rendition of the grafted square.

The next few trials yielded successful patterns of 16-MHDA patches grafted in a background of 11-MUD. Figure (4.12) shows one of these trials to graft 4 squares of size 500 nm X 500 nm and the patterns resulting from the successful grafting attempts.

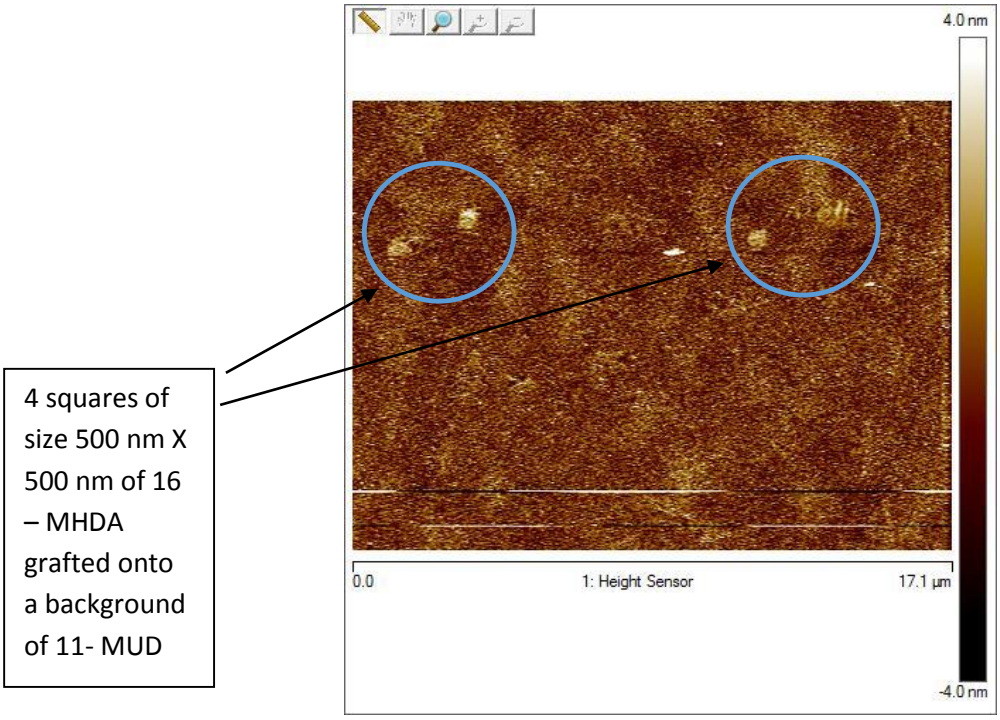

(a)

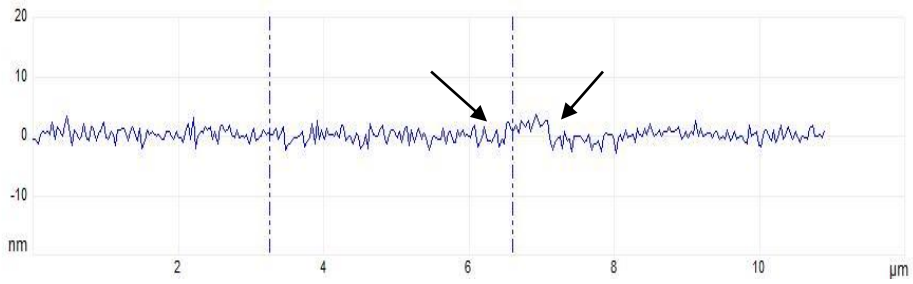

(b)

Figure (4.12): (a)The image shows 4 grafted squares of 16-MHDA of size 500 nm X 500 nm can be visibly seen against the background of 11-MUD in a height image performed by AFM. The squares are indicated by the circles placed on the image. (b): A cross sectional measurement of the height profile of the structure shows that the height difference between the background and the grafted areas is around 0.6 nm on average corresponding to the expected length difference between the structure of the background and the active patches. The arrows indicate the edges of the step representing the grafted area. The vertical bars indicate one of the points where height measurements have been performed.

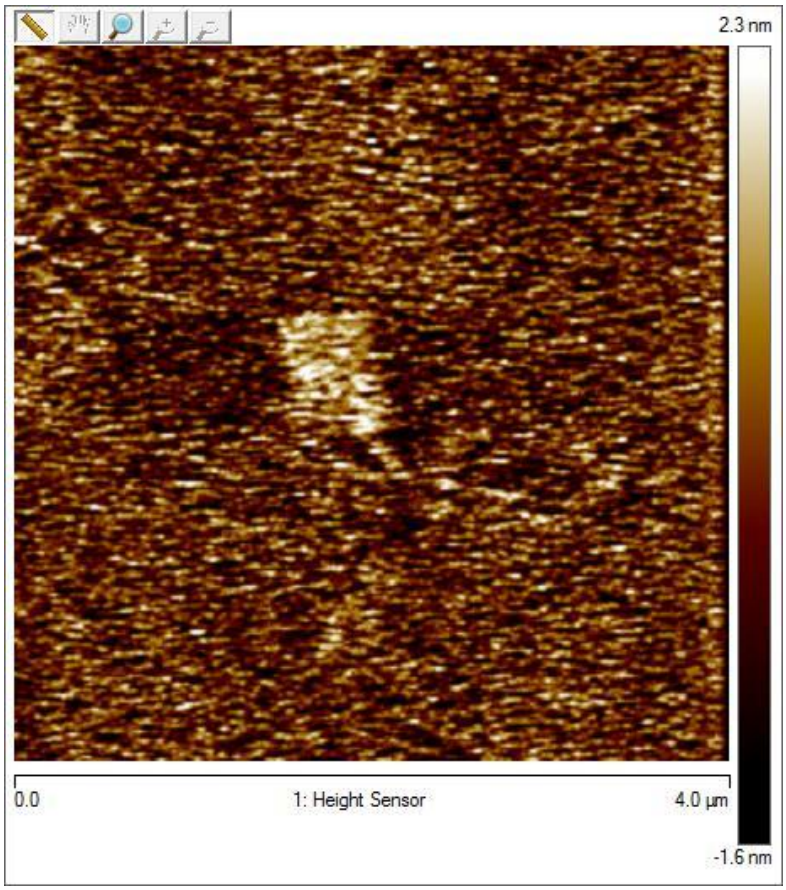

(a)

(b)

Figure (4.13): (a) A zoomed in image of one of the 16 –MHDA squares grafted in an 11 – MUD background. (b) A cross sectional measurement of the height profile of the grafted square of 16 –MHDA. The arrows indicate the edges of the step corresponding to the grafted square. The vertical bars correspond to one of the points at which the average height was measured.

The next major step was to perform the LbL deposition process of PAH with different polymers on the patterned slides. The polymers deposited with PAH were PCBS, PAA, and PSS.

The deposition process was done at different sets of pH levels. The effect of pH was examined in order to optimize the LbL deposition process with respect to secondary effects on selective deposition. The role of the secondary effects was discussed in Prof. Paula Hammond's work as described in chapter 2. [(2)] The idea briefly is that there are several factors that control the preference of the polymer layers in depositing on the surface. When the polymers are fully charged under high pH levels, the predominant factor is the electrostatic interaction and this guides the deposition behavior. Under these conditions, polymers deposit everywhere on the sample but with greater selectivity towards depositing on the grafted patterns. Friction measurements were performed at all pH values used for the deposition process, and the results confirmed changes in the chemistry and morphology of the surface indicating the deposition of polymer layers everywhere on the surface of the sample. This selectivity is seen as a faster rate of thickness increase on the grafted areas when compared to the background in height measurements. Selectivity is also seen in friction measurements as a difference in the friction between the background and the patterned areas due to the different interactions between the tip and the surface in the different places. When the pH is significantly decreased, the polymer layers do not just selectively deposit on the active grafted areas of the surface due to electrostatic interactions alone but also due to other factors such as the type of atoms on the backbone of the polymer and the hydrophobicity vs. hydrophilicity of the polymers used. Changing the pH allowed us to adjust the degree of ionization of the polymer and thus either enhance the electrostatic attraction or diminish its role and allow the secondary effects to take over. This can be pushed to the point that for a certain set of pH levels for the polymers during the LbL deposition, the selective deposition can be completely reversed and the polymers

will prefer to deposit on the –OH terminated background and avoid the active –COOH terminated grafted areas. For the trials performed with PAH and PCBS we kept the pH level of the PAH at ~ 7.0 and varied the pH of the PCBS solution. The experiment was carried at the following 4 different pH values of the PCBS solution: 7.0, 6.0, 5.5, and 5.0. Table (4.1) shows a summary of the results found for these various runs. For pH values of the PCBS of 8 and 4, the selective deposition disappeared and the patterned areas were lost into the background.

The results of the multilayer deposition of the polymers exhibited some interesting correlations. The larger areas of deposition displayed smaller increments of height increase with the repeated bilayer depositions compared to the smaller areas at the same conditions. Also, the maximum height increments between different bilayers were observed at pH 5.5 for the PCBS with noticeable variations between the different cases.

Figure (4.14) shows the progress of depositing several multilayers of polymers (PAH/PCBS) at pH 5.0

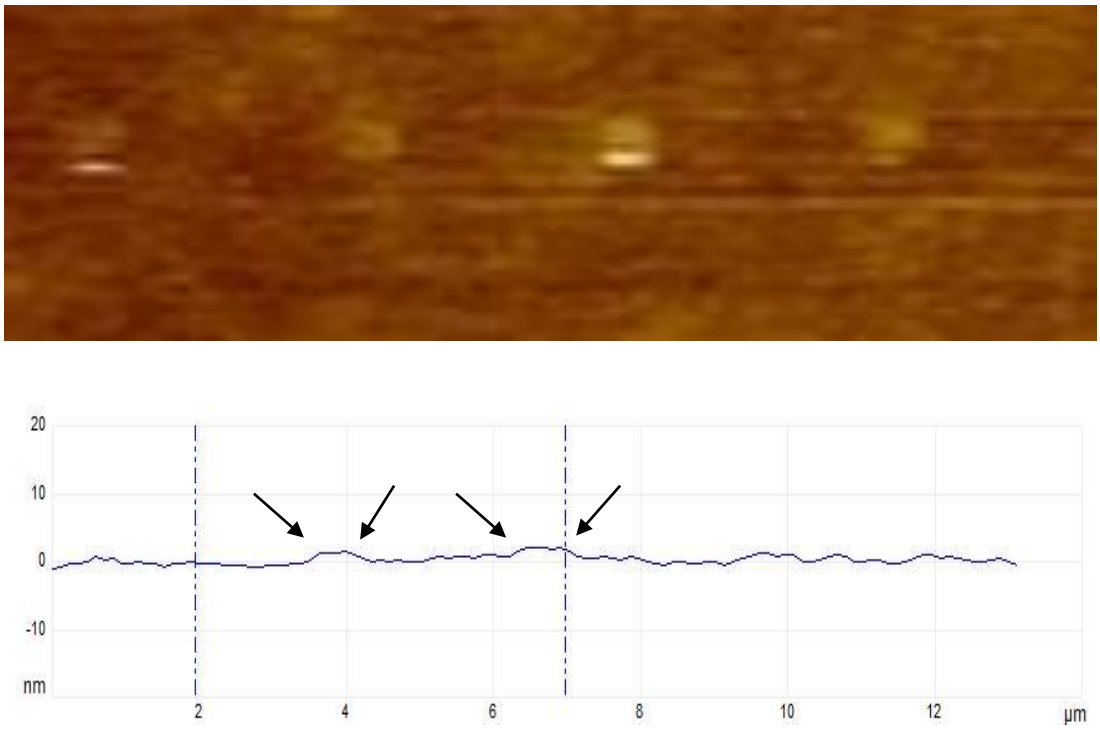

(a)

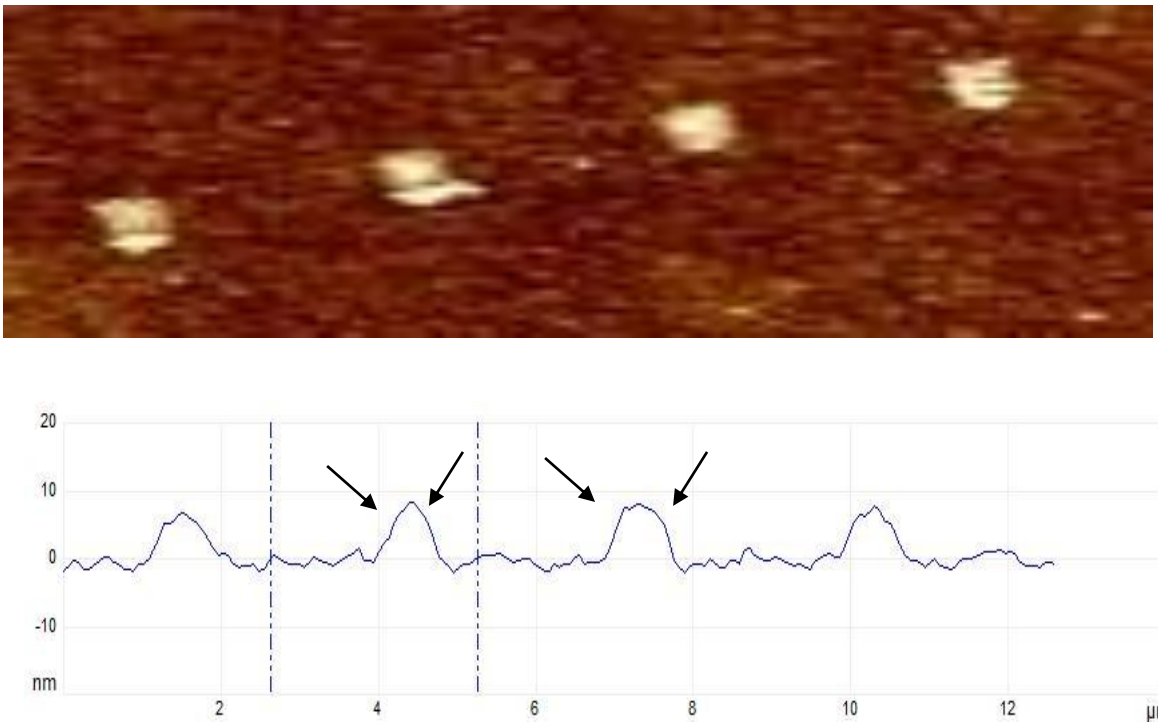

(b)

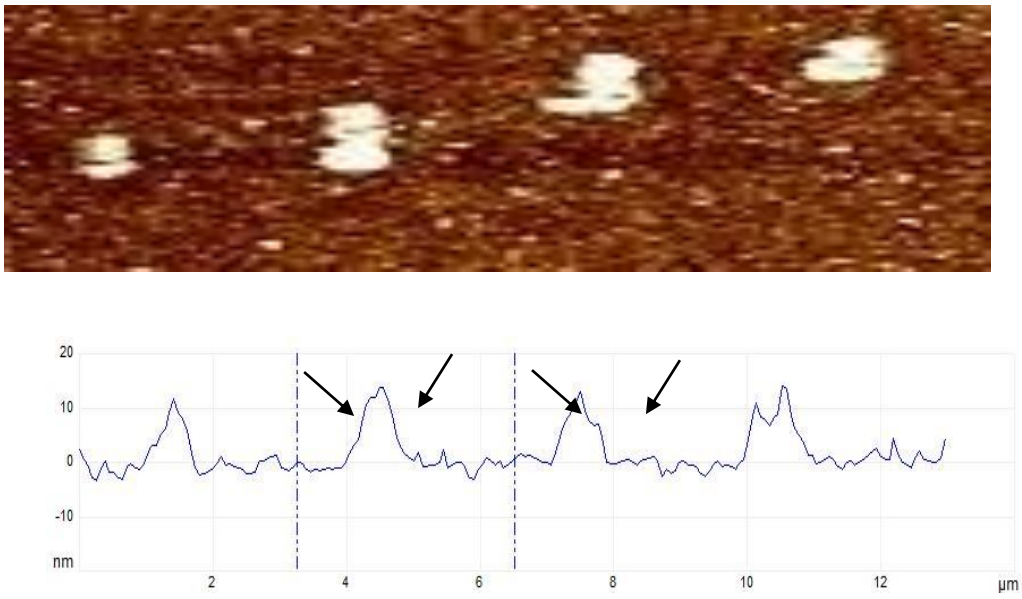

(c)

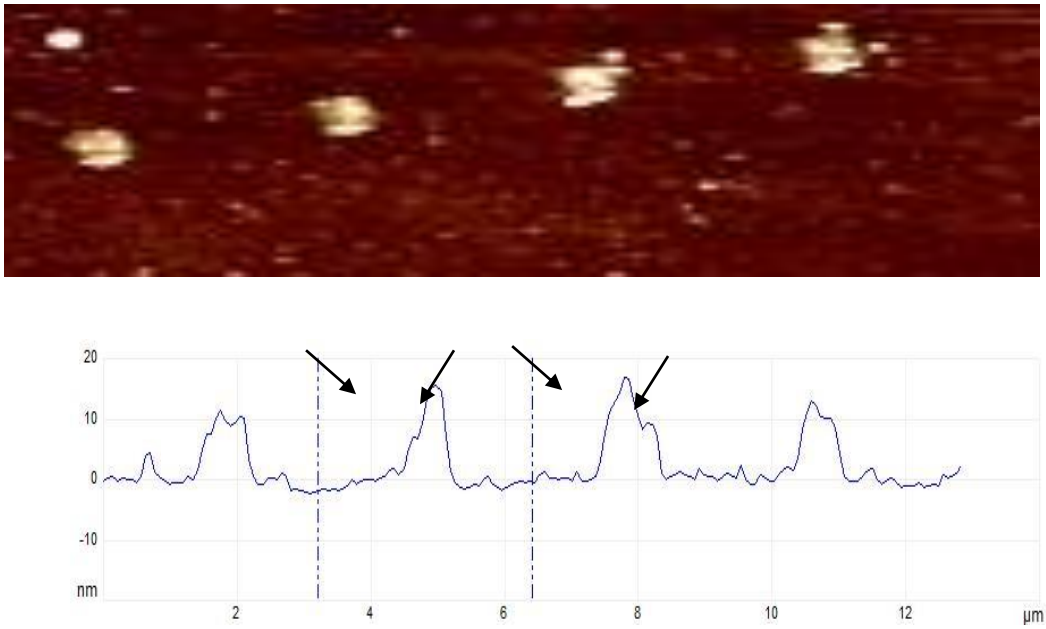

(d)

Figure (4.14): The results of the LbL deposition of PAH and PCBS at pH~5 on squares of 16-Mercaptohexadecanoic acid grafted into a background of 11-Mercaptoundecanol. (a) Immediately after grafting (b) After depositing 2 bilayers. (c) After depositing 4 bilayers. (d) After depositing 6 bilayers. The black arrows point at the edges of the patterned squares.

Figure (4.15) shows the progress of depositing several layers of polymers (PAH/PCBS) at pH ~ 5.5.

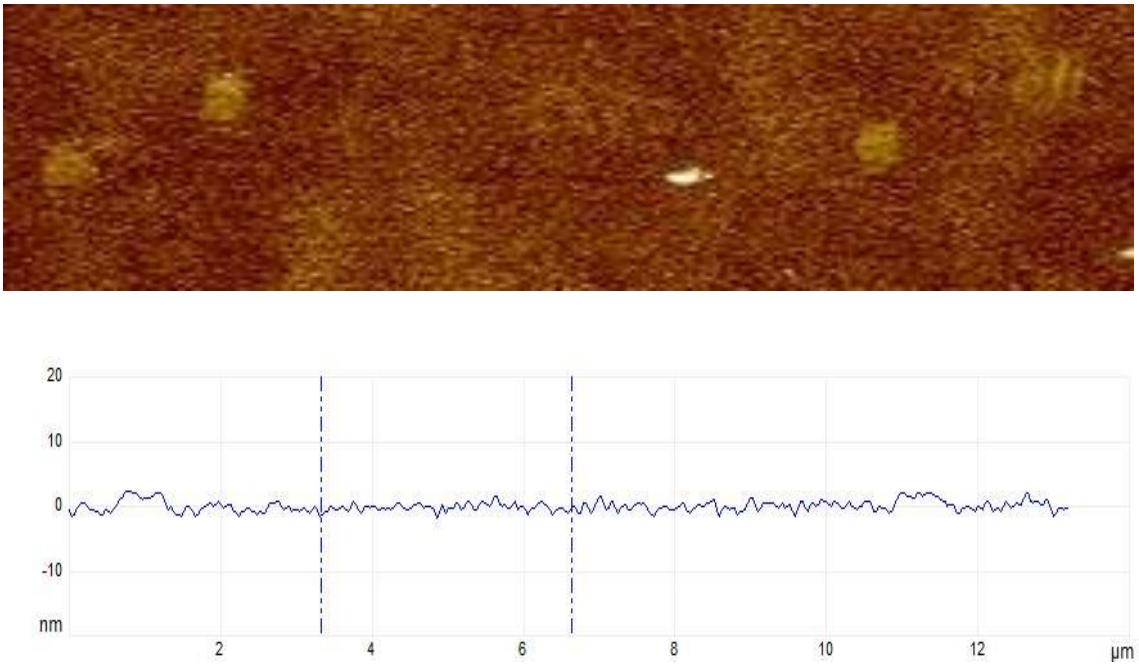

(a)

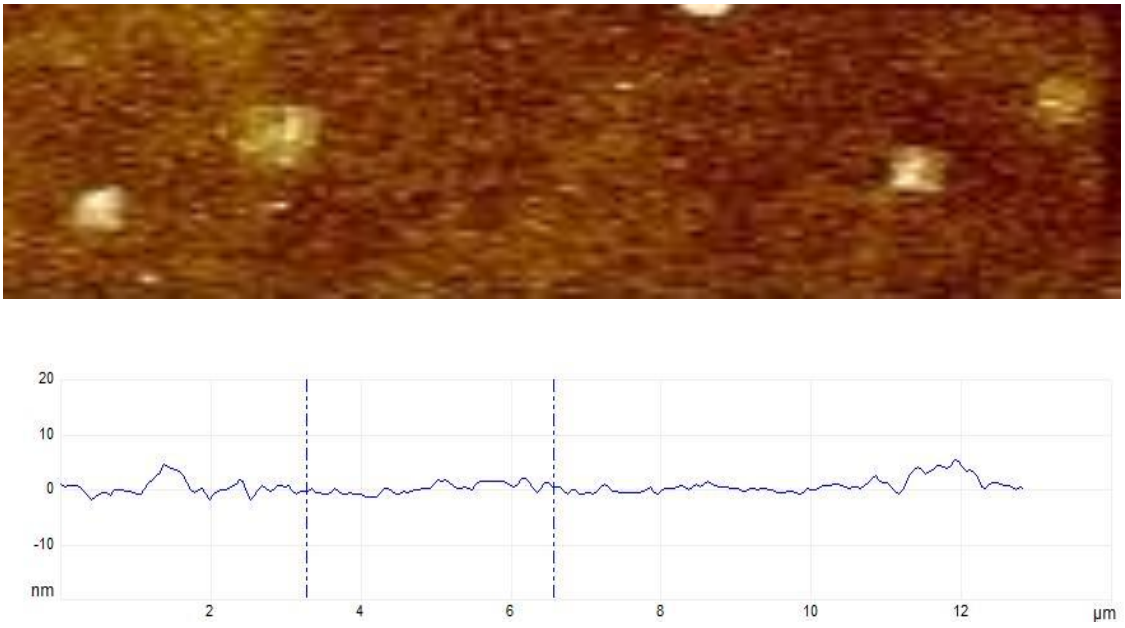

(b)

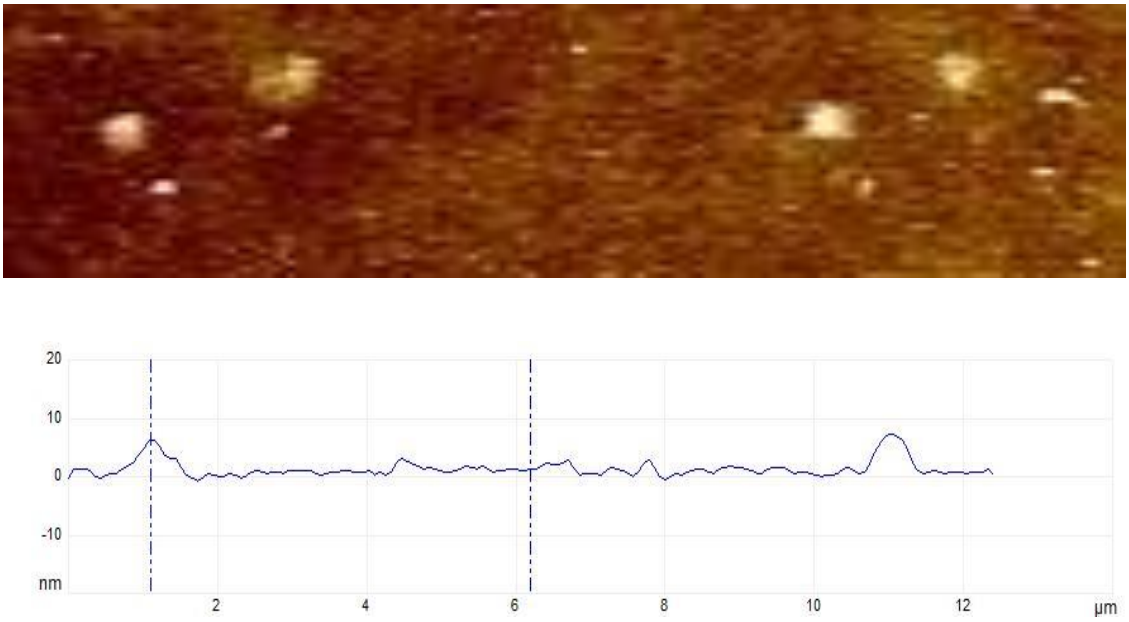

(c)

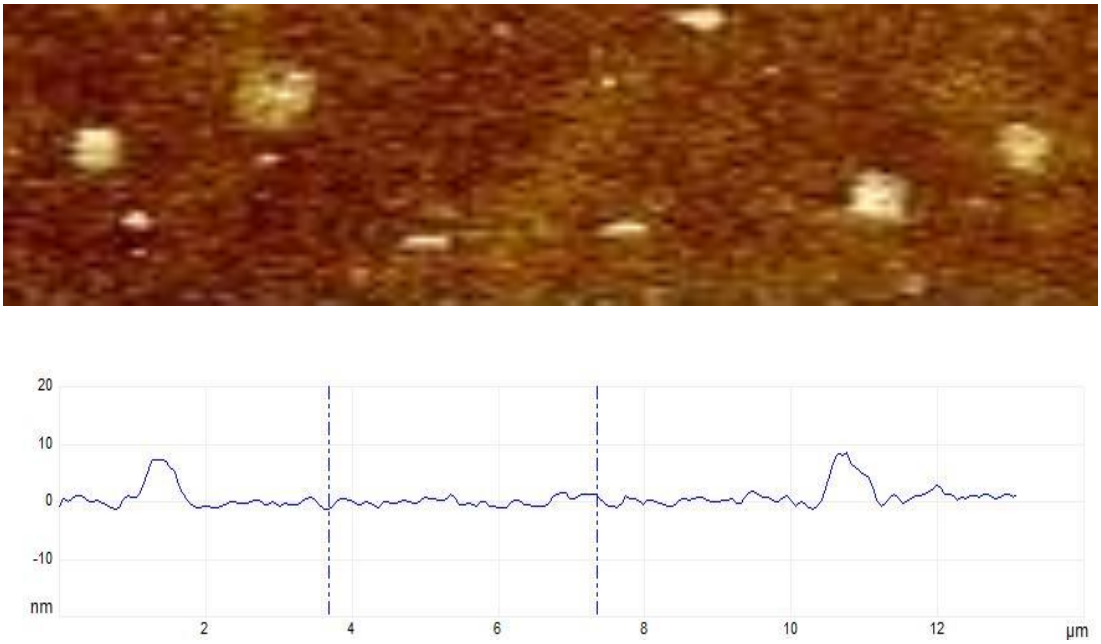

(d)

Figure (4.15): The results of the LbL deposition of PAH and PCBS at pH~5.5 on squares of 16-Mercaptohexadecanoic acid grafted into a background of 11-Mercaptoundecanol. (a) Immediately after grafting (b) After depositing 2 bilayers. (c) After depositing 4 bilayers. (d) After depositing 6 bilayers

Number Of Bilayers	pH 7	pH 6	pH 5.5	pH 5
0	0.5 nm - 1.5nm	0.5 nm - 1.5 nm	0.5 nm – 1.5 nm	0.5 nm – 1.5 nm
2	2.2 nm	2.1 nm	3 nm	6.5 nm
4	4 nm	4.5 nm	5.2 nm	12 nm
6	5.5 nm	5.7 nm	7.1 nm	18.5 nm
8	7 nm	7.2 nm	9 nm	22.5 nm
10	8.2 nm	8.5 nm	10 nm	28.4 nm

Table (4.1): Average height increases measured upon grafting squares of 500 nm X 500 nm of 16-MHDA on an 11-MUD background and then subsequent deposition of bilayers of PAH and PCBS.

The following is a graphical representation of the change in the average thickness of a bilayer with respect to changes in pH.

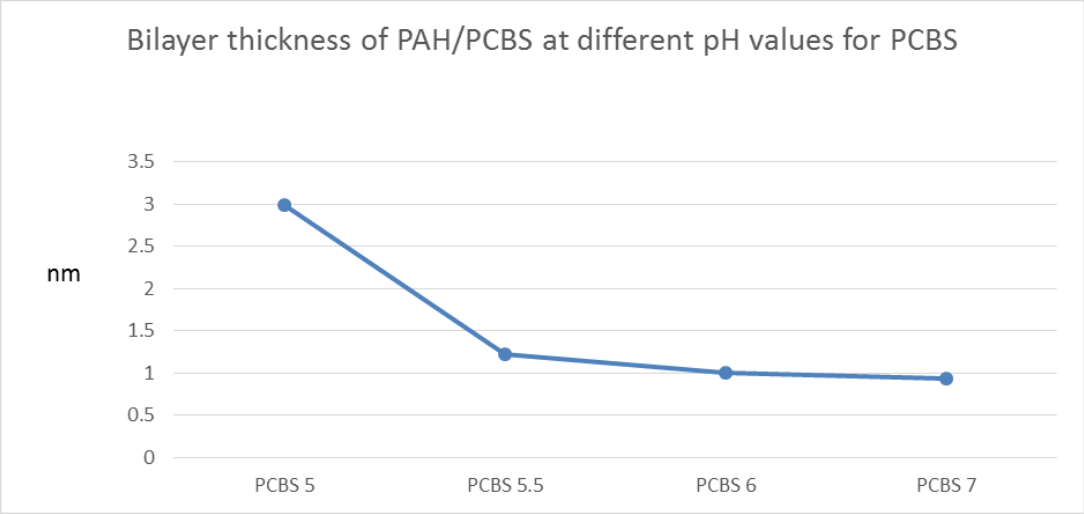

Figure (4.16): A graphical representation of the relationship between the thickness of a single bilayer of PAH/PCBS and the pH of the PCBS solution. The PAH solution was held at pH 7 through out the experiment.

The disproportionate increase of the thickness of a single bilayer of PAH/PCBS deposited at pH 5 for the PCBS can be explained using Rubner's work discussed in detail in chapter 2. If we consider approaching the values of the bilayer thickness from the right side of the graph we will notice a sharp increase in thickness values as the pH of the PCBS solution approaches 5. This can be explained knowing that at pH 7, the PAH solution is fully ionized, while at pH 5, PCBS is partially neutralized (its pK_a is 4.5). A polyelectrolyte is 50% charged at its pK_a and it is 10% ionized and 90% at ionized at +/- one pH unit away from the pK_a. Thus the decreased ionization of PCBS at pH 5.0 leads to thicker adsorbed layers. This increase in thickness is a result of the gain in the enthalpic free energy from spreading the charged polymer layer flat not being able to compensate for the entropic penalty from changing the conformational structure of the polymer. This leads to increased loop structure in the less ionized layer and causes partial segments of it to deposit on the previous layer while the rest of the chain tries to avoid the surface leading to a thick layer formation.[(11)]

Another observation made was that the size of the grafted areas affected the steps of incremental increase in the thickness of the polymer layers deposited on the pattern. For instance, comparing the heights achieved by LbL deposition on squares of sizes 500 nm to squares of size 200 nm showed that the height of the layers deposited over the smaller square increased by 0.4 nm-0.6 nm per bilayer on average for all levels of pH for the polyelectrolyte solutions. Figure (4.17) shows an array of squares of different sizes.

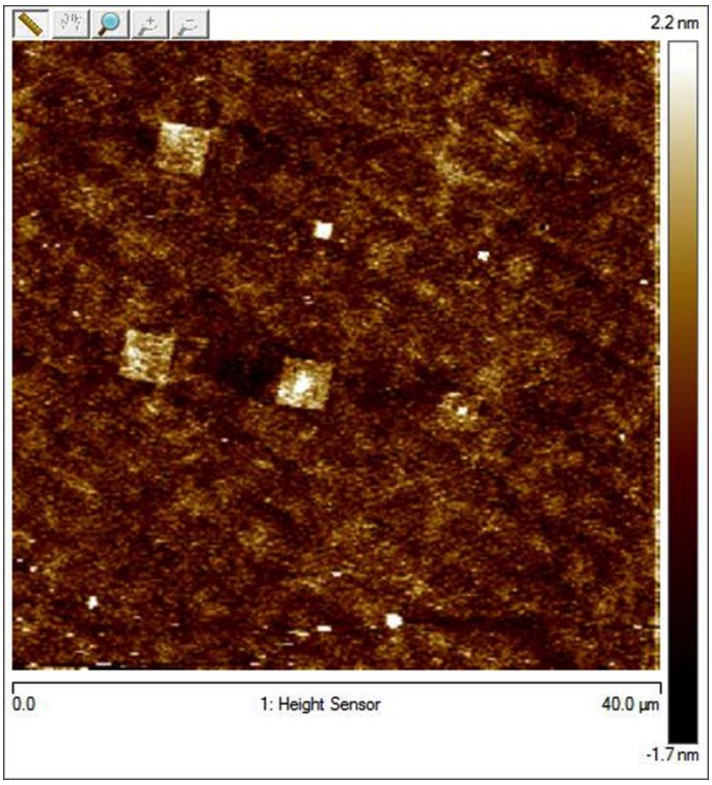

(a)

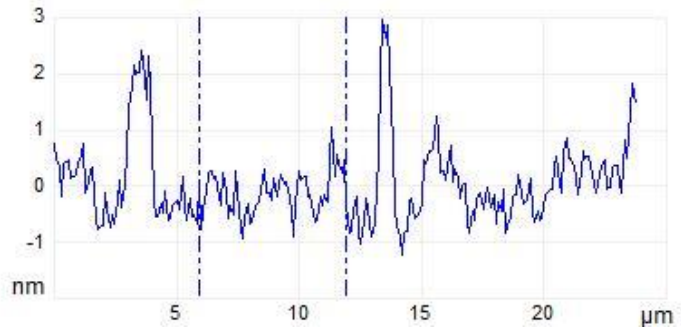

(b)

Figure (4.17): (a) Squares of different sizes of 16-MHDA grafted into a background of 11-MUD and then covered with 4 bilayers of PAH/PCBS at pH ~ 7. We can clearly notice the visible difference in height between the smaller squares of size 200 nm and the bigger squares of sizes 500 nm, 1 um and 3 um. The polymers deposited in thicker films on the smaller squares as opposed to the larger ones. The larger squares were on average 3.5 nm high (for the total of 4 bilayers deposited) while the smaller (200nm) squares were on average 4.3 nm high for 4 bilayers deposited. (b) Height profile of the top row of squares.

Figure (4.18) shows a different part of the array depicted above in Figure (4.17). The height difference is still observable. The sizes of the squares in the image are 3 µm X 3 µm, 1 µm X 1 µm, 500 nm X 500 nm, and 200 nm X 200 nm. The lower row of squares has 3 µm X 3 µm patterns that have unintentional smaller squares inside them. There are two possible reasons for the existence of the smaller squares. The first reason is that the polymers did not adhere well to the larger areas of the 3 µm X 3 µm squares and were partially washed away from the edges of the pattern during the rinsing process. The second possible reason is that due to some misalignment issues with the AFM due to thermal drifting and failure to reposition the AFM tip to specific locations, it is possible that it re-patterned the center of the square during the grafting process causing a higher density of 16-MHDA in the center and thus causing better adhesion there for the polymers.

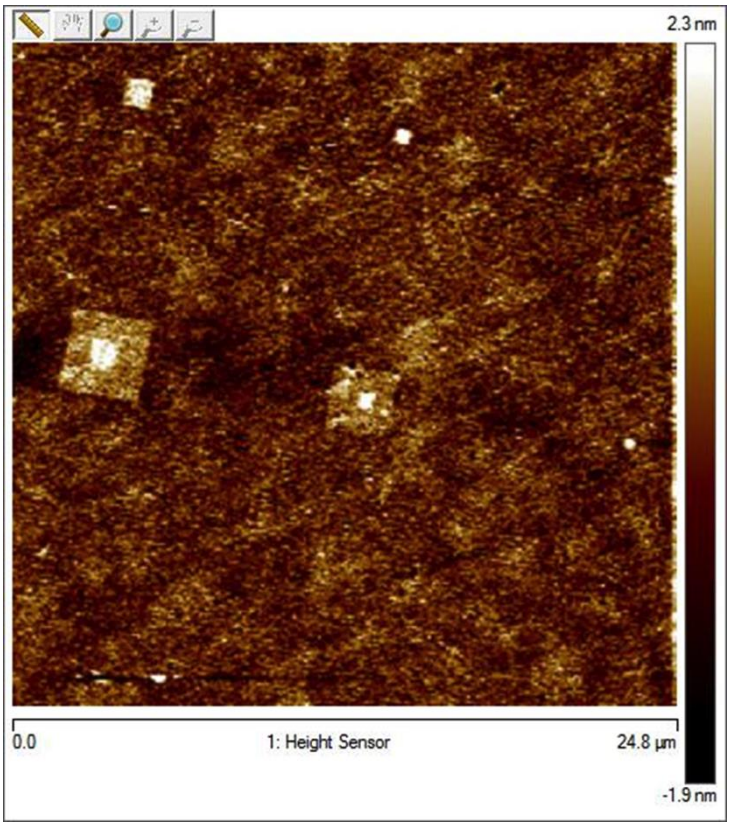

(a)

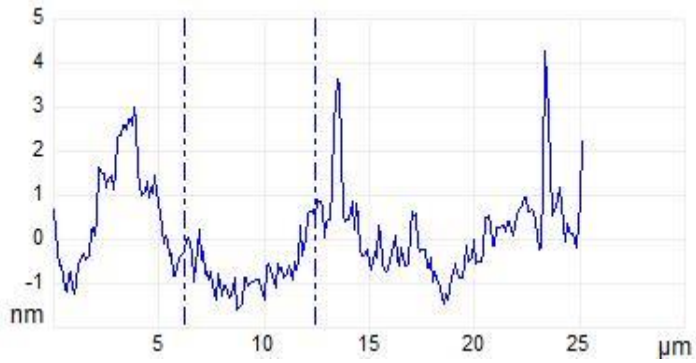

(b)

Figure (4.18): (a) A closer look at the patters of 16-MHDA grafted into 11-MUD and covered with 4 bilayers of PAH/PCBS the difference between the larger squares and the smaller ones is till visible. (b) A cross sectional view of the height profile is shown for the lower row. The sizes of the squares shown in the image are 3 µm X 3 µm, 1 µm X 1 µm, 500 nm X 500 nm, and 200 nm X 200 nm.

Figure (4.19) shows measurements done to compare the heights of the bilayers deposited on each of the squares.

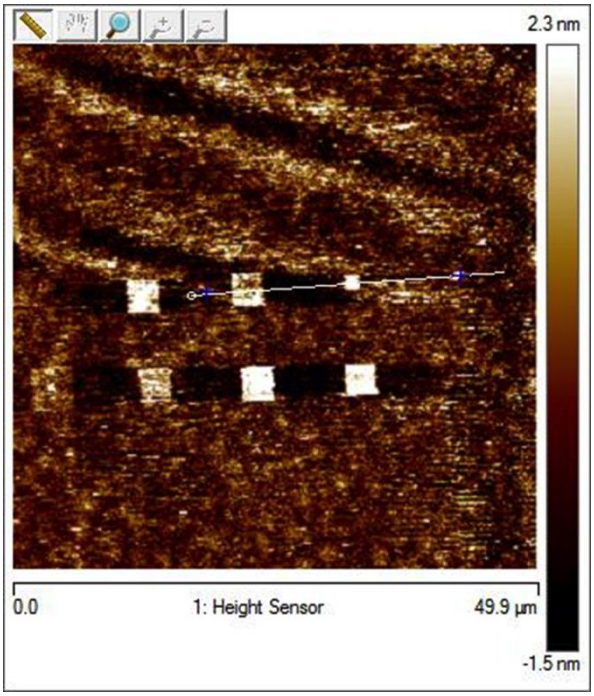

(a)

(b)

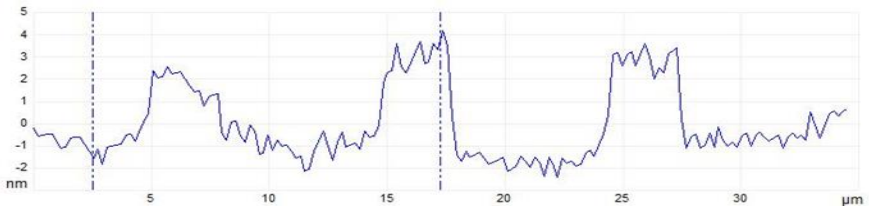

(c)

Figure (4.19): (a) Two rows of squares of 16-MHDA grafted into a background of 11-MUD and covered with 4 bilayers of PAH/PCBS. (b) Cross sectional view of the heights of the polymer layers deposited on patterned areas. We can see that the polymers aggregate in thicker layers on the smaller squares. (c) For comparison, a cross sectional view is taken of the second row of squares of equal sizes. The height of the polymer layers remains the same on average on these squares.

Figure (4.20) shows a comparison between two rows of squares of sizes 500 X 500 nm and 200 nm X 200 nm respectively. The average height for the 500 X 500 nm squares is 5.0 nm while the average height for the 200 X 200 nm square is 6.8 nm.

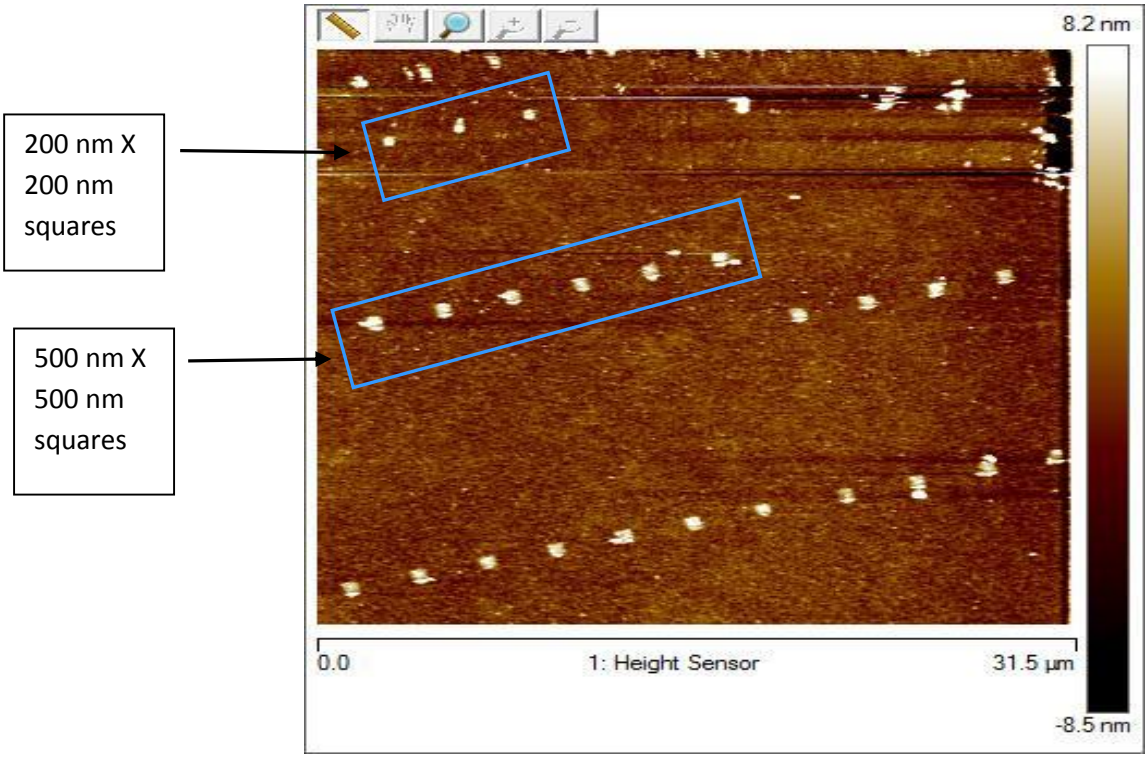

(a)

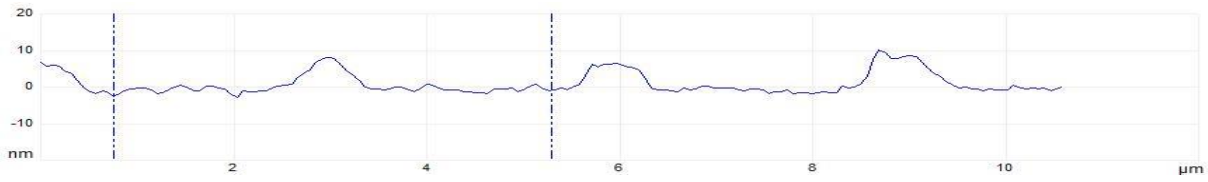

(b)

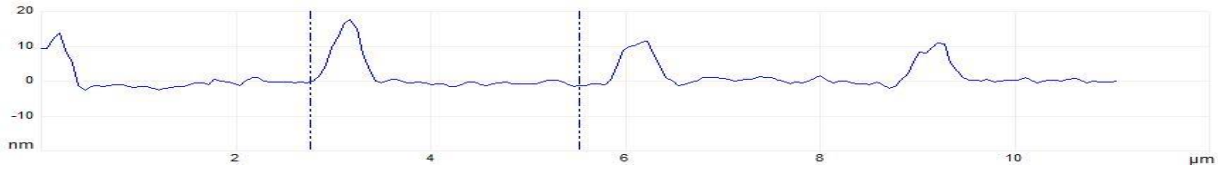

(c)

Figure (4.20): (a) AFM height image of two different sizes of squares 500 nm and 200 nm covered by 4 bialyers of PAH/PCBS using layer-by-layer deposition at pH 5.5. (b) Cross-sectional height measurement of the 500 nm X 500 nm squares. (c) Cross sectional height measurement of the 200 nm X 200 nm squares.

Figure (4.21) shows a comparison between the average thickness of a single bilayer of PAH/PCBS for squares of sizes 3 µm X 3 µm, 500 nm X 500 nm, and 200 nm X 200 nm at different pH levels.

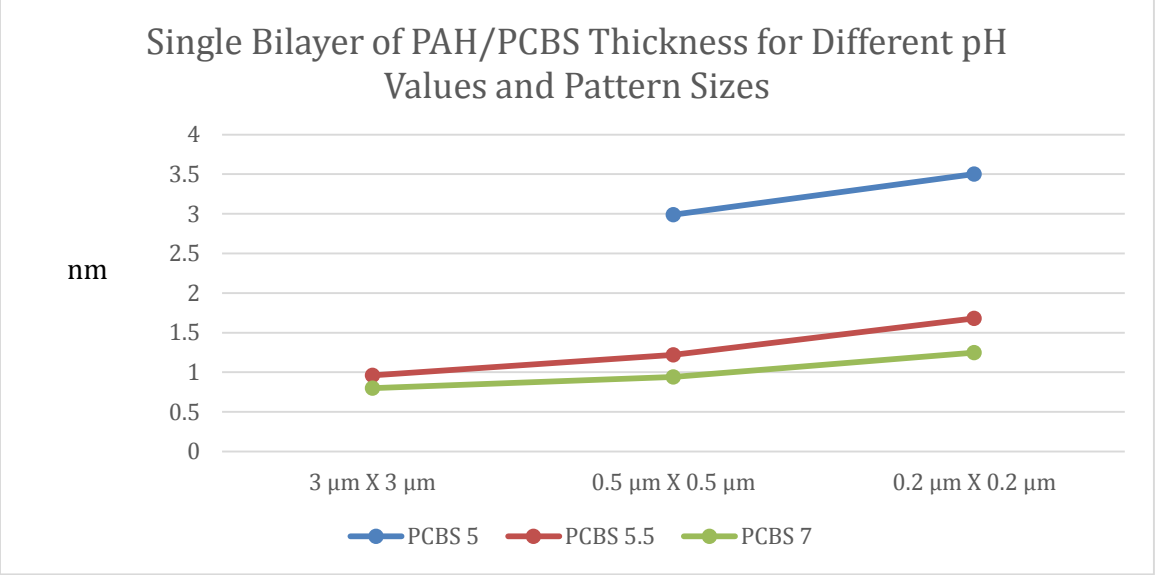

Figure (4.21): A graphical representation of the comparison between the single bilayer thickness of PAH/PCBS as a function of pH for different square sizes.

One possible explanation for smaller patterns having a higher value for the thickness of the layer depositing on them could be attributed to polymer chains folding on top of themselves on the square due to its small size and the inability of the patterned area to accommodate the entire polymer chain in a horizontal manner. But this effect clearly needs more study.

We carried out another comparative study to examine the feasibility of using selective deposition techniques with different polymers. For this study, we used gold-coated slides of the same type used previously. As before, the slides were cleaned by boiling them in ethanol for 45 mins. Then the slides were dipped in 10 mM solution of 11-MUD in ethanol for 48 hours. Then different patterns were constructed on the 11-MUD layer on the gold surface by using nanografting techniques to introduce patches of 16-MHDA into the background matrix. Then we dipped the patterned samples into polyelectrolytes using LbL deposition techniques to achieve selective depositions. The dipping trials were done using two different combinations of polymers. For the first set we used a combination of PAH/PAA. The polyelectrolyte solutions were used at various pH levels. Trials were carried where the pH levels of PAH/PAA were at 3.0/3.0, 5.0/5.0, 9.0/9.0, 3.0/5.0, 3.0/9.0, 5.0/3.0, 5.0/9.0, 9.0/3.0, and 9.0/5.0. The dipping for each of the layers was carried out manually for 3 minutes at room temperature of 23.5 °C. Each dip was followed by a thorough rinse with DI water. Imaging was carried out in liquid. The liquid used was DI water at pH 7.0. Imaging was done after depositing 2 bilayers, 6 bilayers, and 10 bilayers. The procedure was then repeated for the polyelectrolytes PAH/PSS using the same steps. Given that PSS is a strong polyelectrolyte, we kept its pH at 3.0 for the entire experiment. The general form of the patterns is shown in Figure (4.22) and Figure (4.23), which shows images of the patterns after nanografting and prior to deposition of polyelectrolytes.

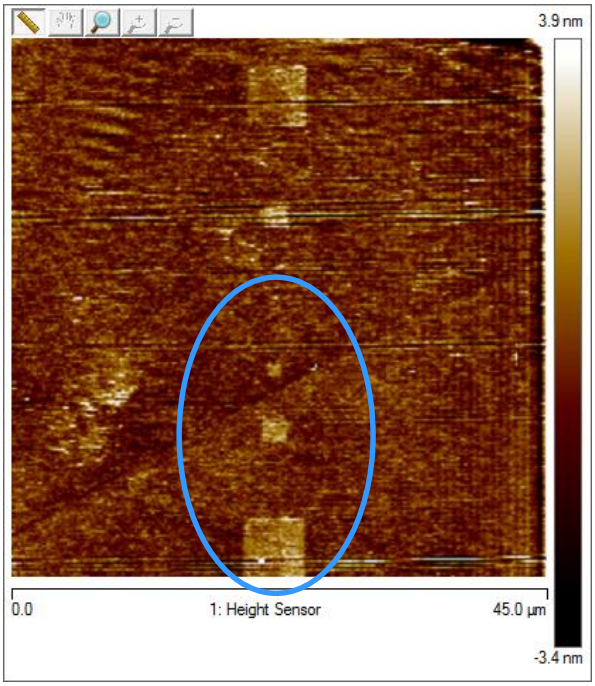

(a)

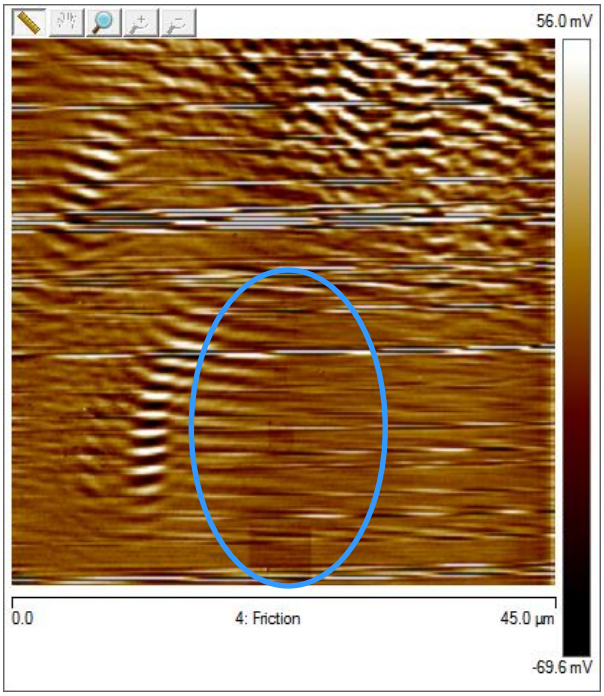

(b)

Figure (4.22): (a) Topographic image of the patterns of 16-MHA grafted onto a background of 11-MUD. The squares were made in sizes of 5 µm, 2 µm, 1 µm, 500 nm, 200, nm, 100 nm, and 50 nm. (b) Friction images of the patterns. The darker areas represent higher friction. Imaging is done in ethanol.

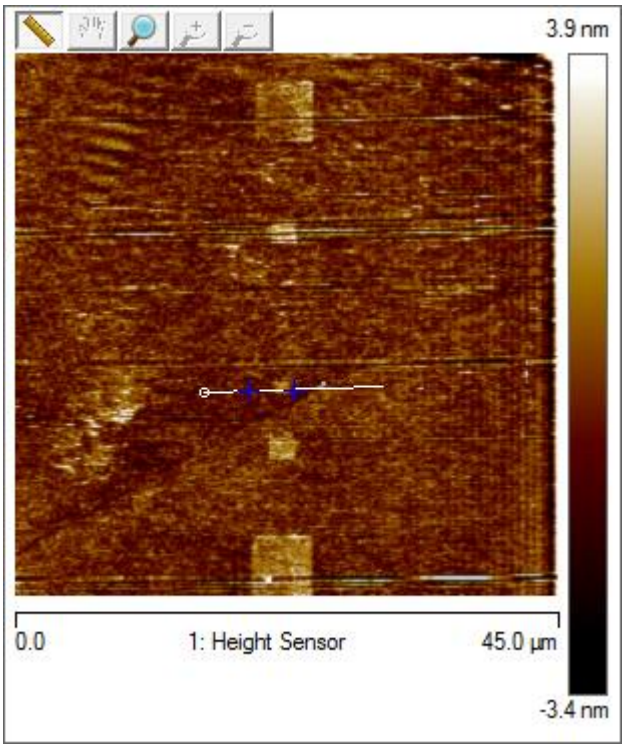

(a)

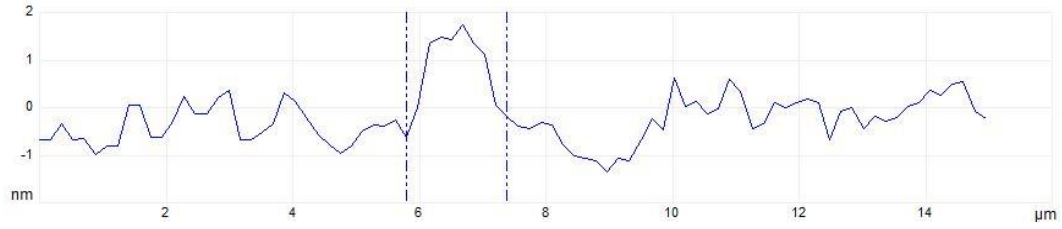

(b)

Figure (4.23): (a) A topographic map of the patterned area of 16-MHA grafted onto a background of 11-MUD showing where the height profile measurements were taken. (b) Height profile measurements for one of the patterned areas. The height profile measurement combined with roughness measurements yield a height difference of 0.55 nm on average between the background and the grafted patch. This height corresponds to the height difference in the chain length difference between the 11-MUD molecule in the background matrix and the 16-MHDA molecule in the grafted area.

In what follows, we show a sample of the images that were taken after 2 bilayer, 6 bilayer and 10 bilayer deposition for PAH/PAA at different pH levels for each. Figures (4.24) through (4.26) are for the case of both polyelectrolytes at pH 9.0

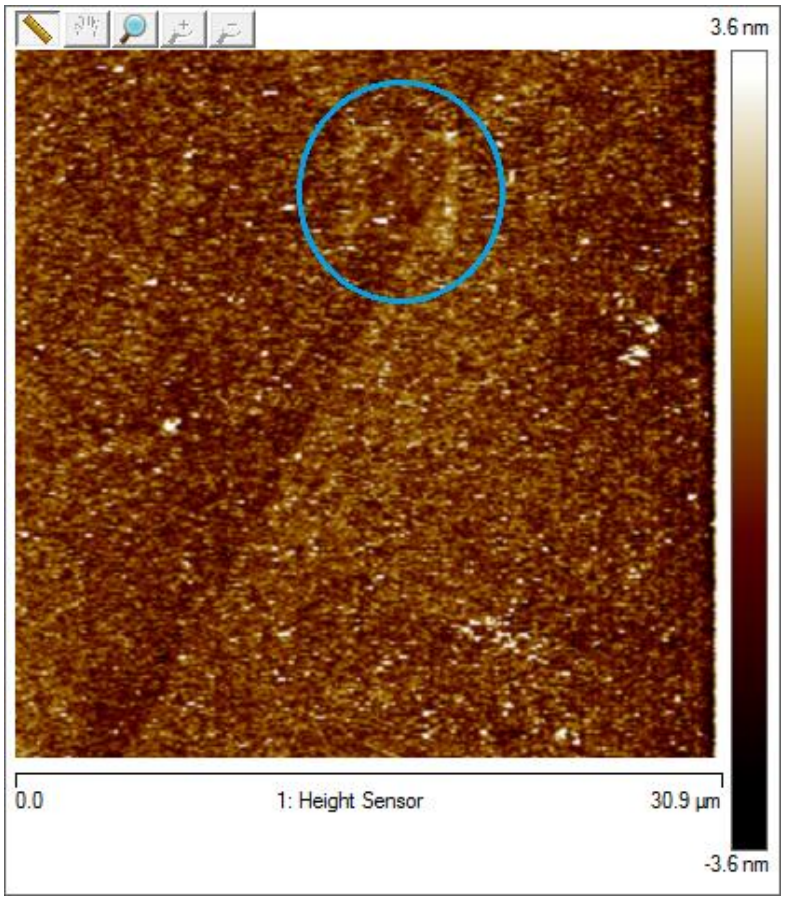

(a)

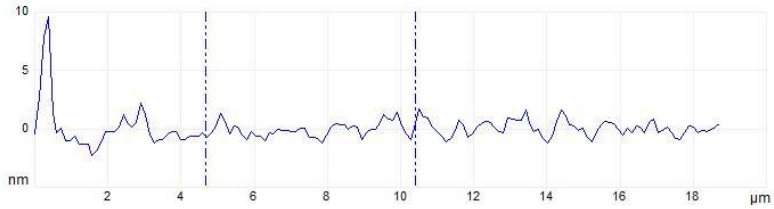

(b)

Figure (4.24): (a) Image of a 5 µm square after 2 bilayers of PAH/PAA at pH 9/9 were deposited on it. The height profile is barely noticeable. Roughness measurements indicate a height difference on the order of 0.7 nm. The change in the morphology of the entire surface including both the background and the patterned areas indicate that the polymers deposited on both the background and the patterned square. (b) Height profile image where the markers indicate the edges of the square. No height difference is observable here.

Examining the friction image of the sample reveals that the background has the same fiction as the patterned square suggesting that the polymers are depositing on background and the patterned square alike.

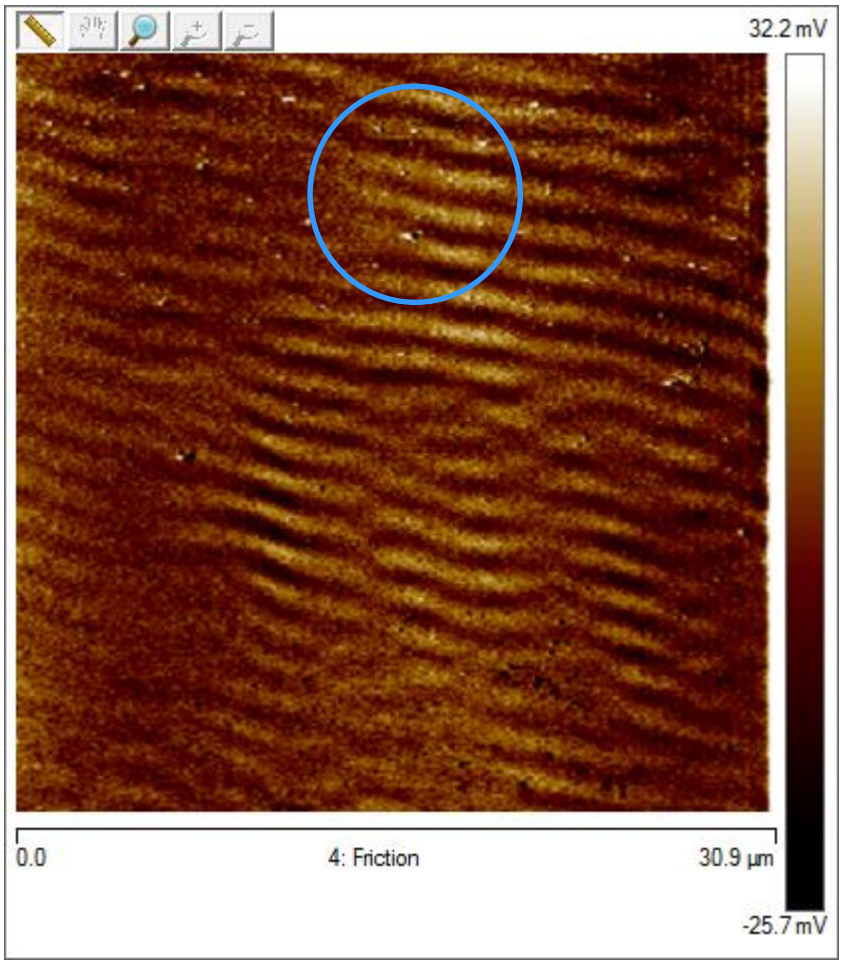

Figure (4.25): Friction image of the 2 bilayers deposited on the square in Figure (4.24). The lack of any distinction in the friction between the background and the patterned square indicates the polymers are depositing everywhere on the surface. We can also see the difference in the morphology of the background compared to the case of a gold surface functionalized with 11-MUD confirming the deposition of the polymer layers everywhere.

After depositing 10 bilayers of PAH/PAA at 9/9 we get the image of Figure (4.26).

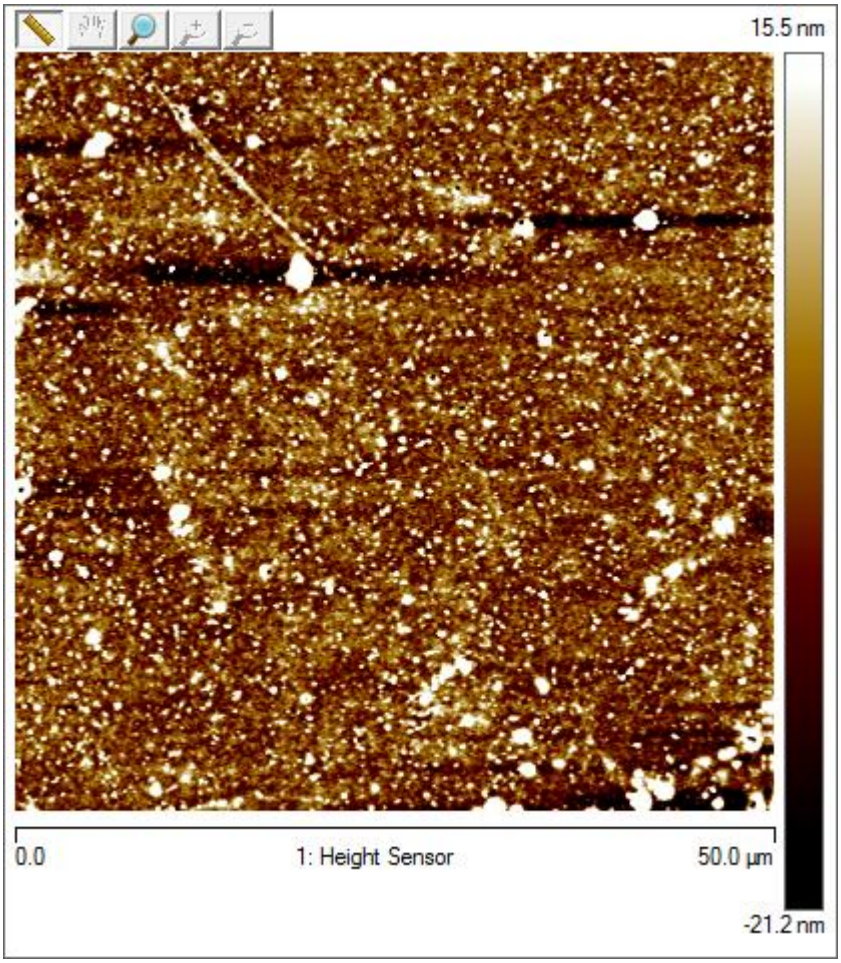

Figure (4.26): After depositing 10 bilayers of PAH/PAA at pH9/9. The patterns have completely disappeared. It is clear that in this case that the polymers have deposited on the entire surface.

After depositing 2 bilayers of PAH/PAA on one of the samples at pH levels 7.0/7.0, the image of Figure (4.27) is obtained.

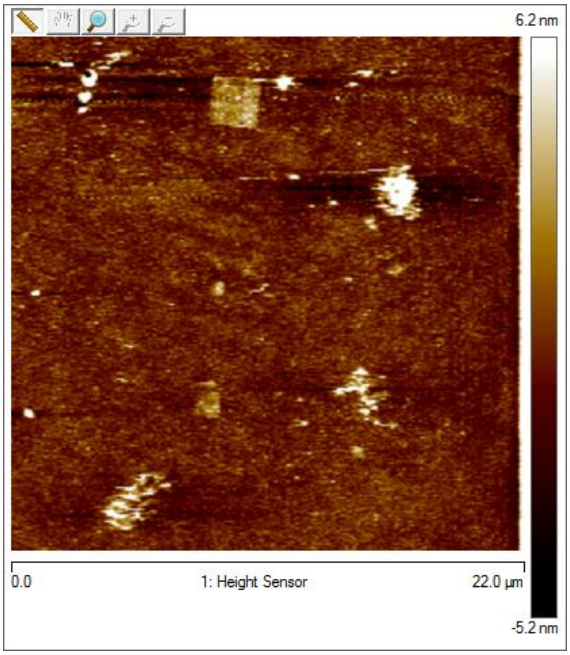

(a)

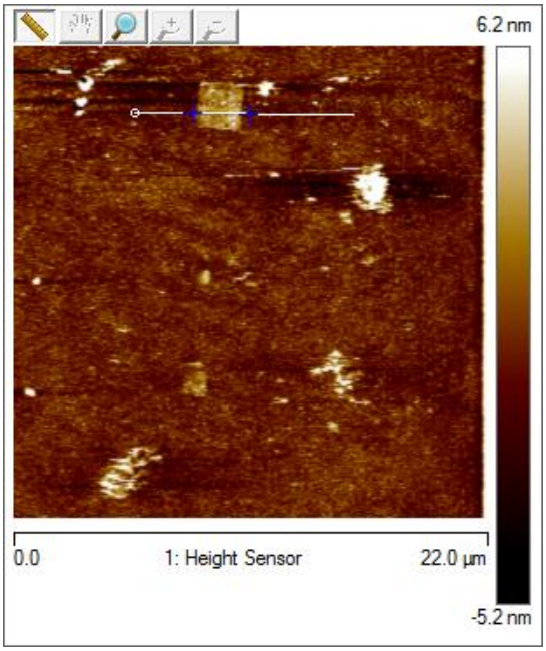

(b)

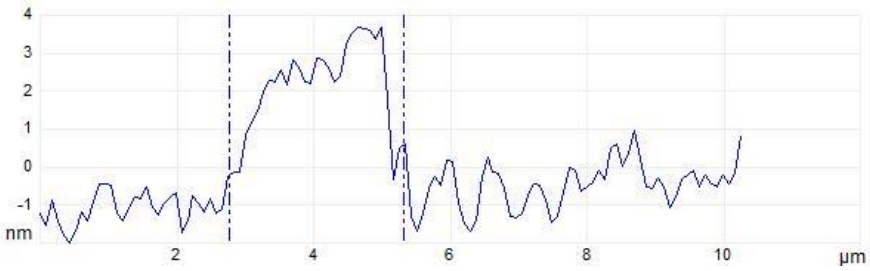

(c)

Figure (4.27): (a) Height image after depositing 2 bilayers of PAH/PAA at pH levels of 7/7. (b) A height image illustrating where the height profile is being measured. (c) Height profile of one of the patterned squares. The average height for these trials was 4 nm.

Imaging again after depositing another 4 bilayers to reach a total of 6 bilayers resulted in Figure (4.28).

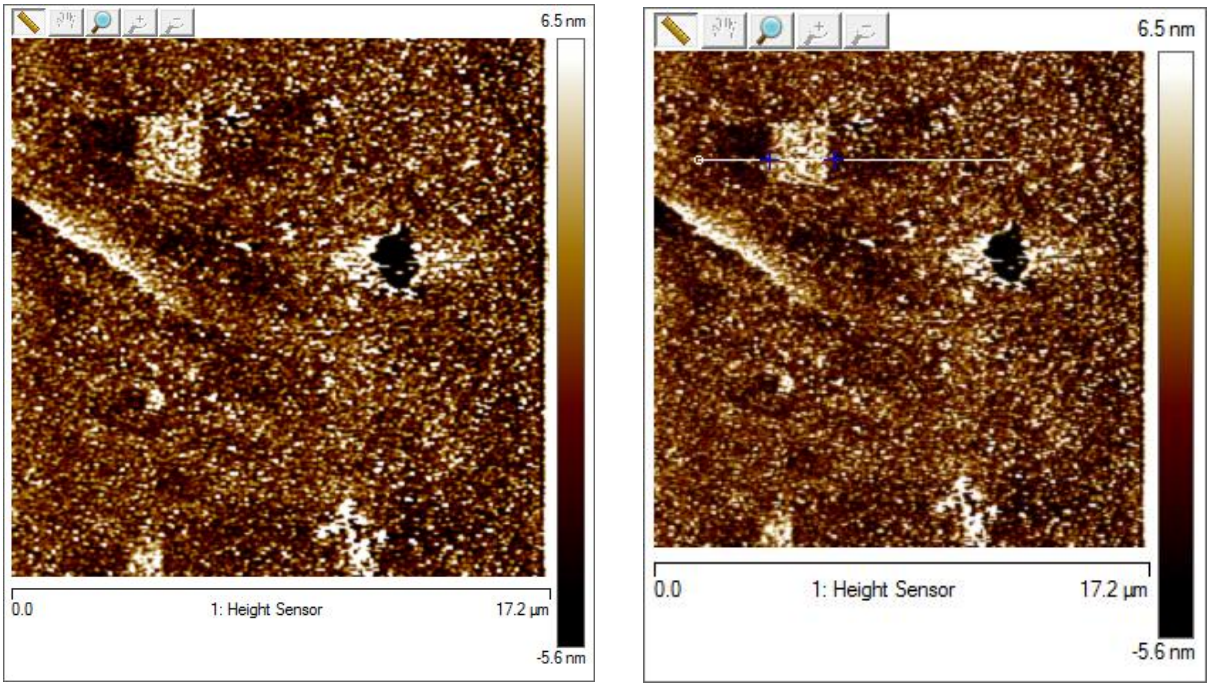

(a) (b)

(c)

Figure (4.28): (a) Height image after depositing 6 bilayers of PAH/PAA at pH levels 7/7. (b) Height image indicating where the height profile is being measured. (c) Height profile for one of the patterned squares. The average for the height of these patterns is 9.5 nm. It is observable from the change in the surface of the entire sample that polymers are depositing everywhere but with stronger affinity to depositing on the patterned area.

Imaging after depositing 10 bilayers of PAH/PAA at pH levels of 7/7 resulted in Figure (4.29).

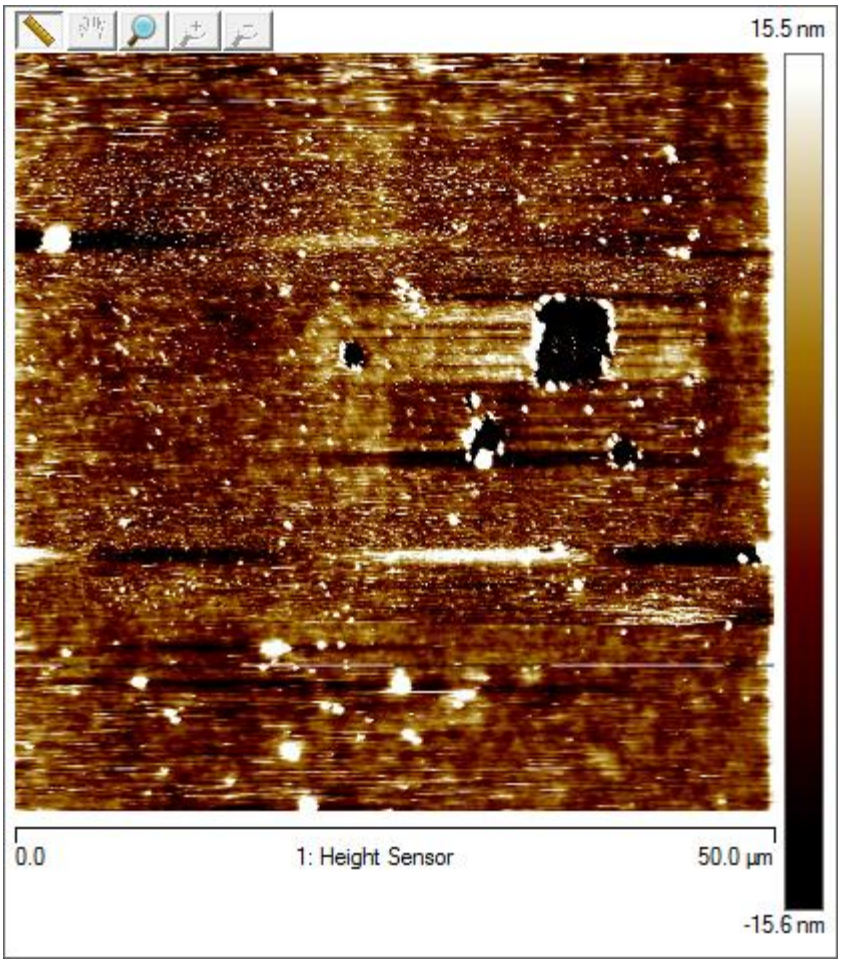

Figure (4.29): Imaging after depositing 10 bilayers of PAH/PAA at pH 7/7 resulted in the polymers depositing everywhere on the sample including the background and the patterned patches to the extent of losing the patterns completely.

Changing the pH levels of the bilayers of PAH/PAA to 9.0/3.0 and performing another round of LbL deposition on patterned areas, we get the following results.

After depositing 2 bilayers, the images of Figure (4.30) are found.

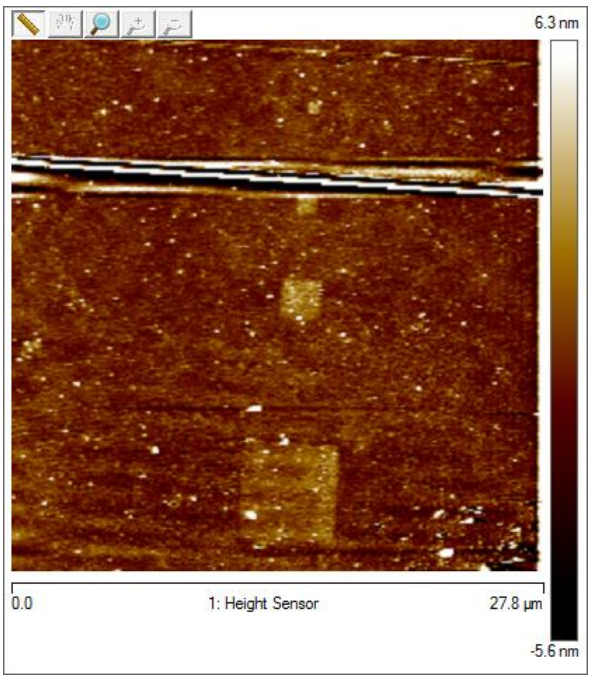

(a)

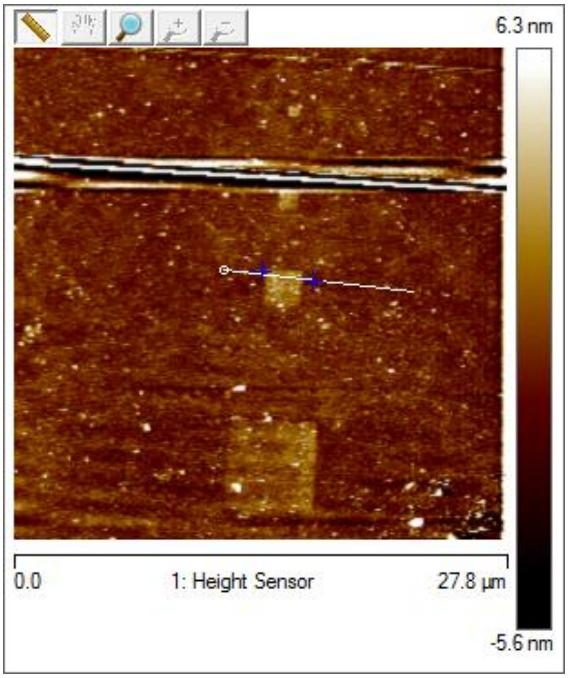

(b)

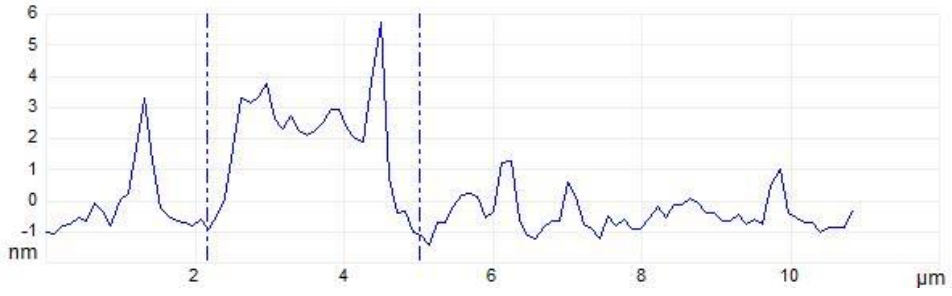

(c)

Figure (4.30): (a) Height image after depositing 2 bilayers of PAH/PAA at pH levels 9/3. (b) Height image indicating where the height profile is being measured. (c) Height profile for one of the patterned squares. The average for the height of these patterns is 4.2 nm.

Imaging after depositing 6 bilayers at the same conditions, we get Figure (4.31).

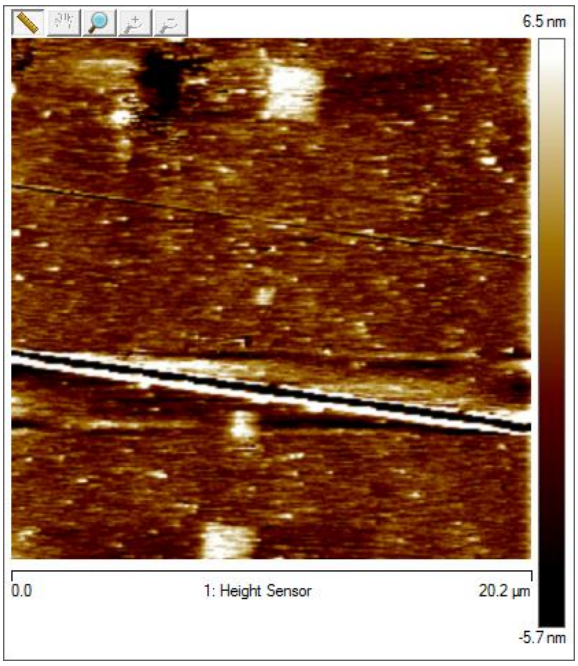

(a)

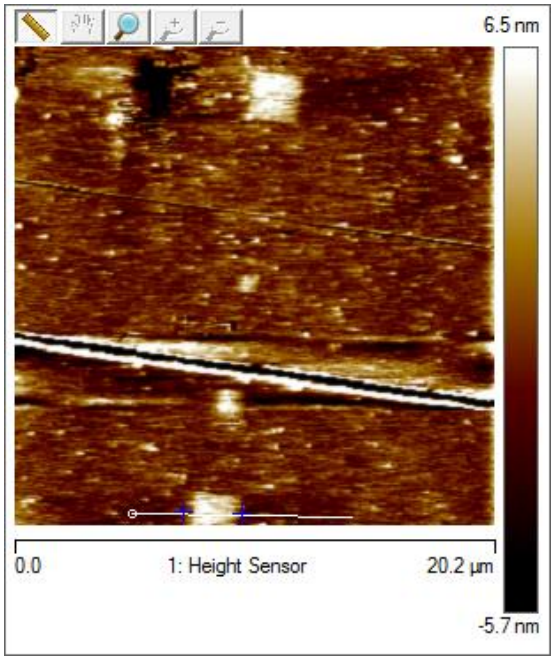

(b)

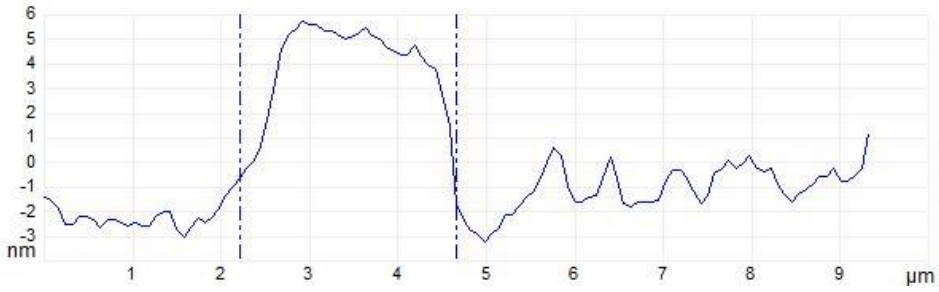

(c)

Figure (4.31): (a) Height image after depositing 6 bilayers of PAH/PAA at pH levels 9/3. (b) Height image indicating where the height profile is being measured. (c) Height profile for one of the patterned square. The average for the height of these patterns is 8.3 nm.

Imaging after depositing 10 bilayers in the same conditions reveals loss of the patterns as seen in Figure (4.32).

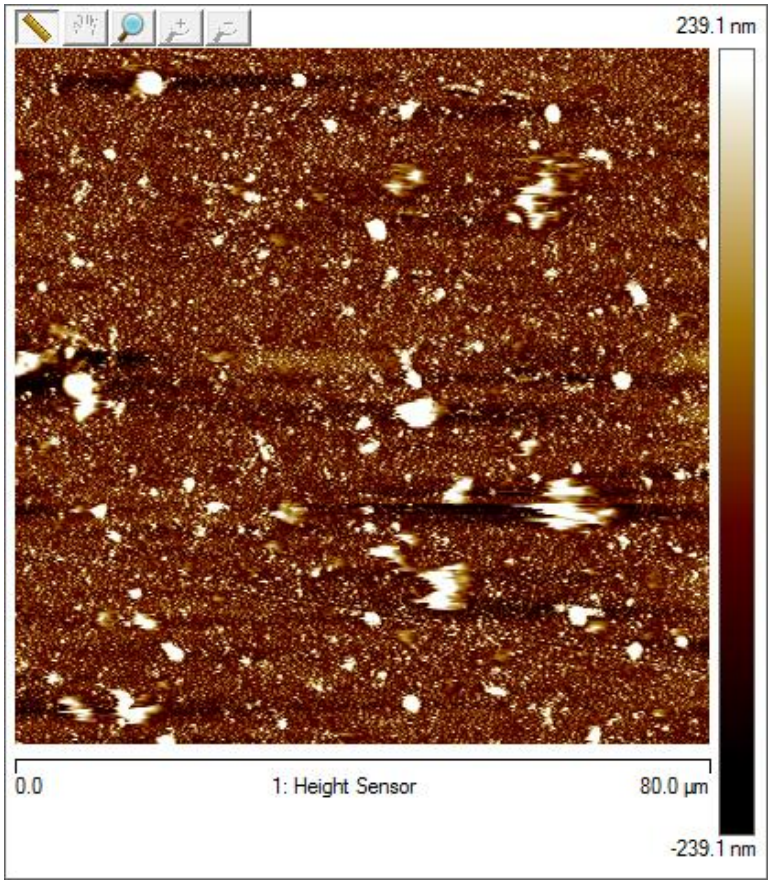

Figure (4.32): A height image after depositing 10 bilayers of PAH/PAA at pH 9/3reveals the loss of the pattern due to the depositing of the polymer layers on the entire sample including the background and the patterned square.

Changing the pH levels of the PAH/PAA dipping solution to 9/7 and continuing the LbL deposition, we deposit 2 bilayers on a new sample and image it to get Figure (4.33).

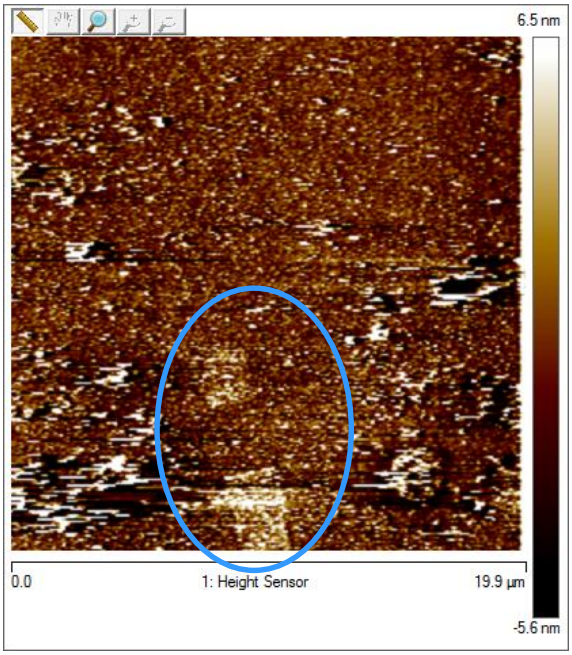

(a)

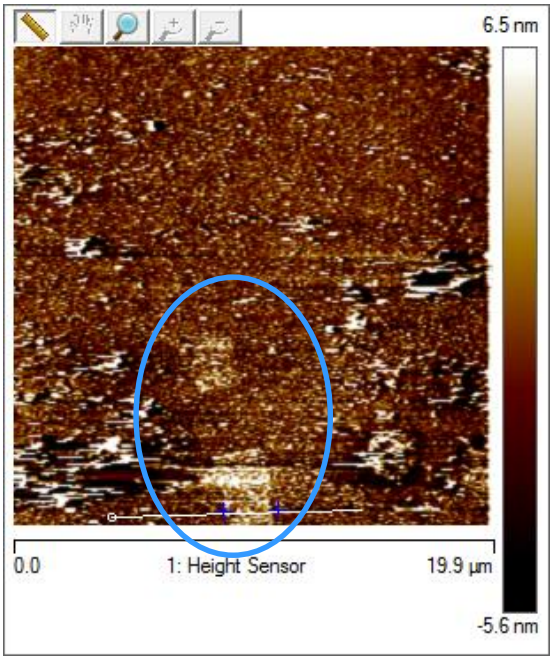

(b)

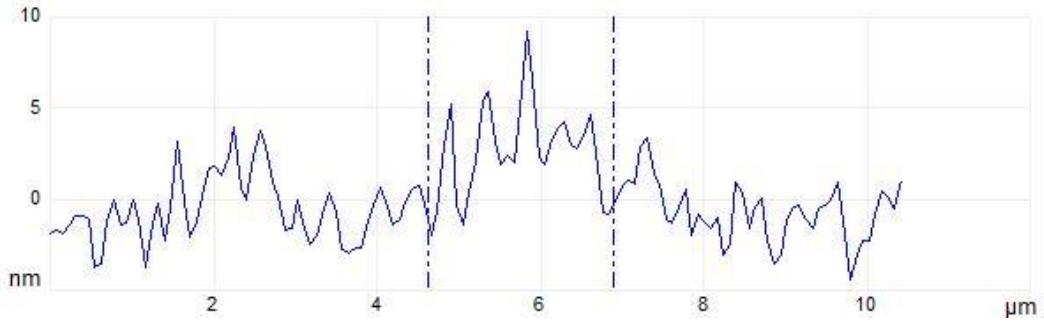

(c)

Figure (4.33): (a) Height image after depositing 2 bilayers of PAH/PAA at pH levels 9/7. (b) Height image indicating where the height profile is being measured. (c) Height profile for one of the patterned square. The average for the height of these patterns is 3.9 nm.

Depositing 6 bilayers at the same conditions and imaging the result gives us Figure (4.34).

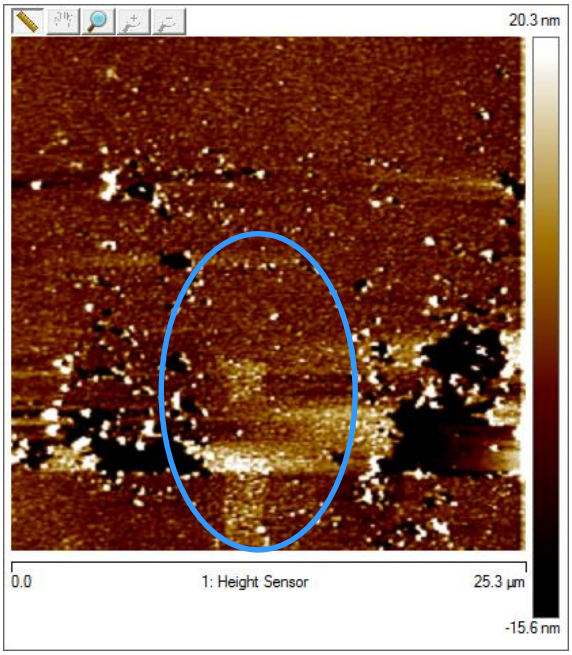

(a)

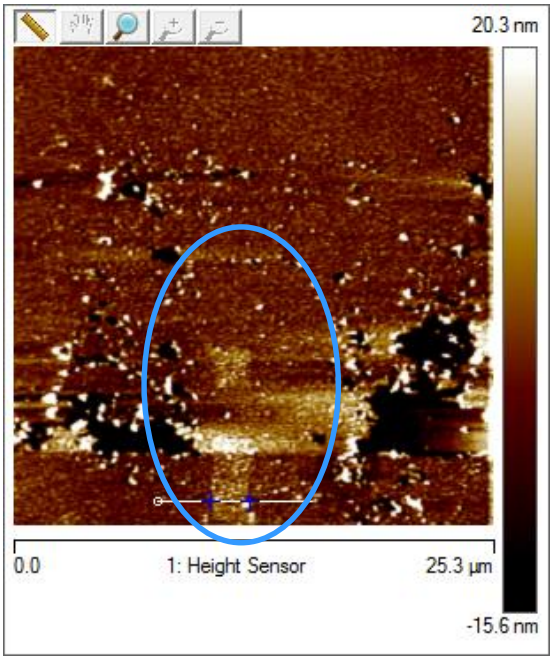

(b)

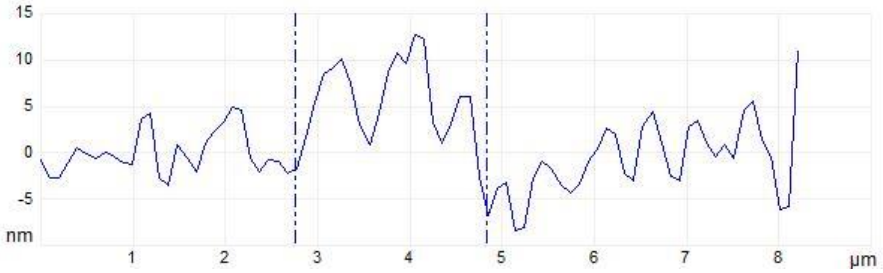

(c)

Figure (4.34): (a) Height image after depositing 6 bilayers of PAH/PAA at pH levels 9/7. (b) Height image indicating where the height profile is being measured. (c) Height profile for one of the patterned square. The average for the height of these patterns is 8.7 nm.

Depositing 10 bilayers at the same conditions and imaging shows that the patterns disappear due to the polymers depositing everywhere as seen in Figure (4.35).

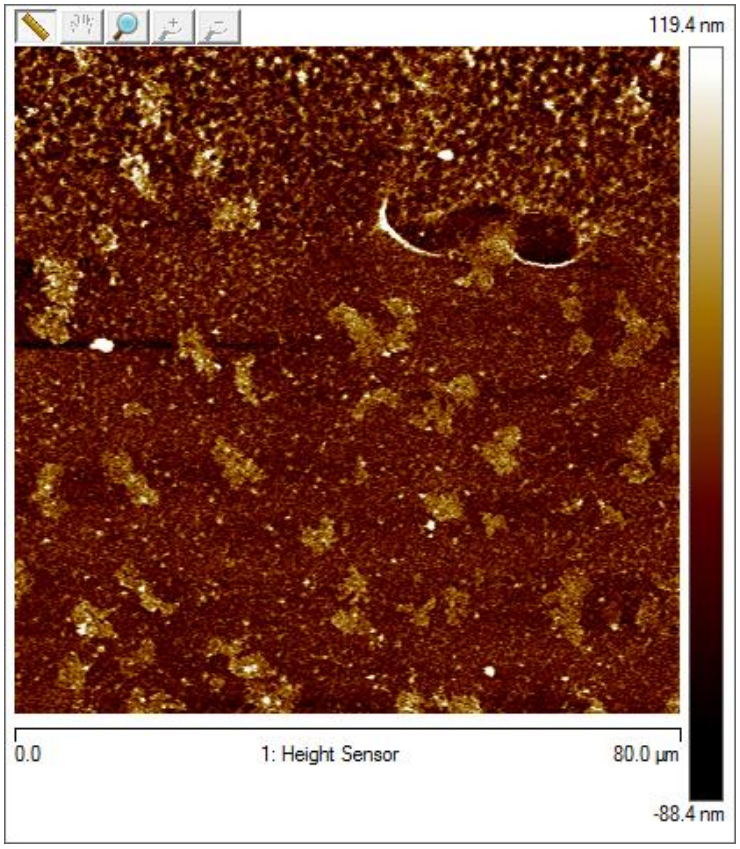

(c)

Figure (4.35): A height image after depositing 10 bilayers of PAH/PAA at pH 9/7reveals the loss of the pattern due to the depositing of the polymer layers on the entire sample including the background and the patterned square.

The experiments performed using PAH/PAA multilayers revealed that the bilayers deposit to some extent everywhere on the substrate in a nonselective manner leading to the eventual loss of patterns

rapidly. Such nonselective deposition can be seen from the friction images where the distinction between patterned areas and the passivated background disappear rapidly.

When the polyelectrolytes were changed to PAH/PSS and the pH level of the PAH was alternated between 3.0, 7.0 and 9.0 while keeping the PSS solution at pH 3.0 we got the results of Figure (4.36) for depositing 2 bilayers of PAH/PSS at pH levels 7/3.

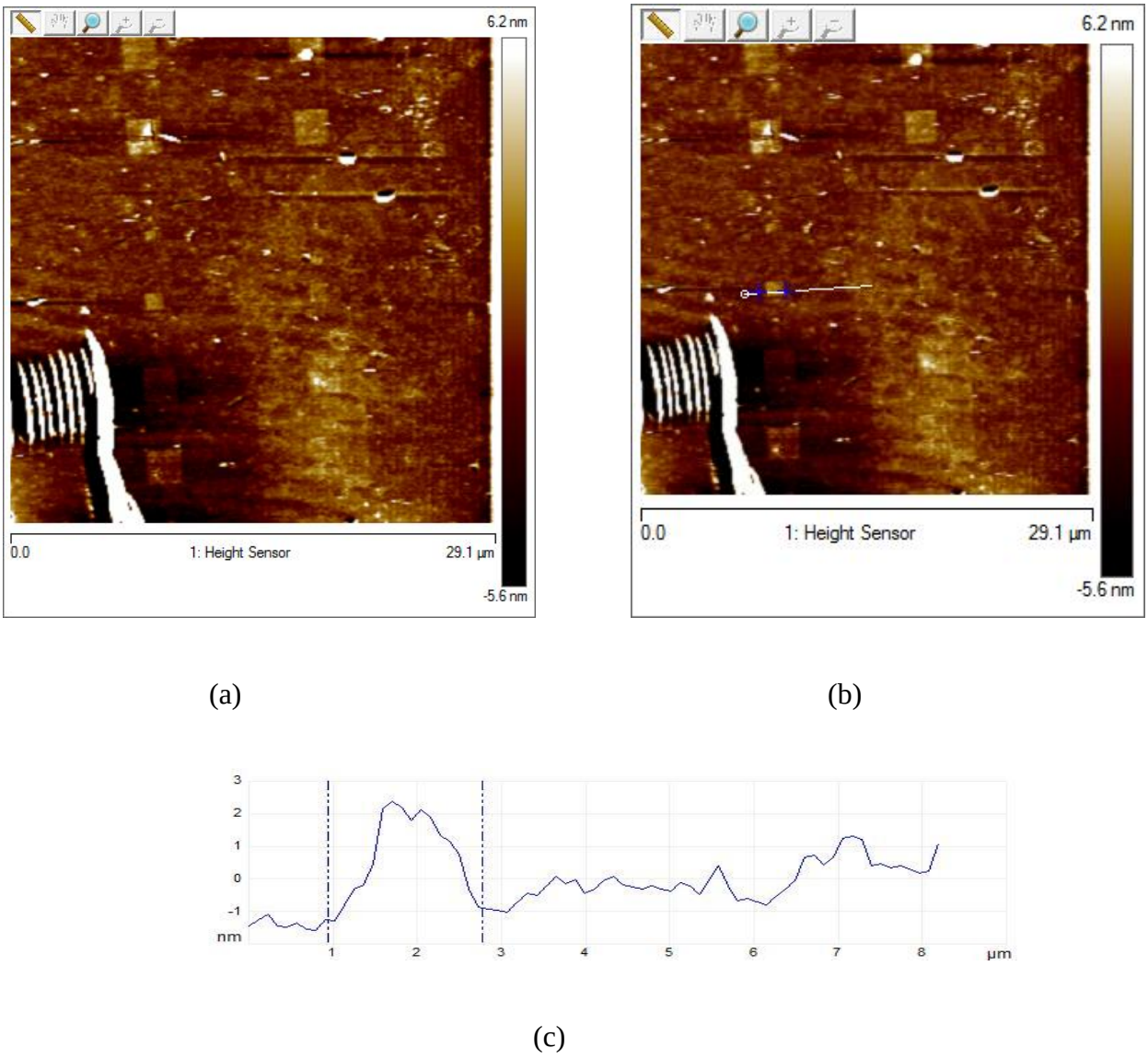

Figure (4.36): (a) Height image after depositing 2 bilayers of PAH/PSS at pH levels 7/3. (b) Height image indicating where the height profile is being measured. (c) Height profile for one of the patterned square. The average for the height of these patterns is 3.16 nm.

Depositing 6 bilayers at the same conditions and imaging gives us Figure (4.37).

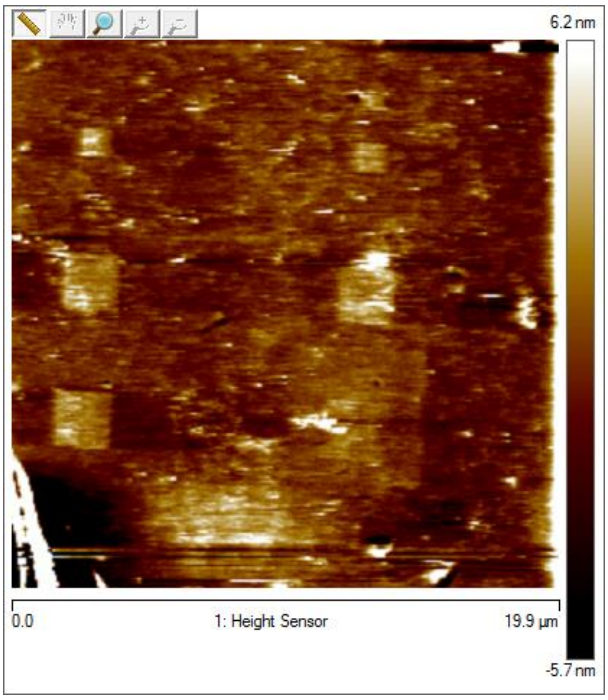

(a)

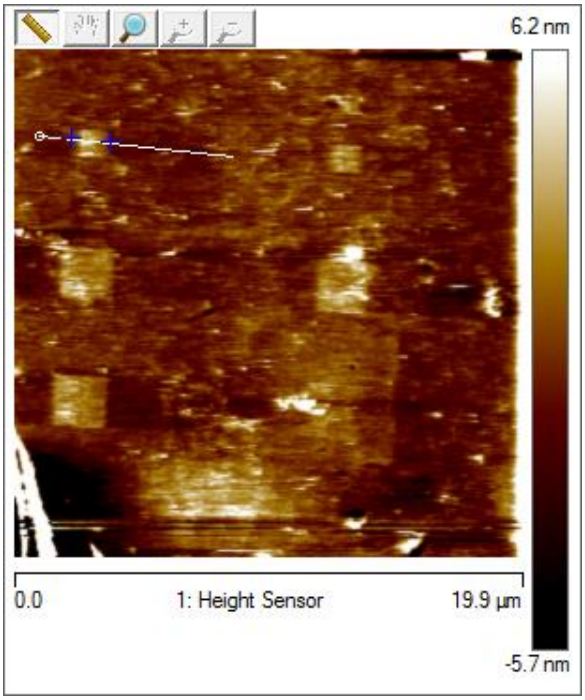

(b)

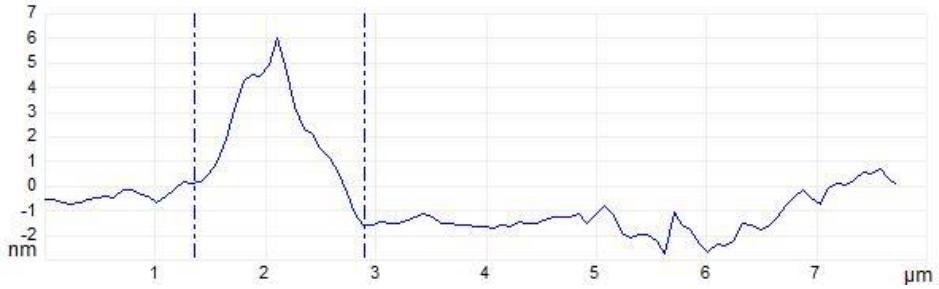

(c)

Figure (4.37): (a) Height image after depositing 6 bilayers of PAH/PSS at pH levels 7/3. (b) Height image indicating where the height profile is being measured. (c) Height profile for one of the patterned squares. The average for the height of these patterns is 6.5 nm.

Depositing 10 bilayers and imaging results in Figure (4.38).

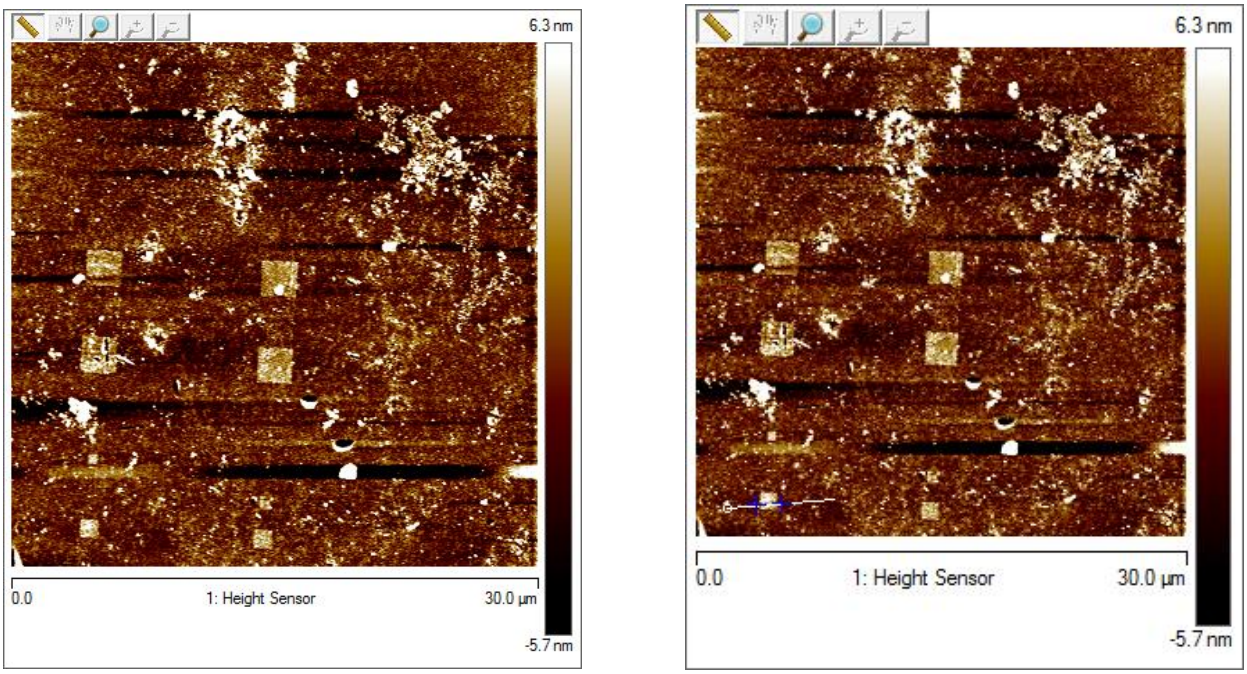

(a) (b)

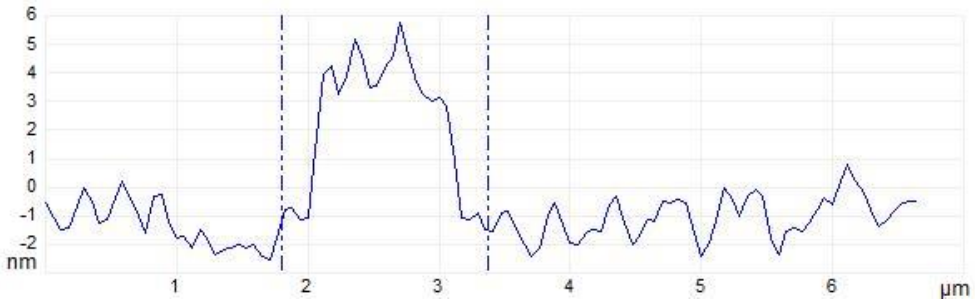

(c)

Figure (4.38): (a) Height image after depositing 10 bilayers of PAH/PSS at pH levels 7/3. (b) Height image indicating where the height profile is being measured. (c) Height profile for one of the patterned squares. The average for the height of these patterns is 8.2 nm.

All of the results for the different pH levels and recorded multilayer thicknesses for PAH/PAA are presented in Figure (4.39). The general observation is that, for most pH combinations, preferential adsorption on the patterned COOH region is observed for low numbers of bilayers but is lost in all cases upon adsorption of ten bilayers. This can be compared to the work of Hammond discussed in Section 2.4.1 and summarized in Figure (2.26). Since Hammond maintained equal pH values for the two solutions, the cases that can be directly compared are the cases for pH 2.5/2.5 (with case 3.0/3.0 here) and pH 7.0/7.0. In both of those cases, Hammond observed deposition on both the COOH and OH surfaces, but with greater adsorption on the COOH surface. This is consistent with our observations, since one would expect that, in the case where deposition occurs on both surfaces, the preference for one surface over the other would eventually get lost as the number of bilayers is increased and the effects of the surface are obscured by the thick film on top of it. One can also consider comparison of the results of Figure (4.39) with the work of Rubner on pH dependence of film thickness. We would expect that total film thickness would generally be less for PAH at pH 3.0 and 7.0 compared to pH 9.0 and for PAA at pH 7.0 and 9.0 compared to pH 3.0, due to the effects of degree of ionization on film thickness (greater ionization results in thinner films). But it is difficult to make any conclusions in this regard with our results, since we are only able to measure the difference in film thickness between the COOH and OH regions as opposed to the absolute thickness on the COOH region. Thus, although the film thickness on the COOH region may follow the expected trends, the thickness of the film adsorbed on the OH region may follow the same trend and obscure the trend with respect to our measurements.

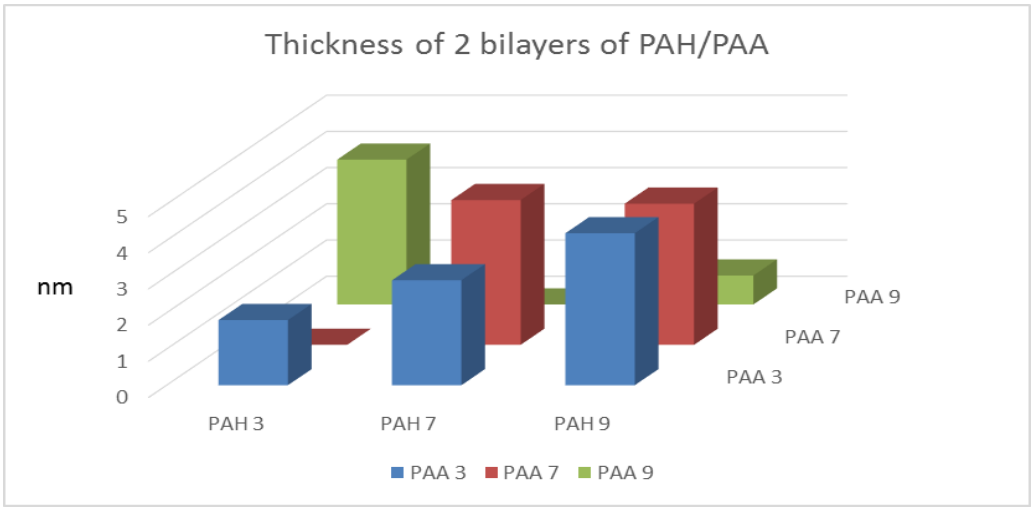
Thickness of 2 bilayers of PAH/PAA
nm
5
4
3
2
1
0
PAH 3
PAH 7
PAH 9
PAA 3
PAA 7
PAA 9
PAA 3 PAA 7 PAA 9

(a)

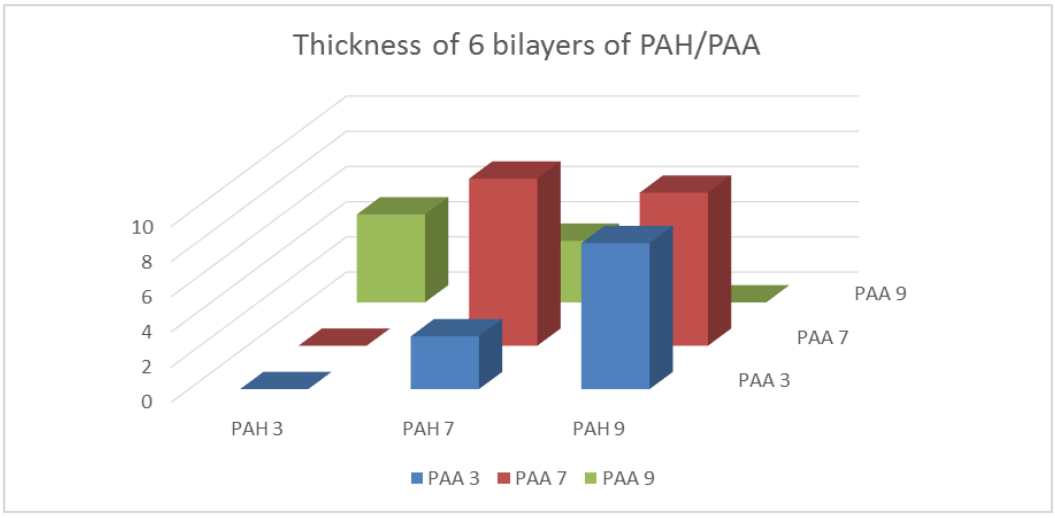
Thickness of 6 bilayers of PAH/PAA
10
8
6
4
2
0
PAH 3
PAH 7
PAH 9
PAA 3
PAA 7
PAA 9
PAA 3 PAA 7 PAA 9

(b)

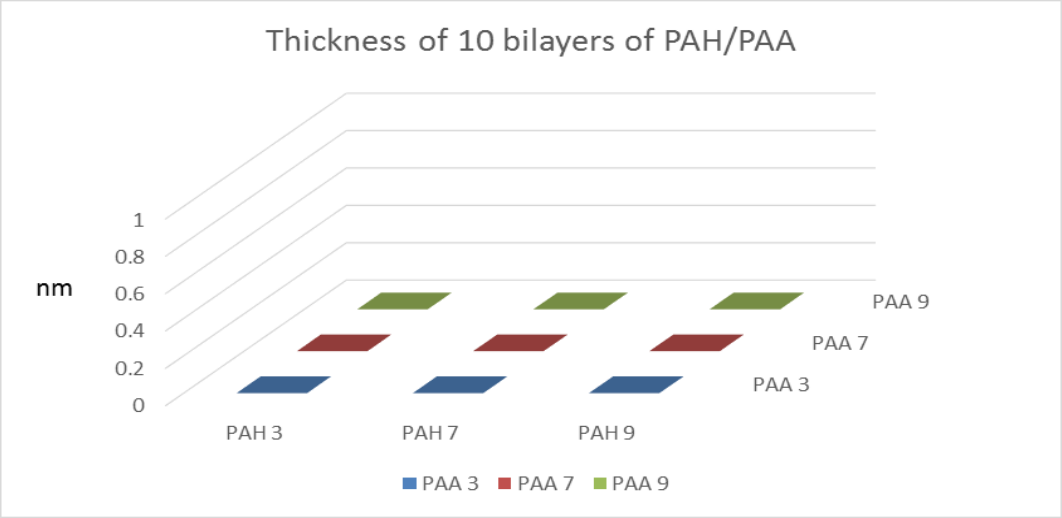

(c)

Figure (4.39): (a) The measured thickness of 2 bilayers of PAH/PAA deposited on patterned areas for a matrix of pH values for the PAH and the PAA solutions. (b) The measured thickness for 6 bilayers of PAH/PAA deposited on the same patterned areas shown in (a) at the same matrix of values of pH for both electrolytes. (c) The measured values for the thickness of 10 bilayers of PAH/PAA. The zero values refer to the inability to distinguish the patterns from the background due to polymer layers depositing everywhere on the sample.

The results from using LbL deposition with the two polymers PAH and PSS where the PAH was alternated between pH levels of 3.0, 7.0, 9.0 and the PSS kept at pH 3.0 are represented Figure (4.40). While the selectivity is lost at ten bilayers for the cases of PAH at pH 3.0 and 9.0, it is maintained at pH 7.0. One would generally expect little difference between the pH 3.0 and 7.0 cases, since PAH is highly charged in both instances and less charged at pH 9.0. However, we do observe a lack of selectivity at pH 9.0 when the PAH is less charged and secondary hydrogen-bonding interactions can lead to adsorption on the OH surface as well as the COOH pattern.

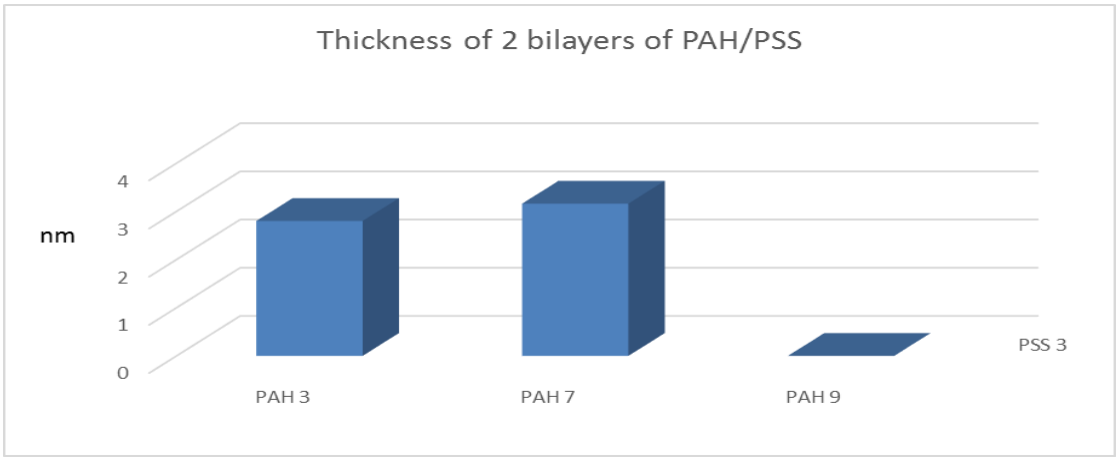
Thickness of 2 bilayers of PAH/PSS
nm
4
3
2
1
0
PAH 3
PAH 7
PAH 9
PSS 3

(a)

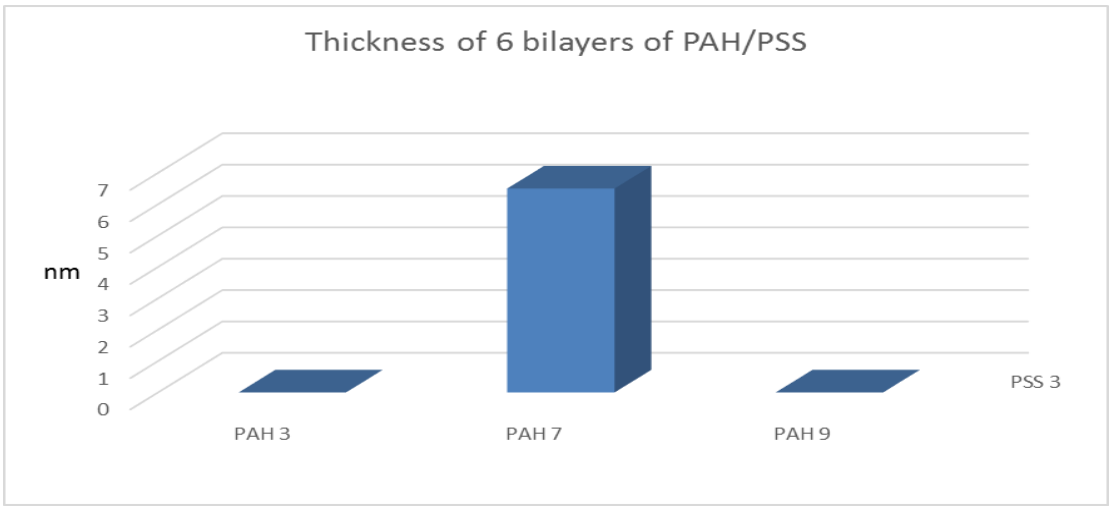
Thickness of 6 bilayers of PAH/PSS
nm
7
6
5
4
3
2
1
0
PAH 3
PAH 7
PAH 9
PSS 3

(b)

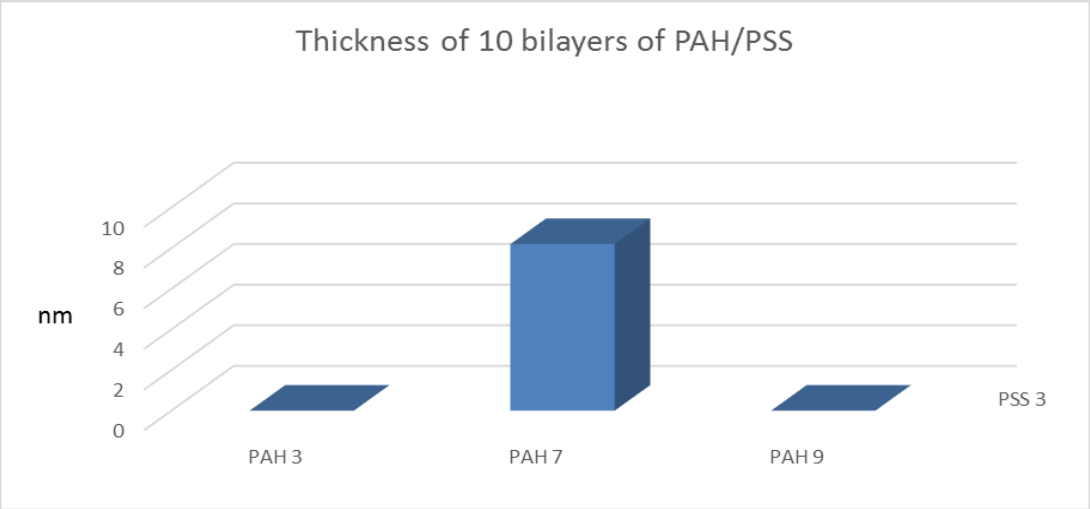

(c)

Figure (4.40): (a) The measured thickness of 2 bilayers of PAH/PSS deposited on patterned areas for three values of pH for the PAH while the PAA solution was held at pH 3. (b) The measured thickness for 6 bilayers of PAH/PSS deposited on the same patterned areas shown in (a) at the same matrix of values of pH for both electrolytes. (c) The measured values for the thickness of 10 bilayers of PAH/PSS. The zero values refer to the inability to distinguish the patterns from the background due to polymer layers depositing everywhere on the sample surface.

A closer look at the friction images after the deposition of 2 bilayers at the different pH levels we examined provides a glimpse into the the selectivity of the deposition process. Friction images that correspond to a highly selective process display a higher contrast between the background and the patterned areas where the polymers are supposed to deposit while avoiding the background. However, when we examine the friction images from the samples we prepared after depositing 2 bilayers of polymers on them, we notice that the friction contrast is fading and that the entire surface of the sample is staring to be homogeneous in both friction and morphology indicating that the polymer multilayers are depositing everywhere. This effect was also noted by Paula Hammond

and co-workers in her papers addressing selective deposition which we summarized in Chapter 2.[2],[3],[4] Figure (4.41) shows various friction images from the samples we prepared after depositing 2 bilayers of PAH/PAA and PAH/PSS on them.

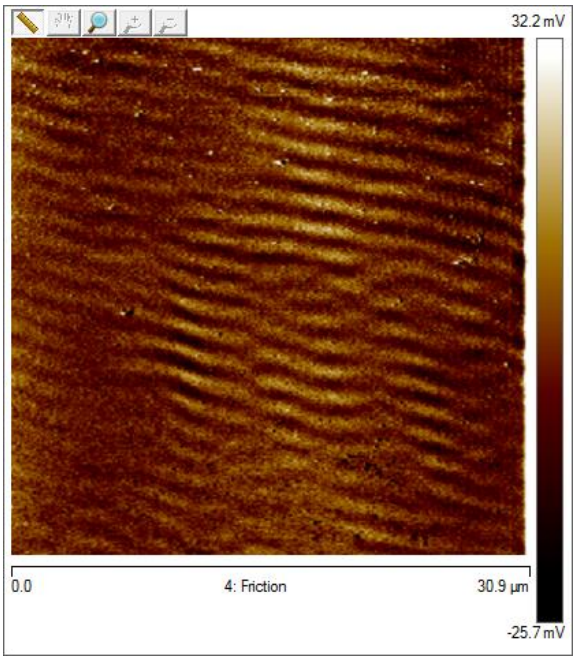

(a)

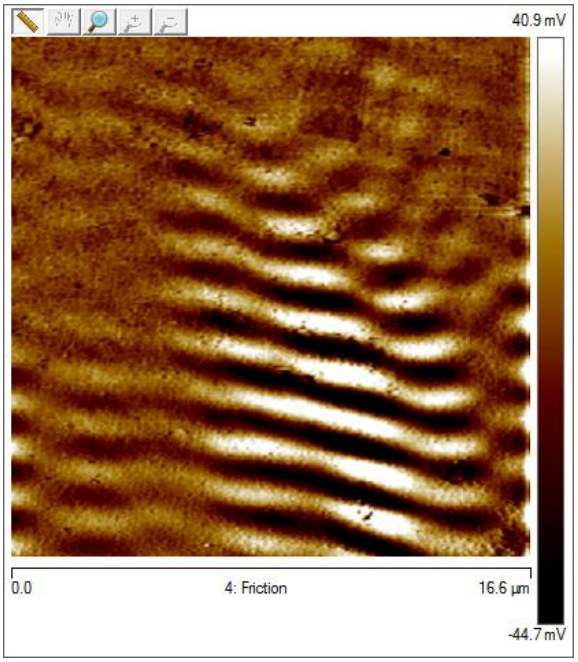

(b)

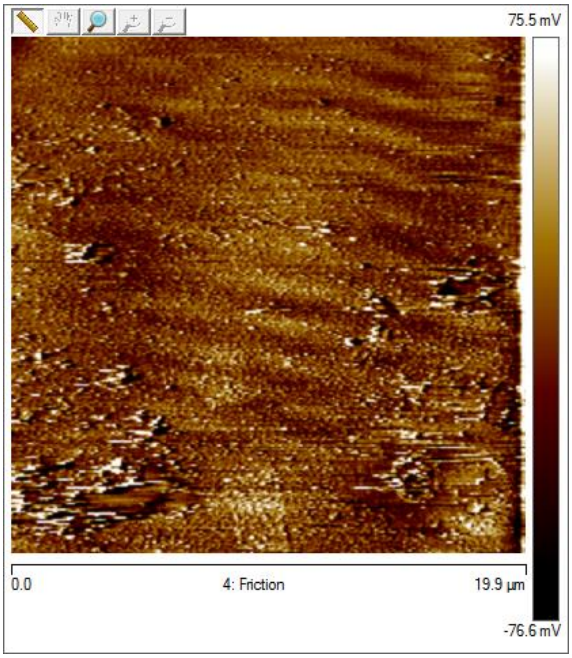
75.5 mV
0.0
4: Friction
19.9 µm
-76.6 mV

(c)

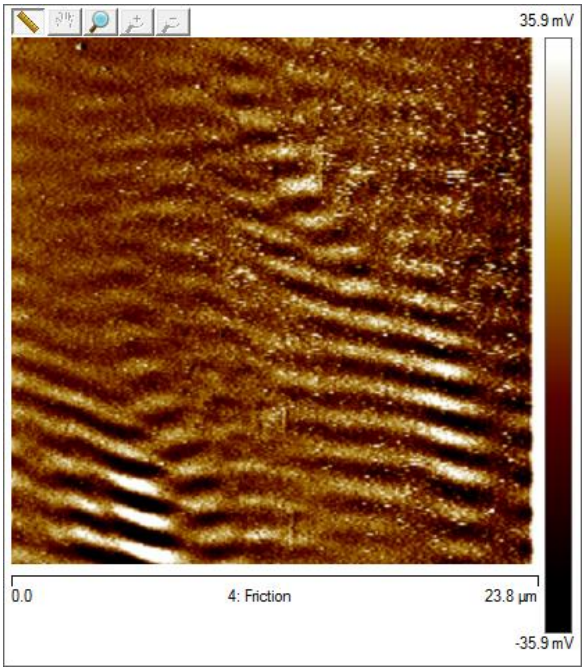
35.9 mV
0.0
4: Friction
23.8 µm
-35.9 mV

(d)

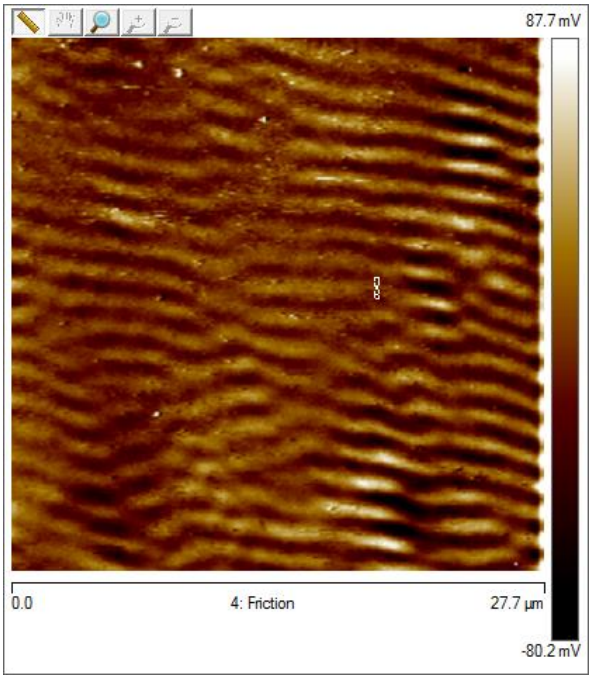
87.7 mV
0.0
4: Friction
27.7 µm
-80.2 mV

(e)

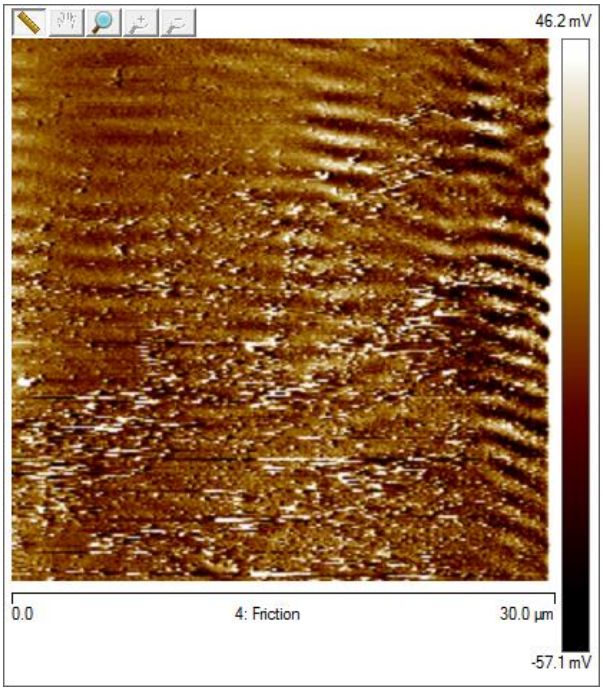
46.2 mV
0.0
4: Friction
30.0 µm
-57.1 mV

(f)

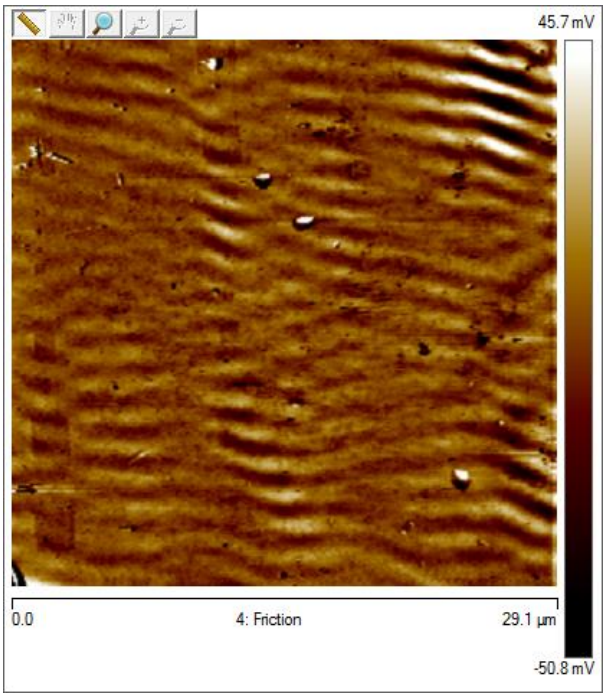
45.7 mV
0.0
4: Friction
29.1 µm
-50.8 mV

(g)

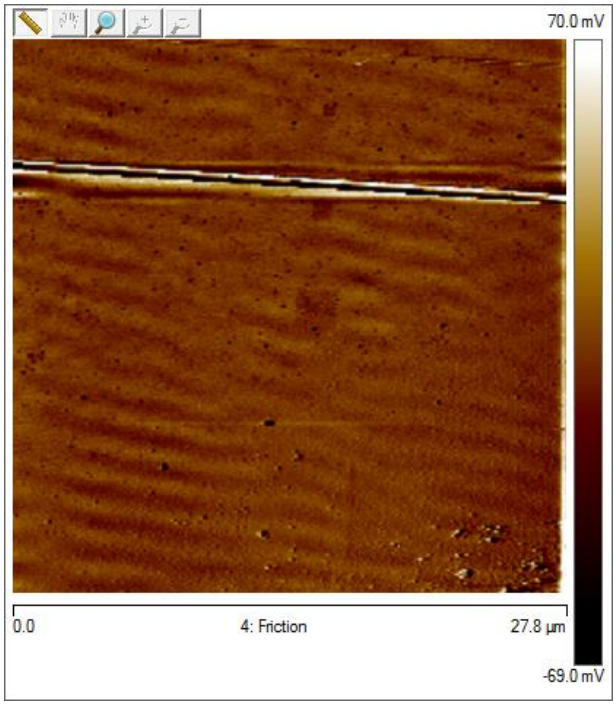
70.0 mV
0.0
4: Friction
27.8 µm
-69.0 mV

(h)

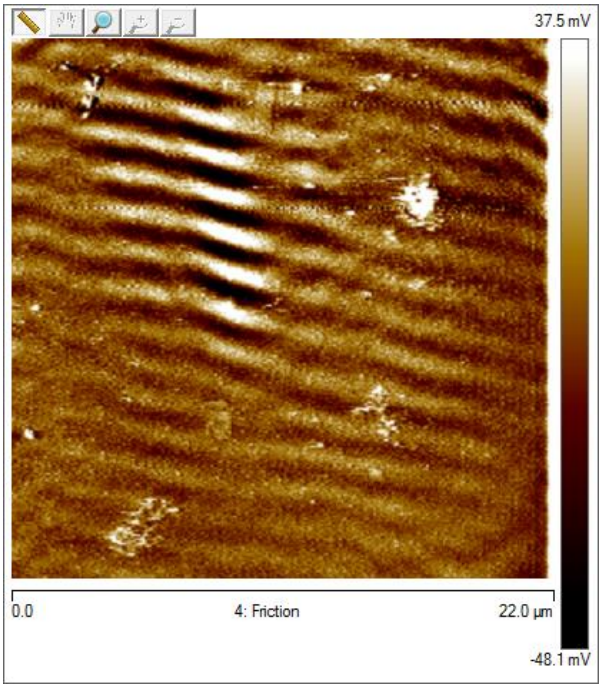
37.5 mV
0.0
4: Friction
22.0 µm
-48.1 mV

(i)

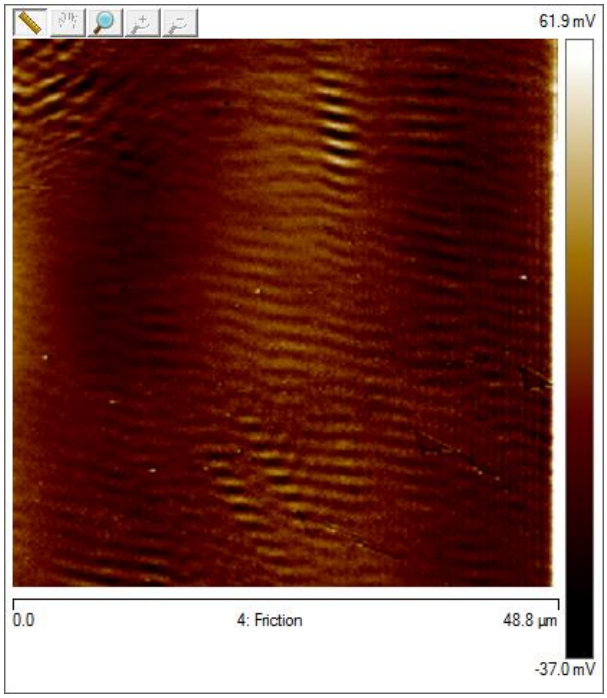
61.9 mV
0.0
4: Friction
48.8 µm
-37.0 mV

(j)

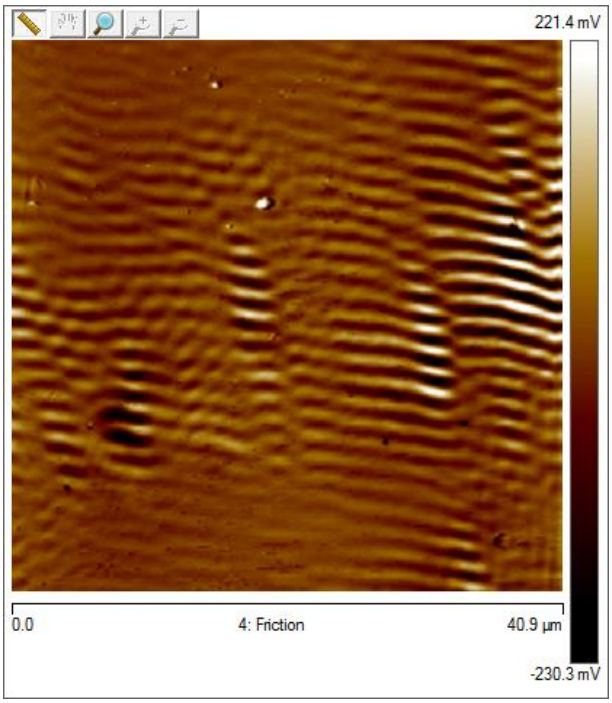

(k)

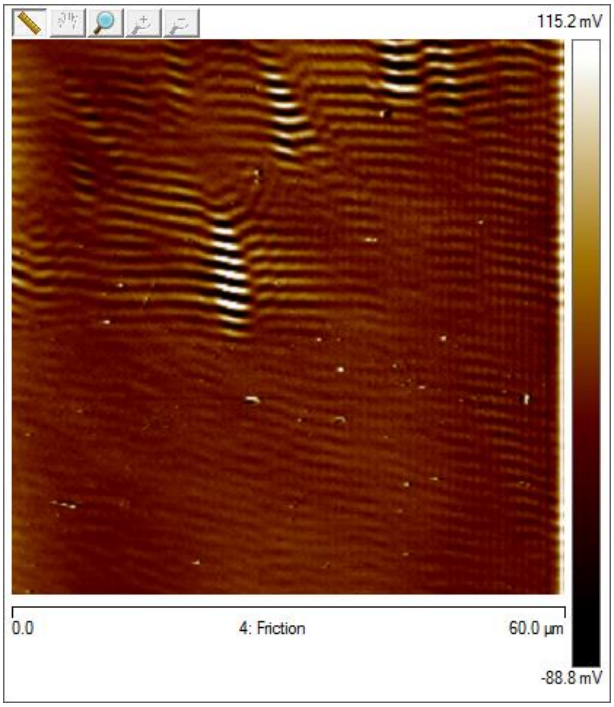

(l)

Figure (4.41): Friction images of patterning samples after depositing 2 bilayers of polymers on them. (a) PAH/PAA at 9/9 (b) PAH/PAA at 3/9 (c) PAH/PAA at 9/7 (d) PAH/PAA at 7/3 (e) PAH/PSS at 3/3 (f) PAH/PAA at 3/3 (g) PAH/PSS at 7/3 (h) PAH/PAA at 9/3 (i) PAH/PAA at 7/7 (j) PAH/PAA at 3/7 (k) PAH/PSS at 9/3 (l) PAH/PAA at 7/9

The lack of selectivity can be understood in terms of a complex interaction between the degree of ionization of the different polyelectrolytes used at the various levels of pH we examined and the secondary effects that guide the selective deposition when electrostatic interactions do not dominate the interaction due to low degrees of ionization of the polymer chains. This can be seen by comparing the friction images in Figure (4.41) to the friction images in Figure (4.42) obtained from the trials of depositing PAH and PCBS where higher selectivity was evident along with the tendency to maintain the discernable patterns over higher numbers of bilayer depositions.

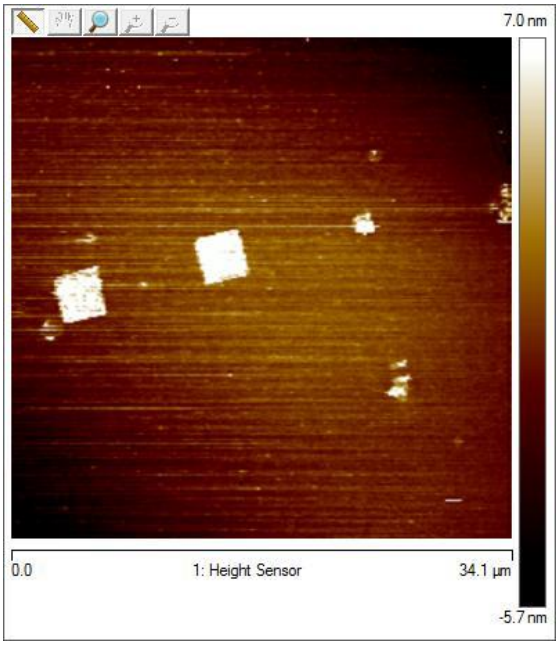

(a)

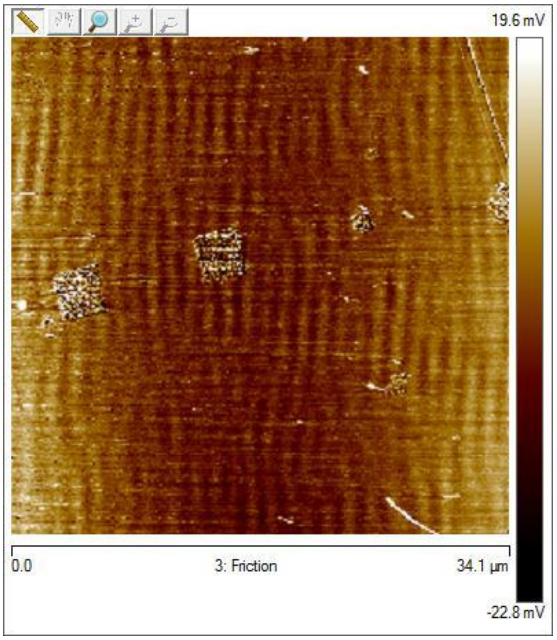

(b)

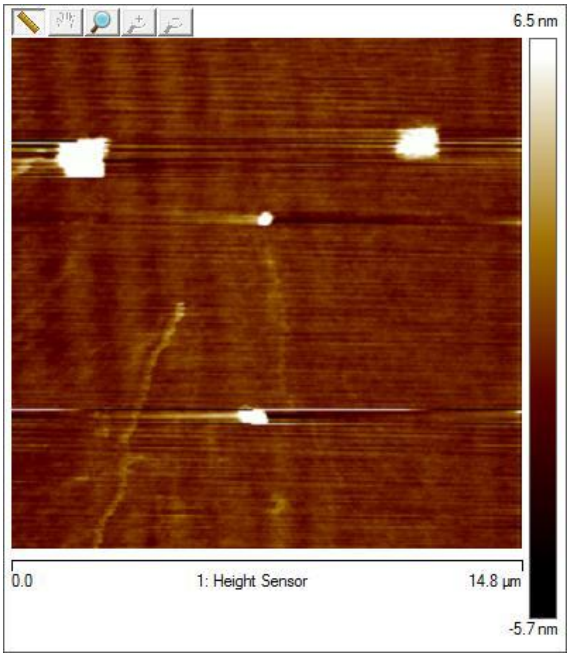

(c)

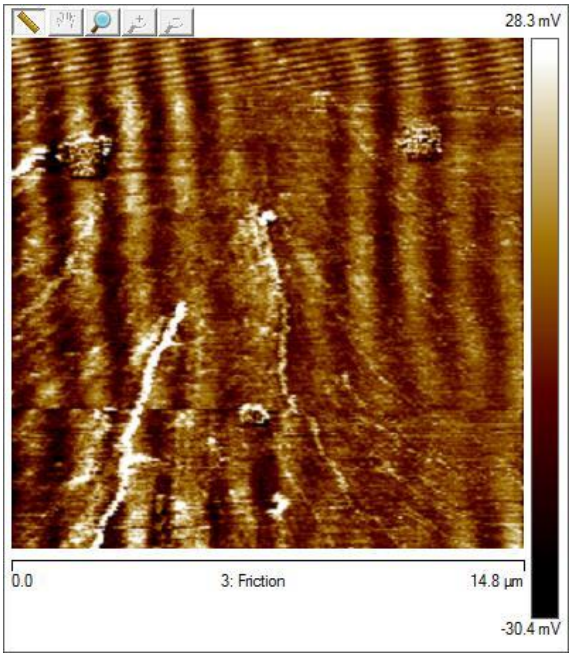

(d)

Figure (4.42): (a) and (b) Height image of patterned squares after the deposition of 2 bilayers of PAH/PCBS at pH 7/5. (c)and (d) Friction images of the patterns in (a) and (b) respectively

When we compare these friction images in Figure (4.42) to the ones in Figure (4.41) we can see clearly that there is a difference in the visibility of the patterns in the friction images in favor of Figure (4.42). Such a difference can be correlated to the better selectivity of deposition we have seen in the deposition process when depositing PAH/PCBS at pH 7.0/5.0. This selectivity was also seen in the higher increases of the thickness of the patterns in the case of PAH/PCBS and that the patterns were not lost until we exceeded 10 bilayers.

4.5 Conclusion

In this chapter we studied the selective deposition of PAH with PCBS, PAA, and PSS. The purpose of the study is to examine optimum conditions for selective deposition through LbL deposition. Determining such optimum conditions will enable us to utilize this method of delivery of molecular components to the circuit elements we would eventually like to build. To that end, we passivated gold surfaces with 11-MUD and then used AFM nanografting to pattern squares of different sizes of 16-MHDA onto the passive background. We followed that by multilayer deposition of PAH as a polycation with PCBS, PAA, and PSS as polyanions. For the case of PAH and PCBS, the pH of PAH was kept at 7.0 while the pH for PCBS was set to four different values 5.0, 5.5, 6.0, and 7.0. For the case of depositing PAH with PAA, both polymers were deposited at a range of pH values to examine the effects of combining different values for pH of the deposition process. For the case of depositing PAH with PSS, the pH for PSS was fixed at 3.0 given that it is a strong polyelectrolyte and the degree to which it is ionized is not dependent on the pH of the solution.

The repeated trials revealed that there is a very strong correlation between the pH level and the deposition selectivity of the polymers that in turn affected the visibility of the patterns and consequently their functionality. The strongest selectivity and ability to maintain the pattern and build on it occurred at pH ~5.0 for PCBS deposited with PAH at pH ~7.0. Once we lowered the pH of the PCBS solution below 5.0 we lost the selectivity completely and the multilayers deposited everywhere on the substrate. The combination of PAH/PCBS at pH 7.0/5.0 also gave us the ability to maintain the patterns up to 10 bilayers. The deposition of PAH with PAA and PSS exhibited some selective deposition behavior on the patterned areas. However, for both the PAA and PSS, the polymers also deposited everywhere on the sample in such rates that made it hard to maintain the patterns past 6 bilayers.

Another observation made is the higher incremental thickness of deposition on patterns of smaller size. There is a difference of 0.4 – 0.6 nm per bilayer of polymers deposited on the patterned areas between the large squares measuring 500 nm X 500 nm, 1 µm X 1 µm, and 3 µm X 3 µm compared to the 200 nm X 200 nm squares. The bilayers deposited on the 200 nm X 200 nm squares were higher than the ones deposited on the larger squares for the same conditions and pH.

Such a study of optimum conditions for multilayer deposition must be carried out before we start using any new polymers. This will help determine the best conditions for using those polymers.

Refrences:

1. A. Tulpar, Z. Wang, C.-H. Jang, V. Jain, J.R. Heflin, W.A. Ducker, "Nanoscale Patterning of Ionic Self-Assembled Multilayers", Nanotechnology **20**, 155301:1-5 (2009).
2. Sarah L. Clark and Paula T. Hammond, "The role of secondary interactions in Selective Electrostatic Multilayer deposition", Langmuir **16** (26), pp 10206-10214, (2000).
3. Sarah L. Clark, Martha F. and Paula T. Hammond, "Ionic Effects of Sodium Chloride on the Templated Deposition of Polyelectrolytes Using Layer-by-Layer Ionic Assembly", Macromolecules **30**, 7237-7244, (1997).
4. Sarah L. Clark and Paula T. Hammond, "Engineering the Microfabrication of Layer-by-Layer Thin Films", Advanced Materials, Volume 10, Issue 18, Pages 1515-1519, December (1998).
5. Gang-Yu Liu, Song Xu,Yile Qian "Nanofabrication of Self-Assembled Monolayers Using Scanning Probe Lithography,", Acc. Chem. Res. **33**, 457-466, (2000).
6. Luis G Rosa and Jian Liang, "Atomic force microscope nanolithography: dip-pen, nanoshaving, nanografting, tapping mode, electrochemical and thermal nanolithography", J. Phys.: Condens. Matter 21 483001, (2009).
7. Paulo Samori, "Scanning probe microscopies beyond imaging ", J. Mater. Chem. **14**, 1353-1366, (2004).
8. Song Xu and Gang-Yu Liu, "Nanometer-Scale Fabrication by Simultaneous Nanoshaving and Molecular Self-Assembly", Langmuir **13**, 127-129, (1997).
9. Nicole Herzer, Stephanie Hoeppener and Ulrich S. Schubert, "Fabrication of patterned silane based self-assembled monolayers by photolithography and surface reactions on silicone-oxide substrates", Chem. Commun. **46**, 5634 – 5652, (2010).

10. Mauzi Liu, Nabil A. Amro, and Gang-Yu Liu, "Nanografting for Surface Physical Chemistry", Ann. Rev. Phys. Chem **59**: 367 – 86 (2008).
11. Shiratori, S. S., and Rubner, M. F., "pH Dependent Thickness Behavior of Sequentially Adsorbed Layers of Weak Polyelectrolytes", Macromolecules, **33**, 4213-4219, (2000).

Chapter 5

Atomic Force Microscope Patterning of Monolayers of Silanes on Silicon Substrates.

5.1 Introduction

In this chapter, we discuss experimental work that was performed to pattern silane monolayers deposited on silicon substrates. The ultimate purpose behind these experiments is to be able construct nanoscale circuit elements. To this end we use two different patterning methods. The first method is nanografting, which we have used before and discussed in extensive detail in Chapters 3 and 4 of this thesis. The second method is electrochemical modification of the surface of the silane monolayer[(1),(2)]. This second method depends on providing a potential difference between the sample surface and the AFM tip. Such a potential difference paired with the existence of ambient humidity oxidizes the areas on which the AFM tip passes leading to a change in the chemical properties of these tracks.[(3)] This method has also been discussed in detail in Chapter 3 of this dissertation. Both methods, nanografting and surface electrochemical modification, aim to change the chemistry of a chosen area on the surface of the monolayer. While nanografting achieves this by replacing some of the molecules adsorbed on the surface by some other molecules that carry the desired chemical property as a functional group, surface chemical modification works on modifying the already existent functional group and turning it into a more suitable one for the designer's purposes. The silane used as a passive background formed a monolayer terminated with a $–CH_3$ group. In the nanografting part of the experiment, this silane was shaved off and replaced, in a nanofrafting process, by another silane which is terminated with an $–NH_2$

group. The $–NH_2$ group served the purpose of guiding the selective deposition of gold nanoparticles and later multilayers of polymers in a selective deposition process[4],[5]. In the electrochemical modification part of the experiment, the applied potential difference between the tip and the monolayer on the surface of the sample changes the surface functional groups from $-CH_3$ to –COOH. The –COOH functional groups functioned as guides for the selective deposition of gold nanoparticles and polymers[4],[5].

5.2 Experimental details

5.2.1 Silanes

The silanes used in this endeavor are a class of compounds containing a silicon atom connected to 3 different atoms (or molecules) at one end of the molecule and then a hydrocarbon chain that connects that to a functional group. One of the silanes that was used in this part of the experiment is chlorodimethyloctadecylsilane. Figure (5.1) shows the molecular structure for this compound. This compound is selected for its ability to form a moderately strong bond with the silicon substrates on which it is deposited such that it can be shaved off using the AFM as opposed to other compounds that can present a problem to the grafting process[6]. The product was purchased from Sigma-Aldrich. We used toluene as a solvent for this silane to prepare a 10 mM solution to deposit a silane monolayer from it on the silicon substrates.

Chlorodimethyloctadecylsilane

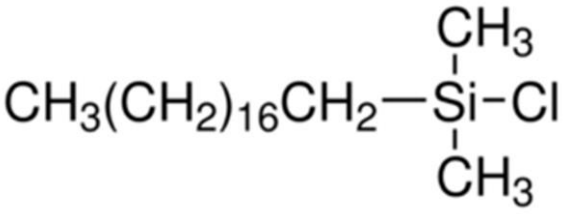

Figure (5.1): Chlorodimethyloctadecylsilane with two methyl groups and a chlorine atom attached to the silicon atom and a methyl group as a functional group.[17] Reproduced with permission from: http://www.sigmaaldrich.com/catalog/product/aldrich/71034?lang=en&region=US

The second silane used is (mercaptopropyl)trimethoxysilane. This silane functioned as a replacement silane that was grafted into a background of chlorodimethyloctadecylsilane. Figure (5.2) shows the structure for this silane. We chose this silane because of the mercapto functional group. This will serve the purpose of attracting gold nanoparticles to the grafted areas[4]. This product was purchased from Sigma-Aldrich. It is in a liquid form and was used as received.

(Mercaptopropyl)trimethoxysilane

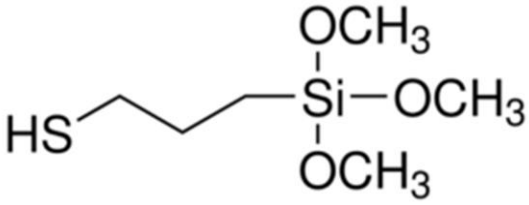

Figure (5.2): (Mercaptopropyl)trimethoxysilane with three methoxy groups attached to the silicon atom and a sulfur atom at the functional group.[17] Reproduced with permission from: http://www.sigmaaldrich.com/catalog/product/aldrich/175617?lang=en&region=US

The third silane used in this work is AminopropylMethyl – Diethoxysilane. This silane was also used as a replacement silane to be grafted into a background of the passivating

chlorodimethyloctadecylsilane. Figure (5.3) shows the structure for this silane. This silane was chosen because of the amine functional group and the ability of amines to bind to gold to help with the selective deposition of the gold nanoparticles on the selected sites[4]. We used this silane as a 10 mM solution dissolved in toluene. This product was purchased from Sigma-Aldrich and used as received.

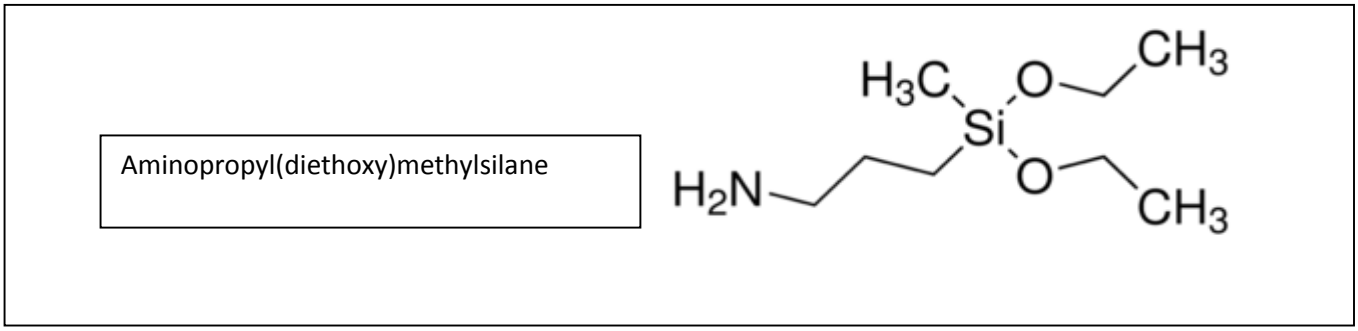

Figure (5.3): Aminopropyl(diethoxy)methylsilane with two ethoxy groups and a methyl group attached to the silicon atom and an amine functional group. [17] Reproduced with permission from:
http://www.sigmaaldrich.com/catalog/product/aldrich/371890?lang=en&region=US

5.2.2 Polymers

The polymers used in this case were PAH and PCBS. Both products were used in the form of 10 mM solutions. Both of these products were purchased from Sigma-Aldrich and used as received.

5.2.3 Gold Nanoparticles

The gold nanoparticles used in this work were negatively-charged and had an average radius of 3 - 4 nm. The gold nanoparticles were bought from Purest Colloids Inc. and used as received. The concentration was 20 ppm.

5.2.4 Atomic Force Microscope System

The system used in this experiment was a Bruker Dimension Icon® with a NanoScope V controller.

5.2.4.2 Tips

The tips used in this series of experiments were Bruker's TESPA, which are made out of antimony-doped silicon. They have a 0.01 – 0.025 Ohm-cm resistivity. And they have a nominal value for their spring constant of 42 N/m. These tips are conductive and have relatively high nominal spring constants. We needed the tips to be conductive to be able to perform electrochemical surface modification on silane monolayers. We also needed the high spring constant for the nanografting attempts since silanes are known to bind strongly to the silicon surface.

5.2.5 Silicon wafers

The silicon wafers used for this experiment as the substrate on which the monolayer of silanes is deposited and later undergoes the patterning were bought from DNS Electronic Materials. The wafers are polished 10 cm silicon wafers of thickness 525 ± 15 μm. The wafers had an SiO_2 layer of 1000 Å.

5.2.6 Photolithography mask

The photolithography mask used in this work was designed using the DraftSight software. This software is an open-source design software that resembles AutoCAD to a great extent. The design for the mask is shown in Figure (5.4). The mask was made by the masking house Photo Sciences Inc. The mask contains six testing circuits. Each of these circuits contains three testing pads that are 4 mm X 4 mm. Each of the testing pads has a 2 mm extended bridge connected to the testing pad. Two of the testing pads are facing each other with a gap of 0.5 μm gap between the bridges. The third testing pad is aligned to the side of the other two testing pads where the third bridge makes a 90° angle with the other two bridges and meets them at the center. The separation between the third bridge and the other two is 20 μm. The intention of this design is that the first two pads can serve as source and drain while the third pad could serve as the gate in a field-effect transistor configuration. The use of a positive photoresist for the photolithography process allows us to perform a metallization and lift-off process where these patterns become conductive electrodes. The goal for designing this mask is to establish connections that would allow us to perform measurements using macroscopic scale instruments on the nanoscale devices we are building. The gaps between the bridges are essentially gaps between the electrodes in which we can construct nanoscale circuit elements.

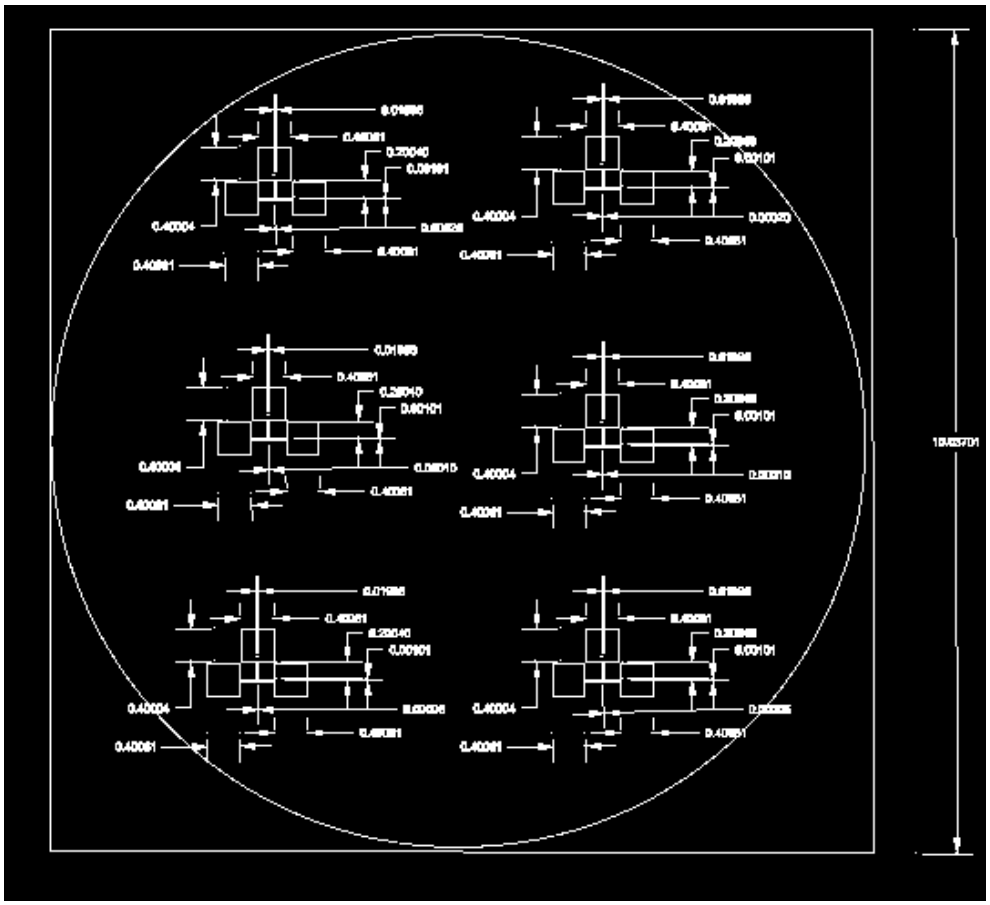

Figure (5.4): The photolithography mask design. The mask had six sites for constructing wires and transistor channels between macroscopic electrodes. The design was done using DraftSight.

Figure (5.5) shows the mask after it was made. The mask is made out of Soda lime and the plating is chromium.

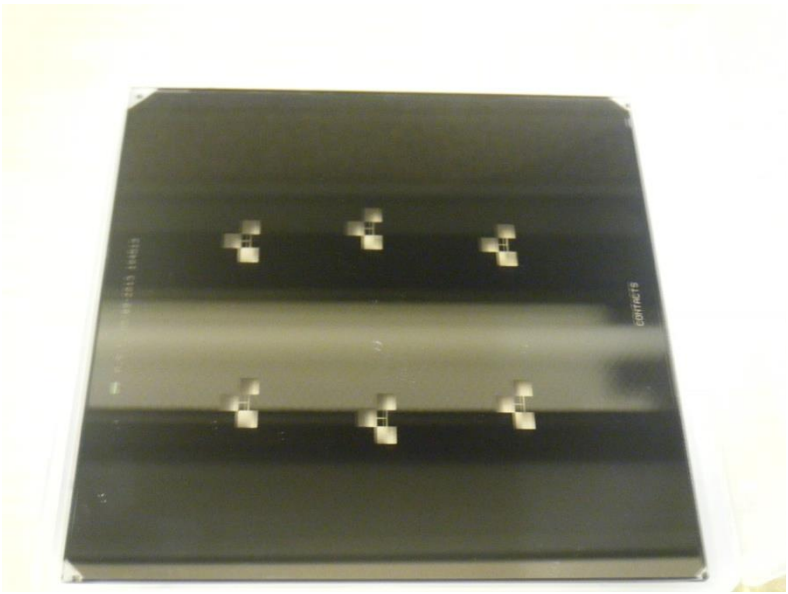

Figure (5.5): The photolithography mask used to make the testing pads for the nanostructures. It is a soda lime 4” chromium on glass mask with the smallest dimension on the mask being 0.5 µm.

5.2.7 Cleanroom equipment

The clean room facility is a 1900 square foot class 100 facility in Whittemore Hall. The facility is run by the ECE department. Figure (5.6) shows a picture of the facility.

Figure (5.6): The cleanroom facility at Virginia Tech is a 1900 sq foot class 100 facility equipped with all equipment needed for a wide range of semiconductor micro-fabrication processes.

5.2.7.1 Photoresist

We used a Microposit® S1813® positive photoresist optimized for G-line exposure. The S1813® was provided by the Cleanroom facility management and was used as received.

5.2.7.2 Mask aligner MA-6

The mask aligner used was a Karl Suss MA-6 – Contact mask aligner capable of producing 0.5 um features on 2" – 150 mm substrates with backside alignment. The system is also retrofitted with BA-6 hardware for wafer to wafer alignment. 365 nm and 405 nm exposure wavelengths. Figure (5.7) shows a picture of the system used in this work.

Figure (5.7): The Karl Suss MA-6 mask aligner located in the cleanroom at Virginia Tech. It was used to expose the wafers using our mask for fabricating testing leads for the nanostructures of our experiment.

5.2.7.3 Kurt – Lesker Ion beam evaporation system PVD-250

The ion beam device used for the metallization part of the testing leads construction is KJL PVD-250 e-beam evaporator – 7cc 4-pocket e-beam evaporator with substrate heating, rotational substrate holder and Kauffman Ion gun for assisted evaporations. Figure (5.8) shows a picture of the device used.

Figure (5.8): Kurt-Lesker PVD e-beam evaporator Located at the cleanroom facility at Virginia Tech. This evaporator was used in the metallization step of the testing leads fabrication process.

5.3 Experimental Procedure

We started the procedure for this work by designing a photolithography mask compatible with the standard cleanroom semiconductor technology standards[7]. The design and implementation of the mask comes as the first step in a procedure that allows us to build a testing frame for the nanostructures we are building. The process is aimed at enabling the construction of nanowires and nanotransistors whose functionality can be tested. [8], [9] For the case of nanotransistors, the design allows for a fixed transistor channel and for the transistor gate to either be on the side or the bottom of the channels.[9] The two options dictate different channel lengths which offers a wider range of variables to test. The mask allowed us to construct a structure that will contain nanowires and nanotransistors between macroscopic testing pads that can be used to perform the tests we need using equipment that is readily available in our labs and allows us to avoid the problem of performing direct contact on the nanoscale. The construction of the testing structures took place in Virginia Tech's cleanroom. The process of building the testing structures started by cleaning the silicon substrates by using the piranha cleaning method which is, briefly, a mix of concentrated sulfuric acid and hydrogen peroxide at a ratio of 3:1 that is heated to 80 °C and used to clean glass and silicon substrates.[10] Following that the substrates were coated with a photoresist. The photoresist used is Micropsoit® S1813® which is a positive photoresist. The photoresist was placed on the spin coating equipment and was spun at 4000 rpm to ensure a uniform coating of the substrate. The next step was for the substrate with the photoresist to be baked at 100 °C for 1 minute as per instructions for applying the photoresist. After letting the substrates cool down for two minutes, I used the photo mask aligner MA-6 to further process the wafers by exposing it to ultraviolet (UV) light. The UV light used had a wavelength of 325 nm

and the exposure time was calculated to be 25 seconds using the hard exposure option on the mask aligner. After that, the wafers were treated using the photoresist developer AZ 400K® which had to be diluted 1:4 with DI water to ensure a controlled development and not complete stripping of the photoresist layer. Developing the photoresist is accomplished by dipping the exposed silicon wafers in the developer for 2 seconds. If the development time is extended farther than this, we either lose the precise measurements for the gaps in the pattern or the entire pattern gets stripped along with the entire photoresist layer. Finally, the wafers were rinsed with DI water and then dried with nitrogen. Since the photoresist used is a positive photoresist, this meant that the exposed parts of the photoresist to the UV light got stripped by the developer leaving the silicon surface underneath it exposed. After rinsing the developed wafers with DI water and drying them with nitrogen, the wafers were inserted into a Kurt Lesker PVD-250 e-beam evaporator to complete the metallization process and fabricate the metal testing pads for the circuits.(11) The metal we chose to evaporate on the circuit is titanium. We chose titanium because it binds very well with silicon to the extent that it is normally used as an adhesion layer between silicon and other metals and it does not exhibit any tendencies for binding with the silanes we are using in this experiment. Such adhesion between titanium and silanes if present would have led to a loss in the selectivity of the deposition of the polymers and other materials we are targeting. Figure (5.9) shows a silicon wafer after the metal evaporation part of the metallization process has been done.

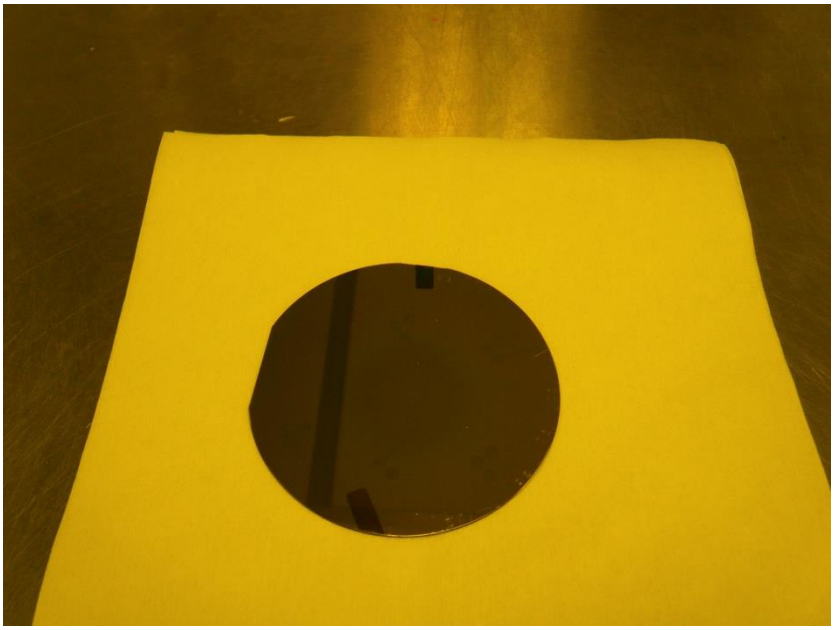

Figure (5.9): One of the substrates after evaporating titanium on it in a PVD-250 e-beam evaporation chamber.

After this step, a lift-off step was performed to rid the circuit from the excess metal film that is deposited now on top of the photoresist layer that is still on the surface of the silicon wafer.[12] In this process we put the wafer with the evaporated titanium layer in a Nalgene jar and covered completely with acetone and sonicated the jar for 15 minutes. Figure (5.10) shows the metallized circuit leads after the lift-off process. Figure (5.11) shows a zoomed in image on one of the circuits.

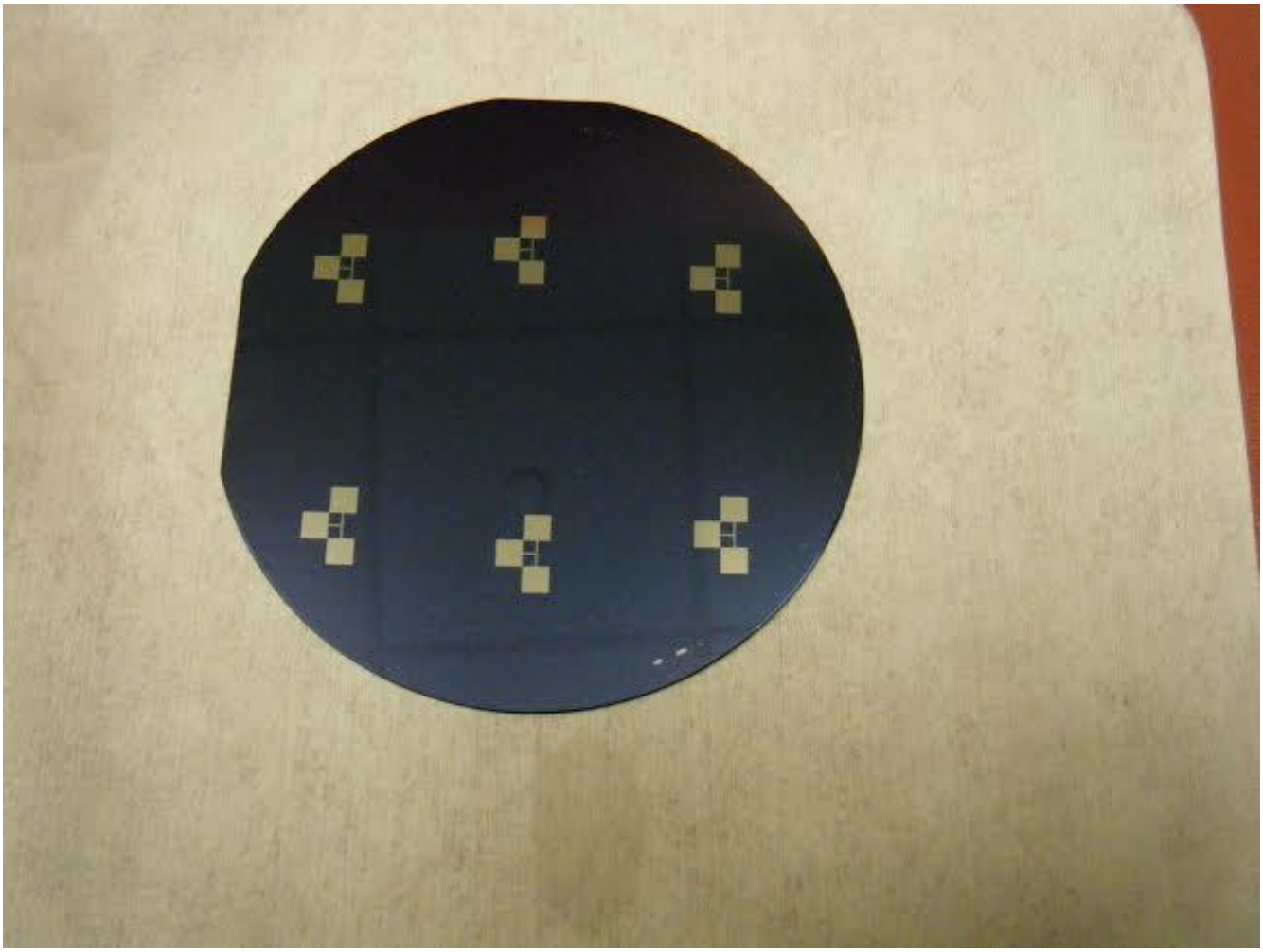

Figure (5.10): A wafer after metallization and lift-off. The process was carried out in Virginia Tech's cleanroom.

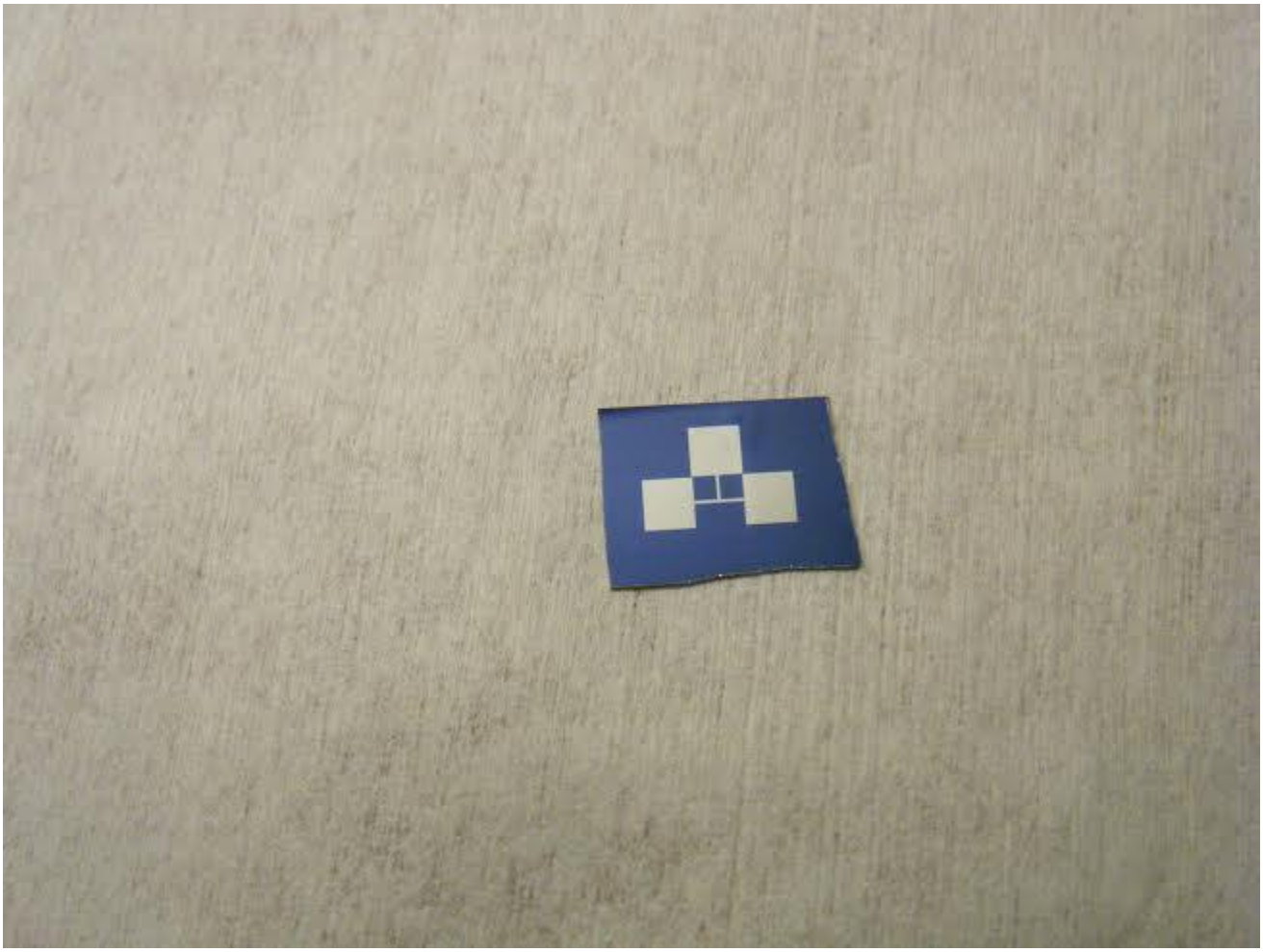

Figure (5.11): One of the circuits designed for testing the nanostructures investigated in our lab.

After this step was completed, we dipped the wafer in a 10 mM solution of chlorodimethyloctadecylsilane and covered the containers for 48 hours to assure a homogeneous covering by a monolayer of the silane on the silicon surface. After the 48 hours period, we picked up the samples from the solution and rinsed it with fresh toluene. The samples were then sonicated in toluene for 5 minutes to ensure getting rid of any physisorbed molecules on the surface of the

silane monolayer. In our nangrafting trials the process proceeded by inserting the sample into the in-house designed AFM liquid cell. The nanografting trials were performed using two different silanes, Aminopropyl(diethoxy)methylsilane and (Mercaptopropyl)trimethoxysilane.

5.4 Results and discussion

5.4.1 3-Aminopropyl(diethoxy)methylsilane

In this trial, the liquid cell was filled with a 10 mM solution of aminopropyl(diethoxy)methylsilane dissolved in toluene. The grafting was done using Bruker -made tips, TESPA, with a nominal spring constant K = 42 N/m. We applied a force around 3 uN to the surface of the monolayer. The strong force applied to the tip was needed to break the bonds between the silane molecules and the silicon substrate. The choice for the passive background of chlorodimethyloctadecylsilane is due to reports in the literature that other silanes, which would have been suitable for the process, like octadecyltrichlorosilane, were impossible to liberate from the substrates using AFM tips.[(6)(13)] Such reports indicated partial shaving only of the molecules and that complete removal of the passive background of octadecyltrichlorosilane was not possible. The height difference represents the difference in length between the two chains for the different molecules. Figure (5.12) shows the results of the grafting process. The large features shown in Figure (5.12) are two of the three electrodes. The gap between these two electrodes is 0.5 µm. The space in which the grafting is taking place is a 20 µm gap between the two electrodes shown in the image and the third (side) electrode that is perpendicular to them.

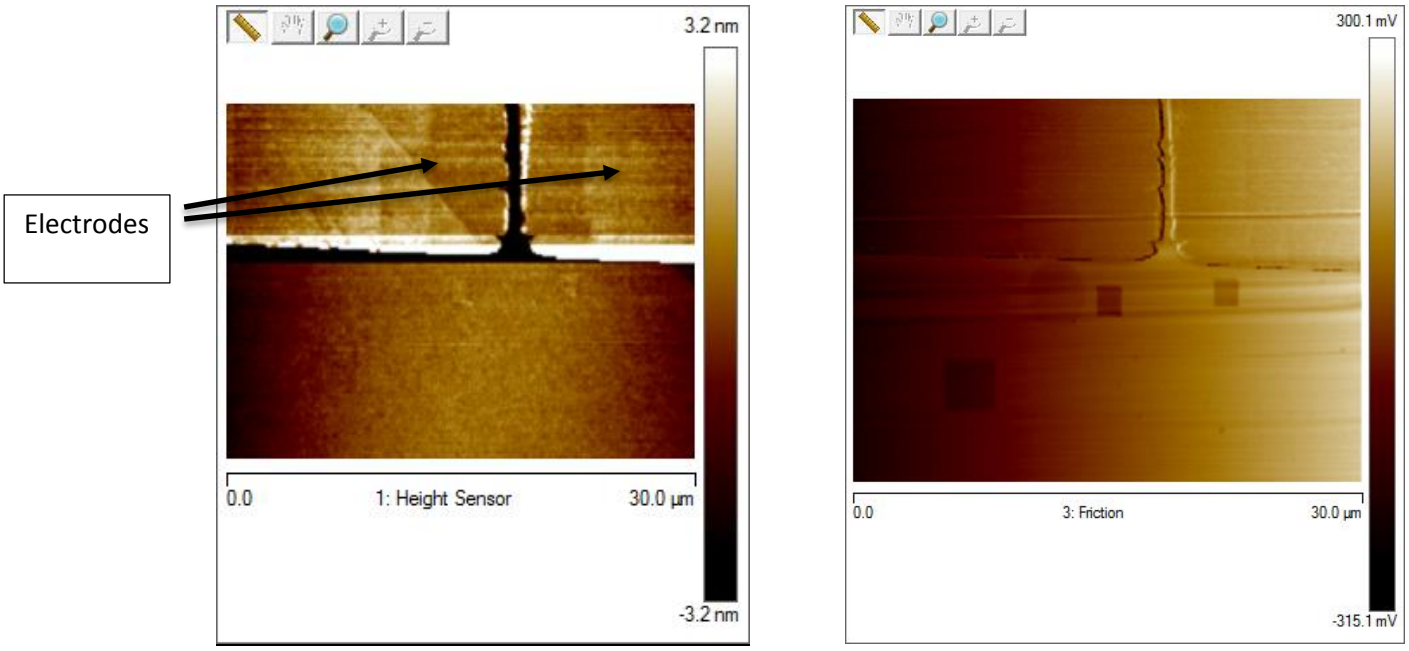

Figure (5.12): (a) The height image of two different patterns grafted of 3-aminopropyl(diethoxy)methylsilane into a background of chlorodimethyloctadecylsilane. We can see that there is no visible difference in height. (b) A friction image of the two different patterns where the effect of having two different functional groups is visible. (c) A cross sectional plot of the height image for the patterned areas.

After the grafting operation was done, we rinsed the samples with fresh toluene to make sure that there are no physisorbed molecules left on top of the monolayer on the surface of the substrate and that all the molecules left are bound to the surface. The samples were then dipped in a colloidal solution of gold nanoparticles that are negatively charged. The gold nanoparticles were between 2 nm and 4 nm in radius on average. Figure (5.13) are the images of the gold nanoparticles stuck to the surface of the sample at the grafted sites.

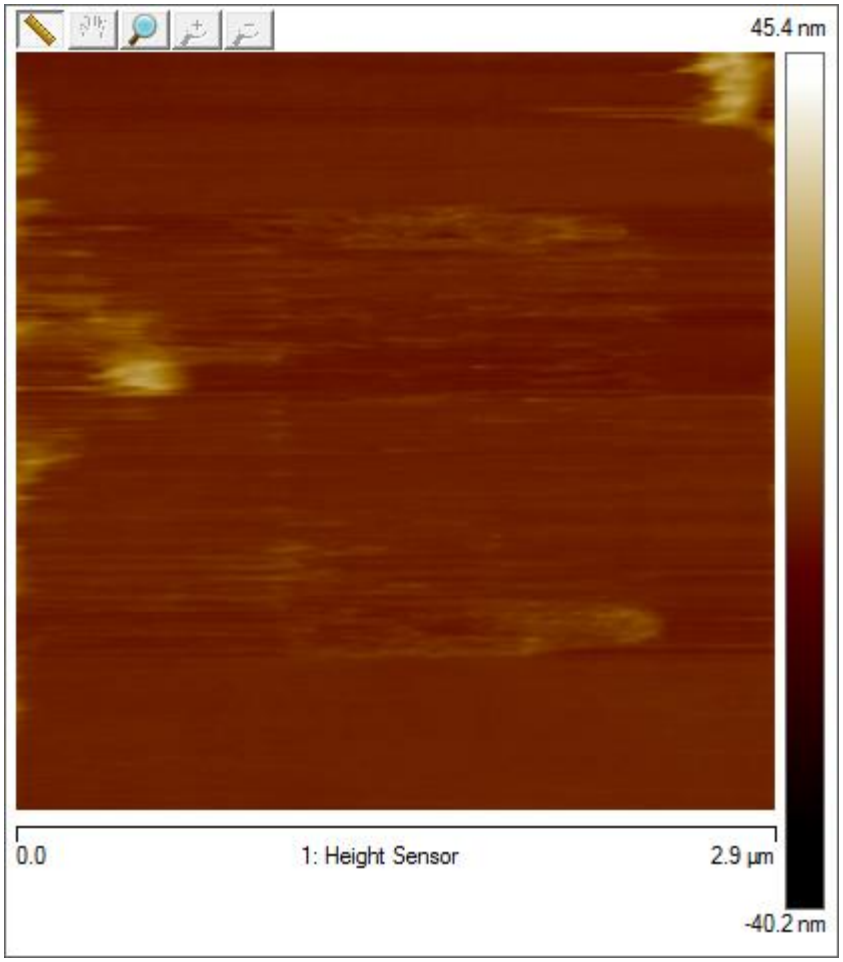

Figure(5.13): A square grafted of aminopropyl(diethoxy)methylsilane onto a background of chlorodimethyloctadecylsilane after being dipped in a gold nanoparticle solution for 3 hours.

We noticed that the adhesion between the gold nanoparticles and the aminopropyl(diethoxy)methylsilane pattern is not strong enough and that the gold nanoparticles are removed with repeated imaging. A conductivity/resistance test was performed for the case of a single wire constructed in the 500 nm gap and three wires in the 20 um gap. The test showed that the scattered gold nanoparticles did not affect the conductivity at all and that the electrodes between which the wires were grafted remained disconnected. Figure (5.14) shows an image of the single wire constructed between the electrodes in the 500 nm gap.

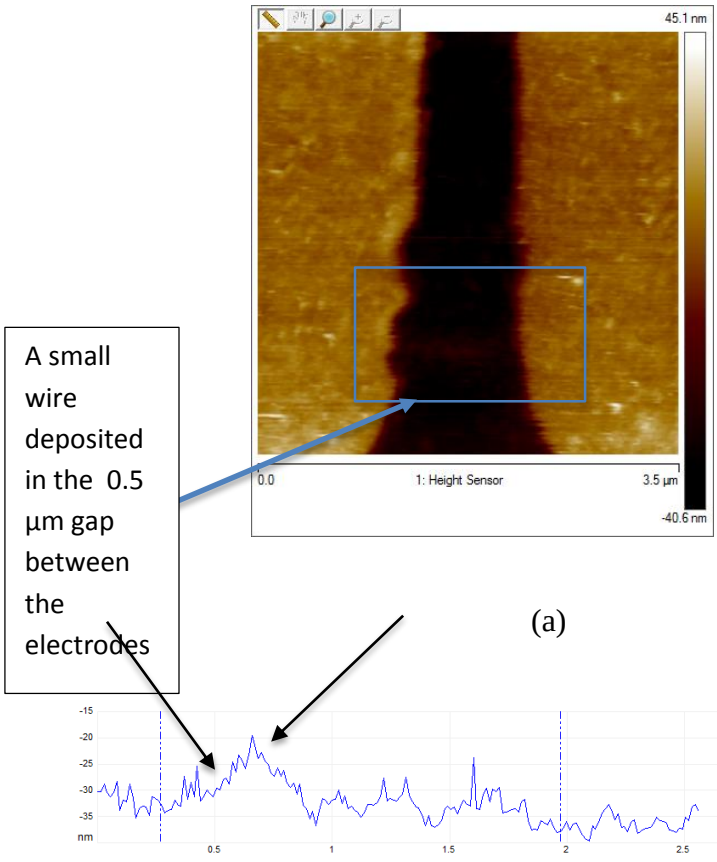

Figure (5.14): (a) A wire constructed between two electrodes. The image is taken after depositing 30 bilayers of gold nanoparticles and PAH on the sample using LbL method. (b) A cross sectional image for the wire. The arrows on the graph indicate the rise in the height profile representing the area where the wire is formed. The wire is 0.5 µm long and 0.5 µm wide. The wire is around 5 nm high. Given that the electrodes are around 50 nm high it is hard to see the wire in the image.

Repeated trials with 60, 80, and 100 bilayers of PAH and gold nanoparticles did not show any improvement in the density of deposition of the gold nanoparticles on the PAH surface.

5.4.2 (3-Mercaptopropyl)trimethoxysilane

In this part of the experiment, we graft (Mercaptopropyl)trimethoxysilane in a background of chlorodimethyloctadecylsilane in different patterns. The choice of using (mercaptopropyl)trimethoxysilane was made in the hope of strengthening the selective deposition of gold nanoparticles on the mercapto functional groups terminating the (mercaptopropyl)trimethoxysilane patterns. The choice of using chlorodimethyloctadecylsilane was made for the same two reasons described above. The first reason being that the $-CH_3$ functional groups will act as a passive background. And the second reason being that it was easy to shave off the chlorodimethyloctadecylsilane using nanografting. Figure (5.15) shows patterns that have been grafted into the chlorodimethyloctadecylsilane.

(a) (b)

Figure (5.15): (a) The height image of the grafted squares of (3-mercaptopropyl)trimethoxysilane in background of chlorodimethyloctadecylsilane. (b) Deflection Error image of the same spot as (a)

The grafting steps were exactly the same as we did for the previous case except that the (mercaptopropyl)trimethoxysilane was used as neat solution in the liquid cell.[6] After the rinsing step, the samples were dried with nitrogen for 2 minutes to allow all the toluene used in the rinsing to evaporate from the surface of the sample. After the samples were dried with nitrogen, they were dipped in a gold nanoparticle solution. The deposition of gold nanoparticles after a single 3 hour dip session was greater than in the case of grafting aminopropyl(diethoxy)methylsilane in a chlorodimethyloctadecylsilane background. Figure (5.16) shows the image of one of the squares shown in Figure (5.15) after it has been dipped in a gold nanoparticle solution for 3 hours under constant agitation.

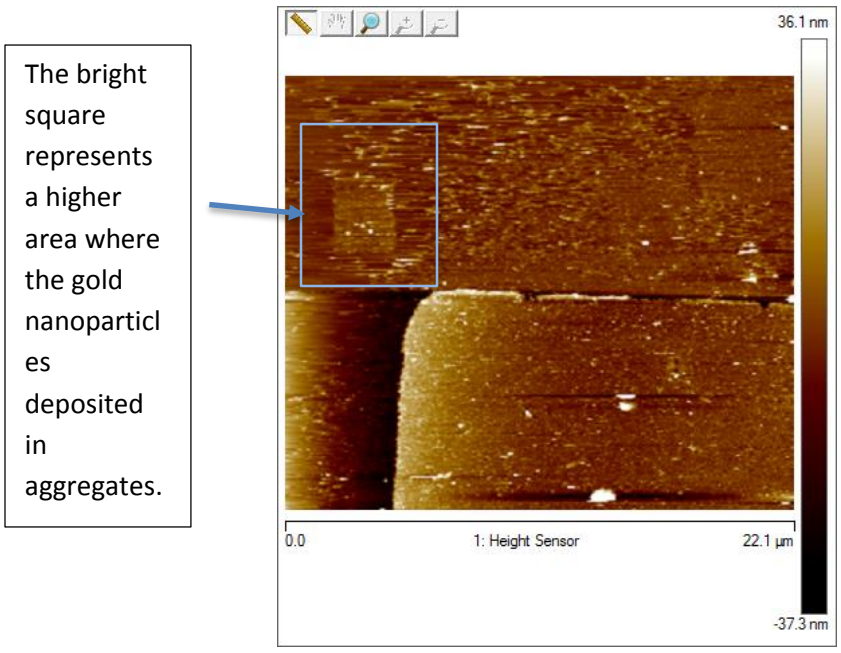

Figure (5.16): A square of (mercaptopropyl)trimethoxysilane in background of chlorodimethyloctadecylsilane after it has been dipped in gold nanoparticles for 3 hours under constant agitation. We can see that gold nanoparticles have aggregated on the grafted square in the top left corner. We can also see that gold nanoparticles have deposited on the background.

In an attempt to improve the adhesion of gold nanoparticles to the surface of the grafted areas, we used LbL deposition to alternate layers of gold nanoparticles and PAH. This resulted in a better adhesion of the gold nanoparticles to the patterned areas. However, the higher the number of bilayers we used the more we suffered from a loss of selectivity in the deposition of the different layers and thus gradually lost the patterns. Such behavior was observed before when working with thiols deposited on gold and was reported elsewhere in the literature and discussed in the literature review in Chapter 2 of this dissertation. [(14)] Figure (5.17) shows the results of depositing 55 bilayers of gold nanoparticles and PAH.

Resistivity tests were performed using a regular multimeter to try to determine the effect of using the LbL method on constructing connections between the electrodes. The electrodes remained disconnected and the resistance was measured as an infinite value on the digital multimeter. Figure (5.18) shows three wires constructed using nanografting after depositing 30 bilayers of PAH and gold nanoparticles on the sample.

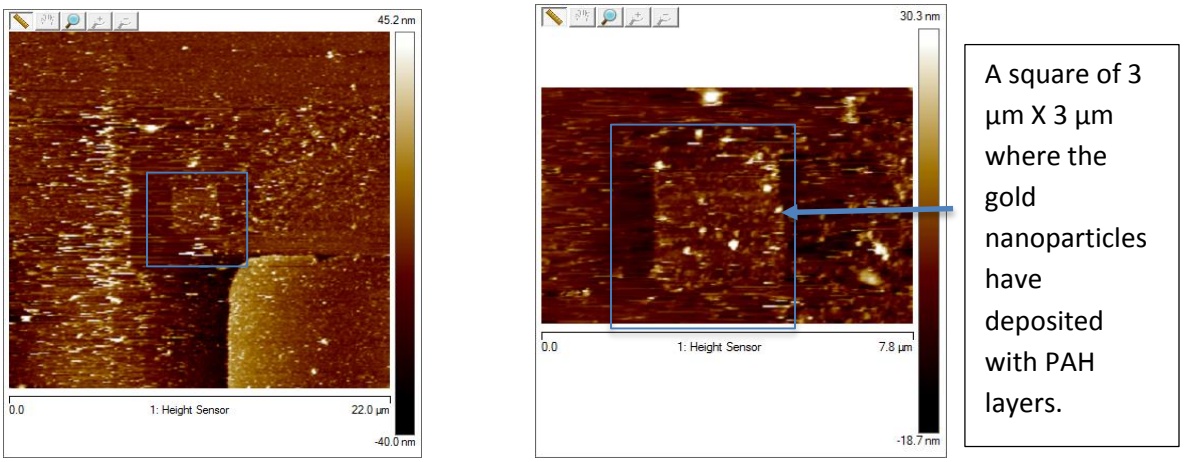

(a) (b)

Figure (5.17): (a) Height image of square of (mercaptopropyl)trimethoxysilane in background of chlorodimethyloctadecylsilane after depositing 55 bilayers of gold nanoparticles and PAH. (b) A zoomed in image on the square in (a)

Patterned areas in the form of wires where gold nanoparticles and layers of PAH have deposited. The wire is 500 nm wide.

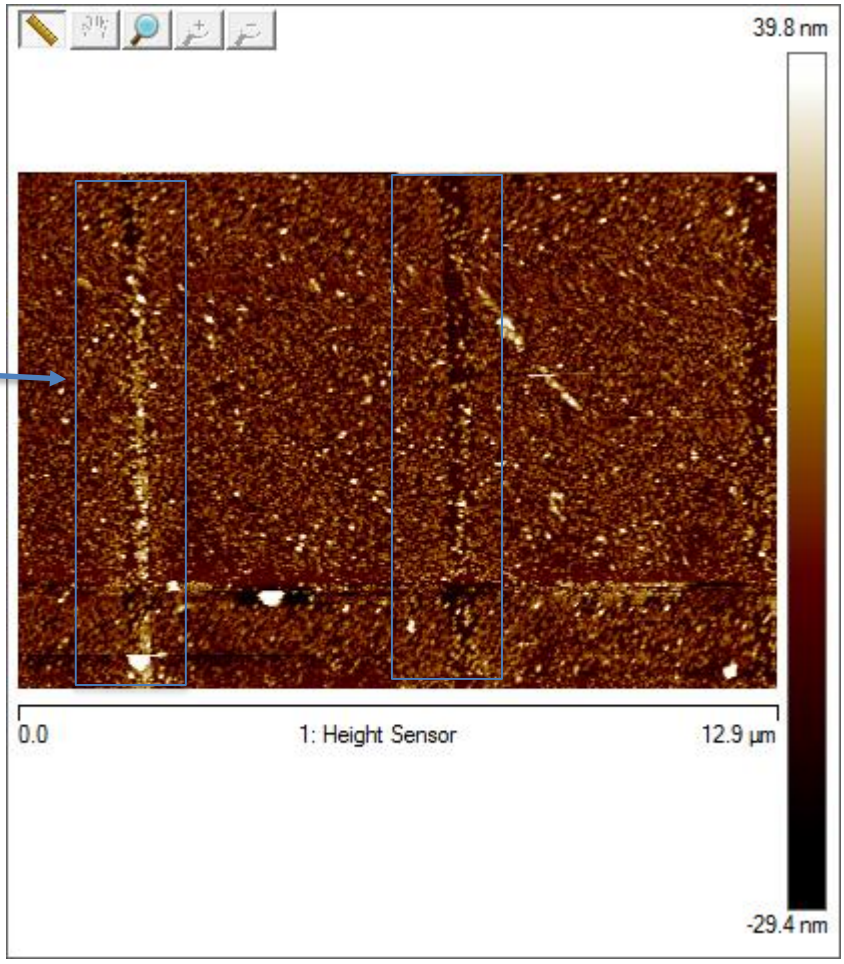

Figure (5.18): Image of three wires grafted of mercaptosilane into a background of chlorosilane after dipping in gold nanoparticles and then depositing 30 bilayers of PAH and gold nanoparticles in an alternating manner. Two wires on the right out of the three show very little adsorption of nanoparticles. The wire on the left shows better adsorption density for the gold nanoparticles and the polymer layers. However, we can see strong nonselective adsorption of gold nanoparticles and PAH layers on the background.

Another attempt at grafting (mercaptopropyl)trimethoxysilane in a background of chlorodimethyloctadecylsilane and then depositing 30 bilayers of PAH and gold nanoparticles on the pattern is depicted in Figure (5.19).

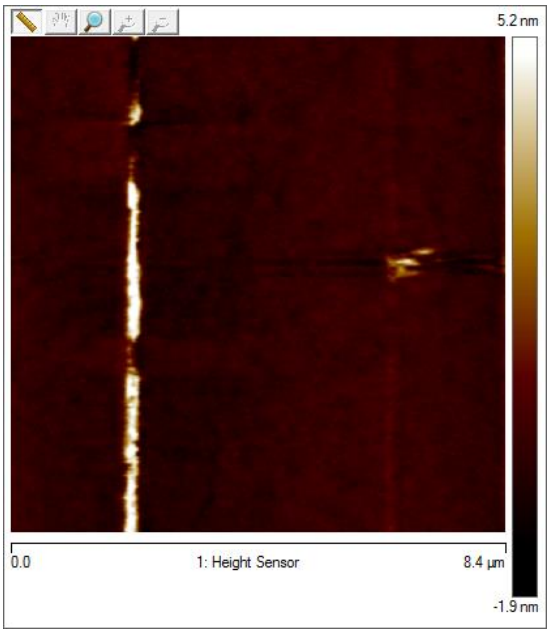

(a)

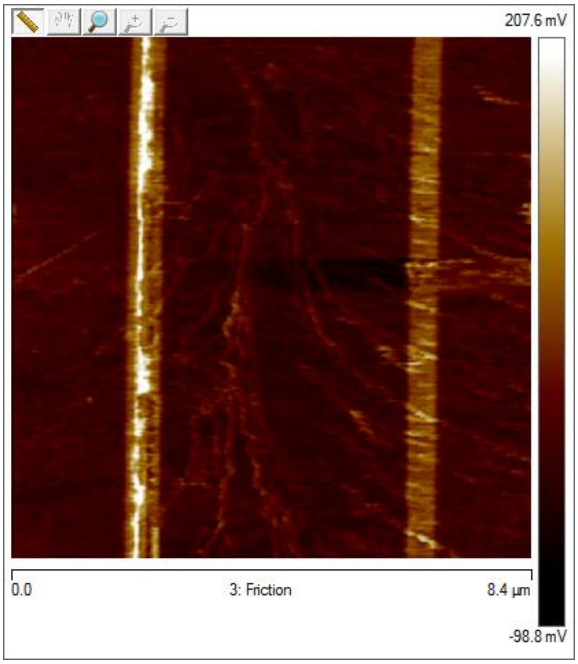

(b)

Figure (5.19): (a) The height image of grafting wires of (mercaptopropyl)trimethoxy silane in background of chlorodimethyloctadecylsilane after depositing 30 bilayers of gold nanoparticles and PAH on the wires. (b) Friction images of the same spot depicted in (a) where we notice the change in the functional group in the grafted areas is very visible in the friction image as opposed to the height image where it is barely visible.

Figure (5.20) shows the results of grafting wires of (mercaptopropyl)trimethoxysilane in background of chlorodimethyloctadecylsilane between the electrodes in the narrow gap and then dipping the substrate in gold nanoparticles for 30 minutes.

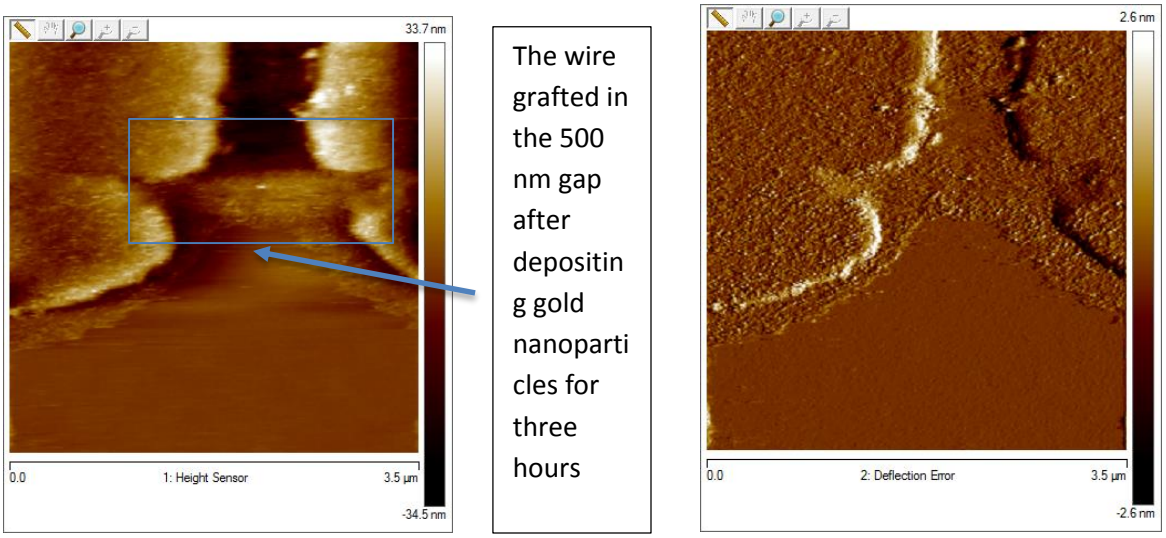

Figure (5.20): (a) Patterning a wire between the two electrodes in the 500 nm gap between them by grafting (mercaptopropyl)trimethoxysilane in background of chlorodimethyloctadecylsilane and then depositing gold nanoparticles on the grafted areas for 3 hours under constant agitation led to the establishment of a connection between the two electrodes. (b) A deflection error image for the wire. (c) A cross sectional view of the height profile of the wire. The arrows on the cross section indicate the beginning of the height difference representing the height of the wire. The height on average was found to be 8 nm. There is observed nonselective deposition of gold nanoparticles around the electrode.

Grafting (mercaptopropyl)trimethoxysilane in background of chlorodimethyloctadecylsilane again between the electrodes in the narrow 500 nm gap and using layer-by-layer deposition to alternately deposit 30 bilayers of PAH and gold nanoparticles yields the results shown in Figure (5.21).

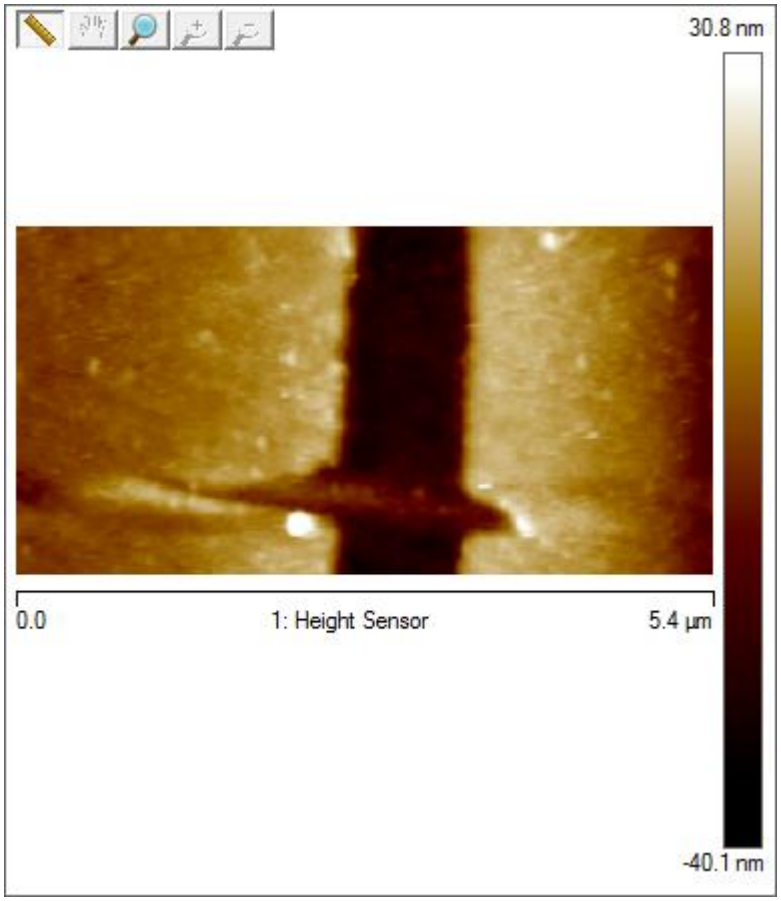

Figure (5.21): The results of grafting (mercaptopropyl)trimethoxysilane in background of chlorodimethyloctadecylsilane again between the electrodes in the narrow 500 nm gap and using layer-by-layer deposition to alternately deposit 30 bilayers of PAH and gold nanoparticles.

We performed measurements of resistance between the electrodes before we started every trial to make sure they are disconnected. After the grafting and gold nanoparticles deposition between the two electrodes in the narrow gap the resistance dropped to zero. We suspect that the nonspecific deposition resulted in a large cross-sectional bridge of gold nanoparticles between the two electrodes over scales much larger than the patterned area.

5.4.3 Surface Electrochemical modification.

As an alternative to the nanografting method, we decided to use an electrochemical surface modification method. This method depends on creating a potential difference between a conductive AFM tip (which functions as a cathode in this case) and the surface of the sample. By creating such a potential difference, we manage to change the functional group at the end of the silane monolayer in the areas patterned.[(1),(2)] The water vapor in the atmosphere surrounding the AFM tip creates a meniscal water droplet that connects the AFM tip to the sample surface and serves to transport electric current between the tip and the surface of the sample.[(3)]

Figure (5.22) shows the effects of reducing the functional group of the monolayer of chlorodimethyloctadecylsilane from a methyl group, $-CH_2$, to a -COOH group. The patterns shown in Figure (5.22) include squares of different sizes. The squares on the left have sizes ranging from 5 μm X 5 μm to 1 μm X 1 μm. Some of these squares are overlapping. The overlapping areas are showing higher oxidation levels. On the right hand side there are several equally spaced 1 μm X 1 μm squares. There are also concentric squares. The concentric squares showed up on the patterned surfaces due to the AFM tips retaining their charge after the patterning was done and oxidizing the functional groups of the monolayer while I was imaging to check the effect of the first round of patterning. Such a side effect will be shown again in Figure (5.28). The circular patterns are some

sort of contamination that appeared on the surface of the purchased substrates and only showed up in the friction measurements.

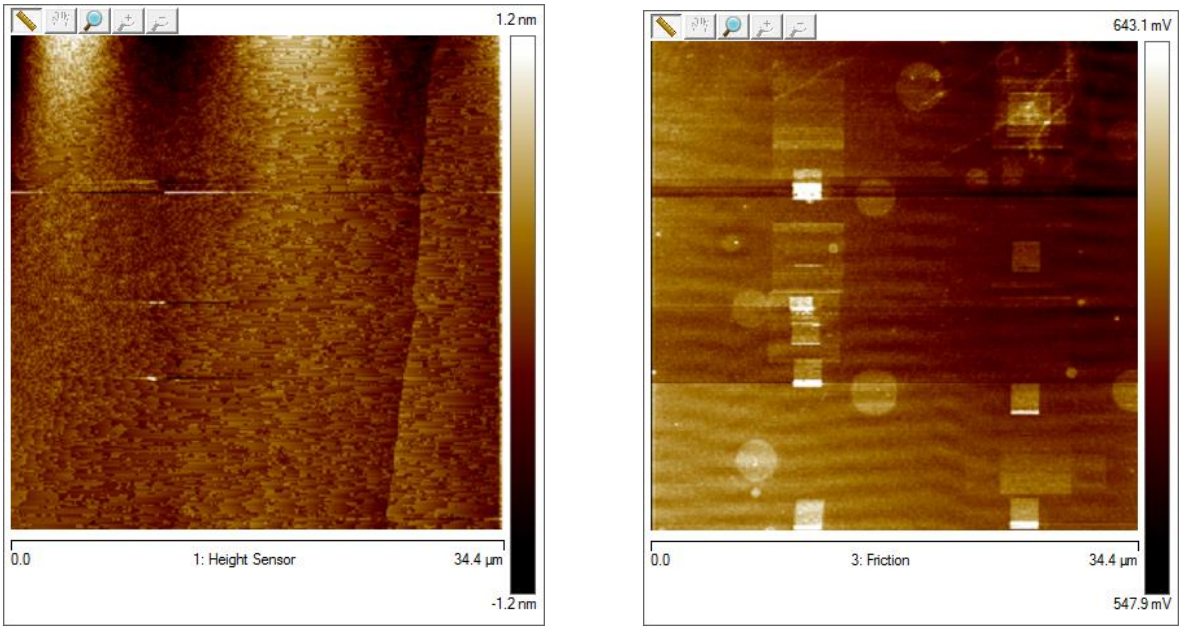

(a) (b)

Figure (5.22): (a) :The height image of a monolayer of chlorodimethyloctadecylsilane after being oxidized. No noticeable differences in height between the background and the patterned areas are observable at all, as expected. (b) The same frame depicted in (a) where the friction on the monolayer is assessed during the imaging and we can clearly see the effect of the change in the chemistry of the functional group.

One of the main things to observe in this case is the fact that on the height image from the AFM there is no observable difference in height between the background and the modified areas. This is expected since there is only a very small change in the total length of the molecule. The modified patterns now terminated with –COOH appear, instead, on the friction images. The friction

measurement mode depends on observing the difference in the interaction between the AFM tip and the surface material in the horizontal direction. The normal mode of operation depends on observing these interactions in the vertical direction, which allows us to construct an image for the height and topography of the surface. The interactions in the horizontal direction are affected by the chemistry of the surface, among other things. When the AFM tip traverses areas where the terminal functional group is different on the monolayer, this causes a different lateral force on the tip leading to a qualitative differentiation between the different species of the functional groups on the surface.

In some cases when the potential difference was too high, above 8V, or when the patterning time was too long, the silane monolayer was dissolved and a fresh layer of the Si substrate was exposed. Such an exposure led to the instantaneous oxidation of the Si layer and the formation of SiO_2. The layer of SiO_2 is higher than the monolayer deposited on the surface and we saw a difference in the height on the height images of the AFM. Figure (5.23) illustrates how this process happens. The difference in height is due to the large amount of current injected into the surface under large potential differences as opposed to the oxidation process that oxidizes a layer on top of the Si wafer under normal circumstances of exposure to the atmosphere[(2)].

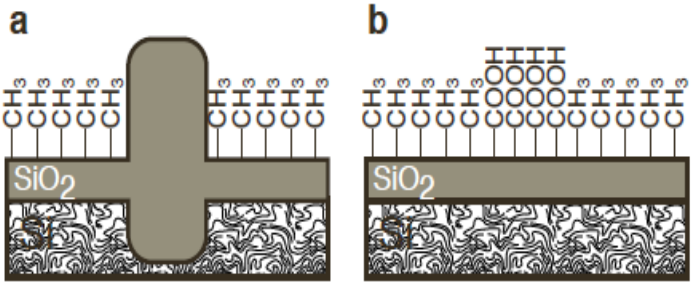

Figure (5.23): (a) The effect of injecting too much current into the surface of the sample is to cause the silane monolayer to dissolve and to cause the freshly exposed layer of Si to oxidize to an extent where it becomes higher than the surrounding background. (b) If the voltage difference between the tip and the surface of the sample is kept under 8 V the functional group of the silane monolayer changes while keeping the silane monolayer intact.[(2)] [Fair use]: Hiroyuki Sugimura, Nagahiro Saito, Kazuyuki Hayashi, Noriya Maeda and Osamu Takai, "Scanning Probe Surface Modification: Chemical Conversion of Terminal Functional Groups on Organosilane Self-Assembled Monolayers", Scanning Tunneling Microscopy/Spectroscopy and Related Techniques: 12th International Conference

Figure (5.24) shows an image of one of the cases when we applied 12 V of potential difference between the sample and the tip. The height difference observed that identifies the patterns is very clear in the height images.

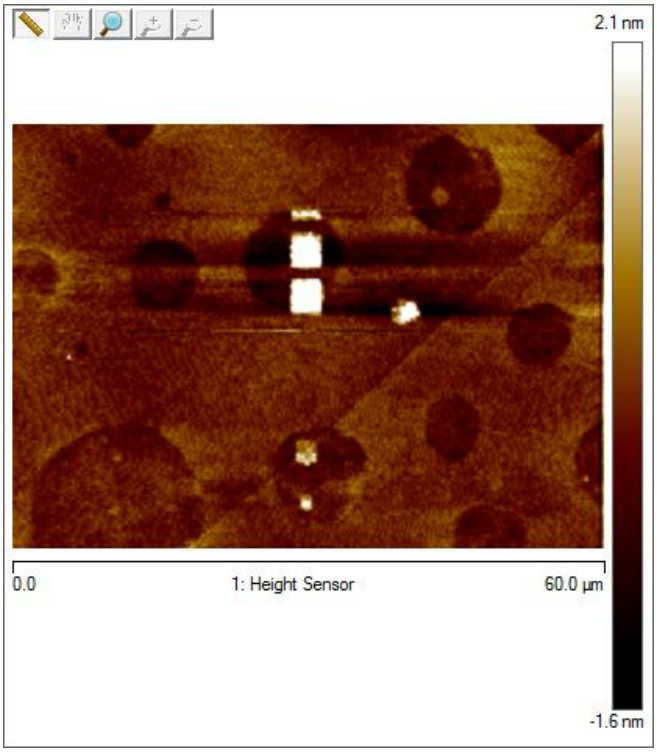

Figure (5.24): Supplying 12V of potential difference between the AFM tip and the surface led to the injection of a large current into the surface of the sample melting the silane monolayer and oxidizing the underlying Si layer to cause the observed difference in height.

Given the crucial role that humidity plays in determining the sizes and shapes of the patterns constructed using electrochemical surface modifications, we performed an extensive study to determine the effects of relative humidity on the patterning process. To this end, we examined pattern sizes and shapes at relative humidity values of 50%, 55%, 60%, 65%, and 70%. The following is a sample of the data collected in this process.

At humidity levels below 50% there were no patterns observed, and consequently we considered this to be our cutoff value.

The studies we performed targeted patterning thin wires and squares on the silane monolayer. The results below show the observation at different humidity levels.

Figure (5.25) shows AFM height and friction images at two levels of magnification for a wire written under 50% humidity. This wire was intended to be 50 nm wide. Due to the meniscal water droplet, it ended up being 110 nm in width

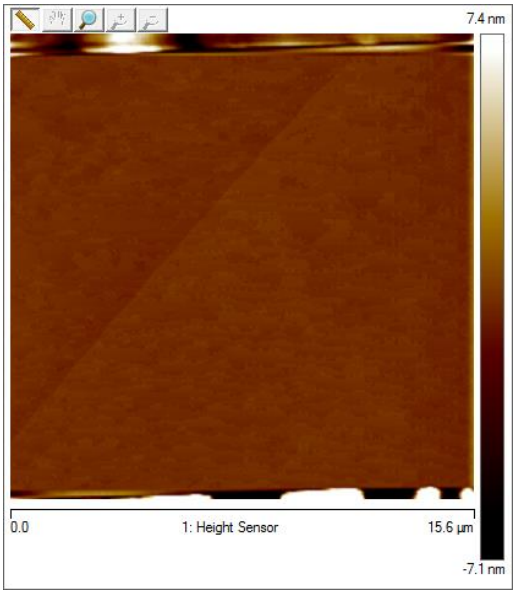

(a)

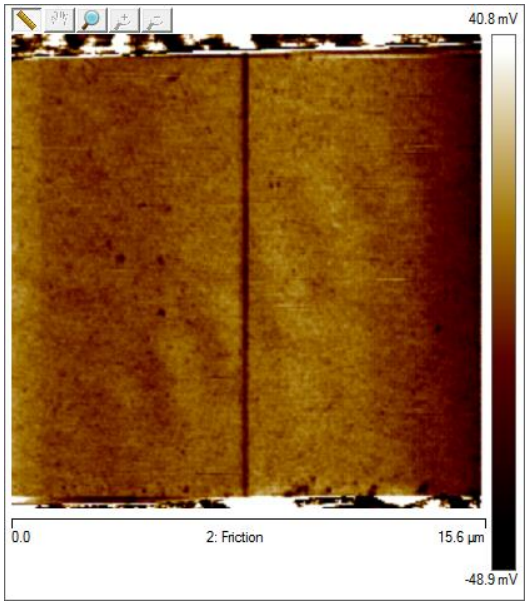

(b)

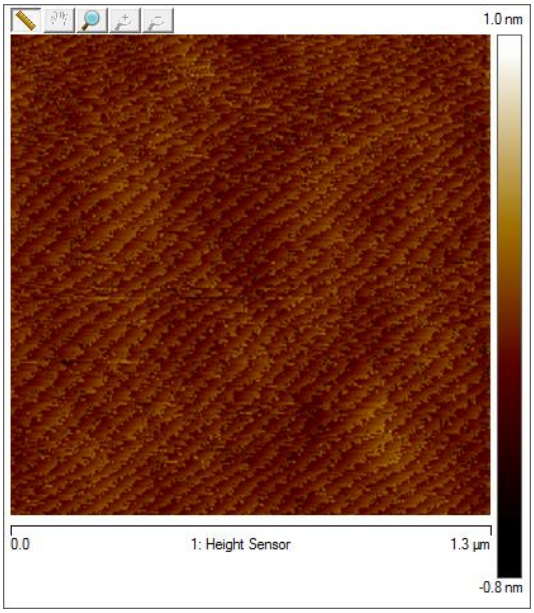

(c)

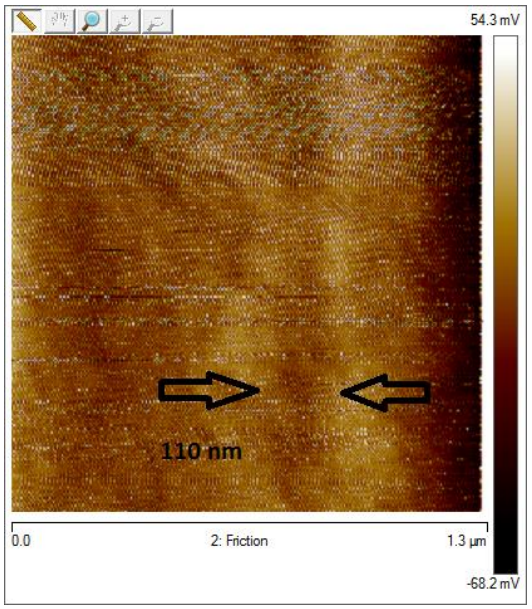

(d)

Figure (5.25): (a) The height image for a wire (b) Friction image for the same wire where notice that we can see the wire in the friction image but not in the height image (c) Zoomed in height image on the wire (d) Zoomed in friction image of the wire. This wire was intended to be 50 nm wide. Due to the meniscal water droplet it ended up being 110 nm in width.

Figure (5.26) shows AFM height and friction images at two levels of magnification for a wire written under 55% humidity. This wire was intended to be 50 nm wide. Due to the meniscal water droplet, it ended up being 125 nm in width

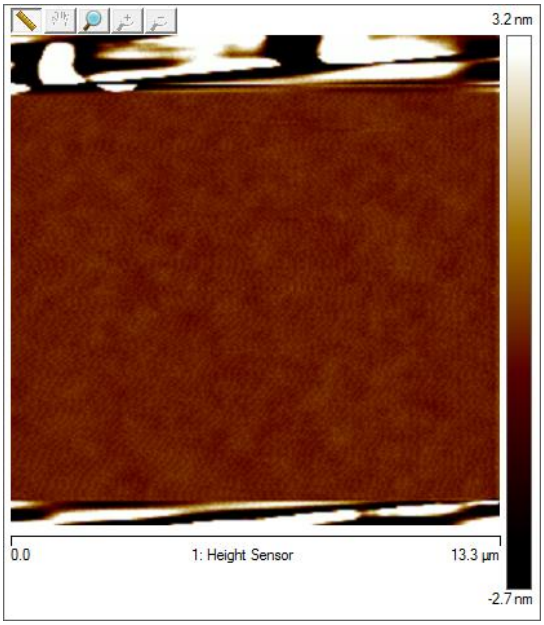

(a)

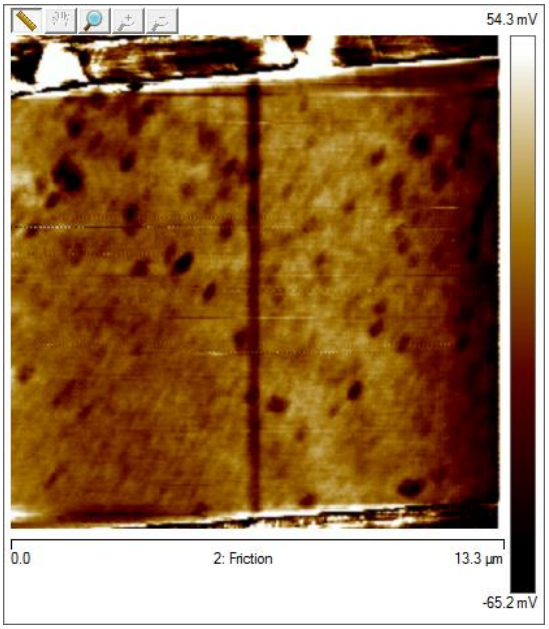

(b)

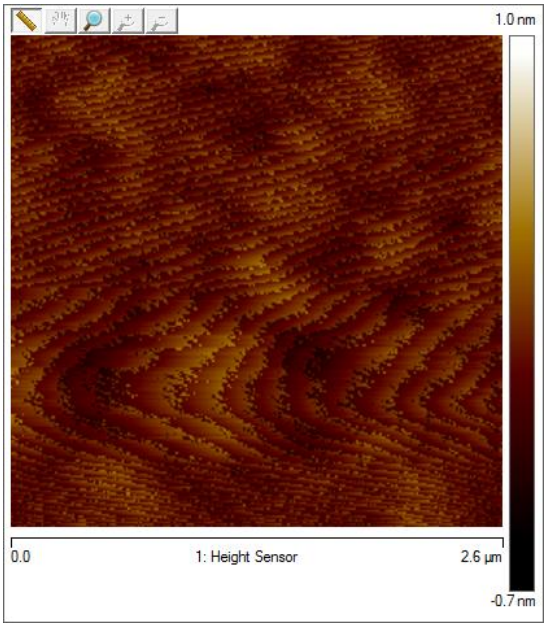

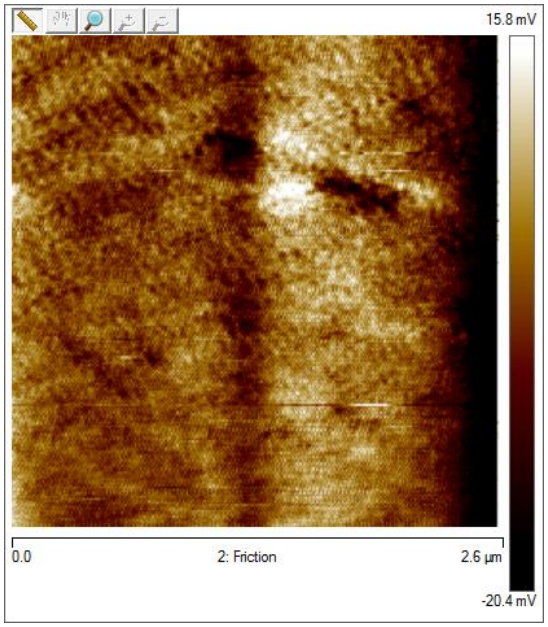

(c) (d)

Figure (5.26): (a) The height image for a wire (b) Friction image for the same wire where notice that we can see the wire in the friction image but not in the height image (c) Zoomed in height image on the wire (d) Zoomed in friction image of the wire. This wire was intended to be 50 nm wide. Due to the minuscule water droplet it ended up being 125 nm in width

Figure (5.27) shows AFM height and friction images at two levels of magnification for a wire written under 60% humidity. This wire was intended to be 50 nm wide. Due to the meniscal water droplet, it ended up being 136 nm in width.

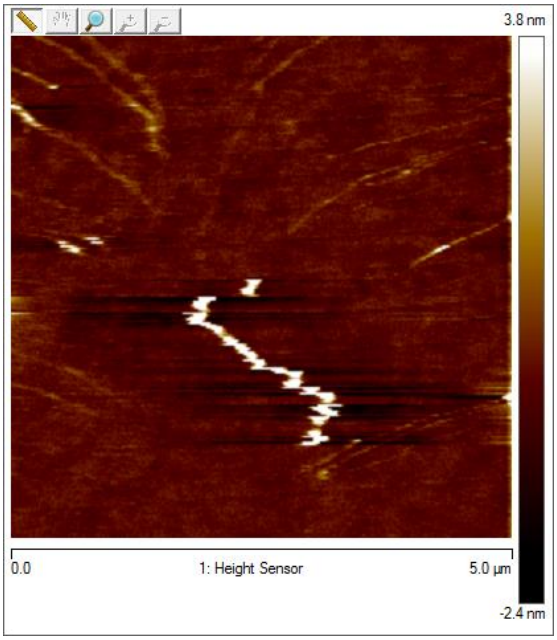

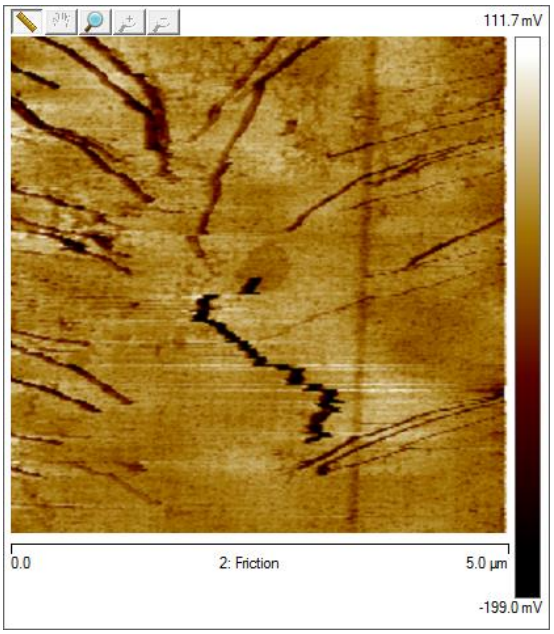

(a) (b)

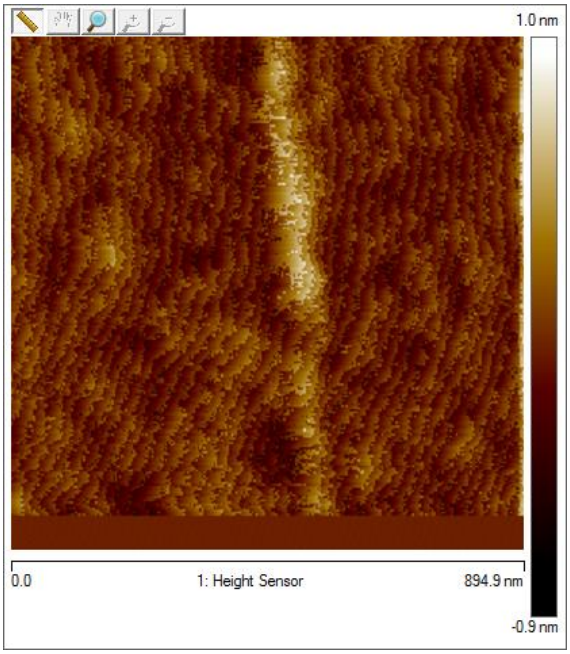

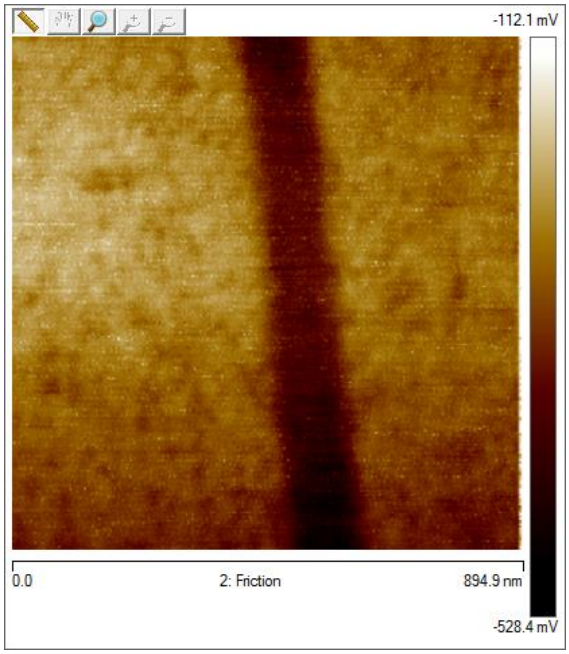

(c) (d)

Figure (5.27): (a) The height image for a wire (b) Friction image for the same wire where notice that we can see the wire in the friction image but not in the height image (c) Zoomed in height image on the wire. (d) Zoomed in friction image of the wire. This wire was intended to be 50 nm wide. Due to the minuscule water droplet it ended up being 136 nm in width

Figure (5.28) shows AFM height and friction images at two levels of magnification for a wire written under 65% humidity. This wire was intended to be 50 nm wide. Due to the meniscal water droplet, it ended up being 145 nm in width.

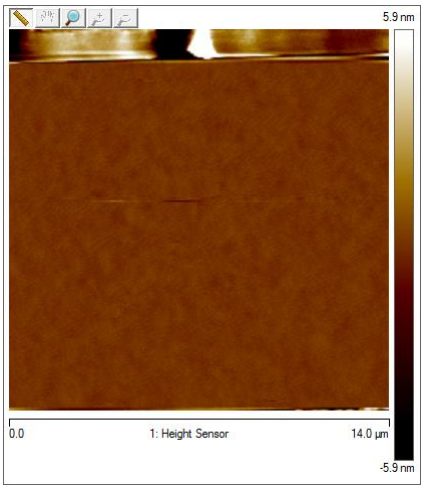

(a)

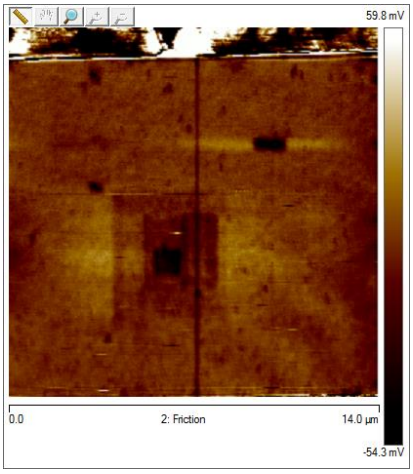

(b)

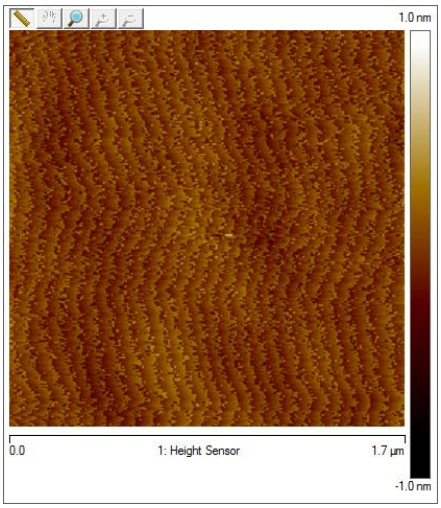

(c)

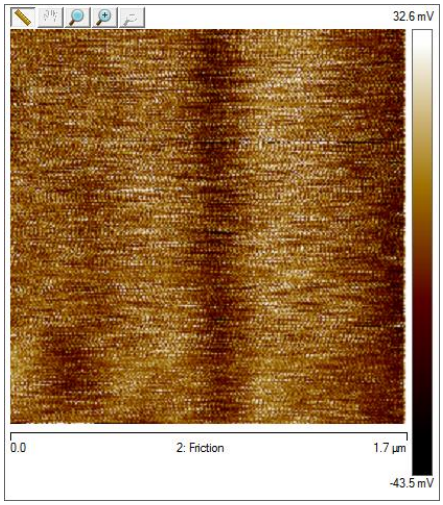

(d)

Figure (5.28): (a) The height image for a wire (b) Friction image for the same wire where notice that we can see the wire in the friction image but not in the height image. The square is due to the tip retaining charge while imaging leading to the oxidization of the imaged area (c) Zoomed in height image on the wire. (d) Zoomed in friction image of the wire. This wire was intended to be 50 nm wide. Due to the minuscule water droplet it ended up being 145 nm in width

Figure (5.29) shows AFM height and friction images at two levels of magnification for a wire written under 70% humidity. This wire was intended to be 50 nm wide. Due to the meniscal water droplet, it ended up being 280 nm in width

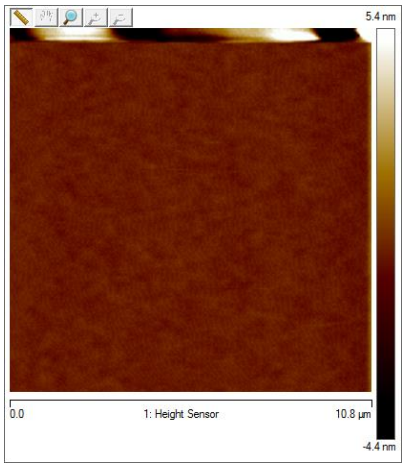

(a)

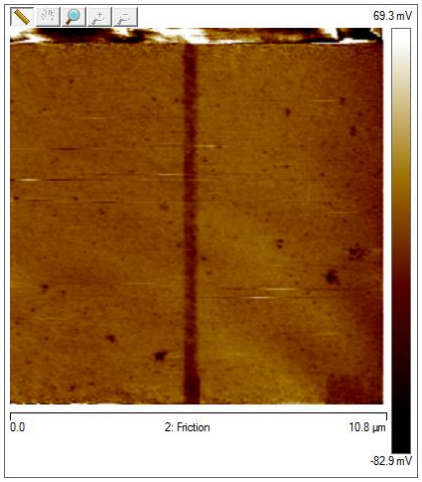

(b)

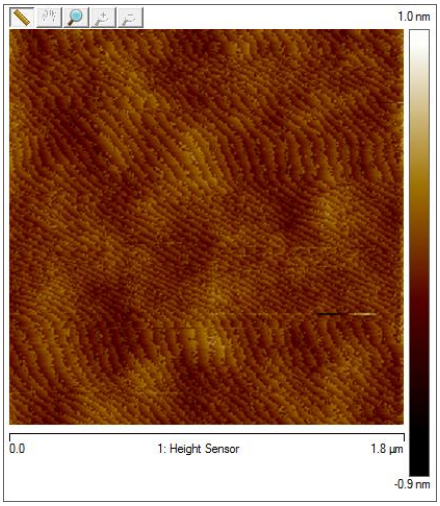

(c)

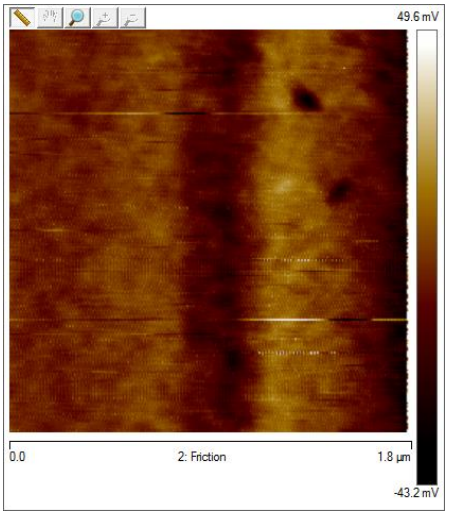

(d)

Figure (5.29): (a) The height image for a wire (b) Friction image for the same wire where notice that we can see the wire in the friction image but not in the height image. (c) Zoomed in height image on the wire. (d) Zoomed in friction image of the wire. This wire was intended to be 50 nm wide. Due to the minuscule water droplet it ended up being 280 nm in width

Figure (5.30) shows the relationship between relative humidity and the width of the wires produced using electrochemical modification of the silane monolayer. A slow increase in line width with increased humidity is observed for humidity in the range 50% to 65% followed by a very sharp rise at 70%. It is important to note that even at 50% humidity, the effect of the meniscal water droplet leads to a much larger wire width than the region over which the AFM tip is directly moved.

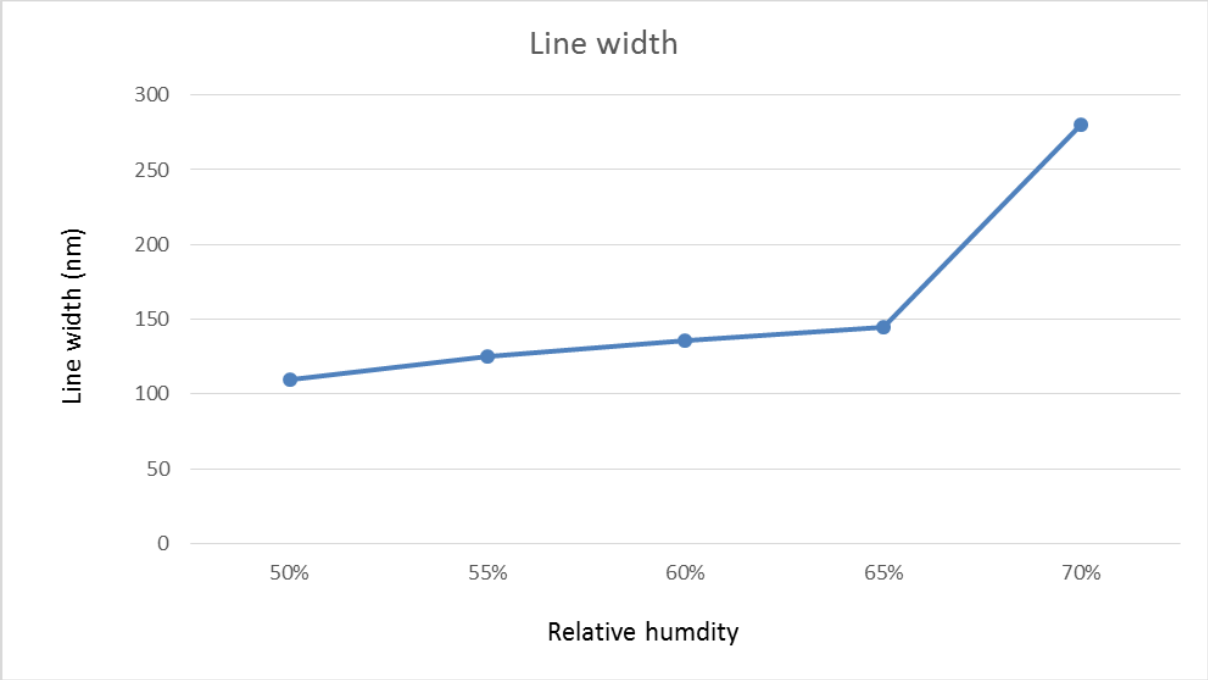

Figure (5.30): A graph showing the relationship between the relative humidity in which electrochemical modification of silane monolayers is carried out and the resulting line width.

Another set of trials we carried out targeted examining the effects of relative humidity on different shapes patterned using electrochemical modification. In this case, we constructed squares of different sizes ranging from 5 μm to 50 nm. The results are shown below. Figure (5.31) shows the results of patterning squares of different sizes under 50 % humidity. The smallest size for the

squares were intended to be 50 nm X 50 nm in size. However, due to the effects of meniscal water droplet, the patterns lost the square shape and became irregularly shaped with a width of 120 nm at the widest part.

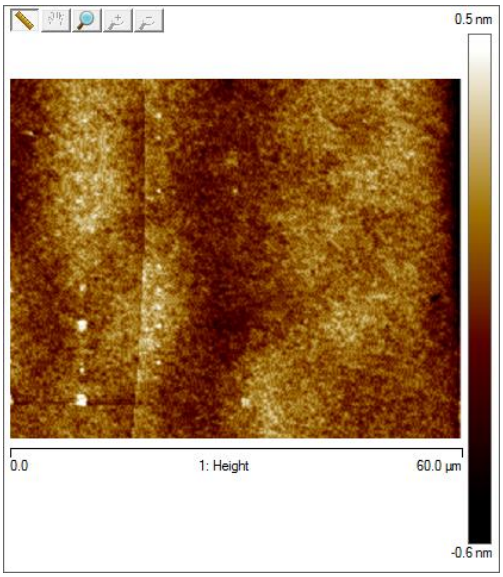

(a)

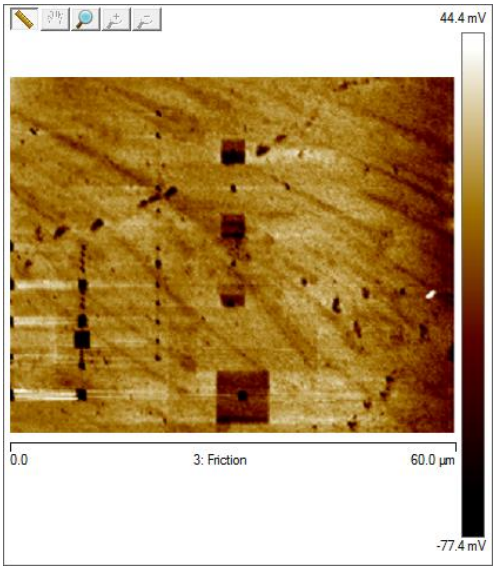

(b)

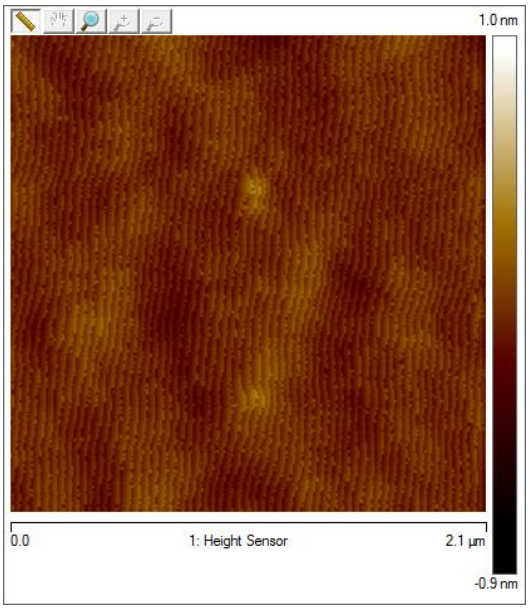

(c)

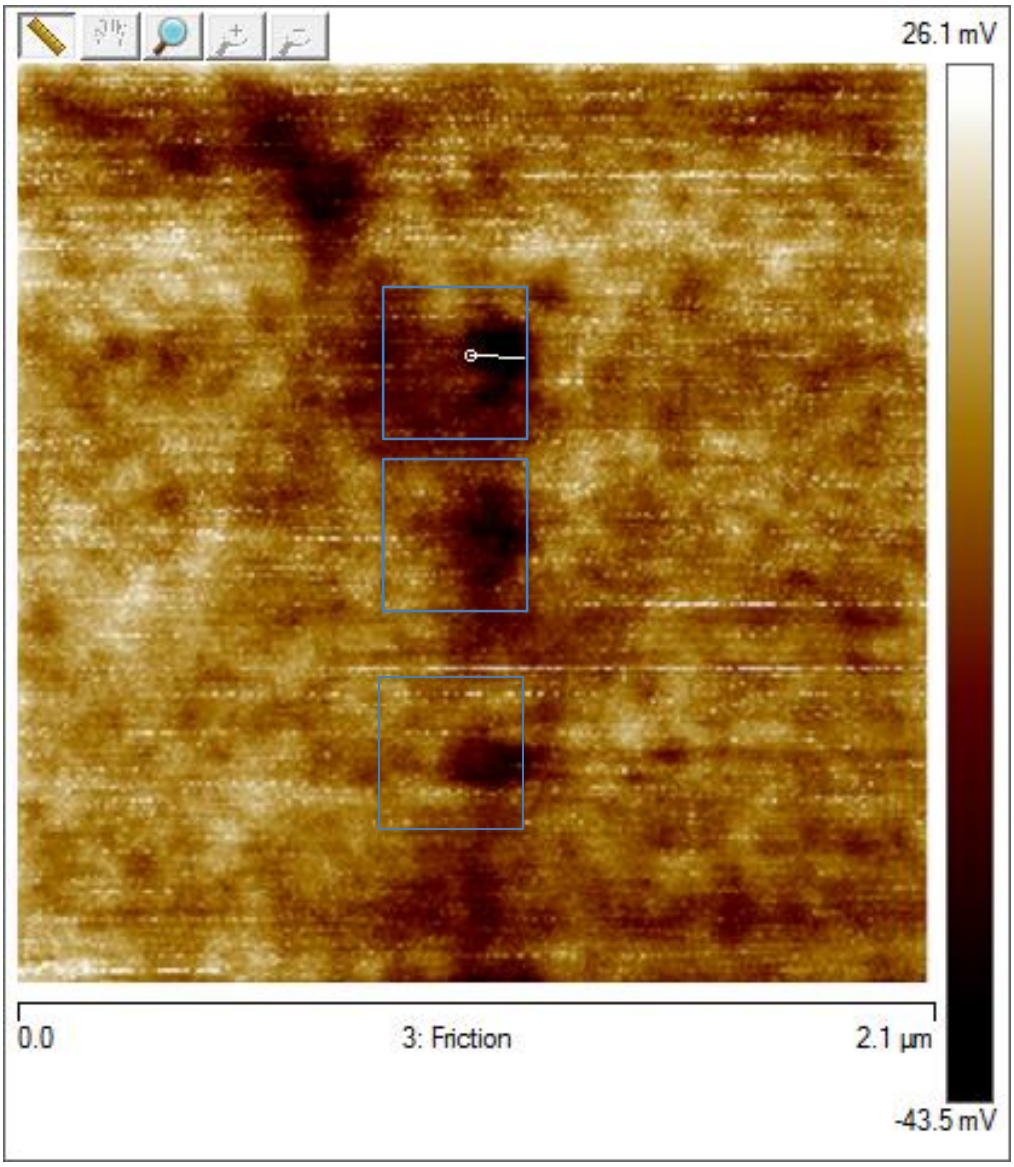

(d)

Figure (5.31): (a) Height images of the patterned areas. There is no noticeable height difference between the patterned squares and the background. (b) A friction image of the patterned areas. Darker colors indicate higher friction. (c) A zoomed-in height image of some of the patterns. (d) A zoomed in friction image of the patterns. The patterns were supposed to be squares of 50 nm sides but due to the meniscal water droplet, they lost the square shape and are 120 nm in the widest part of their irregular shapes.

Figure (5.32) shows the results of patterning squares of different sizes under 60 % humidity. The smallest size for the squares were intended to be 50 nm X 50 nm in size. However, due to the effects of meniscal water droplet, the patterns lost the square shape and became irregularly shaped with a width of 260 nm at the widest part.

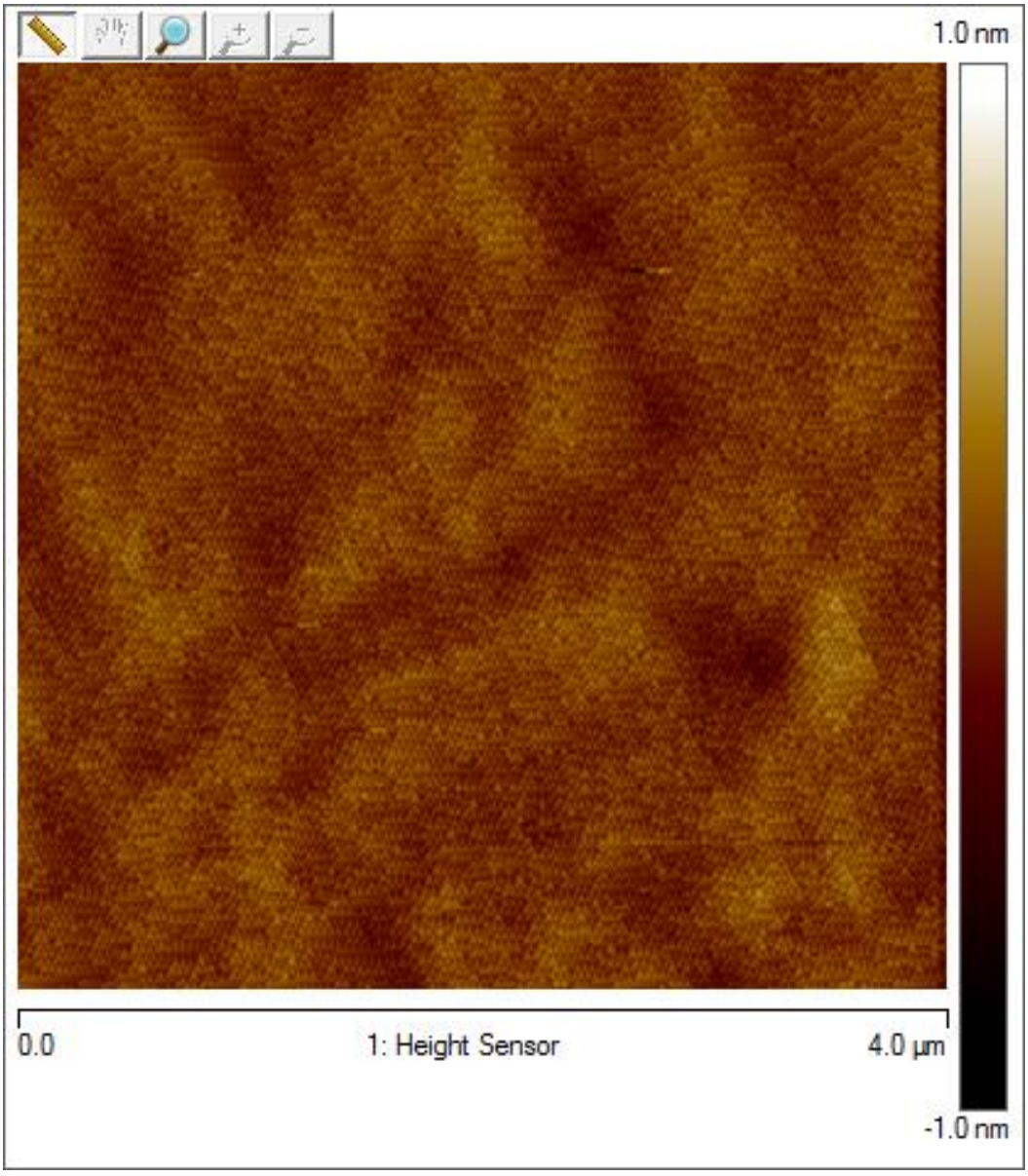

(a)

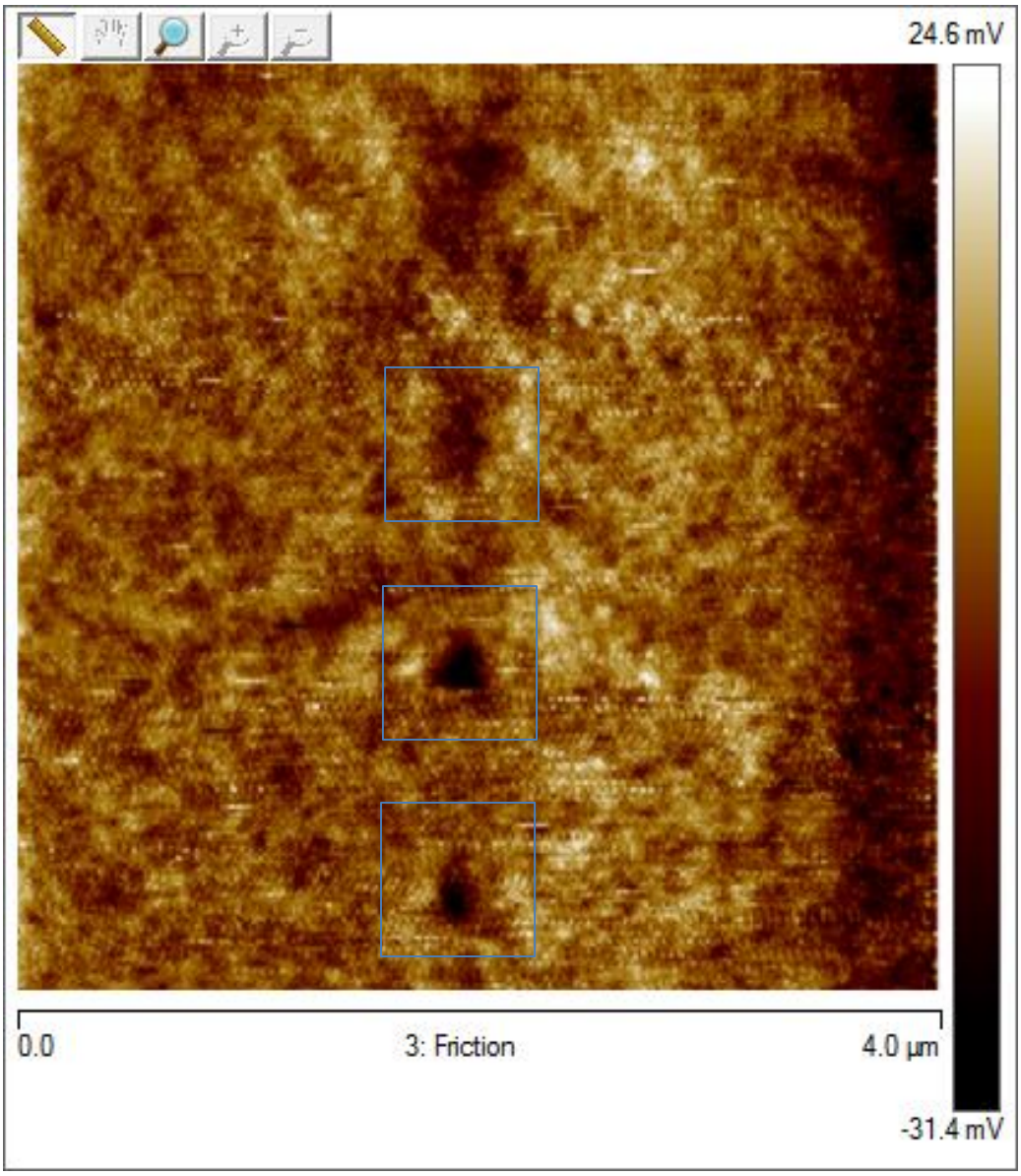

(b)

Figure (5.32): (a) Height image of squares patterned on the silanes by using electrochemical surface modification. There is no noticeable height difference. (b) A friction image of the squares in (a). These patterns were supposed to be 50 nm on each side but due to the water meniscus, they lost the square shape and are now 260 nm in the widest part.

Figure (5.33) shows the results of patterning squares of different sizes under 70 % humidity. The smallest size for the squares were intended to be 50 nm X 50 nm in size. However, due to the effects of meniscal water droplet, the patterns lost the square shape and became irregularly shaped with a width of 500 nm at the widest part.

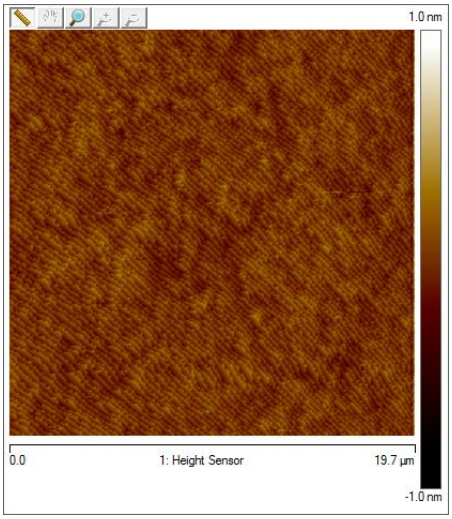

(a)

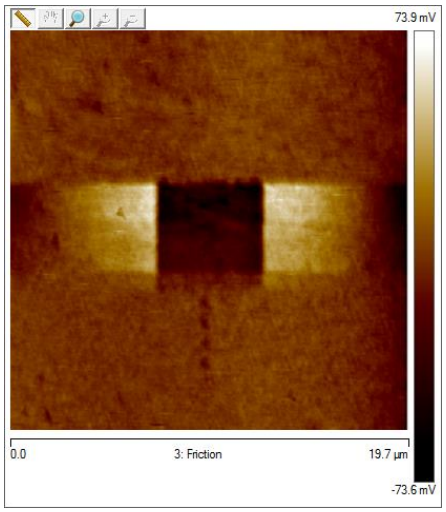

(b)

Figure (5.33): (a) The height image of patterned areas using electrochemical surface modification doe at 70% relative humidity. No difference is observed in the height between the patterned area and the background. (b): A friction image of patterns in (a). The small squares were patterned to be 50 nm on the side. Due to the meniscal water droplet, they are at 500 nm wide at the widest part of their irregular shape.

Although the resultant features sizes are larger than the patterns written by the AFM tip, the electrochemical surface modification technique does provide a reliable method of producing a charged template on the surface that can be used for deposition of various materials by layer-by-layer deposition. In our attempts to deposit gold nanoparticles onto these templates, one of the

main problems that persisted in this case was the weak binding between the gold nanoparticles and the patterned areas even after large numbers of bilayer depositions of PAH and gold nanoparticles.

A search in the literature revealed that there is a possible solution using what is known as a seeding method for the gold nanoparticles to form more uniform conductive surfaces when the gold nanoparticles are deposited on polymers.[5], [15], [16] The procedure starts with depositing a layer of PAH from a 10 mM solution at pH ~7.0 on the patterned areas that are now terminated by a functional –COOH group. The next step is to deposit a layer of the negatively-charged gold nanoparticles on top of the PAH layer. Then, the patterned samples are suspended in a 200 ml DI water solution of 2.6 mg hydroxylamine hydrochloride and 20 mg of $HAuCl_4 \cdot 3H_2O$ for 30 minutes under constant agitation.[5] Repeating the process of dipping the template samples in the negatively-charged gold nanoparticles and then in the chloroauric acid solution leads to the increased growth and uniformity of the deposited gold layer. After repeating the seeding procedure three times, the wires seemed to have a more uniform structure and surface. Figure (5.34) shows the results after we patterned two wires using surface oxidation, deposited an initial layer of negatively-charged gold nanoparticles and performed the seeding procedure three times.

Among the cons for using the nanografting technique while working with silanes is that we either had to use the replacement silane neat or dissolve it in toluene. Both of these options proved harsh and damaging to the liquid cell seal and potentially dangerous to the AFM. Another disadvantage is that AFM use either for imaging or grafting under liquid conditions is very difficult compared to imaging in air. One more disadvantage is that the AFM tips were dulled very quickly with the high forces applied to achieve the grafting needed. The main advantage for the grafting method is that the wires could be very narrow given that the width of the wires depended only on the diameter of the tip and the noise levels. In using the surface chemical modification methods, we found that

the wires are much wider than in the grafting case. The added width is attributed to the dependence of the patterning process on the meniscal water droplet forming between the AFM tip and the surface. Figure (5.35) shows a sample of three wires constructed using the grafting method. The difference in the wire sizes is very clear. The size of the water droplet also depends on the humidity of the atmosphere surrounding the AFM. This patterning trial was performed at relative humidity 70%.

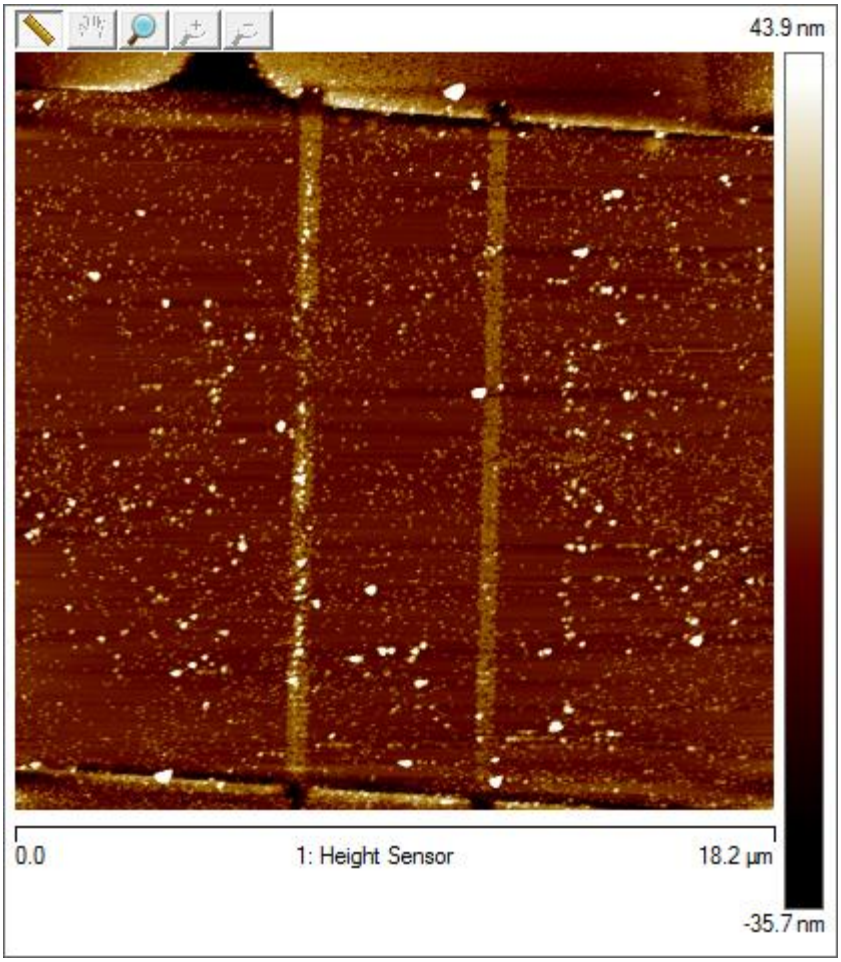

Figure (5.34) Height image of the two wires that were fabricated by using a seeding technique on areas patterned using electrochemical modification of the surface. The increase in the density of deposited gold particles is visible in the image. The resistance measurement for this construction was 86 MΩ.

Figure (5.35) shows the friction image of three grafted areas onto the passive background. The Nanoman® automated grafting program produced very thin lines of 30 nm width.

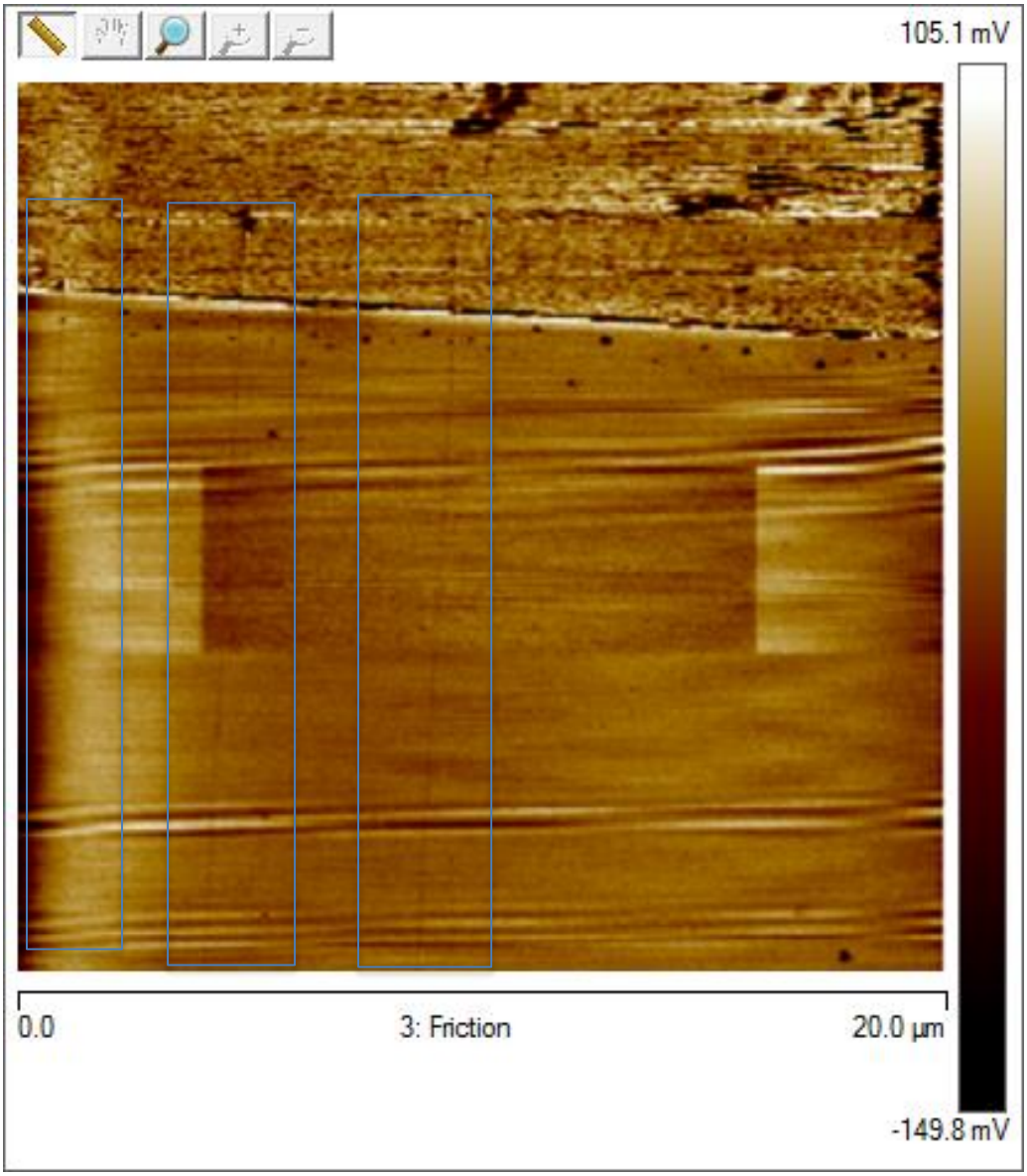

Figure (5.35): Three wires grafted using the nanografting technique and utilizing the Nanoman® automated nanolithography mode on the AFM. The wires are very thin compared to the ones patterned using surface chemical modification. Unfortunately, there was no success in depositing gold nanoparticles on them.

One of the problems we faced was the deposition of gold nanoparticles everywhere on the surface. Figure (5.36) shows a picture taken of the AFM tip that shows the tip shaving off some of the gold nanoparticles that were deposited on the surface of the sample.

Figure (5.36): Nonspecific binding of gold particles to the entire surface remains a problem for constructing nanowires using nanografting. After we dipped the samples in colloidal gold nanoparticle solution we noticed that the gold nanoparticles have deposited on the entire sample. As the AFM tip scans the surface while we are imaging the patterns we constructed we noticed that it is shaving some of the weakly adsorbed gold nanoparticles from the surface. This can be seen in the above image as a lighter color square right underneath the tip marking the area which was scanned by the AFM.

But once these weakly adsorbed particles were removed we could see wire patterns that were clearly visible. Excessive imaging caused the patterns to disintegrate. Figure (5.37) shows the wires that emerged after a small force was applied to the tip to remove the weakly bound gold nanoparticles.

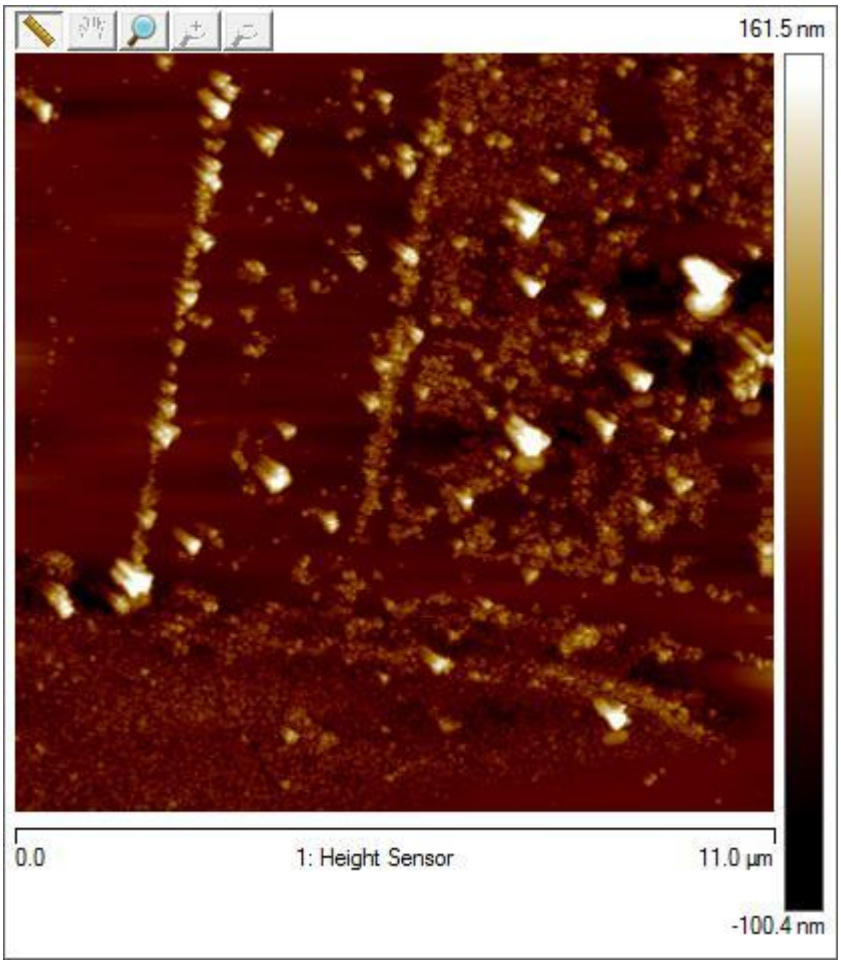

Figure (5.37): Two areas of selective deposition for gold nanoparticles and reduced gold atoms constituting two wires. We can see gold particles depositing on the background but in such a manner that did not cause any electric conductance between the electrodes.

Resistance measurements were performed on the wires constructed here. Wires of width 100 nm had values of resistance of 157 MΩ per wire on average. For these wires the measurements were carried out twice for two different wires. The values were 175 MΩ and 139 MΩ. For wires that were 500 nm in width the resistance per wire was 105.5 MΩ on average. Measurements for the resistance of the 500 nm wires were carried out twice for two different wires. The two values measured were 125 MΩ and 86 MΩ. When two wires 500 nm in width were constructed in parallel between two electrodes their resistance dropped to 46.2 MΩ, which is approximately half the value for a single wire as would be expected. The measurement for the two parallel wires was carried out only once. However, these values for the resistance should not be considered definitive. Given the problems we had with selective deposition of gold nanoparticles on the patterned wires, it was very difficult to build enough wires to establish a statistically coherent result. Much more rigorous examination of the resistance of these wires is required before any conclusions can be made.

5.5 Conclusion

In this chapter we examined the possibility of extending the selective deposition techniques from being guided by thiols deposited on gold to being guided by silanes deposited on silicon. The goal behind this is to study optimal conditions for using LbL deposition techniques as a vehicle for delivering molecular building blocks to nanocircuit elements.

The first step in establishing selective deposition is the patterning process. In this chapter we examined two different pattering methods. The first method we examined is nanografting. Transferring the procedure of nanografting to be performed on silicon substrates coated with a monolayer of silanes proved successful. However, the success of this procedure was limited by the severe wear on the AFM tips after a very limited number of runs and the harsh environment to

which the AFM was exposed because of the silane solutions. Grafting (3-mercaptopropyl)trimethoxysilane onto a background of chlorodimethyloctadecylsilane proved more successful than grafting 3-aminopropyl(diethoxy)methylsilane into a background of chlorodimethyloctadecylsilane with respect to selectively depositing layers of PAH and gold nanoparticles on the patterned areas. The smallest features of the patterns were on the order of a 300 nm grafted wires that did not exhibit any gold nanoparticles deposition. The smallest feature size of a wire where some gold nanoparticles deposition was observed was 100 nm. However, the density of the deposited gold particles did not lend itself to the construction of conductive paths.

The second patterning method we examined is electrochemical surface modification using anodic oxidation utilizing an AFM. Switching the patterning method to electrochemical surface modification allowed for the construction of patterns where the smallest feature is again on the order of 100 nm. Reducing gold atoms onto the selectively deposited gold nanoparticles allowed for the establishment of conductive paths.

We also performed a study of the relationship between humidity and the pattern sizes obtained using electrochemical surface modification. The results revealed some limitations on the smallest sizes that we can achieve using this method. The smallest feature size observed was 100 nm at 50% humidity and increased with increased humidity.

References:

1) Daan Wouters and Ulrich S. Schubert, "Constructive Nanolithography and Nanochemistry: Local Probe Oxidation and Chemical Modification", Langmuir **19**, 9033-9038, (2003).

2) Hiroyuki Sugimura, Nagahiro Saito, Kazuyuki Hayashi, Noriya Maeda and Osamu Takai, "Scanning Probe Surface Modification: Chemical Conversion of Terminal Functional Groups on Organosilane Self-Assembled Monolayers", Scanning Tunneling Microscopy/Spectroscopy and Related Techniques: 12th International Conference STM'03. AIP Conference Proceedings , Volume 696, pp. 150-157, (2003).

3) N. Saito, N. Maeda, H. Sugimura, and O. Takai, "Generation of Amino -Terminated Surfaces by Chemical Lithography Using Atomic Force Microscopy", Langmuir **20**, 5182-5184, (2004).

4) Rachel K. Smith, Penelope A. Lewis, Paul S. Weiss, "Patterning self-assembled monolayers", Progress in Surface Science **75**, 1-68, (2004).

5) Lakshmi Supriya, Ph.D. dissertation, Virginia Polytechnic Institute and State University, 2005.

6) Michael V. Lee, Kyle A. Nelson, Laurie Hutchins, Hector A. Becerril, Samuel T. Cosby, Jonathan C. Blood, Dean R. Wheeler, Robert C. Davis, Adam T. Woolley, John N. Harb, Mathew R. Linford, "Nanografting of Silanes on Silicon Dioxide with Applications to DNA Localization and Copper Electroless Deposition", Chem. Mater. 2007,19, 5052-5054.

7) Jaeger, Richard C. *Introduction to Microelectronic Fabrication* 2nd ed. (Upper Saddle River: Prentice Hall, 2002).

8) Thomas L. Floyd, *Electronic devices (Convensional Current Version)*, 9th ed. (Prentice Hall, 2011).

9) Yi Cui, Zhaohui Zhong, Deli Wang, Wayne U. Wang, and Charles M. Lieber, "High Performance Nanowire Field Effect Transistor", Nano Letters, Vol 3 No. 2, 149 -152, (2003).

10) http://www.enma.umd.edu/LAMP/Sop/Piranha_SOP.htm

11) Peter Van Zant, *Microchip Fabrication*, 5th edition. (McGraw-Hill Professional, 2004).

12) Stanford Nanofabrication Facility, Lift Off, https://snf.stanford.edu/SNF/processes/process-modules/photolithography/lift-off-lol-procedures/liftoff

13) Headrick, J. E., Armstrong, M., Cratty, J. Hammond, S., Sheriff, B. A., Berrie, C. L., "Nanoscale patterning of alkyl monolayers on silicon using the atomic force microscope", Langmuir, **21**, 4117-4122 (2005)

14) Sarah L. Clark and Paula T. Hammond, "The role of secondary interactions in Selective Electrostatic Multilayer deposition", Langmuir **16** (26), pp 10206-10214, (2000).

15) James M. Burkstrand, "Metalpolymer interfaces: Adhesion and xray photoemission studies", Journal of Applied Physics **52**, 4795, (1981).

16) Nikhil R. Jana, Latha Gearheart, and Cathrine J. Murphy, “seeding Growth for Size of 5-40 nm Diameter Gold Nanoparticles”, Langmuir, **17**, 6782-6786, (2001)

17) http://www.sigmaaldrich.com

Chapter 6

Swelling and Deswelling of Nanostructured Multilayer Polymer Films Using an Atomic Force Microscope

6.1 Introduction

In this chapter, we examine a new phenomenon that has been observed while performing some of our atomic force microscope based lithography experiments using thiols SAMs on gold substrates. During our experimental trials we observed that swelling and deswelling of multilayers of polymers can be achieved mechanically using an atomic force microscope. Scanning areas of the deposited polymer multilayers in contact mode with high forces resulted in flattened (pushed down, indented) areas that could be clearly seen in images taken in tapping mode. Rescanning parts of the flattened areas in contact mode with a medium force resulted in pulling up these areas noticeably. Also, in the process of achieving and reproducing the above-mentioned phenomenon, a direct method has been developed and tested to examine the phenomenon reported by Rubner of chemically swelling and de-swelling polymer multilayers which we discussed in detail in Chapter 2.[(1),(2),(3),(4),(5)]

The phenomenon observed and discussed here concerns the changing of the thickness of the deposited multilayers. The thickness of the polymer layers can change depending on several factors. The first factor that affects it is the pH of the solution from which it was deposited on the substrates. For weak polyelectrolytes, the pH of the solution determines the degree of ionization of the polymer. The lower the pH the more ionized a polycation is and vice versa. The opposite is true for polyanions where they are highly ionized at high pH. The second factor that can affect the

thickness of the layers is the deposition time used to deposit the multilayers on the substrates. The third factor that can affect the layer thickness is the pH of a solution they are submerged in after deposition. The change in the polymer layers' thickness examined in this experiment and reported here, unlike any of the cases reported before, is done via mechanical means. A chemical way of inducing changes in the thickness of the deposited polymer multilayers, described as swelling and deswelling , has been reported by Rubner.[(1),(2),(3)] In this chapter, we discuss a new method for achieving swelling and deswelling of polymer multilayers using an atomic force microscope (AFM).

6.2 Experimental details

6.2.1 Poly(allylamine hydrochloride) (PAH)

PAH is a positively-charged polymer when in solution. This polymer was used in a 10 mM solution in DI water at pH~7.0. It was purchased from Sigma-Aldrich and used as received.

6.2.2 poly[1-[4-(3-carboxy-4-hydroxyphenylazo)-benzensulfonamido]-1,2-ethanediyl sodium salt] (PCBS)

PCBS is a negatively-charged polymer when in solution. We used this polymer as a 10 mM solution in DI water at pH~7.0.

6.2.3 Poly(acrylic acid, sodium salt) solution (PAA)

PAA is a negatively charged polymer when in solution. We used this polymer as a 10 mM solution at pH~7.0.

6.2.4 Slides

We used glass slides that are coated with a gold layer of thickness 1000 Å deposited on an adhesive layer of Cr of thickness 50 Å. The slides were purchased from EMF Corp.

6.2.5 Atomic Force Microscope (AFM)

The AFM used in this experiment is a Veeco multimode with a NanoScope V controller.

6.2.6 AFM tips

The tips used were silicon nitride and silicon tips made by Veeco. The spring constants for the tips used varied between 0.6 N/m and 24 N/m. The softer tips, up to 4 n/m, were used for imaging and mechanically swelling and deswelling the polymer multilayers. The harder tips, k > 10 N/m, were used for shaving off polymer layers.

6.3 Experimental procedure

This experiment starts by cleaning the gold slides by boiling them in ethanol as described in Chapter 4. Then this is followed by depositing 2 bilayers of PAH/PCBS and PAH/PAA on a gold slide that has a monolayer of 16-mercaptoundecanoic acid formed on it. [(6), (7)] The deposited layers were then imaged using an AFM. While doing the imaging, we noticed that applying large forces to the AFM tip while imaging in contact mode causes areas of indentation in the layers. These indented areas correspond to the scanned areas. Rescanning the indented areas again with a medium force in contact mode and imaging the results in tapping mode shows a tendency for the medium force scans in contact mode to pull up areas of the previously indented multilayers. The difference in height between the areas that were flattened and the areas pulled up is measured and analyzed for various combinations of polymer multilayers. In the first case examined, we cleaned

a gold plated glass slide and dipped it for 48 hours in 16-mercaptoundecaoic acid. The cleaning process was a very gentle one and consisted of boiling the slide in ethanol for 45 minutes. After the boiling was completed, the slide was rinsed with fresh ethanol and then dried with pure nitrogen. The solution in which the slide is dipped was a 10 mM solution of 16-mercaptoundecaoic acid dissolved in ethanol. The slide was left in the solution for 48 hours to ensure a smooth and well-packed structure of the thiol on the gold surface of the slide. After the 48 hour dipping period was over, the slide was rinsed with fresh ethanol and then sonicated for 2 minutes in ethanol to make sure we get rid of any physisorbed molecules. Finally, the slide was rinsed again with fresh ethanol and dried with pure nitrogen. The slide was then inserted in the liquid cell of a Multimode AFM, and we proceeded to deposit four bilayers of PAH/PCBS while the slide is in the liquid cell. Both the PAH and the PCBS solutions were prepared as 10 mM solutions with their pH levels adjusted to 7.0.

6.4 Results and discussion

Scanning an area of 5μm X 5μm multiple times in contact mode using a strong imaging force and then switching to tapping mode and imaging the results, we notice that the strong force used in contact mode imaging pushed down the entire

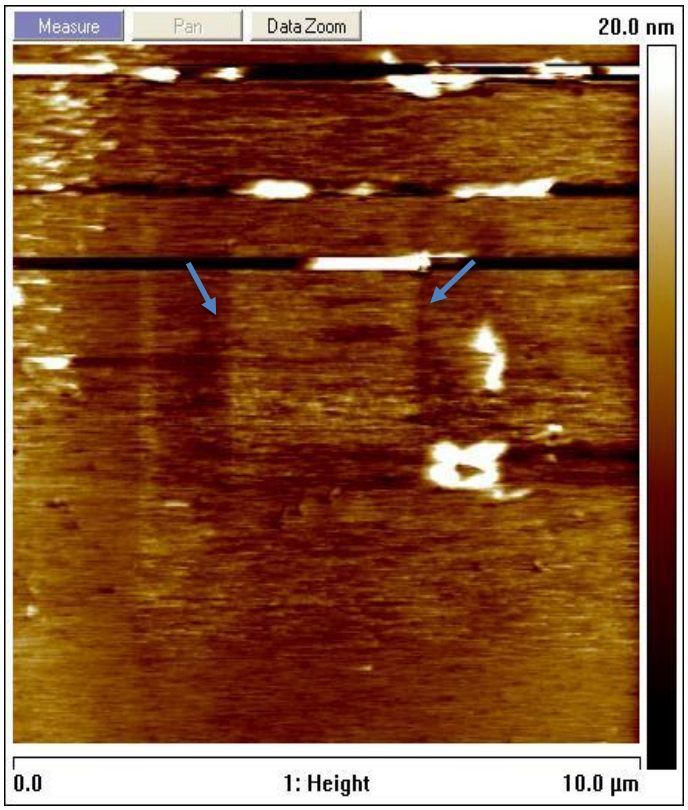
Measure
Pan
Data Zoom
20.0 nm
0.0
1: Height
10.0 µm

(a)

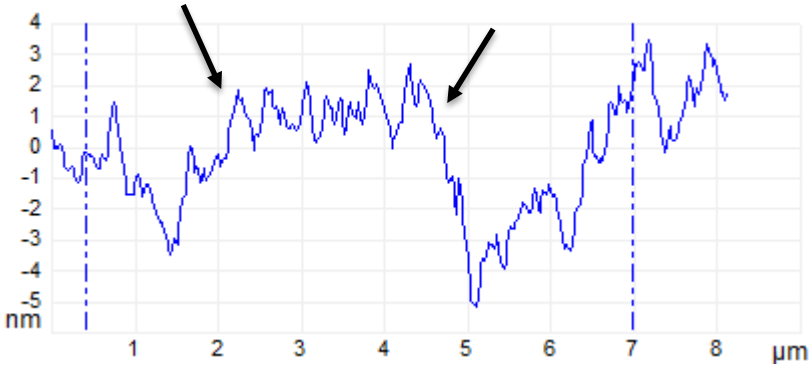
4
3
2
1
0
-1
-2
-3
-4
-5
nm
1
2
3
4
5
6
7
8
µm

(b)

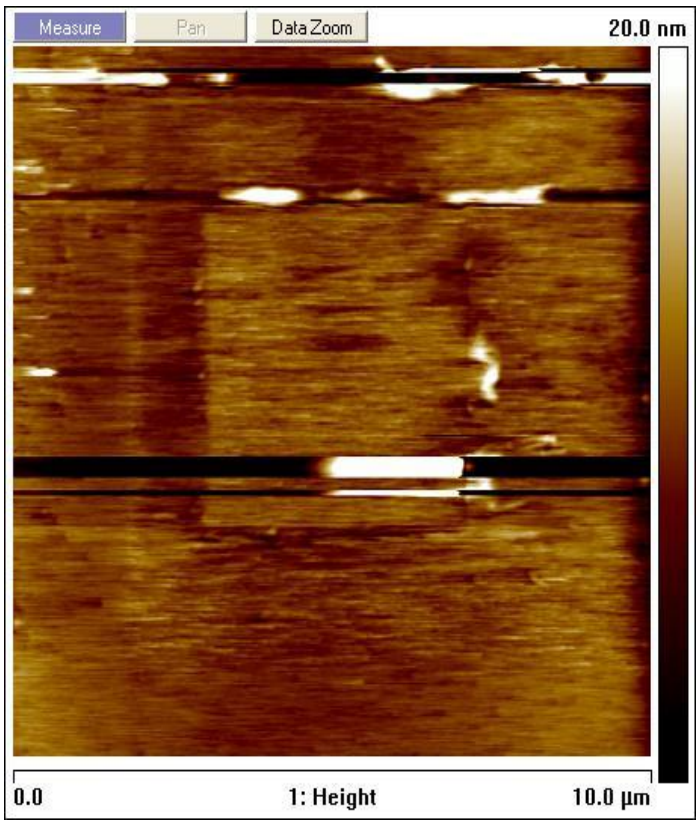
Measure
Pan
Data Zoom
20.0 nm
0.0
1: Height
10.0 µm

(c)

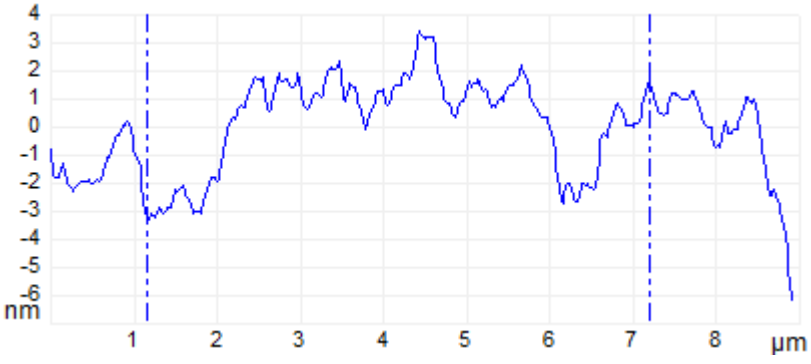
4
3
2
1
0
-1
-2
-3
-4
-5
-6
nm
1
2
3
4
5
6
7
8
µm

(d)

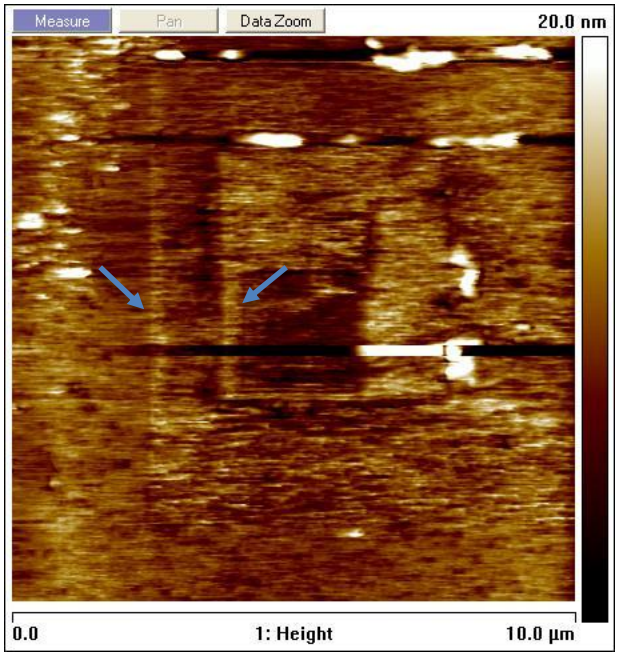

(e)

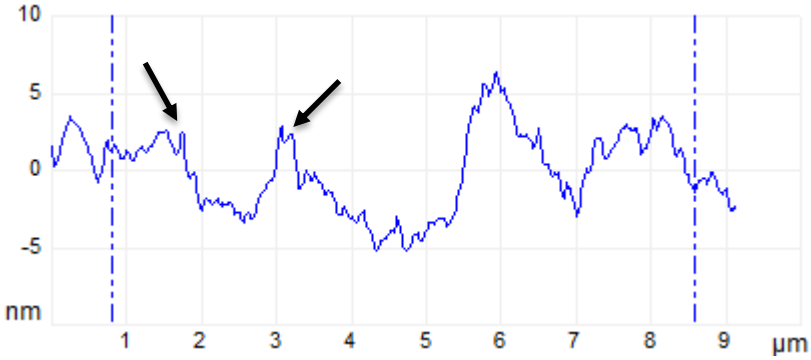

(f)

Figure (6.1): (a,b) Four bilayers of PAH/PCBS are deposited on the gold surface and then an area of 5 µm X 5 µm is pushed down and then an area of 3 µm X 3 µm is pulled up in the center. (c,d) in the same square we pull up an area of 4 µm X 4 µm. (e,f) In the center of the previous square we go back to push down an area of 2 µm X 2 µm.

scanned area. The height difference between the high area and the pushed down part is 7.8 nm on average. In Figure (6.1), we can see the difference between the flattened background of an area of 5 μm X 5 μm and various sub-regions that were pulled up and flattened again, as described in the figure caption.

The second case examined in the experiment proceeded to use a different combination of polymers. The combination used in this case was PAH/PAA with their pH adjusted to 7.0. When the experimental procedure was repeated with 2-bilayers of PAH/PAA, we noticed a similar situation to the previous case. In Figure (6.2), we can see the effect of flattening and then pulling up an area of 3μm X 3μm with a square of 1 μm X 1 μm in the center. The same phenomenon is observed again with an average difference of 3.5 nm between the flattened and pulled up areas.

A possible explanation for the mechanism behind these observations can be attributed to the fact that the tips used are made of silicon and silicon nitride and consequently the tips have affinity for having polyelectrolytes adsorbing on them and thus providing the surface of the tips with a net electric charge due to the acquired polymer coating. When an oppositely-charged tip is scanning near the polymer surface deposited on the slide it exerts an upward force on the polymer surface. There is definitely an interplay between how much force is applied from the tip on the surface and how much attraction is provided by the electric charge and this determines whether the surface is to be pushed down or pulled up.

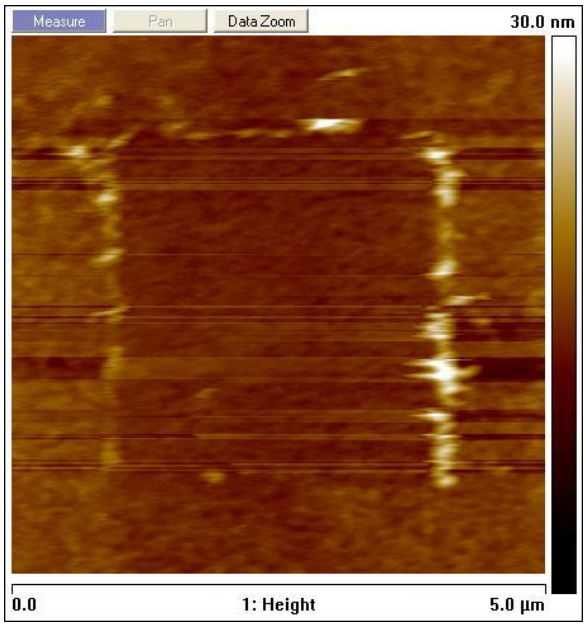

(a)

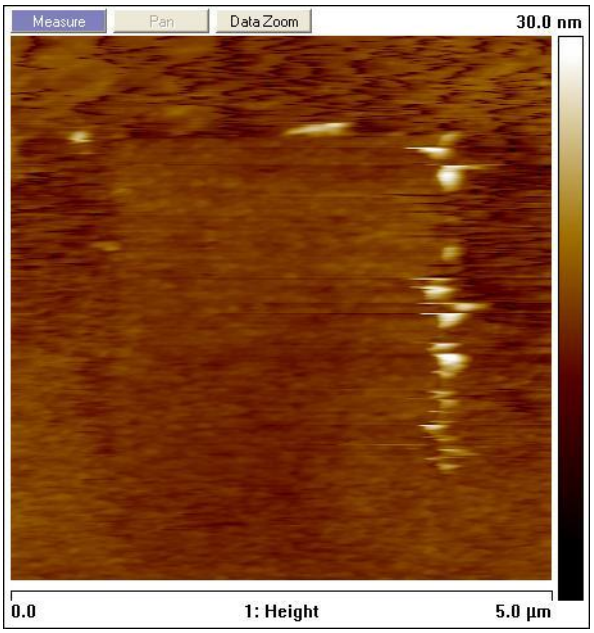

(b)

Figure (6.2): (a) Two bilayers of PAH/PAA were deposited on gold and then an area of 3 µm X 3 µm was pushed down using imaging in contact mode with a high force applied to the tip. (b) The same area of 3 µm X 3 µm was pulled up revealing a restoration of the thickness of the two bilayers due to mechanical swelling.

In performing the mechanical swelling and deswelling experiments we observed that it is possible to use the AFM tip to shave off some of the deposited polymer multilayers. However, this polymer multilayer shaving required the use of an AFM tip that is clean and has not been used before. Once the tip was used to shave any parts of the polymer multilayers it was not possible to use it for shaving anymore. This is believed to be due to the effect of some of the polymer layers getting attached to the AFM tip during the shaving process.

Another observation made during the mechanical swelling and deswelling experiment was noticing that polymer multilayers deposited on the AFM tip if the multilayer deposition was carried out inside the AFM liquid cell where the AFM tip is exposed to the polymer solutions. This effect was noticed through the failure of using a tip exposed to the multilayer deposition in the liquid cell in performing any deposited multilayer shaving regardless of the force that was applied to the tip. Also, a tip that has been exposed to the deposition process in the liquid cell consistently produced images of very poor quality suggesting that the tip is contaminated. Given that the AFM tips that we used for this experiment are made out of silicone, it seemed reasonable to assume that the polymer multilayers deposited on the tips as well during the deposition process.

To illustrate these two cases we deposited 3 bilayers of PAH/PCBS at pH 7/7 on a gold substrate functionalized with 16-MHA. The deposition took place in the AFM liquid cell while a tip was loaded in the cell. Using this tip for imaging resulted in the mechanical swelling of the layers as seen in Figure (6.3.a). The imaging was done using a new AFM tip to obtain a good imaging resolution. After the imaging was done we selected a different area of the surface where the 3 PAH/PCBS bilayers were deposited and by applying a high force during imaging a 3 μm X 3 μm square was shaved off as seen in Figure (6.3.b)

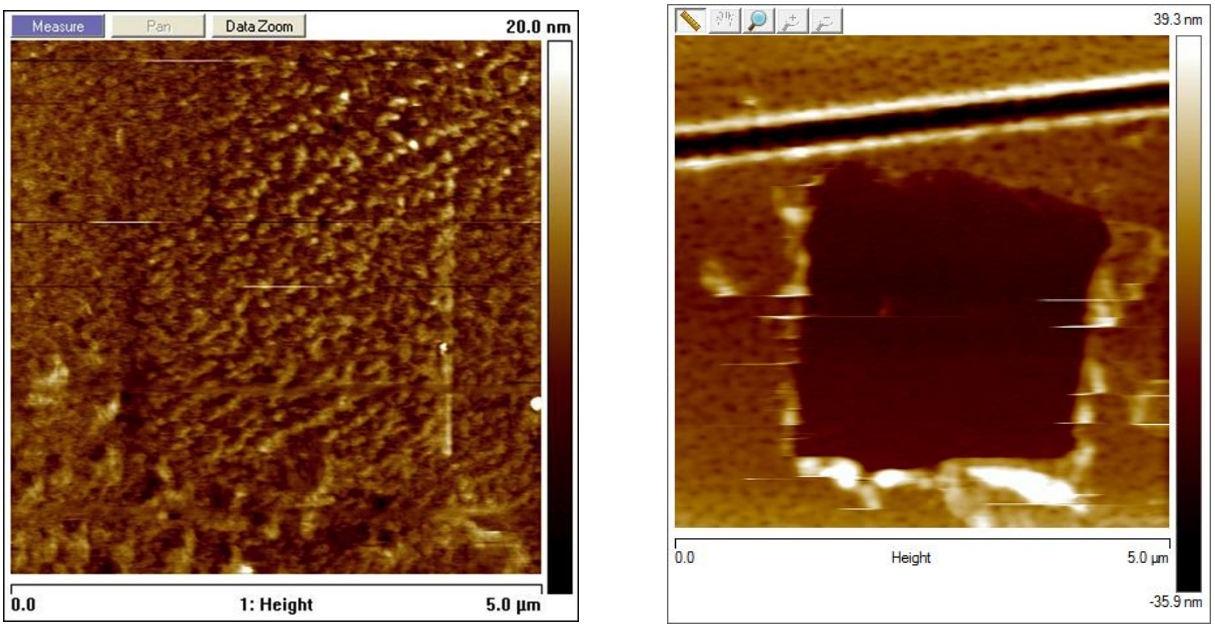

(a) (b)

Figure (6.3): (a) An area covered by 3 bilayers of PAH/PCBS after being pulled up using an AFM tip on which we deposited multilayers of polymers. (b) An area of 3 bilayers of polymer that was shaved off using a new AFM tip.

Using the AFM to shave off some regions on the gold surface from the polymer multilayers allowed us to compare this phenomenon to the pH-induced swelling and deswelling of polymer multilayers reported by Rubner.[(2)] Shaving an area of 3 µm X 3µm from the adsorbed polymer multilayers, exposing the substrate to DI water at pH ~ 10.0, letting the sample sit in the water inside the liquid cell for 20 minutes and then imaging revealed an average thickness for the 2 bilayers of PAH/PAA of 3.7 nm. Varying the pH level of the water all the way down to pH~1.0 and then back to pH~10.0 while waiting for 20 minutes at each pH level before imaging, we get the results summarized in Table (6.1). Figure (6.4) shows the change in height of the polymer multilayers with the 3um square of 2 bilayers of PAH/PAA shaved off.

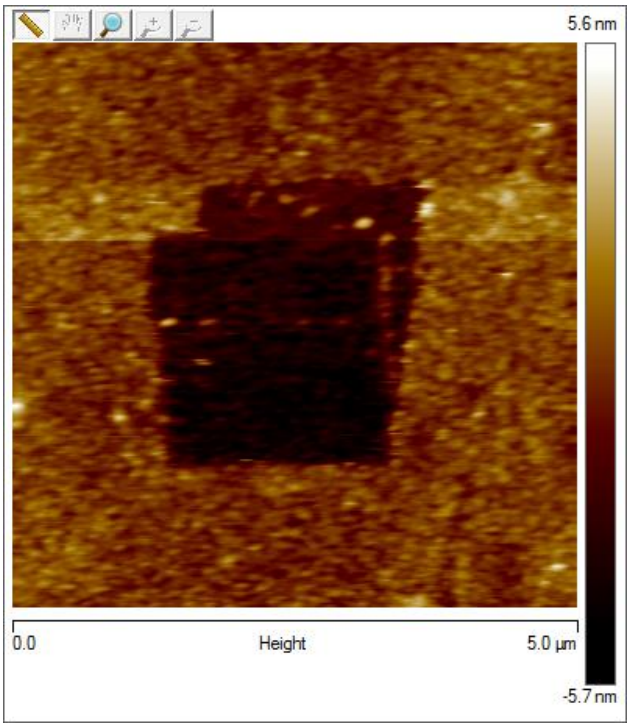

(a)

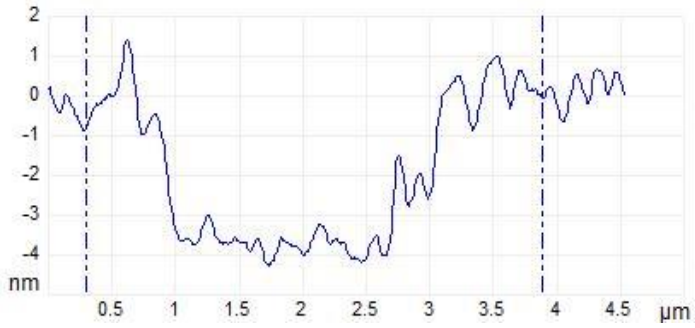

(b)

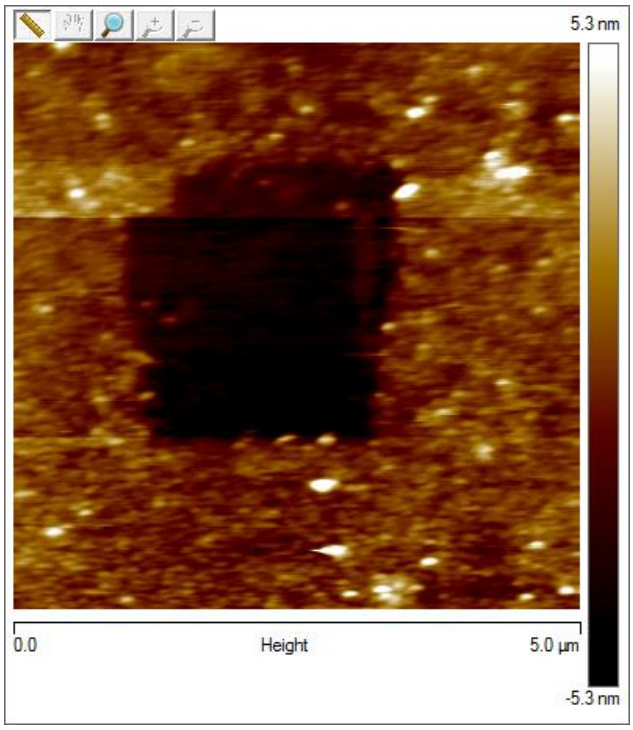

(c)

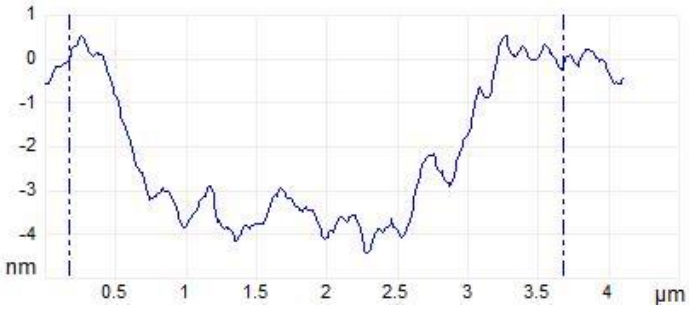

(d)

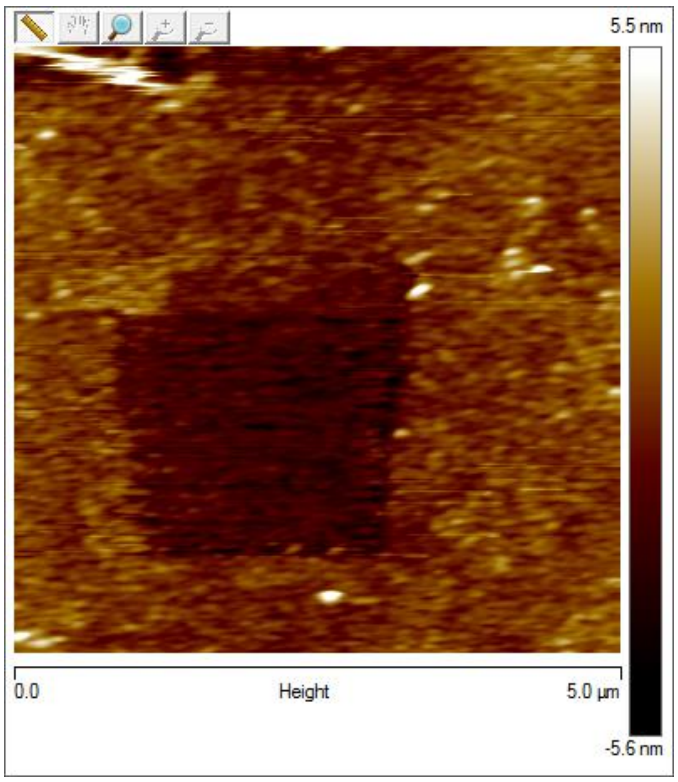

(e)

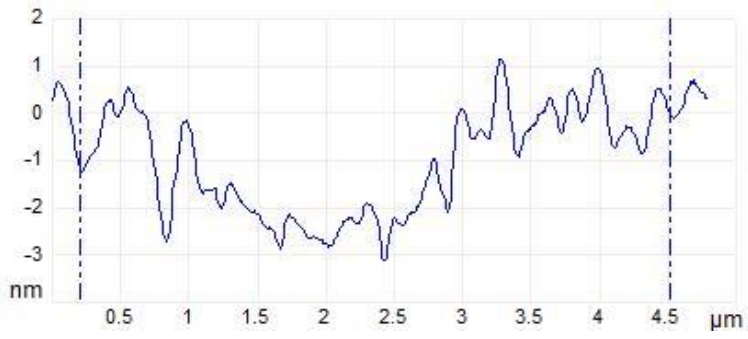

(f)

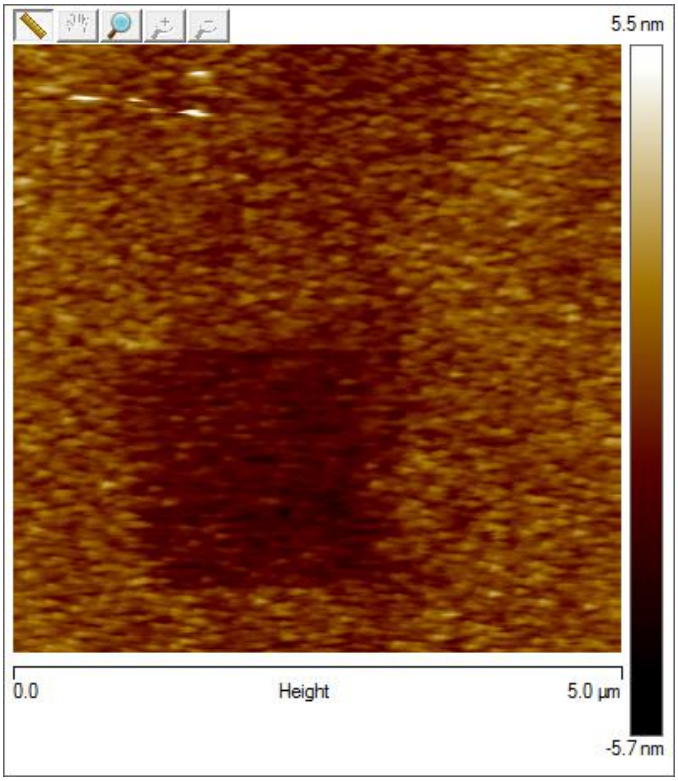

(g)

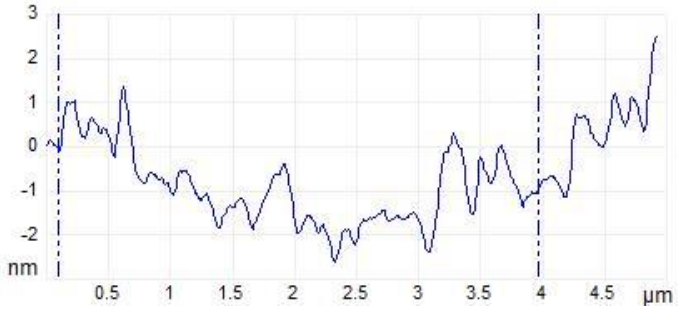

(h)

Figure (6.4): (a): After shaving a 3 µm X 3 µm area the polymer multilayers were submerged in DI water at pH~10.0 for 20 minutes. (b) A height cross section of (a). (c) The same shaved area at pH~7.0. (d) A height cross section of (c). (e) The same shaved area at pH~4.0. (f) A height cross section of (e). (g) The same shaved area at pH~ 1.0. (h) Height cross section of (g).

pH Level	Layers thickness while decreasing the pH	Layers thickness while increasing the pH
10	3.7 nm	2.9 nm
9	3.2 nm	2.8 nm
7	2.4 nm	2.2 nm
6	2.3 nm	1.2 nm
4	2.3 nm	1.3 nm
3	2.1 nm	1.1 nm
2	1.3 nm	1.1 nm
1	0.95 nm	0.95 nm

Table (6.1): The difference in height between an area that has been cleared of the polymer multilayers and another that is covered with the polymer as we change the pH of the solution for two bilayers of PAH/PAA each at pH 7.0. The height measurements are made using an atomic force microscope.

Figure (6.5) shows a plot of the thickness changes of the PAH/PAA bilayers as we change the pH of the solution.

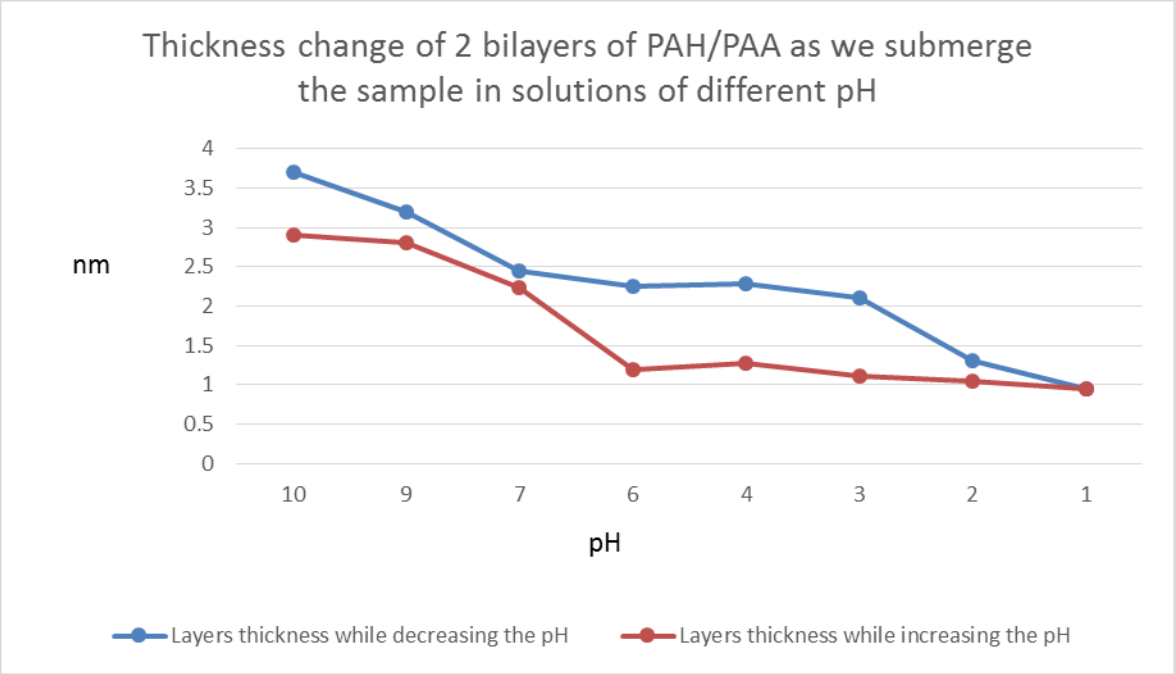

Figure (6.5): Changes in the thickness of 2 bilayers of PAH/PAA that were deposited at pH 7.0 as a response to the bilayers being immersed in DI water of different pH.

The results seen in these graphs agree with Rubner's conclusions, which we discussed in detail in Chapter 2. [(1),(2),(3),(4)] According to Rubner, the initial deposition conditions of polymer multilayers containing PAH layers affect the swelling response they have. This can be attributed to the fact that depositing PAH layers at pH < 8.5 means that they are almost fully ionized and this will decrease the number of the free amine groups on the chains through their interacting with the neighboring layers establishing bonds. When the PAH layers are deposited at high enough pH (pH 9 or higher), the chains are partially ionized which means that there will be a large number of free (non-ionized/non-interacting) amine groups left on the chains of PAH. This will allow these free amine groups to be completely ionized when they are exposed to low pH solutions. When these

free amine groups are fully ionized post-assembly, they allow for electrostatic interactions between the layers to break thorough deposition energy minima governing layer thicknesses. Such behavior leads to the observed trends in swelling of polymer multilayers containing weak polyelectrolytes such as PAH. On the other hand, when polymer multilayers containing PAH are deposited at pH values where the majority of the amine groups are ionized such as our case here where the deposition pH of the PAH was 7.0, the ionized amine groups establish electrostatic connections with the neighboring layers and are not free to exert the same effect as the free amine groups. This leads to polymer multilayers containing PAH deposited at pH < 8.5 exhibiting a low increase or decrease of their thickness in response to changes of pH of solutions in which they are immersed. The benefit of the method we have used in reexamining this phenomenon is that it is a direct measurement between areas covered with polymer multilayers and others where the polymer layers have been stripped off completely. In all of the experiments done before examining this phenomenon, indirect methods have been used such as ellipsometry or Fourier transform infrared analysis (FT-IR).

6.5 Conclusion

In this chapter, we performed experiments to examine a phenomenon we observed while working on nanografting of thiols on gold followed by layer-by-layer assembly. The observation was that if we allow an AFM tip to have polyelectrolyte layers to be adsorbed on it while we are adsorbing them on the surface and then pass this tip over the surface of a substrate that is covered with multiple layers of polymers using a medium force while the AFM is in contact mode, it causes the polymer multilayers to swell. Repeating the scanning with greater force caused the polymer

multilayers to be compressed with visible indentations in the scanned areas. Repeated swelling and deswelling was observed to be possible. This was only possible when a tip is used after it has been covered in polymer multilayers. Using a fresh AFM tip led to the degradation of the polymer multilayers and their removal in some cases.

A direct method for testing the swelling and deswelling of polymer layers in response to changes in pH of the solutions they are submerged in was devised. We changed the pH of the solution in which the samples were submerged and observed the changes in the thickness of the bilayers of PAH/PAA. The results of the direct method developed are in agreement with the reported behavior published in the literature.

References

1. Hiller. J, Mendelsohn. J. D., Rubner. M. F. Reversibly Erasable Nanoporous Anti-reflection Coatings from Polyelectrolyte Materials. Nat. Mat. 59-63.

2. Itano. K., Choi. J., Rubner. M. F. Mechanism of the pH-Induced Discontinuous Swelling/Deswelling Transitions of Poly(allylamine hydrochloride)-Containing Polyelectrolyte Multilayer Films. Macromolecules **38**, 3450-3460, (2005).

3. Hiller. J., Rubner. M. F. Reversible Molecular Memory and pH-Switchable swelling transitions in Polyelectrolyte Multilayers. Macromolecules **36**, 4078-4083, (2007).

4. Lee. D., Nolte. A. J., Kunz. A.L., Rubner. M. F., Cohen. R. E. pH-Induced Hysteretic Gating of Track-Etched Polycarbonate Membranes: Swelling/Deswelling Behavior of Polyelectrolyte Multilayers in Confined Geometry. J. AM. CHEM. SOC. **128**, 8521-8529, (2006).

5. Zhai. L., Notle. A. J., Cohen. R. E., Rubner. M. F. pH-Gated Porosity Transitions of polyelectrolyte Multilayers in Confined Geometries and Their Application as Tunable Bragg Reflectors. Macromolecules **37**, 6113-6123, (2004).

6. Gero Decher. Fuzzy Nanoassemblies : Toward Multilayerd Polymeric Multicomposites. Science **277**, 1232 (1997).

7. R. K. Iler (1966). "Multilayers of co lloidal particles". *Journal of Colloid and Interface Science* **21**: 569

Chapter 7

Conclusion and Future Work

The experiments discussed in this dissertation focused on developing a novel method that has the potential to fabricate nanoscale electronic devices. The main motivation for pursuing the techniques in this dissertation were to find a relatively cheap and simple method to further down scale the dimensions of electronic components. Utilizing an AFM and self-assembled polymer layers and nanoparticles offer both these advantages and more. The lithography technique demonstrated here was done in a standard lab using bench top equipment without any need for special environments and accommodations such as vacuum or cleanroom environment. The equipment utilized is on the low end of cost with respect to other approaches for fabrication of nanoscale devices. The materials used were inexpensive and readily available.

7.1 Selective deposition of polymers using templates of thiols on gold substrates

The first part of our investigations led to the establishment of a method to pattern self-assembled monolayers of thiols using an AFM. An 11-MUD monolayer was deposited on a gold substrate through a two-phase process dependent on the attachment of the sulfur head groups of the thiol molecules to the gold substrate. Placing the thiol coated gold substrates in a liquid cell in the AFM and using nanografting techniques led to establishing patterns of different 16-MHDA embedded in a matrix background of the passivating 11-MUD. Using LbL deposition of PAH as polycation to be deposited with PCBS, PAA, and PSS as polycations from an aqueous solution allowed us to investigate and establish optimum conditions for the selectivity of polymer deposition on the patterned charged surfaces. For the study performed using PAH and PAA, the pH of the

polyelectrolyte solutions was varied over values of 3.0, 5.0, and 9.0 for both solutions. The polymer multilayers deposited everywhere on the substrate with a slight preference for depositing on the patterned areas. The best condition for depositing PAH/PAA layers selectively was found to be achieved at pH 9.0 for PAH and pH 7.0 for PAA. Such slight selectivity in the deposition was observed until the deposition of 6 bilayers of PAH/PAA. The selectivity in deposition disappeared completely after depositing 10 bilayers of PAH/PAA.

For the study performed using PAH and PSS, PAH was deposited at pH 3.0, 5.0, and 9.0. However, given that PSS is a strong polyelectrolyte and the degree of ionization of its chains does not depend on the pH of the solution, its pH was kept constant at 3.0. The polymer layers deposited everywhere on the substrate with preference towards depositing on the patterned areas. The best conditions for depositing PAH/PSS multilayers selectively was found to be at pH 7.0 for the PAH solution and pH 3.0 for PSS. Such selectivity was noticeable after depositing 10 PAH/PSS bilayers where the patterns were clearly disguisable in height measurements.

For the study performed using PAH and PCBS, the pH of PAH was kept at a constant value of 7.0 while PCBS was deposited from solutions of pH 7.0, 6.0, 5.5, and 5.0. It was observed that polymer multilayers deposit everywhere on the samples but with higher thickness for the multilayers on the patterned areas. A strong correlation was observed between the pH level of the polymer solution and the height of the individual monolayers deposited on the patterned areas, which can be explained based on the dependence of degree of ionization of the polymer chains of the weak polyelectrolyte on the pH of the solution. Repeated trials revealed that we get the largest increases in the height and the best selectivity for the deposited polymer layers when we used bilayers of PAH/PCBS where the pH of the PAH solution was 7.0 and the pH of the PCBS solution was 5.0. Such conditions allowed for the best selectivity observed throughout our study. Such selectivity

was observable after depositing 10 bilayers of PAH/PCBS. The patterns observed were very clear and distinguishable from the background. The observation that the bilayer thickness was ~3 nm for a PCBS pH of 5.0 compared to ~1 nm for pH values of 6.0 and 7.0 is consistent with the established properties of layer-by-layer polyelectrolyte films for which the thickness is found to increase as the charge density of the polymer decreases in the vicinity of the pK_a, which is ~4.5 for PCBS.

We also observed an interesting increase in the bilayer thickness for decreased template size. For each of the pH values studies, a 20-50% increase in bilayer thickness was observed for 200 nm X 200 nm templates compared to 500 nm X 500 nm and 3 μm X 3 μm. While this effect is not yet fully understood, we hypothesize that it is related to the confinement of the polyelectrolyte chains onto an area smaller than that to which they equilibrate on the larger templates.

The study of the selectivity and thicknesses of polymer multilayers on nanoscale charged templates presented here can be useful in designing an experiment or a procedure to ensure the selective delivery of polymers, nanoparticles or other materials considered as building blocks for nanoscale electronics.

7.2 Selective deposition on templates of silanes on silicon

Using nanografting on monolayers of chlorodimethyloctadecylsilane deposited on silicon allowed us to pattern the monolayer by introducing patches of aminopropyl(diethoxy)methylsilane onto the passive background. Such a technique allowed us to establish patterns of very small dimensions down to 30 nm in width. Attempts to further selectively deposit gold nanoparticles and polymer layers on these patterned areas were only partially successful. Nanografting silanes on silicon substrates proved extremely harsh on the AFM tips and caused them to wear down very easily.

Also, the solvents used to dissolve the silanes provided a very aggressive environment for the AFM components used with the liquid cell to perform the grafting. The results were limited also in terms of the ability to deposit gold nanoparticles on the patterned areas of sufficient density to construct conductive paths. In an attempt to improve the selectivity of the deposition of gold nanoparticles on the patterned areas we used LbL deposition of PAH and negatively charged gold nanoparticles. The PAH and gold nanoparticles deposited everywhere on the surface of the sample with no selectivity.

Given the limited success with the nanografting attempts for silanes on silicon substrates, I attempted a different method for patterning the silane monolayers. This method depended on applying a potential difference between a conductive AFM tip and the silane monolayer. The silane used as a monolayer on the silicon was chlorodimethyloctadecylsilane. The potential difference applied between the tip and the monolayer while holding the monolayer at negative potential caused a reduction reaction in the functional group of the chlorodimethyloctadecylsilane monolayer changing it from $-CH_2$ to –COOH. This introduced a pattern into the background matrix. Such a patterning process was successful in establishing selective deposition of polymers and gold nanoparticles. This selective deposition led to the establishment of clearly visible areas of preferred deposition for PAH and gold nanoparticles on the patterned areas. However, the gold nanoparticle deposition was not dense enough to make the paths conductive. Adding a step of reducing more gold atoms on top of the gold nanoparticles was successful in establishing enough density in the particle deposition so that the paths became conductive. The wires I successfully constructed had widths that ranged from 100 nm to 500 nm. The width of the template created and the resultant gold nanowire depended strongly on the ambient humidity due to the effect of the water meniscus between the tip and surface that mediates the oxidation process. For templates for

which the AFM tip traced out a 50 nm width feature, the width of the gold nanowire varied from 100 nm at 50% humidity to >250 nm at 70% humidity. For humidity <50%, no feature was observed, presumably due to insufficient water meniscus in this case. The resistance measurements for the 100 nm wide wire yielded an average value of 157 MΩ. The resistance measurements for the 500 nm wide wires yielded an average value of 105.5 MΩ, while two wires of 500 nm width had a resistance of 46 MΩ.

7.3 Swelling and deswelling of polymer multilayers using an AFM

After depositing multilayers of PAH and PCBS on a gold surface functionalized with 16-MHDA, we were able to manipulate the thickness of the polymer multilayers using the AFM tip. The multilayers were shown to swell and deswell as a response to AFM imaging. This swelling and deswelling of the polymer layers was accomplished by mechanical means as opposed to the pH-induced effects described in the literature. When an AFM tip was covered with multiple bilayers of PAH and PCBS deposited at pH 7 for both solutions, and then passed over the PAH and PCBS bilayers deposited on the gold substrate under the same conditions while applying medium force to the AFM tip, it caused increased thickness of the layers. This effect was found to be reversible when the fore exerted by the tip on the surface was increased. When we increased the force applied to the AFM tip and scanned an area covered with polymer multilayers, it was shown to decrease its thickness. Alternating the swelling and deswelling of a specific area of the polymer multilayers was shown to be possible by alternating the imaging force applied to the AFM tip.

Nanoshaving an area of 2 bilayers of PAH and PAA deposited on a gold substrate functionalized with 16-MHDA and successively changing the pH levels of the DI water in which the samples were submerged in the liquid cell of the AFM led to a direct method of observing the swelling and

deswelling phenomena of the polymer multilayers in response to changes of pH levels. The values recorded in our experiment matched and are explained by Rubner's work discussed in Chapter 2. Since the deposition of the PAH/PAA bilayers took place for pH 7 for both solutions, it met the condition of pH < 8.5 that characterized the relatively small changes in thickness as observed by Rubner and in our experiment.

7.4 Future Work

The immediate next step in the project is the enhancement of the selectivity of the deposition process. One of the key factors in the improvement of selectivity of the self-assembly process is the material used for passivating the substrate's background. It has been shown in the literature that passivating the background with 11-mercaptoundecyl-tri(ethylene glycol) compounds yields satisfactory levels of selectivity for the self-assembly process.[(1),(2)]

Lowering the noise levels under which the AFM is operated by providing further vibrational and acoustic noise insulation should allow us to reduce the sizes of the patterns made using nanografting and provide improved imaging conditions to detect very small patterns. Also, establishing a better and more consistent control mechanism for the humidity levels in which samples are patterned by providing more consistent humidification devices and highly sensitive hygrometers integrated with a feedback circuit should allow us to make smaller patterns. Such control and ability to further downscale the sizes of the patterns is critical to enabling reproducible features at length scales currently possible with photolithography.

The most important future direction of the project is the use of selective deposition of semiconducting polymer multilayers and carbon nanotubes on patterned areas of silanes on silicon substrates. For nanotubes, this approach could allow assembly of nanotubes functionalized with

poly(aminobenzene sulfonic acid) (PABS) into desired locations onto a substrate, which is still a challenging problem. This is in contrast to all the extra steps normally required for nanotube FETs such as having to determine the location of the nanotubes on the substrate and then using ion beam lithography to place the electrodes. Similarly, the use of charged conjugated polymers such as charged polythiophene and sulfonated polyaniline in the LbL films assembled on the substrate would allow construction of nanoscale transistors from these materials as well as enable detailed studies of the conduction mechanism.

References

1. Seung Woo Lee, Raymond G. Sanedrin, Byung-Keun Oh, and Chad A. Mirkin, "Nanostructured Polyelectrolyte Multilayer Organic Thin Films Generated via Parallel Dip-Pen Nanolithography", Adv., **17**, 2749–2753, 2005.

2. Sarah L. Clark and Paula T. Hammond, "The role of secondary interactions in Selective Electrostatic Multilayer deposition", Langmuir **16** (26), pp 10206-10214, (2000).